Ultimate Capacity of Aluminium Plates under Multiple Loads, Considering HAZ Properties

Dr.Ing. Thesis

by

Odd Halvdan Holt Kristensen

Trondheim, 2001

Department of Marine Structures
Faculty of Marine Technology
Norwegian University of Science and Technology

URN:NBN:no-1307

Abstract

The purpose of this work has been to investigate the ultimate capacities of aluminium plates. The aluminium plates are supposed to be part of a marine structure. Their behaviour has been explored by taking advantage of non-linear finite element simulations. The loading conditions included axial compression, transverse compression, pure shear loading, axial compression in combination with transverse compression and axial compression in combination with shear loading.

Different patterns of heat affected zones have been studied with particular attention on conventionally welded plates and extruded, welded plates. The plates have been given realistic boundary conditions in addition to boundary conditions believed to represent the extremities in plate collapse behaviour. The initial deflection patterns chosen, were generally conservative, and the variations in collapse capacities for different initial deflection patterns have been investigated. The initial deflection amplitudes were systematically varied to cover all values of the initial deflection amplitudes likely to occur.

In addition to studying different patterns of the heat affected zones, systematic variations of the breadths of the heat affected zones have been performed. Systematic variations in the magnitudes of the residual stresses and systematic variations of the reductions of the 0.2 percent tensile proof stresses in the heat affected zones have also been carried out. Three different aluminium alloys were studied. They were believed to represent a high, medium and low utilised aluminium alloy. The aspect ratio of the plates was varied to cover both plates that were completely square to plates with a length equal to five times the breadth of the plates.

It was found that axially loaded plates with heat affected zones along loaded edges had lower ultimate capacities than plates with heat affected zones along unloaded edges, and if the plates had heat affected zones along loaded edges, having additional heat affected zones along unloaded edges did not alter the buckling capacities. The reduction in ultimate capacity could be modelled to vary linearly with the breadth of the heat affected zones, and the reduction in ultimate capacity could be modelled to vary linearly with the relationship between the value of the 0.2 percent tensile proof stress in the heat affected zones and the 0.2 percent tensile proof stress of the base material.

The ultimate capacities of transversally loaded plates could be found as the sum of a square plate and a plate strip, even if the plates contained heat affected zones. Square plates and plate strips with relevant patterns of heat affected zones had to be employed. Biaxial interaction curves showed a considerable slenderness dependence for all values of the aspect ratio investigated. The biaxial interaction curves were only slightly affected by introduction of different patterns of heat affected zones. The stress corresponding to equal elastic and plastic strain was better suited as the normalising stress than the more commonly used 0.2 percent tensile proof stress. One design curve could be used to represent all the different aluminium alloys investigated. Changing the aluminium alloy did not change the shape of the biaxial interaction curves.

Based on the detailed study of the collapse behaviour of aluminium plates carried out, and established practice, new ULS design formulas for axial compression, transverse compression, pure shear loading, axial compression in combination with transverse com-

URN:NBN:no-1307

pression and axial compression in combination with shear loading were proposed. The new design formulas accounted for reductions in ultimate capacities due to heat affected zones, including heat affected zones along loaded edges. They took full advantage of non-linear residual strength for slender plates; and the slenderness dependence and aspect ratio dependence for biaxial interaction curves were systematically incorporated.

URN:NBN:no-1307

Acknowledgements

The work was carried out under the supervision of Professor Torgeir Moan, to whom the author wishes to express his gratitude.

Sincere thanks are given to Professor Carlos Guedes Soares, Dr.ing. Sverre Valsgård and Professor Jørgen Amdahl for their willingness to serve as members of the doctoral committee.

This research was funded by Faculty of Marine Technology. I would like to thank the faculty for the generous contributions.

Thanks are extended to Dr.ing. Arne Aalberg and Professor Magnus Langseth at Department of Structural Engineering. Their help and comments have been both useful and encouraging.

Bjørn Østbye and Seyed Mostafa Jalali are thanked for their support regarding hardware and software applications. You have been more than helpful. I will really miss your excellent service.

I have had numerous instructive conversations with students at Faculty of Marine Technology. I can't name you all, but you have been of great help.

My thanks to my colleagues at Department of Marine Structures, Department of Marine Hydrodynamics and MARINTEK. I know some of you better than others, but, in addition to the technical advice, all the cinemas, dinners and trips in mother nature have really been appreciated.

During my many years of stay in Trondheim I have enjoyed my favourite hobby, dancing. Thanks to all friends at Trondheim Dancing Club, Da'capo Dancing Club and 'Kom og Dans'. You have not only been appreciated as dancing colleagues. Regularly meeting people outside the university has brought both new impulses and really widened my horizon.

Last, but not least, I will like to thank all my family. You have all been very supportive.

URN:NBN:no-1307

Contents

Nomenclature

General

- Symbols are generally defined where they appear in the text for the first time

Roman Symbols

A	Front area of plate
C	Elastic buckling coefficient
C_1	Longitudinal elastic buckling coefficient
C_2	Transverse elastic buckling coefficient
C_3	Elastic shear buckling coefficient
E	Young's modulus
F_{red}	Reduction in buckling force due to introduction of heat affected zones along long edges
F_x	Axial compression force
G	Shear modulus
K	Reduction factor due to heat affected zones
HAZ	Abbreviation for heat affected zones
R_x	Longitudinal strength ratio of plate in biaxial compression
R_y	Transverse strength ratio of plate in biaxial compression
R_τ	Shear strength ratio of plate in biaxial compression
a	Length of plate
a_{eff}	Effective length of plate
a_{mn}	Eigenmode amplitude in double Fourier series component mn
b	Breadth of plate
b_{HAZ}	Breadth of heat affected zone
b_{eff}	Effective breadth of plate
b_{hard}	Breadth of part of plate without reduced material properties
f	Coefficient in approximate eigenmode equation
i	Deflection amplitude number
k	factor determining the magnitude between stresses in different directions; constant in equation determining the exponent, n, in the Ramberg-Osgood law
m	Number of sine half waves in longitudinal direction
n	Number of sine half waves in transverse direction; knee factor in the Ramberg-Osgood law
n^*	Reduced knee factor in the Ramberg-Osgood law in the heat affected zones
p_1	Eigenmode amplitude for eigenmode with one half wave in longitudinal direction
p_2	Eigenmode amplitude for eigenmode with two half waves in longitudinal direction
p_3	Eigenmode amplitude for eigenmode with three half waves in longitudinal direction
p_5	Eigenmode amplitude for eigenmode with five half waves in longitudinal direction
s	Coefficient in approximate eigenmode equation
t	Plate thickness

w	Plate out-of-plane deflection
w_0	Eigenmode amplitude
w_i	Normalising constant for plate out-of-plane deflection
w_{max}	Maximum out-of-plane deflection
w_{mn}	Initial deflection contribution from double Fourier series component mn
x	Longitudinal co-ordinate of plate
y	Transverse co-ordinate of plate

Greek Symbols

Δa	Longitudinal end shortening
Δa_{max}	Maximum longitudinal end shortening
α	Reduction factor for 0.2 percent tensile proof stress in the heat affected zones
β	Longitudinal slenderness of plates
γ	Shear strain; design curve exponent
$\gamma_{0.2}$	Elastic shear strain
γ_n	Normalised shear strain
ε	Strain
ε_0	Residual strain corresponding to conventional elastic limit
$\varepsilon_{0.2}$	Elastic strain
$\varepsilon_{2.5}$	2.5 times elastic strain
ε_{elpl}	Strain corresponding to equal elastic and plastic strain
ε_n	Normalised strain
ε_t	Elongation at rupture
ε_x	Longitudinal strain
ε_y	Transverse strain
$\bar{\lambda}$	Normalised slenderness
μ	Coefficient in equation determining the effective breadth of a plate
ν	Poisson's coefficient
ξ	Design curve exponent
σ	Stress
$\sigma_{0.1}$	0.1 percent tensile proof stress
$\sigma_{0.2}$	0.2 percent tensile proof stress
$\sigma_{0.2}^*$	0.2 percent tensile proof stress in the heat affected zones
σ_E	Elastic buckling capacity
σ_{Ex}	Elastic longitudinal buckling capacity
σ_{Ey}	Elastic transverse buckling capacity
σ_R^+	Residual stresses in tension
σ_R^-	Residual stresses in compression
σ_Y	Conventional yield stress of material
σ_{cr}	Actual buckling capacity or critical compressive stress
σ_{elpl}	Stress that corresponds to equal elastic and plastic strain
σ_j	Equivalent stress or Mises stress
σ_n	Normalised stress
σ_{red}	Reduction in buckling stress due to introduction of heat affected zones along long edges
σ_t	Ultimate tensile strength

σ_x	Longitudinal stress
σ_{mx}	Mean longitudinal stress
σ_{mux}	Mean uniaxial ultimate longitudinal stress
σ_{muxHAZ}	Mean uniaxial ultimate longitudinal stress for plates with specified breadth of the heat affected zones
$\sigma_{muxbasic}$	Mean uniaxial ultimate longitudinal stress for plates consisting of the base material only
$\sigma_{muxfreesimply}$	Mean uniaxial ultimate longitudinal stress for plates with free, simply supported edges
σ_{muxres}	Mean uniaxial ultimate longitudinal stress for plates with residual stresses only
$\sigma_{muxsoft}$	Mean uniaxial ultimate longitudinal stress for plates with soft zones only
$\sigma_{muxtotal}$	Mean uniaxial ultimate longitudinal stress for plates with both residual stresses and soft zones
$\sigma_{mux,\ w=0.0025b}$	Mean uniaxial ultimate longitudinal stress for plates with maximum initial deflection amplitude equal to 0.0025 times the breadth of the plate
σ_y	Transverse stress
σ_{my}	Mean ultimate transverse stress
σ_{muy}	Mean uniaxial ultimate transverse stress
σ_{muyHAZ}	Mean uniaxial ultimate transverse stress for plates with specified breadth of the heat affected zones
$\sigma_{muybasic}$	Mean uniaxial ultimate transverse stress for plates consisting of the base material only
$\sigma_{muyfreesimply}$	Mean uniaxial ultimate transverse stress for plates with free, simply supported edges
$\sigma_{muytotal}$	Mean uniaxial ultimate transverse stress for plates with both residual stresses and soft zones
$\sigma_{muy,\ w=0.0025b}$	Mean uniaxial ultimate transverse stress for plates with maximum initial deflection amplitude equal to 0.0025 times the breadth of the plate
$\sigma_{\varepsilon 0}$	Conventional elastic limit
τ	Shear stress
$\tau_{0.2}$	0.2 percent tensile shear stress
τ_E	Elastic shear buckling capacity
τ_{elpl}	Shear stress corresponding to equal elastic and plastic strain
τ_m	Mean shear stress
τ_{mu}	Mean uniaxial ultimate shear stress
$\tau_{mubasic}$	Mean uniaxial ultimate shear stress for plates consisting of the base material only
τ_n	Normalised shear stress
ϕ	Biaxial compression angle
χ	Coefficient in equation determining the exponent, n, in the Ramberg-Osgood law
ω	Aspect ratio of plate (ω=a/b)

Chapter 1

Introduction

1.1 Background

The interest in using aluminium alloys in marine vessels is increasing. Aluminium alloys are employed in both monohulls, catamarans and offshore structures. Either the entire vessel or parts of the vessel are built in aluminium. The main reason for choosing aluminium alloys instead of steel is their light weight. Weight sensitive structures will experience increased speed and cargo capacity and reduced fuel consumption. Building parts of a vessel, principally the sections located high up, will also increase stability.

Because the research done on aluminium plates in marine structures is limited, it is useful to begin by looking at the significant and extensive research done on steel plating.

It started out by using classical linear elastic buckling with Johnson Ostenfeld correction. Later, one went on to use the effective flange or effective width concept. Douglas Faulkner (1975) verified the effective width concept proposed by Caldwell (1965). The axial capacities of long plates were described by a modified von Karman approach. Carl A. Carlsen (1980) adjusted the effective width formula to account for residual stresses.

Sverre Valsgård (1980) confirmed the adjusted effective flange formula proposed by Carlsen by using numerical simulations. He also documented that the ultimate transverse capacities of long plates could be found by summing the axial capacity of a square plate and a plate strip. Sverre Valsgård has in addition performed extensive studies on biaxial in-plane compression.

Carlos Guedes Soares, J. M. Gordo, M. Kmiecik and A. P. Teixeira (Soares, 1988, Soares and Kmiecik, 1993, Soares and Gordo, 1996a and 1996b, and Teixeira and Soares, 2001) have investigated the ultimate strength of rectangular plates. Both axial compression, transverse compression, biaxial compression and the effect of lateral pressure are investigated. Based on the results from experiments and numerical simulations they have proposed new design formulas for collapse strength of rectangular steel plates. Their design formulas explicitly account for plate slenderness, residual stresses, initial distortions and boundary conditions.

Initial imperfections, or post welding distortions, of steel plates have been extensively studied by M. Kmiecik, Jurek Czujko and Carl A. Carlsen (Czujko and Kmiecik, 1975, Carlsen and Czujko, 1978, Kmiecik et al, 1995). Their results are the foundation for the tolerance limits specified in the design rules given by Det Norske Veritas AS. A. C. Antoniou, M. Lavidas and G. Karvounis (Antoniou, 1980, and Antoniou et al, 1984) have also done comprehensive studies of post-welding deformations in ship plating. The post welding deformations are described by a two-dimensional Fourier series, and statistical distributions of the Fourier series components are developed.

Other extensive studies of collapse of rectangular steel plates can be found in Fukumoto et al (1983), Fukumoto and Itoh (1984), Yao et al (1991), Fujikubo et al (1997) and Marsh (1998).

The collapse strength of aluminium alloy plates has been studied both experimentally and numerically. Little (1981) performed numerical simulations of the uniaxial collapse capacity of rectangular aluminium plates with different slenderness, aluminium alloys and initial deflections, but without heat affected zones.

Mofflin and Dwight (1984) did laboratory tests on 76 aluminium plates with controlled initial out of flatness and heat affected zones. Their axial collapse capacities were compared with two theoretical models, a finite strip approach and a yielding edge zones approach. The collapse behaviour of the plates tested by Mofflin and Dwight has also been simulated using non-linear finite element simulations (Hopperstad and Langseth, 1994, and Kristensen, 1997).

The work by Little, Mofflin and Dwight form much of the foundation for the development of British Standard 8118 (1991) and Eurocode 9 (1998).

Hopperstad et al (1997) did laboratory tests on plate elements in aluminium and showed that given the actual initial deflection patterns and the actual distributions of residual stresses and soft zones, numerical simulations could predict the collapse strength of aluminium plate elements found in laboratory tests with excellent accuracy.

Numerical simulations have also shown excellent agreement with laboratory tests for stiffened aluminium plates. This is shown in Aalberg et al (1998, 1999a and 1999b) and Zha and Moan (2001a and 2001b). Numerical simulations can even predict the collapse strength of aluminium test specimens exposed to elevated temperatures (Amdahl et al, 2001).

1.2 Aim and Scope of Work

Most steel design rules use linear elastic buckling with Johnson Ostenfeld correction or a modified von Karman approach as the basis for axial strength determination of steel plating. When design codes for aluminium plates are developed, a direct copying of the design formulas for steel structures is employed. The yield stress for steel is replaced by the 0.2 percent tensile proof stress of the base aluminium alloy, and the elastic modulus for steel is replaced by the elastic modulus for aluminium alloys. In addition, a requirement that the mean average stresses of the plates cannot exceed the reduced 0.2 percent tensile proof stresses of the aluminium alloys in the heat affected zones is enforced.

Eurocode 9 (1998) have a correction for heat affected zones that is dependent of the breadth of the heat affected zones, but only heat affected zones along long edges of the plates is considered, and no reduction is performed if the mean average stresses are below the reduced 0.2 percent tensile proof stresses of the aluminium alloys in the heat affected zones.

Based on the numerical simulations carried out in Chapter 5, the assumption that the reduction in axial collapse strength due to introduction of heat affected zones disappears if the mean average stresses are below the reduced 0.2 percent tensile proof stresses in the heat affected zones, is questioned. Even for plates with heat affected zones along all long edges only, plates with the lowest mean average stresses (or highest values of the slenderness, β) show the largest percent reduction in ultimate capacities due to heat affected zones. It is also shown that plates with heat affected zones along all edges (conventionally welded plates) or plates with extruded patterns of the heat affected zones have considerably larger reductions in collapse strength than plates with heat affected zones along long edges only.

Marine design codes with an axial ULS design formula that considers heat affected zones along all edges or extruded patterns of the heat affected zones, and systematically treat variations of the breadths of the heat affected zones and different reductions of 0.2 percent tensile proof stresses due to welding, do not exist. In Chapter 10 such a design formula is developed.

In Chapter 7 the concept proposed by Valsgård to find the transverse ultimate capacity by summing the capacity of a square plate and a plate strip is extended to aluminium plates containing heat affected zones. Corresponding design formulas are developed in Chapter 10.

Compared with previous work, mainly for steel plates, and the design formulas in design codes, the numerical simulations for biaxilly loaded plates carried out in Chapter 7, demonstrates a systematic slenderness dependence that is either not imposed or very different from existing design formulas. New design formulas based on the numerical simulations carried out are presented in Chapter 10.

Also for plates loaded in pure shear, there have been systematic studies of reductions in collapse strength due to introduction of heat affected zones (Chapter 5) with corresponding design formula development in Chapter 10. The interaction curves for axial compression in combination with shear loading will be limited by pure elastic interaction, which will always be conservative, and plastic correction, which does not take buckling into account at all. The interaction formulas for pure elastic interaction and the interaction formula for plastic correction are quite similar (see Chapter 11), so slenderness dependence is limited; but the slenderness dependence observed is incorporated in the design formulas proposed in Chapter 10. Some design codes allow interaction beyond plastic correction (Eurocode 9, 1998, and Lloyd's, 1996), and these interaction curves should be replaced by more conservative interaction curves.

To the author's knowledge no systematic studies of post welding distortions in marine structures built in aluminium have been performed. The maximum initial deflection used in most of the analyses is equal to 0.5 percent the breadth of the plates. This is half the value of the maximum imperfections allowed by Det Norske Veritas AS in the design rules for steel plating. Due to the uncertainty connected with finding representative values of initial imperfections, the initial imperfection amplitudes have been systematically varied in Chapter 8, to cover all values of the initial deflection amplitudes that will be likely to occur. The initial deflection patterns are also varied, and the initial deflections used in the design formula development are compared with initial deflection patterns found in test-specimens, although these initial distortions will not be representative for a whole erected marine structure.

Using the 0.2 percent tensile proof stress as the normalising stress is debated in Chapter 9. In the author's opinion using the stress corresponding to equal elastic and plastic strain will be more representative. Due to the huge variations in yield stresses for different aluminium alloys the stresses corresponding to equal elastic and plastic strain are believed to represent points on the different stress-strain curves that are more equally utilised. The results found are in accordance with the numerical predictions found by Little (1981). One design curve can be used to represent all aluminium alloys, not 3 different curves which are used in Eurocode 9.

Chapter 2

Characteristics of Aluminium Alloys

2.1 General Considerations

Aluminium alloys are used as a structural material in a wide variety of engineering fields, such as the aeronautical industry, the transportation industry, the construction industry and the marine industry. Planes, containers, railway coaches, roofs, wall cladding, ladders, bridges, towers, masts, fast ferries, cranes, superstructures and helidecks are all built by the use of aluminium alloys (Bayley, 1987, Sharp, 1993, Mazzolani, 1995, Kissel and Ferry, 1995, Dwight, 1999).

Aluminium alloys are often used as an alternative to structural steels, a more commonly used material. The main reason for choosing aluminium alloys is that aluminium alloys have material yield strengths that are in the same order of magnitude as the most commonly used mild steels. The density of aluminium alloys is approximately one-third the density of structural steels. This gives a higher strength/weight ratio. Some of this advantage is outweighed by the fact that the elastic modulus of aluminium alloys is only one third that of steel. A structural component consisting of an aluminium alloy will have larger deformations and be more susceptible to instability than a geometrically similar structural component made of steel or stainless steel. Aluminium alloys also show poorer fatigue properties than structural steels.

Table 2.1 : Room temperature properties of a typical aluminium alloy, steel and stainless steel

	Aluminium	**Steel**	**Stainless steel**
Yield stress (Nmm^{-2})	255	235	240
Average weight density ($kg\ m^{-3}$)	2700	7850	7900
Young's modulus ($N\ mm^{-2}$)	70000	206000	206000
Melting point (°C)	658	1450-1530	1450
Linear thermal expansion Coeffisient ($°C^{-1}$)	24×10^{-6}	12×10^{-6}	17.3×10^{-6}
Specific heat ($cal\ g^{-1}$)	0.255	0.12	0.12
Thermal conductivity ($cal\ cm^{-1}s^{-1}°C^{-1}$)	0.52	0.062	0.035
Electrical resistivity ($\mu\Omega$ cm)	2.84	15.5	70

Normally aluminium needs no protection against atmospheric or chemical corrosive agents. The corrosion process is naturally inhibited. Aluminium in contact with oxygen forms aluminium oxide. Aluminium oxide is more stable than aluminium and acts as a protective shell. Pure aluminium has the highest resistance to corrosion. The corrosion resistance for

aluminium alloys depend on chemical composition, the fabrication process, the heat treatment and the stress field.

In addition to bolting, riveting and gluing, aluminium alloys can also be welded. For some aluminium alloys welding considerably reduces material strength. The effects of welding are elaborated on in Chapter 2.5.

When using aluminium alloys, one also has the advantage of the extrusion fabrication process. A structural part can be given a shape that simultaneously gives the minimum weight and the highest structural efficiency. For instance, the stiffeners of a stiffened aluminium panel can be given a much more complicated and idealised shape than what would have been possible in a steel panel, and the stiffeners will not have to be welded to the plate. The plates with their stiffeners on top are produced in one single process.

Taking all the mechanical properties of aluminium alloys into consideration one can say that aluminium alloys are well suited in long span systems with low live loads, in cases where lightness means economy of power under service or transport, in structures situated in corrosive or humid environments and in structures with difficult maintenance conditions.

2.2 Classification of Aluminium Alloys

Normally aluminium alloys are classified either with respect to the fabrication process (casting alloys and wrought alloys) and to the heat treatment (heat treated alloys and non heat treated alloys), or with respect to the chemical composition. The first way of classifying the aluminium alloys makes it possible to group families with similar mechanical behaviour.

Unfortunately, the nomenclature for aluminium alloys is different in each country. Either a numerical designation (USA, UK, Spain, Canada) or an alphanumerical designation (most European countries, ISO normalisation) are used, but the designations vary for each country.

A four-digit combination or a group of letters indicate the chemical composition. The most common alloying elements are copper, manganese, silicon, magnesium, zinc, nickel and iron. The designation indicating the chemical composition is followed by symbols giving the metallurgical fabrication stage of the alloy.

The main fabrication stages in the classification provided by the Aluminium Association in the USA are : rough stage of fabrication, annealed stage, work-hardened stage, tempered non-stabilised stage and heat treated stage. All these stages are symbolised by letters (F, O, H, W and T), and the main fabrication stages are subdivided even further by the use of numbers and additional letters following the characters of the main fabrication stage.

It is also possible to identify an alloy by parameters indicating strength. The most common mechanical properties then are $\sigma_{0.2}$, the conventional yield limit corresponding to a permanent deformation of 0.2 percent, σ_t, the ultimate tensile strength, and ε_t, elongation at rupture.

2.3 Stress-strain curves

The challenge when dealing with aluminium alloys is that there is an enormous variability in the mechanical properties. The values of the 0.2 percent tensile proof stresses for aluminium alloys suitable for structural applications ranges from 10 N/mm^2 to 500 N/mm^2, and the 0.2 percent tensile proof stresses may vary both with respect to different directions in the material (anisotropy) and be different in tension and compression. Even the same alloy has different characteristics depending on the fabrication process and heat treatment, and the material properties can be drastically altered when the alloy is exposed to welding.

The elastic modulus, on the other hand, seems to be reasonably constant. It is approximately 70000 N/mm^2, but according to Mazzolani (1995) it varies from 68500 to 74500 depending on the different alloys considered. In spite of huge individual variations it is possible to find material laws that describe the stress-strain relationships of the different alloys. On the other hand, they have to be more sophisticated than material laws of mild steels because the continuous behaviour of the σ-ε curve cannot be modelled as an elastic/perfectly plastic material curve.

The stress-strain relationship of aluminium alloys is normally divided into three parts. The first part is linear, and the slope is equal to the elasticity modulus. The elastic portion of the curve goes up to the proportional stress, σ_p, usually taken to correspond to a residual strain of 0.01 percent. The linear part of the curve is followed by a non-linear portion up to a knee and a strain-hardening portion. The sharpness of the knee and slope of the strain-hardening portion differ depending on the different alloys. The stress corresponding to 0.2 percent residual strain is assumed to be the stress beyond which the behaviour of the material is no longer elastic, and $\sigma_{0.2}$ is internationally used in structural computations, with the same meaning as the yield stress in steel.

Excellent mathematical models have been proposed by Baehre (1966), Mazzolani (1972) and Ramberg and Osgood (1943). In this dissertation the Ramberg-Osgood law will be used. The reason for choosing this model is that all parts of the σ-ε-curve can be expressed by one equation only, and despite it's simplicity, the Ramberg-Osgood law shows excellent agreement with experimental values (Mazzolani, 1995, page 59 and following pages).

The Ramberg-Osgood law can be expressed as:

$$\varepsilon = \frac{\sigma}{E} + \varepsilon_0 \left(\frac{\sigma}{\sigma_{\varepsilon_0}} \right)^n \tag{2.1}$$

E is the Young's modulus, $\sigma_{\varepsilon 0}$ the conventional elastic limit and ε_0 the residual strain corresponding to the elastic limit. Normally σ_{ε_0} is set equal to the 0.2 percent tensile proof stress, and Equation 2.1 can be written:

$$\varepsilon = \frac{\sigma}{E} + 0.002 \left(\frac{\sigma}{\sigma_{0.2}} \right)^n \tag{2.2}$$

$$n = \frac{\ln 2}{\ln\left(\frac{\sigma_{0.2}}{\sigma_{0.1}}\right)} \tag{2.3}$$

The higher the value of the exponent, n, is, the sharper the knee of the stress-strain curve, and the slower the slope of the strain-hardening portion of the curve. If the exponent, n, is set equal to infinity, one will have a curve corresponding the linear-elastic/perfect-plastic behaviour, a curve suitable for the behaviour of mild steels.

$\sigma_{0.1}$, the stress corresponding to a residual strain equal to 0.1 percent, or the exponent, n, are normally not provided by the material specifications or in the design rules. Only $\sigma_{0.2}$, the elastic limit, σ_t, the ultimate tensile strength, and ε_t, the elongation at rupture, are given. Based on the value of the 0.2 percent tensile proof stress Steinhardt (1971) has proposed the expression:

$$10n = \sigma_{0.2} \tag{2.4}$$

The reason for choosing this simple expression is that it has been shown by experimental results that there is a connection between the 0.2 percent tensile proof stress and the exponent, n, in the Ramberg-Osgood law. Non-heat-treated alloys have an exponent, n, in the range of 10-20, and heat-treated alloys have an exponent, n, in the range of 20-40. Expressed with other words it might be said that the higher the yield strength of the material is, the sharper the knee and slower the slope in the strain hardening portion of the material stress-strain curve.

Mazzolani (1974) has given a more sophisticated expression taking all the three values in the material specifications into account. Using N, mm as units:

$$n = \frac{\ln 2}{\ln(1 + k\chi)} \tag{2.5}$$

$$\chi = \frac{\sigma_t - \sigma_{0.2}}{10\varepsilon_t}\frac{\sigma_t}{\sigma_{0.2}} \tag{2.6}$$

$$k = 0.028 \tag{2.7}$$

or

$$n = \frac{\ln 2}{\ln\left(1 + 0.0028 \cdot \frac{\sigma_t - \sigma_{0.2}}{10\varepsilon_t} \cdot \frac{\sigma_t}{\sigma_{0.2}}\right)} \tag{2.8}$$

Always using the stress corresponding to 0.2 percent permanent plastic strain has the disadvantage that the elastic part of the strain varies depending on the aluminium alloy considered. As an alternative, one could use the stress corresponding to equal elastic and plastic strain. If the material behaviour is described by the Ramberg-Osgood law (Equation 2.1), the stress giving equal elastic and plastic strain and the corresponding value of the total strain can be written:

$$\sigma_{elpl} = \sigma_{\varepsilon_0}^{\frac{n}{n-1}} \cdot (\varepsilon_0 E)^{\frac{1}{1-n}} \tag{2.9}$$

$$\varepsilon_{elpl} = 2 \cdot \sigma_{\varepsilon_0}^{\frac{n}{n-1}} \cdot \varepsilon_0^{\frac{1}{1-n}} \cdot E^{\frac{n}{1-n}} \tag{2.10}$$

Setting ε_0=0.002 yields:

$$\sigma_{elpl} = \sigma_{0.2}^{\frac{n}{n-1}} \cdot (0.002E)^{\frac{1}{1-n}} \tag{2.11}$$

$$\varepsilon_{elpl} = 2 \cdot \sigma_{0.2}^{\frac{n}{n-1}} \cdot 0.002^{\frac{1}{1-n}} \cdot E^{\frac{n}{1-n}} \tag{2.12}$$

The values of the stresses corresponding to equal elastic and plastic strain will be used for non-dimensioning of material design curves in later chapters. They are believed to be points on the material curves that are in a more similar part of the utilisation of the material.

2.4 Geometrical Imperfections

2.4.1 Out-of-Straightness

Extensive studies have been carried out to determine the post welding shape of welded steel plating in ships (Antoniou et al, 1984, Antoniou, 1980, Carlsen and Czujko, 1979 and 1978, and Kmiecik et al 1995). The most common ways of describing plate deflections is either to measure the largest plate out-of-plane deflection from initial straightness only, or to describe the whole post buckling shape by the use of Fourier analyses.

Carlsen and Czujko (1978) found that the maximum plate out-of-plane deflections plus two times the standard deviations from their measurements performed, could be written as:

$$w_{max} = 0.016b - 0.36t \tag{2.13}$$

The corresponding results found by Antoniou (1980) can be expressed as:

$$w_{max} = 0.014b - 0.32t \tag{2.14}$$

When analysing Fourier components all the authors found that the lowest component (one half wave in both longitudinal and transverse direction) was the dominating one with higher components showing much smaller amplitudes.

Based on these studies Det Norske Veritas has specified the maximum allowable out of plane deflection of stiffened steel plating equal to 0.01b.

The author has not been able to find such systematic studies for post welding distortions of aluminium plates as have been conducted for steel plates. Information of test specimen geometry, however, is available. The post welding shape of aluminium plating in test

specimens will not be equal to the post welding shape of aluminium plating in whole structures, but they may give an indication of what order of magnitude of the post welding plate out-of-plane deflections to be expected.

In the report written by Clarke (1987) on measurements of test panels made by the same building technique as conventional ship builders, he found that the initial imperfection amplitude, w_{max}, varied from 0.0066b to 0.021b. The trend was the same here as for steel plates, slender plates showed larger initial imperfection amplitudes than sturdy plates.

Aalberg et al (1999c) have done imperfection measurements on stiffened aluminium test panels. The plates with their stiffeners on top were extruded and joint by friction stir welding, but the test specimens had no welds at the ends of the plates. Plates with both open L-stiffeners and closed stiffener extrusions were investigated. Plates with open L-stiffeners had a maximum initial deflection of 0.012b (plate thickness 5 mm), and plates with closed stiffener extrusions had a maximum initial deflection of 0.0064b (plate thickness 3 mm).

Moan et al (1999) measured the out-of-flatness for test-specimens where the stiffeners had been welded to the plate. The out-of-flatness was measured as the amplitude of a sine out-of-plane deflection. Typical plate imperfection amplitudes were 2.3 mm. With a plate breadth equal to 200 mm, this corresponds to a out-of-flatness equal to 0.012b.

2.4.2 Variation in Plate Thickness

When aluminium plates are produced, they will have variations in thickness. The plates will have different values of the thickness in different parts of the plates, and the thickness will differ from nominal thickness.

In laboratory tests performed in Norway (Aalberg et al, 2000), measurements on test-specimens showed that the difference in thickness between the thickest and thinnest parts of the plate divided by the thickness of the thinnest part of the plate varied from 1.7 % to 8.6 %. The average value was 5.17 %. The plate with the largest maximum deviation from nominal thickness was 6.40 % thicker than the nominal thickness. The average value of the maximum deviation from nominal thickness was 4.30 %.

All the panels were extruded. For rolled plates, measurements in other laboratory tests (Moan et al, 1999) showed much smaller deviations both regarding the difference between the thickest and thinnest parts of the plate and the maximum deviation from nominal thickness. The difference in thickness between the thickest and thinnest parts of the plate divided by the thickness of the thinnest part of the plate ranged from 0 % to a maximum of 1.0 %, and the average value was as low as 0.37 %. The plate with the largest value of the maximum deviation from nominal thickness had a thickness exceeding the nominal thickness by 2.0 %. The average value of the deviation from nominal thickness was 1.2 %, also this value much smaller than for plates that had been extruded.

The difference between extruded plates and rolled plates are believed to be caused by the fact that the extrusion tools are worn out. Depositions and indentations are created to give inaccuracies. The production methods of rolled plates are more accurate.

Stiffened aluminium panels are made up of several extruded plates with attached stiffener welded together by friction stir welding. If the different aluminium plates making up the panel are produced in different times of the life cycle of the extrusion tool, which is often the case, one will experience greater distinctions than if the plates making up the panels were produced consecutively.

According to Mazzolani (1995) the different national specifications for extruded profiles allow a deviation from nominal thickness equal to 5 percent. This value can reach 10 percent in the case of thin profiles with thickness less than 5 mm.

Other measurements of thickness variations can be found in Clarke and Swan (1985).

2.5 Mechanical Imperfections

2.5.1 Introduction

When aluminium plates are welded, zones with reduced yield strength and residual stresses are created. Close to the welds there will be a zone with reduced yield strength and residual stresses in tension. Further away from the welds there is a corresponding stress field in compression to maintain equilibrium. In a whole structure, that consists of many welded parts, a single component can be exposed to various residual stress fields, but it will only have a reduced yield strength in the part of it that is close to a weld. The residual stress fields are strongly dependent on the sequential order in which the structure has been assembled.

2.5.2 Modelling of Residual Stresses and Soft Zones

2.5.2.1 Patterns of the Heat Affected Zones

The aluminium plates considered in this thesis are located between longitudinal stiffeners and transverse girders.

If the stiffeners on the plates are extruded, the plates will not have welds between the stiffeners and the plates, but the plates with their extruded stiffener on top will be welded together to form a stiffened panel. In most cases these welds will be of the friction-stir type. The friction stir welds can have any location in the plate field between the stiffeners. Normally they are located either in the middle of the plate field or close to one of the stiffeners. The panels made of joined extruded stiffened plates are welded to transverse girders.

As a result of this building technique, extruded plates will have a heat affected zone in the longitudinal direction, and heat affected zones along the two short edges of the plate. Plates that have not been extruded, will be welded to both the longitudinal stiffeners and transverse girders and consequently have heat affected zones along all four edges.

If the friction stir welds of the stiffened extruded plates are located at the position of the stiffeners, extruded plates and conventionally welded plates will have the same pattern of the heat affected zones. In this thesis only extruded plates with friction stir welds located in the middle of the plates are considered.

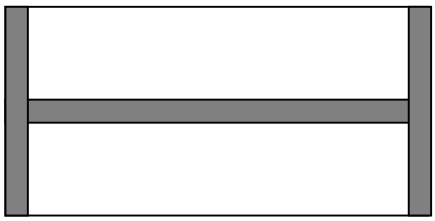

Figure 2.1 : Heat affected zones of an extruded plate (extruded HAZ pattern)

Figure 2.2 : Heat affected zones of a plate that have been conventionally welded, (HAZ along all edges)

The plates in most real structures will have one of the two patterns of heat affected zones given above (Figures 2.1 and 2.2), but other extensions of heat affected zones have also been studied. They are given in Figures 2.3-2.6.

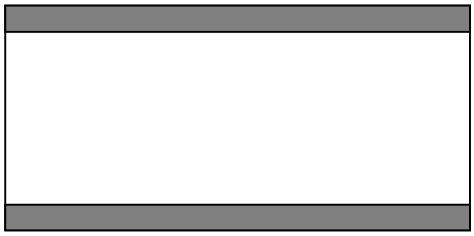

Figure 2.3 : HAZ along long edges

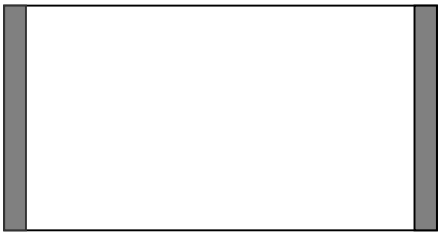

Figure 2.4 : HAZ along short edges

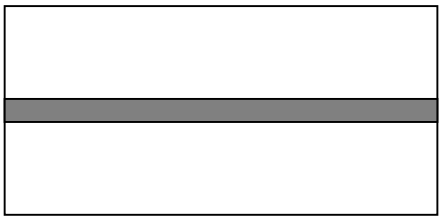

Figure 2.5 : HAZ in the middle, longitudinal direction

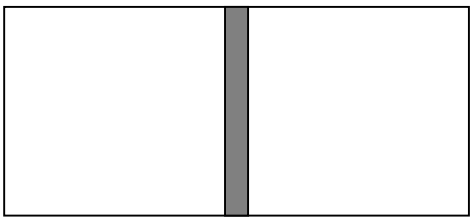

Figure 2.6 : HAZ in the middle, transverse direction

2.5.2.2 Material Behaviour in the Heat Affected Zones

Welding exposes the plates to severe heating. This heating process in most cases ceases the effect of heat treatment and cold working and brings the aluminium alloys back to their annealed state.

The severity of the reduction of material properties due to welding depends on the type of aluminium alloy. Alloys with large increase in strength due to heat treatment and cold working will experience the greatest reduction in material properties, while alloys with properties close to the annealed state will not be affected.

The yield strength, or 0.2 percent tensile proof stress, and the knee-factor, n, in the Ramberg-Osgood law will be reduced in the welding zones (see also Chapter 2.6). The result is a material property in the welded parts of the plates in accordance with an aluminium alloy with lower yield stress. The reduction in material properties is strongest in the regions close to the welds and decreases gradually to reach full strength further away from the welds.

In the zones close to the welds the material will be heated. The surrounding structure prevents the alloy from expanding to such an extent that the material yields plastically. When the temperature decreases after the welding process is finished, the material shrink and gradually re-enter it's elastic capacities. The result is that the material in the welded parts of the structure and close to the welded parts of the structure will be in tension. These tension fields will be balanced by compression stress fields further away from the welding zone.

The zones that in an unloaded condition have stresses in tension or compression, are called residual stress fields. They are dependent on which sequence the structure has been erected, but the zones with reduced material strength will always be in the parts of the structures that have been welded or in the immediate vicinity of the parts of the structure that have been welded.

The extent of the zones with reduced yield strength is dependent on the thickness of the plating. It is also dependent on the welding method used (MIG-welding, TIG-welding, friction stir welding etc.). Other factors that influence the breadth of the heat affected zones are the number of weld passes, the cooling between each weld pass, the distance to neighbouring welds, the distance to the free edges and the number of heath paths.

A very common idealisation (Mazzolani, 1995) is to assume the material properties to be constant in the parts of the structure that is affected by welding. The reduction in 0.2% tensile proof stress, $\sigma_{0.2}$, and knee-factor, n, in the Ramberg-Osgood law are assumed to be of the same order in the whole region. In the parts of the structure not affected by welding, the material properties are assumed to be identical to the parent material.

Following the same approach, the breadth of the zones with residual stresses in tension are assumed to be equal to the breadth of the zones with reduced material properties, and the residual stresses in these parts of the structure are assumed to be uniformly distributed. The corresponding compression fields in the parts of the structure with parent material properties are also assumed to be uniformly distributed. Resulting forces and moments due to the residual stress fields must be equal to zero.

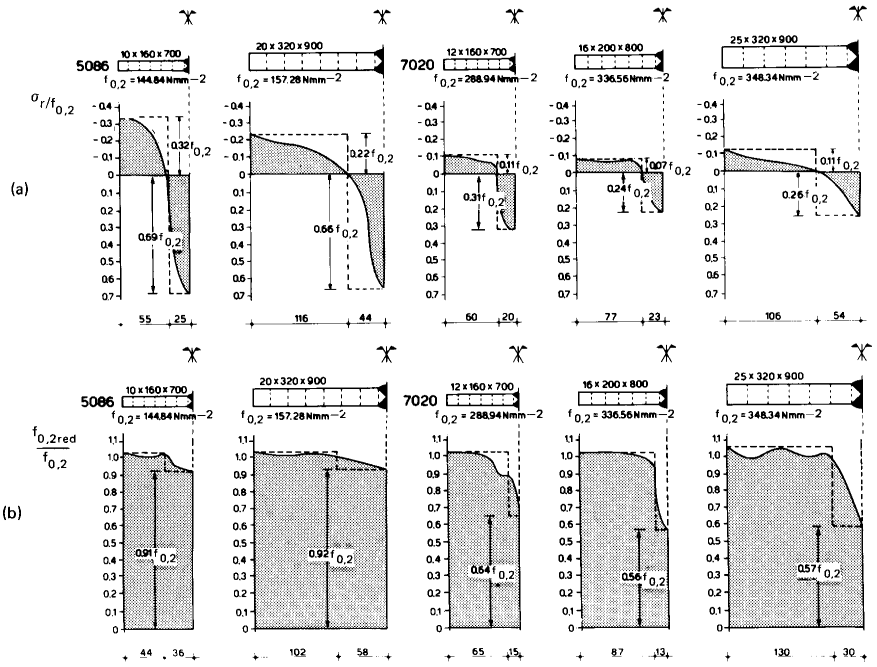

Figure 2.7 : Distribution of residual stresses and reduction of yield strength due to welding in butt-welds. The idealisations of residual stresses and soft zones are also shown (figure taken from Mazzolani, 1995).

The values of the maximum residual stresses in tension varies. A typical interval is between 50 % and 100 % of the 0.2 percent tensile proof stress in the zones with reduced material parameters, and a characteristic value is 75 % percent of the reduced 0.2 percent tensile proof stress (this value was used in most of the analyses performed). The value of the residual stresses in tension can then be written:

$$\sigma_R^+ = 0.75 \cdot \sigma_{0.2}^* = 0.75 \cdot \alpha \cdot \sigma_{0.2} \tag{4.4}$$

Given a plate that have been welded along it's longitudinal edges, the corresponding residual stresses in compression can be found by demanding zero resultant forces.

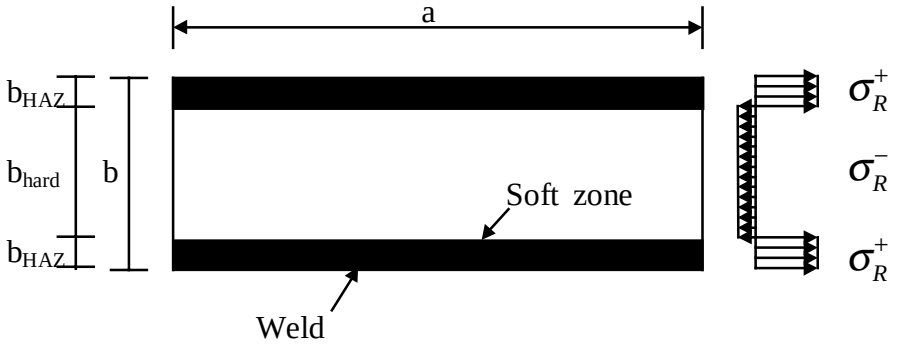

Figure 4.11 : Calculation of residual stress fields

$$\sigma_R^+ \cdot (2b_{HAZ}) + \sigma_R^- \cdot b_{hard} = 0 \tag{4.5}$$

$$b_{hard} = (b - 2b_{HAZ}) \tag{4.6}$$

$$\sigma_R^- = -\frac{\sigma_R^+ \cdot 2b_{HAZ}}{b - 2b_{HAZ}} \tag{4.7}$$

Some of the plates given in Figures 2.1-2.6 do have welds in two perpendicular directions (extruded HAZ pattern and HAZ along all edges). The total residual stress pattern in these plates have been procured by adding two residual stress fields; one residual stress field as if the plates were welded in longitudinal direction only and one residual stress field as if the plates were welded in transverse direction only.

2.5.2.3 Breadth of the Heat Affected Zones

Information of the size (width) of heat affected zones is given in design codes. DNV design codes (Det Norske Veritas Classification AS, 1996) for ships built in aluminium do not specify the breadth of the heat affected zones, only that material yield strength capacity have to be reduced if a part of the structure actually is affected by welding. The same assumptions are made in Lloyd's Register of Shipping (1996). British Standard 8118 (British Standards Institution, 1991) and Eurocode 9 (European Committee for Standardization,1998), on the other hand, specify in detail the breadth of the heat-affected-zones.

Typical breadths of the heat affected zones for plates analysed in this thesis are given in Chapter 4.2.

2.6 Materials Used in the Analyses

Three different alloys, representative for marine structures, have been investigated. The first alloy is 6082-T6 (AlSiMgMn). This is a heat treatable alloy that is solution heat-treated and then artificially aged. The second alloy is 5083-F (AlMg4,5Mn0,7). This is a non heat-treatable alloy in fabricated condition. Alloy number three is alloy 5083-O, with the same alloying elements as 5083-F, but the material is in it's annealed state. The material properties for the different alloys according to Eurocode 9 are given in Table 2.4. The strength values and loss of strength due to welding differ slightly with plate thickness and welding method.

Table 2.4 : Material properties taken from Eurocode 9

Alloy	Minimum 0.2 % tensile proof stress [N/mm^2]	Minimum tensile strength [N/mm^2]	Minimum elongation at failure [%]	Modulus of elasticity [N/mm^2]	Loss of strength due to welding [%]
6082-T6	260	310	6	70000	50
5083-F	175	320	18	70000	0
5083-O	125	275	11	70000	0

The material parameters used in the analyses are not the exact values taken from Table 2.4. They were taken from experimental values in the Ph. D. thesis written by David Shane Mofflin (Mofflin, 1983). The material properties were found from compression rather than tension tests since failure due to buckling is essentially a compression failure. The values presented are true values and not minimum guaranteed values. They represent typical values from a lot of tests performed.

Mofflin found that the material behaviour of the stress-strain relationship for aluminium alloys in compression could be adequately handled by the Ramberg-Osgood law. The same assumptions will be followed in this thesis. The values of the exponent, n, E and $\sigma_{0.2}$ have been experimentally determined in the work done by Mofflin. The material parameters for the different alloys used in the numerical analyses are given in Table 2.5.

Table 2.5 : Material parameters used in the numerical analyses

Alloy	0.2 % tensile proof stress [N/mm^2]	Knee-factor, n, in the Ramberg-Osgood law	Modulus of elasticity [N/mm^2]	Loss of strength due to welding [%]
6082-T6	292	26	70000	50
5083-F	190	15	70000	10
5083-O	91	10	70000	10

When aluminium alloys are welded, the parts of the materials that have been exposed to welding return to their annealed state. Additional strength obtained by either heat treatment or cold working will be lost. As a result the 0.2 percent tensile proof stress of the material will be reduced and the shape of the stress-strain curve will be altered.

In this thesis the reduction of the yield strength will be described by the letter α, the ratio between the reduced 0.2 percent tensile proof stress and the original 0.2 percent tensile proof stress.

$$\sigma_{0.2}^{*} = \alpha \cdot \sigma_{0.2} \tag{2.13}$$

In the Ramberg-Osgood law the shape of the stress-strain curve is given by the exponent, n. According to Equation 2.4 the exponent, n, is proportional to the yield strength of the material, and one might wright:

$$\frac{n^{*}}{n} = \frac{\sigma_{0.2}^{*}}{\sigma_{0.2}} = \alpha \tag{2.14}$$

or

$$n^{*} = \alpha \cdot n \tag{2.15}$$

This approach will be used in the numerical analyses. For alloy 6082-T6 Mofflin found that in the heat affected zones the yield strength was reduced from 292 MPa to 146 MPa, and the exponent, n, decreased from 26 to 12. This is in very close agreement with equation 2.15 which predicts a value of the exponent, n, equal to 13.

Chapter 3

Simple Code Formulations for Buckling and Ultimate Collapse

3.1 Linear Elastic Buckling of Rectangular Plates

There are two methods for determining first buckle of linear elastic plates, either direct solutions of the differential equation for plates or by energy method. This has to be done for a huge amount of load conditions and support conditions. Excellent books are written on the subject; see for instance Timoshenko and Gere (1961).

The detailed solutions of the various load and support conditions will not be derived in this thesis but some of the results will be reproduced.

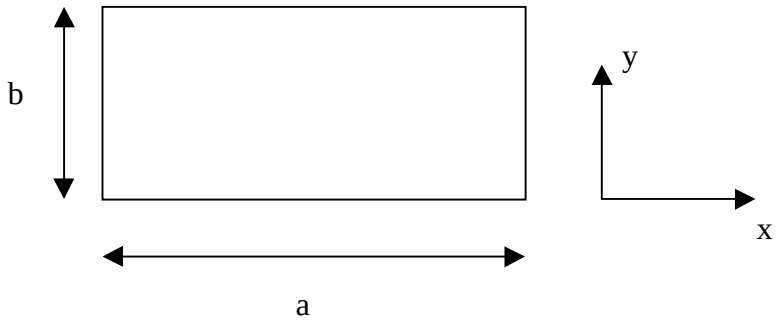

Figure 3.1 : Plate dimensions used in the formulas

3.1.1 Axial Buckling Capacity of Simply Supported Rectangular Plates

The buckling capacity of a plate that is simply supported along all edges and exposed to axial uniform compression, can be written:

$$\sigma_{Ex} = C_1 \frac{\pi^2 E}{12\left(1-\nu^2\right)}\left(\frac{t}{b}\right)^2 \tag{3.1}$$

For a plate with aspect ratio, a/b, greater than unity, the coefficient C_1 will experience a minimum value every time the aspect ratio is an integer. This value is equal to C_1=4. For intermediate values of the aspect ratio, a/b, the coefficient, C_1, will be higher, but never greater than 4.5, and the additional strength for intermediate values decreases as the aspect ratio, a/b, increases.

3.1.2 Transverse Buckling Capacity of Simply Supported Rectangular Plates

A plate that is exposed to transverse uniform compression and is simply supported along all edges will have a buckling capacity given by:

$$\sigma_{Ey} = C_2 \frac{\pi^2 E}{12(1-\nu^2)}\left(\frac{t}{b}\right)^2 \tag{3.2}$$

The aspect ratio, a/b, is assumed to be greater than unity, and for a plate with aspect ratio, a/b, greater than unity, the coefficient C_2 can be expressed as:

$$C_2 = \left[1+\left(\frac{b}{a}\right)^2\right]^2 \tag{3.3}$$

3.1.3 Eigenmodes of Simply Supported Rectangular Plates

For all values of the aspect ratio, a/b, there is a corresponding buckling shape (or eigenmode) that gives the lowest buckling capacity. These eigenmodes can be written as:

$$w = w_0 \cdot \sin\left(\frac{m\pi x}{a}\right)\cdot \sin\left(\frac{n\pi y}{b}\right) \tag{3.4}$$

Transversally loaded plates will buckle with one half wave in both x- and y-direction, m=n=1. Axially loaded plates will also have one half wave in the transverse direction, n=1, but the number of half waves in longitudinal direction will be equal to the aspect ratio, a/b; if the aspect ratio is an integer value. If the aspect ratio, a/b, is not an integer value, the number of half waves will be equal to either the integer value below or above the value of the aspect ratio, whichever gives the lowest buckling capacity.

This is the reason why the coefficient C_1 exceeds the value of 4 for non-integer values of the aspect ratio, a/b. The plate cannot buckle into an integer number of completely square buckles. The buckles get a rectangular shape with increased energy absorption and increased buckling capacity as the result.

3.1.4 Shear Buckling Capacity of Simply Supported Rectangular Plates

When using the energy method, the plate deflections are expressed by a double Fourier-series, and many terms have to be included to achieve acceptable accuracy. An expression giving good accuracy with the exact solution for a simply supported plate exposed to pure shear load is given in Timoshenko and Gere (1961).

$$\tau_E = C_3 \frac{\pi^2 E}{12(1-\nu^2)}\left(\frac{t}{b}\right)^2 \tag{3.5}$$

$$C_3 = 5.35 + 4\left(\frac{b}{a}\right)^2 \tag{3.6}$$

Table 3.1 : Comparison of exact and approximate solution for simply supported plate exposed to pure shear load

a/b	1	1.2	1.4	1.5	1.6	1.8	2.0	2.5	3	4
C_3, exact	9.34	8.0	7.3	7.1	7	6.8	6.6	6.1	5.9	5.7
C_3, Eq. 3.6	9.35	8.1	7.4	7.1	6.9	6.6	6.4	6.0	5.8	5.6

An approximate equation for the eigenmode of an infinitely long plate exposed to pure shear load is also given.

$$w = w_0 \cdot \sin\frac{\pi y}{b} \cdot \sin\frac{\pi}{s}(x - fy) \tag{3.7}$$

$$s = b\sqrt{1 + f^2} \tag{3.8}$$

$$f = \frac{1}{\sqrt{2}} \tag{3.9}$$

The exact solutions will vary with different aspect ratios, a/b, but Equation 3.7 describes a typical shear buckling shape. The eigenmode consists of one half wave in the shortest direction of the plate and cantilevered half waves along the longest direction of the plate.

3.1.5 Buckling of Simply Supported Rectangular Plates Compressed in Two Perpendicular Diretions

The calculation of the buckling capacity of a rectangular plate that is submitted to the action of uniformly distributed compressive stresses in two perpendicular directions is straigth forward. The deflection of the plate is described by a double Fourier-series.

$$w_{mn} = a_{mn} \sin\frac{m\pi x}{a} \sin\frac{n\pi y}{b} \tag{3.10}$$

Only one term in the double Fourier-series should be considered in calculating the critical values of the stresses. For a chosen term in the double Fourier-series the corresponding biaxial interaction equation can be written:

$$\sigma_x m^2 + \sigma_y n^2 \frac{a^2}{b^2} = \frac{\pi^2 E}{12(1-\nu^2)}\left(\frac{t}{a}\right)^2\left(m^2 + n^2\frac{a^2}{b^2}\right)^2 \tag{3.11}$$

As can be seen there is a linear connection between the stresses in longitudinal and transverse direction. The integer pair (m,n) corresponding to the lowest capacities has to be chosen. The choice of integer pair (m,n) is dependent on loading condition and aspect ratio a/b. It can be useful to express the stresses in the transverse direction as a fraction of the stresses in the longitudinal direction.

$$\sigma_y = k\sigma_x \tag{3.12}$$

Equation 3.11 can then be rewritten:

$$\sigma_x = \frac{\pi^2 E}{12(1-\nu^2)}\left(\frac{t}{a}\right)^2 \frac{\left(m^2 + n^2\frac{a^2}{b^2}\right)^2}{\left(m^2 + kn^2\frac{a^2}{b^2}\right)} \tag{3.13}$$

Equation 3.11 can also be used if one of the stress components is in tension

3.1.6 Buckling of Simply Supported Rectangular Plates Exposed to Axial Compression in Combination with Shear Loads

For a plate exposed to uniformly distributed axial stresses combined with uniformly distributed shear stresses Bathdorf and Stein (1947) has produced an interaction curve.

The ratio between the axial stresses and the critical value of the axial stresses when they act alone is written:

$$R_x = \frac{\sigma_{mx}}{\sigma_{mux}} \tag{3.15}$$

An equivalent expression for the shearing stresses is:

$$R_\tau = \frac{\tau_m}{\tau_{mu}} \tag{3.16}$$

The interaction curve is very simple and takes the form:

$$R_x + R_\tau^2 = 1 \tag{3.17}$$

This curve can also be used for tensile axial stresses.

3.2 Non-Linear Solution Methods

The formulas given in Chapter 3.1 only predict linear initial buckling loads of plates. The plates are assumed to behave linearly with stresses uniformly distributed along the sides of the plate. No consideration is made neither of yielding nor additional strength of the plate due to geometrical changes.

Some of the factors influencing ultimate strength of plates are type of loading, edge restraint, aspect ratio, initial distortions, heat affected zones and plate slenderness.

In this chapter selected concepts of treating the ultimate strength of plates will be elaborated on. The theories and their application is mainly from the calculation methods developed for steel plates.

3.2.1 Johnson-Ostenfeld Correction

This is a simple correction that takes elasto-plastic behaviour into account (Bleich, 1952). The plate is assumed to have a capacity equal to the linear elastic buckling capacity if the linear elastic buckling stress is less than half the yield stress of the material. For higher values of the linear elastic buckling load, the buckling capacity is modified by a parabolic equation.

$$\sigma_{cr} = \sigma_E \qquad \sigma_E \le \frac{\sigma_Y}{2} \tag{3.17}$$

$$\sigma_{cr} = \sigma_Y\left(1 - \frac{\sigma_Y}{4\sigma_E}\right) \qquad \sigma_E > \frac{\sigma_Y}{2} \tag{3.18}$$

It is convenient to express the Johnson-Ostenfeld formulas in terms of normalised slenderness. The normalised slenderness is defined as:

$$\bar{\lambda} = \sqrt{\frac{\sigma_Y}{\sigma_E}} \tag{3.19}$$

The Johnson-Ostenfeld correction then takes the form:

$$\frac{\sigma_{cr}}{\sigma_Y} = 1 - \frac{1}{4}\bar{\lambda}^2 \qquad \bar{\lambda} \le \sqrt{2} \tag{3.20}$$

$$\frac{\sigma_{cr}}{\sigma_Y} = \frac{1}{\bar{\lambda}^2} \qquad \bar{\lambda} > \sqrt{2} \tag{3.21}$$

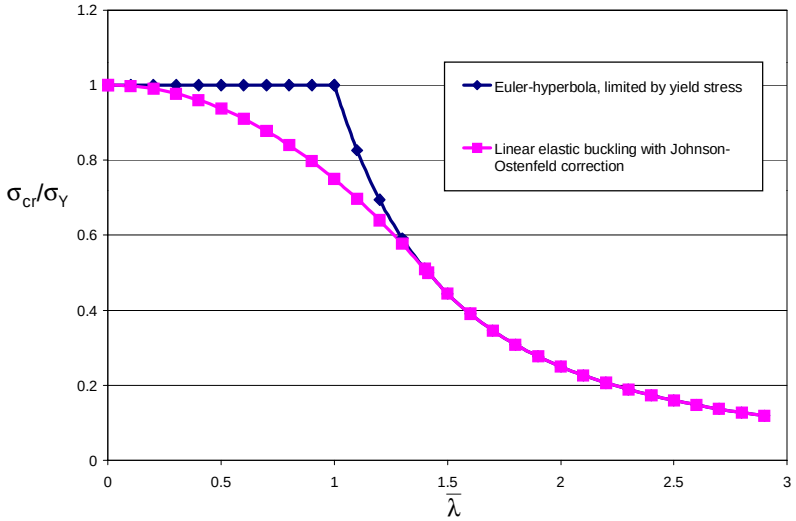

Figure 3.2 : Linear elastic buckling with Johnson-Ostenfeld correction

The Johnson-Ostenfeld correction is commonly used, for instance in the design rules by Det Norske Veritas (1996) and Lloyd's (1996). The effect of hardening beyond proportional limit is not taken into account if this approach is utilised.

Plates are often normalised with an other slenderness parameter, designated β.

$$\beta = \frac{b}{t}\sqrt{\frac{\sigma_Y}{E}} \tag{3.22}$$

The relation between, β, and the reduced slenderness, $\bar{\lambda}$, is:

$$\beta = \bar{\lambda}\sqrt{\frac{\pi^2 C}{12\left(1-\nu^2\right)}} \tag{3.23}$$

The use of Equation 3.23 presupposes that the buckling capacity of the plate can be expressed by the equation:

$$\sigma_E = C\ \frac{\pi^2 E}{12\left(1-\nu^2\right)}\left(\frac{t}{b}\right)^2 \tag{3.24}$$

Setting C=4 and ν=0.3 yields:

$$\bar{\lambda} = \frac{\beta}{1.9014} \tag{3.25}$$

3.2.2 Effective Width Concept

When plates are axially loaded beyond proportional limit, the stresses along the plates will no longer be uniformly distributed. The centre of the plate starts to buckle and loses most of it's load carrying capacity. The load carrying capacity in the middle of the plate does not go to zero, but it will reach a capacity almost identical to a plate strip.

The edges of the plate are prevented from lateral displacement and the stresses along the edges of the plate increases until they reach the yield stress. The breadth of the zone with yield stresses and stresses in the range of the yield stress vary with the slenderness of the plate. The more sturdy the plate is, the larger the extension of the zone. The stresses then gradually decays and reach the plate strip capacity in the middle of the plate.

Transversally loaded plates show the same kind of behaviour, but the middle part of the plate, with stresses almost identical to a plate strip, is much wider. The total capacity of the plate can be regarded as the sum of an axially loaded plate, with the same breadth as the transversally loaded plate, plus the capacity of a plate strip, with a length equal to the difference between the total length of the plate and the breadth of the plate.

$$\frac{\sigma_{muy}}{\sigma_Y} = \frac{b}{a}\left(\frac{\sigma_{muy}}{\sigma_Y}\right)_{\substack{\text{square}\\ \text{plate}}} + \left(1-\frac{b}{a}\right)\left(\frac{\sigma_{muy}}{\sigma_Y}\right)_{\substack{plate\\ strip}} \tag{3.26}$$

The simplest way of describing the effective width concept for an axially loaded plate is to assume that the plate has axial stresses equal to the yield stress in a zone of breadth $b_{eff}/2$ at the longitudinal edges of the plate. In the middle of the plate the axial stresses are assumed to be zero. The ultimate axial buckling capacity then becomes:

$$\frac{\sigma_{mux}}{\sigma_Y} = \frac{b_{eff}}{b} \tag{3.27}$$

Several proposals for equations describing the effective breadth of plates have been issued. The equations cover different values of initial distortions, residual stresses and boundary conditions.

One equation proposed by Faulkner (1975) for steel plates takes the form:

$$\frac{b_{eff}}{b} = 1 \qquad \beta < 1 \tag{3.28}$$

$$\frac{b_{eff}}{b} = \frac{2}{\beta} - \frac{1}{\beta^2} \qquad \beta \geq 1 \tag{3.29}$$

This equation accounts for initial deflections in the order of $w_0/t \sim b^2/25$, but not for residual stresses. The edges of the plate are prevented from lateral displacement and the edges are constrained to remain straight. Det Norske Veritas (Valsgård, 1980) has modified this equation to account for residual stresses, and the equation suitable for design purposes of steel plates takes the form:

$$\frac{b_{eff}}{b} = 1 \qquad \beta < 1 \tag{3.30}$$

$$\frac{b_{eff}}{b} = \frac{1.8}{\beta} - \frac{0.8}{\beta^2} \qquad \beta \geq 1 \tag{3.31}$$

Soares (1988) has given an even more sophisticated modification of the Faulkner's formula, accounting for different values of residual stresses, different values of initial distortions, and different boundary conditions. It is very compounded. The main equation can be found on page 308 of the reference, with compounding equations on pages 289-290.

For transversally loaded plates Faulkner has proposed an equivalent curve as to the axially loaded case.

$$\frac{a_{eff}}{a} = \frac{\sigma_{muy}}{\sigma_Y} = \frac{0.9}{\beta^2} + \frac{1.9}{\omega\beta}\left(1-\frac{0.9}{\beta^2}\right) \tag{3.32}$$

$$\omega = \frac{a}{b} \tag{3.33}$$

A new design formula was proposed by Det Norske Veritas (Valsgård, 1980):

$$\frac{a_{eff}}{a} = \frac{b}{a}\left(\frac{b_{eff}}{b}\right) + 0.08 \cdot \left(1 - \frac{b}{a}\right)\left(1 + \frac{1}{\beta^2}\right)^2 \tag{3.34}$$

where b_{eff}/b is given by Equations 3.28-3.29.

The equation given by Valsgård has been additionally modified by Soares and Gordo (1996a):

$$\frac{a_{eff}}{a} = \left[\frac{b}{a}\left(\frac{b_{eff}}{b}\right) + 0.08 \cdot \left(1 - \frac{b}{a}\right)\left(1 + \frac{1}{\beta^2}\right)^2\right] \cdot \left(0.589 + 0.130\frac{a}{b} + 0.252\beta - 0.069\beta\frac{a}{b}\right) \tag{3.35}$$

3.2.3 Biaxial Buckling

When a plate is subjected to two orthogonal compressive stresses, one pair of loads will be acting along the short edges of the plate and the other pair of loads will be acting along the long edges of the plate.

When dealing with biaxial interaction, it is convenient to express the capacities in the different directions as a ratio between the capacities for a given biaxial loading condition and the uniaxial buckling capacities.

$$R_x = \frac{\sigma_{mx}}{\sigma_{mux}} \tag{3.36}$$

$$R_y = \frac{\sigma_{my}}{\sigma_{muy}} \tag{3.37}$$

The collapse phenomena is a combination of yielding and buckling. The nature of the interaction depends mainly on the plate slenderness and aspect ratio. For very slender plates, independently of the aspect ratio, a/b, the interaction will be essentially elastic and tend toward linear interaction.

$$R_x + R_y = 1 \tag{3.38}$$

Very compact or sturdy plates ($\beta < 2/3$, Hughes, 1988) are, independently of the aspect ratio a/b, dominated by yielding and will tend towards the Hencky-von Mises ellipse.

$$R_x^2 - R_x R_y + R_y^2 = 1 \tag{3.39}$$

For intermediate values of the slenderness, β, the interaction mechanisms are very complicated. Collapse begins with elastic buckling, leading to loss of effectiveness of the middle

portion of the plate. The load carrying portions of the plate then turn towards the sides of the plate forming two effective widths in each direction. Collapse ultimately occurs when one pair of plate edges reaches a yield criterion.

Square plates have the simplest and strongest interaction. This is due to the symmetric nature of the interaction. The plate has no weak side; uniaxial ultimate buckling capacity is the same in both directions. The preferred collapse mode is also the same no matter what loading condition that is considered.

The interaction curves are symmetrical with the Hencky-von Mises limiting the interaction for sturdy plates and linear interaction as the boundary curve for very slender plates. A weighted combination of the two boundary equations have shown to be in good accordance with large deflection numerical analyses. The following interaction curve was proposed by Frieze, Dowling and Hobbs (Dowling, Harding and Frieze, 1976).

$$R_x^2 - R_x R_y + R_y^2 + \left(\beta - \frac{\frac{4}{9}}{\beta} \right) \left(R_x + R_y - 1 \right) = 1 \qquad \beta \geq \frac{2}{3} \tag{3.40}$$

Valsgård (1980) has proposed a similar interaction formula for square plates:

$$R_x^2 - \left(3.2 e^{-0.35\beta} - 2 \right) R_x R_y + R_y^2 = 1 \tag{3.41}$$

If the plates become rectangular, the plates will have one strong loading direction and one weak loading direction with a higher uniaxial buckling capacity in the longitudinal direction than in the transverse direction.

A given magnitude of the transverse stress ratio, R_y, will correspond to a lower and lower value of the transverse mean stress the higher the aspect ratio, a/b, becomes. Since the longitudinal buckling capacity is independent of the aspect ratio, a/b, the longitudinal strength will be less and less influenced by the transverse stress, simply due to the fact that the transverse stress is lower for a plate with a high aspect ratio, a/b, than it is for a plate with a small value of the aspect ratio, a/b.

Consequently the longitudinal strength ratio becomes higher and higher for a plate with the same transverse strength ratio the larger the aspect ratio, a/b, becomes. This effect is more distinct for plates of moderate slenderness because very sturdy plates are limited by the Hencky-von Mises ellipse and very slender plates are limited by linear interaction no matter the value of the aspect ratio, a/b.

Soares and Gordo (1996b) have given interaction formulas for biaxially loaded plates with different aspect ratios. The formulas handle different values of residual stresses and initial deflections.

3.2.4 Ultimate Strength under Shear

The ultimate capacity of plates exposed to shear loads have many similarities with axially loaded plates. Very sturdy plates will collapse by pure yielding. Very slender plates will first experience instability by elastic buckling. After the buckling has occurred, a tension field in one of the two diagonal direction is created. This tension field can carry further loads until yielding occurs, and collapse follows.

In plates that have an intermediate slenderness the initial buckling becomes inelastic and less distinct, but the tension field mechanism still occurs.

3.2.5 Plastic Correction for Multiple Loading Conditions

This is a very simple correction, only taking account of the yielding effect. All other effects are disregarded. This correction is utilised on several occasions in the DNV design rules for steel (1995).

The expression for the equivalent stress or Mises stress is:

$$\sigma_j^2 = \sigma_x^2 + \sigma_y^2 - \sigma_x \sigma_y + 3\tau^2 \tag{3.42}$$

Yielding occurs when the equivalent stress is equal to the yield stress.

$$\frac{\sigma_j^2}{\sigma_Y^2} = \frac{\sigma_x^2}{\sigma_Y^2} + \frac{\sigma_y^2}{\sigma_Y^2} - \frac{\sigma_x \sigma_y}{\sigma_Y^2} + \frac{3\tau^2}{\sigma_Y^2} = 1 \tag{3.43}$$

Equation 3.41 can be solved with respect to the longitudinal stress.

$$\frac{\sigma_x}{\sigma_Y} = \frac{1}{2}\left\{\sqrt{4 - 3\left(\frac{\sigma_y}{\sigma_Y}\right)^2 - 12\left(\frac{\tau}{\sigma_Y}\right)^2} - \left(\frac{\sigma_y}{\sigma_Y}\right)\right\} \tag{3.44}$$

If a plate is biaxially loaded with a combination of longitudinal stresses and shearing stresses the reduction in axial capacity due to shearing stresses can be written:

$$\frac{\sigma_x}{\sigma_y} = \sqrt{1 - 3\left(\frac{\tau}{\sigma_Y}\right)^2} \tag{3.45}$$

The corresponding expression for the reduction in axial capacity because of transverse stresses in tension is:

$$\frac{\sigma_x}{\sigma_Y} = \frac{1}{2}\left\{\sqrt{4 - 3\left(\frac{\sigma_y}{\sigma_Y}\right)^2} - \left(\frac{\sigma_y}{\sigma_Y}\right)\right\} \tag{3.46}$$

Chapter 4

Finite Element Models

4.1 Non-Linear Finite Element Program ABAQUS

All the numerical simulations in this doctoral thesis have been done by the help of the non-linear finite element program ABAQUS. This is a versatile program package owned by Hibbitt, Karlsson & Sorensen, Inc. (ABAQUS, 1998). ABAQUS covers almost every field where the finite element method is applicable. This dissertation will only deal with the static stress/displacement analysis part of the program package. It is not possible or desirable to cover every aspect of the finite element modelling and simulation, but selected topics will be elaborated on in the following sections.

ABAQUS is well suited to simulate the collapse behaviour of both stiffened and unstiffened aluminium plates. Documentation where ABAQUS has been calibrated against laboratory test with test specimens made of aluminium alloys can be found in Hopperstad and Langseth (1994), Hopperstad et al (1997), Kristensen (1997), Zha and Moan (2001a and 2001b) and Aalberg et al (1999a, 1999b and 1999c).

4.2 Plates Analysed

All plates analysed had a breadth equal to b=300 mm, but the length of the plates was varied to cover aspect ratios, a/b, equal to 1, 2, 3 and 5. The corresponding plate lengths, a, become 300 mm, 600 mm, 900 mm and 1500 mm

The thickness of the plates analysed is given in Table 4.1. The thickness of the plates was varied to cover slenderness ratios ranging from β=1.0 - 5.0. These values of the slenderness, β, are believed to cover most of the slenderness range of practical interest.

Table 4.1 : The thickness of the plates analysed

β [-]	Thickness alloy 6082-T6 [mm]	Thickness alloy 5083-F [mm]	Thickness alloy 5083-O [mm]
1.0	19.37	15.63	10.82
1.5	12.92	10.42	7.21
2.0	9.69	7.81	5.41
2.5	7.75	6.25	4.33
3.0	6.46	5.21	3.61
3.5	5.54	4.47	3.09
4.0	4.84	3.91	2.70
4.5	4.31	3.47	2.40
5.0	3.88	3.13	2.16

Det Norske Veritas has provided the author with approximately 30 drawings of stiffened aluminium plate designs. Due to confidentiality design details cannot be revealed, but the

slenderness of the plates varied from β=1.10 to β=4.78. Most of the plates in panels with closed box stiffeners had a slenderness in the interval β=1.1-1.6. Most of the plates with open stiffeners had a slenderness in the interval β=3.0-3.7.

The breadth of the heat affected zones in most of the analyses was set equal to 25 mm, but in Chapter 5 parametric studies are performed where the breadth of the heat affected zones are altered. Table 4.2 gives the breadth of the heat affected zones according to British Standard 8118 and Eurocode 9. The materials have been assumed to be at a sufficiently low temperature (60°C or lower) at the start of the deposition of every weld pass and the materials have been assumed to have at least two valid heat paths. The values taken from Eurocode 9 are for MIG welds. For a TIG weld the extent of the HAZ is greater because the heat input is greater than for a MIG weld. According to Eurocode 9 the extent of HAZ is never less than 30 mm for TIG welds.

Table 4.2 : Extent of the heat affected zones according to British Standard 8118/Eurocode 9

Plate slenderness [-]	Extent of HAZ 6082-T6 [mm]	Extent of HAZ 5083-F [mm]	Extent of HAZ 5083-0 [mm]
1.0	26.46/35	25.21/35	23.61/30
1.5	24.31/35	23.47/30	21.63/30
2.0	23.23/30	22.60/30	16.23/20
2.5	22.58/30	18.75/30	12.99/20
3.0	19.38/30	15.63/20	10.83/20
3.5	16.62/20	13.41/20	9.27/20
4.0	14.52/20	11.73/20	8.10/20
4.5	12.93/20	10.41/20	7.20/20
5.0	11.64/20	9.39/20	6.48/20

4.3 Element Models

Three different element models for plates with aspect ratio ω=a/b=3 have been utilised. The most frequently used element model had a 72 by 24 mesh. All elements had the same length and breadth, 12.5 mm. The elements used were quadrilateral four noded stress/displacement thick shell elements with reduced integration of type S4R (ABAQUS notation, see ABAQUS, 1998). Element S4R has the advantage to account for finite membrane strains and it will allow for change in thickness. They are, therefore, suitable for large strain analyses. Large strains occurred locally in many of the numerical analyses performed.

Table 4.3 : Element models used in the analyses

Mesh number	Aspect ratio a/b	Plate length [mm]	Plate width [mm]	Mesh	Number of elements	Element length= element width [mm]
1	1	300	300	24 x 24	576	12.5
2	2	600	300	48 x 24	1152	12.5
3	3	900	300	72 x 24	1728	12.5
4	3	900	300	144 x 48	6912	6.25
5	3	900	300	288 x 96	27648	3.125
6	5	1500	300	120 x 24	2880	12.5

For analyses involving shear stresses and axial compression in combination with shear stresses a finer mesh was used. It had a 144 by 48 mesh with element length and breadth equal to 6.25 mm. The element type was the same, S4R. This element mesh was also used for convergence analyses.

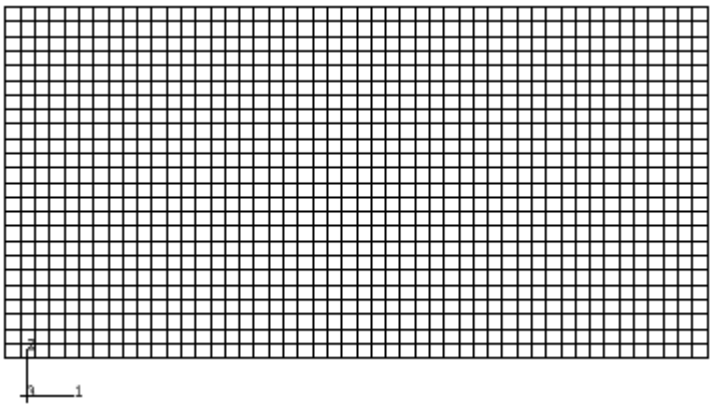

Figure 4.1 : Element mesh no. 2, aspect ratio a/b=2, 48 by 24 elements, 1225 nodes

To verify the accuracy of the element models a very refined element model was developed and used for convergence analyses only. It consisted of a 288 by 96 mesh with the only used element type, S4R. Element length and breadth was 3.125 mm.

For plates with aspect ratio a/b=1,2 and 5 only one element size was utilised, elements with length and breadth equal to 12.5 mm. The element size is identical to the element size of the 72 by 24 element mesh for plates with aspect ratio, a/b=3.

4.4 Boundary Conditions

The boundary conditions for the plates analysed are referred to as the restrictions given to the nodes along the edges of the plates. The edges are given in-plane boundary conditions and bending boundary conditions.

Table 4.4 : Boundary conditions for plates

In-plane boundary conditions	**Bending boundary conditions**
Free edges	Simply supported edges
Straight edges	Clamped edges
Fixed edges	

In-plane boundary conditions describe how the nodes along the edges of the plate can move in their own plane (x-y-plane). The nodes can either be free, straight or fixed. Nodes that are free have no restrictions as to moving in their own plane. Straight nodes can move in their own plane, but all the nodes along the edge of the plate have to stay on a straight line. This is done by the help of the *EQUATION-option in ABAQUS. Nodes that are fixed cannot move at all in the directions in which they are fixed.

The bending boundary conditions of the plate edges describe the capability of the plate edges to transfer bending moments. The bending boundary conditions are referred to as simply supported or clamped . A simply supported edge cannot transfer bending moments and has no restrictions as to rotating around an axis parallel to the edge. A clamped edge is capable of transferring bending moments and is prevented from rotating around an axis parallel to the edge.

Most of the plates analysed had straight, simply supported edges. The reason for choosing the edges to remain straight is that the plates are located between longitudinal stiffeners and transverse girders. At the other side of the stiffeners and girders there will be other plates. Keeping the edges straight is necessary to make sure that the structure stays in one piece. If the nodes were not on a straight line, compatibility will no longer be satisfied.

Keeping the edges straight may be a reasonable assumption for a plate in the middle of a stiffened panel, but closer to the end of the panel the plate will not have the benefit of neighbouring plates keeping it's edges straight. Completely straight edges is an idealised non-conservative condition with completely free edges as the other extremity.

The assumption that the plates are simply supported is believed to be conservative. There will always be some kind of fixation from adjacent structural parts, such as stiffeners, girders and other plates. The degree of fixation will vary with the location within the ship, but the plates will never be completely clamped, which is the other extremity.

4.5 Initial Deflection Patterns Chosen in the Analyses

The problem with choosing initial deflection patterns is divided into two parts, finding the right initial deflection shape and using the right initial deflection amplitude. As have been elaborated on in Chapter 2.4, extensive studies on post welding shapes of aluminium plates have not been conducted.

In most of the analyses performed, the maximum value of the plate out of plane deflection, w_{max}, have been set equal to 0.005b. This is half the value of the tolerance limit in the design rules for steel plates provided by Det Norske Veritas (DNV, 1995). Comparing with the maximum out-of-plane deflections found on the test specimens mentioned in Chapter 2.4, restricting the plate out-of-plane deflection to 0.005b will be non-conservative for most of the plates. On the other hand, there are substantial uncertainty connected with the value of the initial deflection amplitudes in real structures. The initial deflections seem to vary depending on plate dimensions, welding methods, stiffener and girder geometry and the alloy and building methods chosen.

To overcome some of the problems connected with finding the right initial deflection amplitudes, a sensitivity study has been performed in Chapter 8. The initial deflection amplitudes have been systematically varied. As more information become available, the proposed design curves can be adjusted if the initial deflection amplitudes show much larger amplitudes than 0.005b, and the slenderness of the plates considered have such values that the ultimate collapse strengths of the plates are sensitive to the size of the initial deflection amplitudes.

Plates exposed to pure axial compression and pure transverse compression were given the linear elastic eigenmodes as their initial deflection patterns. The only exceptions are found in Chapter 8.3 where a sensitivity study of ultimate strength of plates exposed to different initial deflection patterns is performed. The reason for choosing these eigenmodes was that they were believed to give low values of the ultimate capacity of the plates.

The linear eigenmode of plates exposed to pure transverse compression is very similar to the post buckling shape of a plate in a welded aluminium panel. The Fourier component with one half wave in both longitudinal and transverse direction is dominating, and this Fourier component is identical to the linear elastic eigenmode for transversally loaded plates. Axially loaded plates, on the other hand, have linear elastic eigenmodes different from the post welding shape of aluminium plates. The Fourier component corresponding to the linear elastic eigenmode only contributes for about 30 percent of the total initial deflection amplitudes of aluminium plates in stiffened aluminium panels.

The challenge with biaxial analyses is that the post buckling patterns change upon loading condition. The loading changes from pure axial loading, with the axial post buckling pattern, to pure transverse loading, with the transverse post buckling pattern. The question was what happened for intermediate loading conditions.

Observations from preliminary analyses performed, showed that the transverse post buckling shape (one half wave in both longitudinal and transverse direction) was preferred, except for plates exposed to pure axial loading. Even for the smallest value of the proportionality constant, k (see Chapter 4.7.4), the transverse post buckling shape was preferred.

The initial deflection patterns chosen were a combination of several eigenmodes, allowing the plates to develop preferred post buckling shapes. The initial deflection patterns chosen were actually very similar to the shape in welded structures with the largest contribution from the Fourier component with one half wave in both longitudinal and transverse direction, and higher order components having much smaller amplitudes.

The axial linear eigenmode was also chosen for plates exposed to pure shear loading and axial compression in combination with shear loading. The reason for this choice is in two parts; post welding shapes similar to shear eigenmodes are not believed to be present in welded aluminium plates, and a plate exposed to shear loading with initial deflection patterns corresponding to the axial linear eigenmode and the shear linear eigenmode, respectively, are not believed to have very different collapse capacities. The cantilevering of the collapse mode easily develops even if the linear axial eigenmode is chosen as the initial deflection pattern.

In Chapters 6 and 7 analyses with altered boundary conditions have been performed, but the initial deflection patterns were not changed.

The initial deflection patterns for all values of the aspect ratio ω=a/b and all types of load conditions can be written:

$$w(x,y) = w_i\left[p_1 \sin\left(\frac{\pi x}{a}\right) + p_2 \sin\left(\frac{2\pi x}{a}\right) + p_3 \sin\left(\frac{3\pi x}{a}\right) + p_5 \sin\left(\frac{5\pi x}{a}\right)\right] \cdot \sin\left(\frac{\pi y}{b}\right) \quad (4.1)$$

Table 4.5 : Initial imperfection parameters in Equation 4.1 for rectangular plates

Type of loading	**w_i [mm]**	**p_1**	**p_2**	**p_3**	**p_5**
Axial compression					
ω=a/b=1	1.5	1	0	0	0
ω=a/b=2	1.5	0	1	0	0
ω=a/b=3	1.5	0	0	1	0
ω=a/b=5	1.5	0	0	0	1
Transverse compression					
ω=a/b=1	1.5	1	0	0	0
ω=a/b=2	1.5	1	0	0	0
ω=a/b=3	1.5	1	0	0	0
ω=a/b=5	1.5	1	0	0	0
Biaxial compression					
ω=a/b=1	1.5	1	0	0	0
ω=a/b=2	$\frac{2}{3}\sqrt{3}=1.1547$	1	0.5	0	0
ω=a/b=3	1.1338	1	0.25	0.5	0
ω=a/b=5	1.0	1	0	0	0.5
Pure shear load					
ω=a/b=3	1.5	0	0	1	0
Axial compression in combination with shear loads					
ω=a/b=3	1.5	0	0	1	0

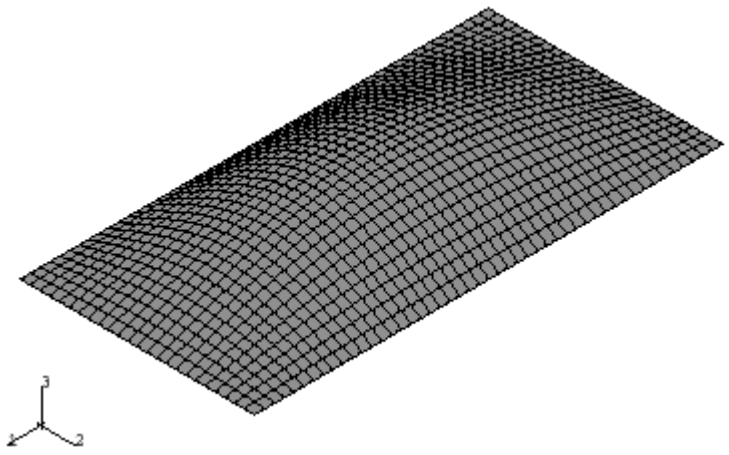

Figure 4.2 : Initial deflection pattern for transversely loaded plate with aspect ratio a/b=2

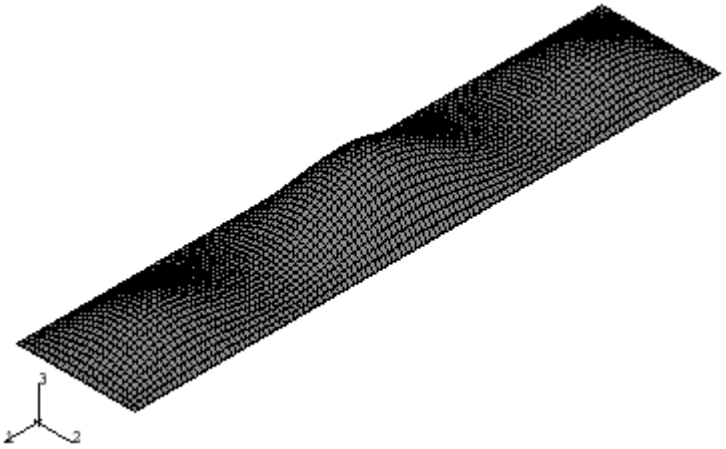

Figure 4.3 : Initial deflection pattern for biaxially loaded plate with aspect ratio a/b=5

4.6 Newtons Method and Arc Length Method

ABAQUS normally uses Newtons Method to solve the differential equations. In this thesis the arc length method has been used instead. This method has the advantage of handling limit points with both snap-throughs and snap-backs.

Instead of using load control or displacement control, the solution is found by following the tangent to the response curve in the state control space. The movement along the tangent is followed by an iteration procedure. Excellent descriptions of the details in the method can be found in Felippa (1996) or Crisfield (1991).

4.7 Load Sequence for Multiple Load Conditions

4.7.1 Introduction

The different kinds of non-linear finite element analyses performed will be explained. This will be done by showing examples of the different types of analyses carried out.

4.7.2 Axial Compression

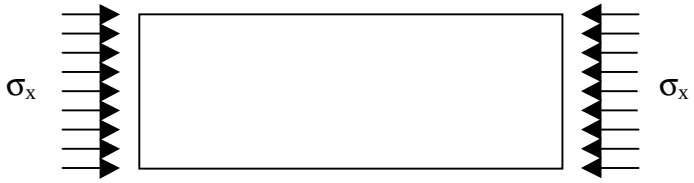

Figure 4.4 : Axial compression of plates

Axial compression means that the plates were strained by giving all the nodes at one of the short edges the same axial displacement. The total force was then recorded by summing the node reaction forces at the other end of the plate.

The plates were compressed until the displacement of the nodes at the short end of the plate corresponded to 2.5 times the yield strain.

$$\varepsilon_{0.2} = \frac{\sigma_{0.2}}{E} \tag{4.2}$$

$$\varepsilon_{2.5} = 2.5 \cdot \varepsilon_{0.2} = \frac{2.5 \cdot \sigma_{0.2}}{E} \tag{4.3}$$

$$\Delta a_{max} = a \cdot \varepsilon_{2.5} = \frac{2.5 \cdot a \cdot \sigma_{0.2}}{E} \tag{4.4}$$

To calculate compressive stresses, the total force was divided by the front area of the plate, and the strain was found by dividing the axial displacement by the length of the plate.

$$\sigma_{mx} = \frac{F_x}{A} \tag{4.5}$$

$$\varepsilon_x = \frac{\Delta a}{a} \tag{4.6}$$

A common way to present the stress-strain curves for plate buckling is to make the curves dimensionless. In most of this dissertation the strain is divided by the yield strain, and the stress is divided by the 0.2 percent tensile proof stress.

$$\varepsilon_n = \frac{\varepsilon_x}{\varepsilon_{0.2}} \tag{4.7}$$

$$\sigma_n = \frac{\sigma_{mx}}{\sigma_{0.2}} \tag{4.8}$$

A typical progress of the stress-strain curves for plates with different values of the slenderness, β, is given in figure 4.5. The plates are made of alloy 6082-T6, they have no heat affected zones, and the edges are free, simply supported.

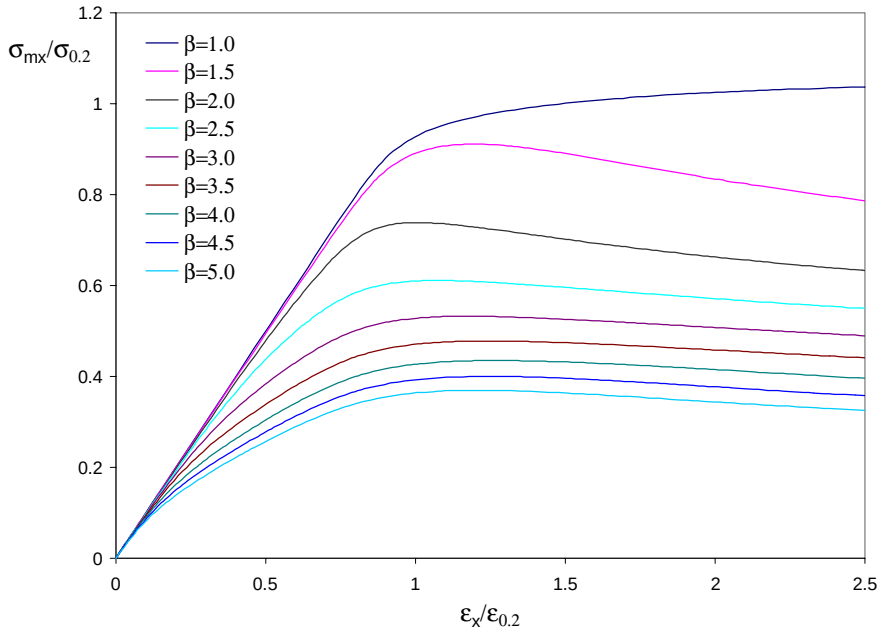

Figure 4.5 : Stress-strain relationships of axially loaded plates with free, simply supported edges. The plates are made of alloy 6082-T6 and consist of the base material only. The stress-strain curves from plates with the smaller value of the slenderness, β, will have the higher top points.

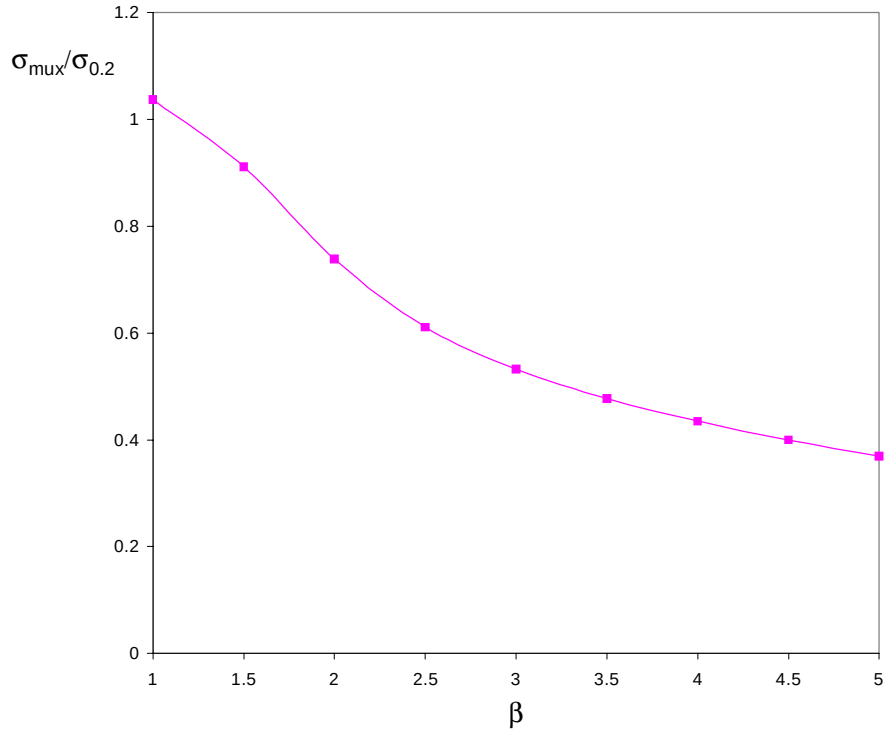

Figure 4.6 : Maximum capacities of axially loaded plates with free, simply supported edges. The plates are made of alloy 6082-T6 and consist of the base material only.

The maximum value of the stress-strain curves is called σ_{mux}. This value is either the top point of the curves or the mean axial stress when the normalised strain equals 2.5 times the yield strain. The latter value was used if the curve was continuously increasing and no top point was passed during the crushing of the plates. Stopping the analyses when the normalised strain equalled 2.5 times the yield strain was a decision made by the author. For most of the analyses the top point of the stress-strain curves was reached for strains in the vicinity of the yield strain. If not the stress-strain curves were continuously growing. Higher collapse values could have been achieved by compressing the plates beyond 2.5 times the yield strain, but stopping at this value is conservative. In Figure 4.6 the axial capacities are plotted for the different values of the slenderness, β.

4.7.3 Transverse Compression

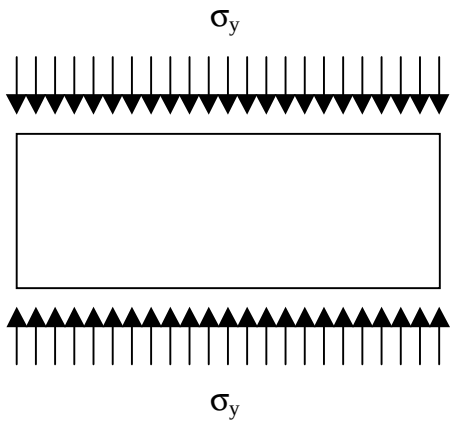

Figure 4.7 : Transverse compression of plates

Transverse compression means that the plates are strained by giving all the nodes at one of the long edges of the plates the same transverse in-plane displacement. The total forces on the plates were recorded by adding the node reaction forces at the other long edge of the plates. The same method for calculating normalised stresses and strains as for axial compression is used.

Figures 4.8-4.9 show the stress-strain curves and maximum stresses for plates with different values of the slenderness, β. The plates are made of alloy 6082-T6, they have no heat affected zones, and the edges are free, simply supported. The reason for not changing to a transverse slenderness parameter has to do with the fact that the transverse capacities of plates will be handle by weighted summing of the capacity of a quadratic plate and the capacity of a plate strip (see Chapters 7 and 10).

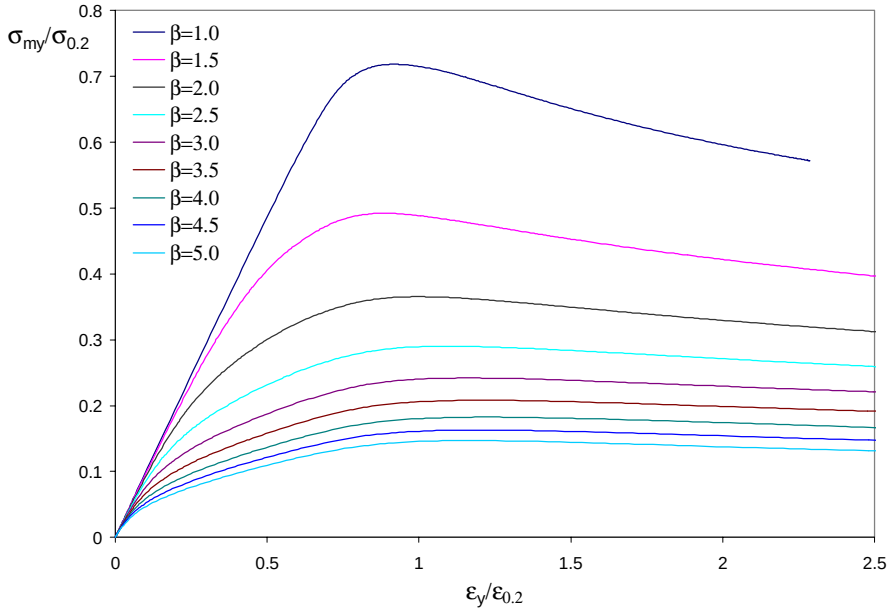

Figure 4.8 : Stress-strain relationships of transversally loaded plates with free, simply supported edges. The plates are made of alloy 6082-T6 and consist of the base material only. The stress-strain curves from plates with the smaller value of the slenderness, β, will have the higher top points.

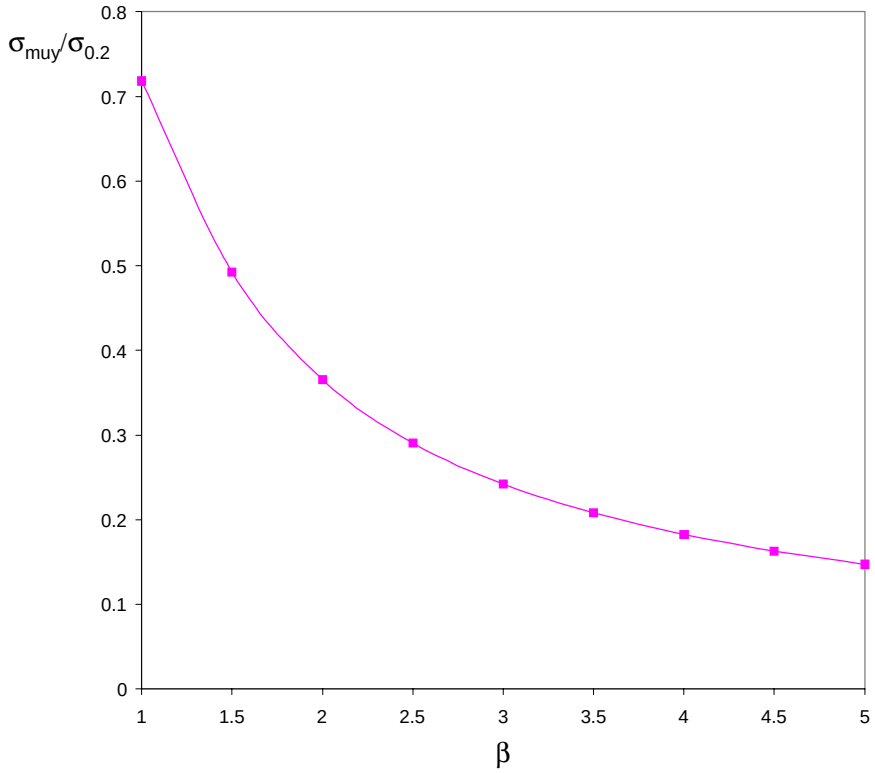

Figure 4.9 : Maximum capacities of transversally loaded plates with free, simply supported edges. The plates are made of alloy 6082-T6 and consist of the base material only.

4.7.4 Biaxial Compression

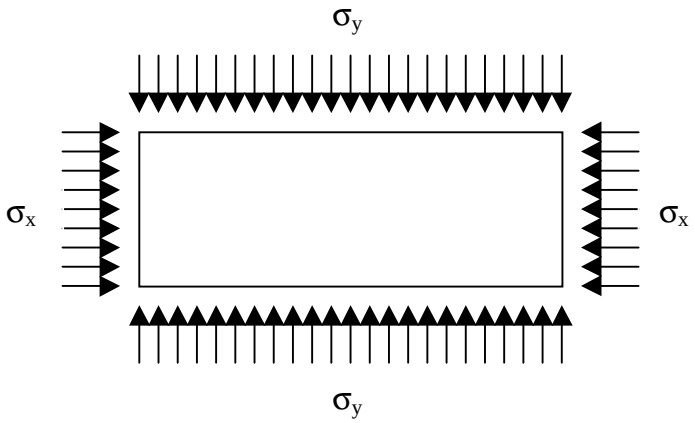

Figure 4.10 : Biaxial compression of plates

Biaxial compression means that the plates are compressed by imposing forces both at the short and long edges of the plates simultaneously. This is done by keeping the edges straight with the help of the *EQUATION option in ABAQUS. Forces are then given to the mid node of one of the short edges of the plates and to the mid node of one of the long edges of the plates. The other short edge and the other long edge are prevented from moving in x- and y-direction. The displacements of the nodes where the forces are enforced, are registered to find strains in x- and y-direction, respectively.

The plates are collapsed with the ratio between average stresses in longitudinal and transverse direction kept constant; ensuring so called proportional loading.

$$\sigma_{my} = k \cdot \sigma_{mx} \tag{4.9}$$

The proportionality constant, k, can be expressed as:

$$k = \tan\phi \tag{4.10}$$

$$\phi = 0^\circ, 9^\circ, 18^\circ, ..., 90^\circ \tag{4.11}$$

The critical stresses in the x- and y-direction are normalised with respect to the ultimate uniaxial strengths in their respective direction.

$$R_x = \frac{\sigma_{mx}}{\sigma_{mux}} \tag{4.12}$$

$$R_y = \frac{\sigma_{my}}{\sigma_{muy}} \tag{4.13}$$

It should be pointed out that the ultimate uniaxial strengths in the x- and y-direction differ slightly from the ultimate uniaxial strengths found in the chapters dealing with uniaxial compression. This is due to the fact that an other initial deflection pattern was used when

biaxial compression was performed (see Chapter 8 for details on the influence of changing initial deflection patterns).

Figure 4.11 show biaxial interaction curves for plates with different values of the slenderness, β. The plates have an aspect ratio, a/b=3. They are made of alloy 6082-T6, and they have heat affected zones along all edges of the plates.

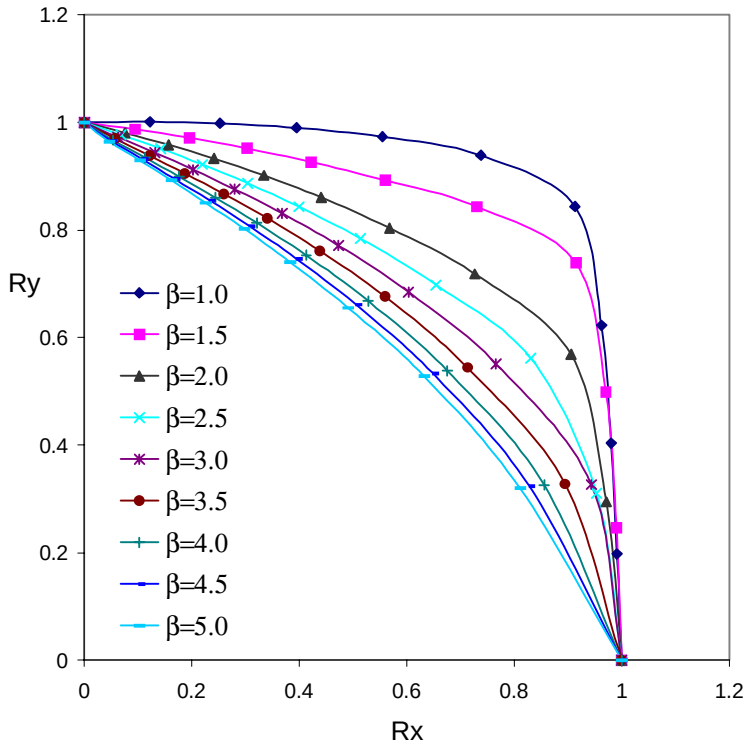

Figure 4.11 : Biaxial interaction curves for plates made of alloy 6082-T6 with aspect ratio a/b=3. The plates have heat affected zones along all edges.

4.7.5 Pure Shear Load

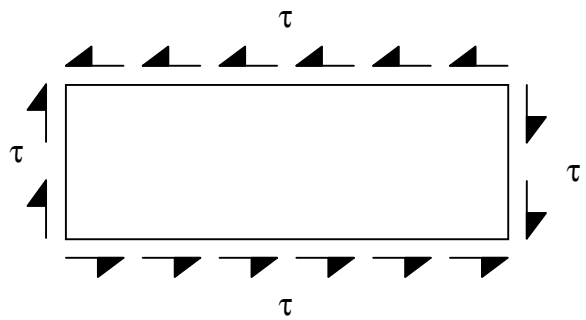

Figure 4.12 : Plates exposed to pure shear load

Giving the plates pure shear loads means that all the nodes along the edges of the plate; except the corner nodes; were exposed to the same shear force (forces parallel to the plate edges), but the directions were varied depending on which side of the plate the forces were enforced.

They were given according to the figure above. The corner nodes were only exposed to half the forces of the other nodes, but they were given forces in two directions, corresponding to the directions of the forces in their neighbouring plate sides.

To allow shear deformation the nodes along the short edges of the plates must no longer have the same axial deflection, but they are forced to stay on the same line. This is done with the help of the *EQUATION command in ABAQUS.

The stresses were normalised with respect to the shear yield stress.

$$\tau_{0.2} = \frac{\sigma_{0.2}}{\sqrt{3}} \tag{4.14}$$

$$\tau_n = \frac{\tau_m}{\tau_{0.2}} \tag{4.15}$$

The shear strain was normalised by dividing by the yield shear strain.

$$\gamma_{0.2} = \frac{\tau_{0.2}}{G} \tag{4.16}$$

$$\gamma_n = \frac{\gamma}{\gamma_{0.2}} \tag{4.17}$$

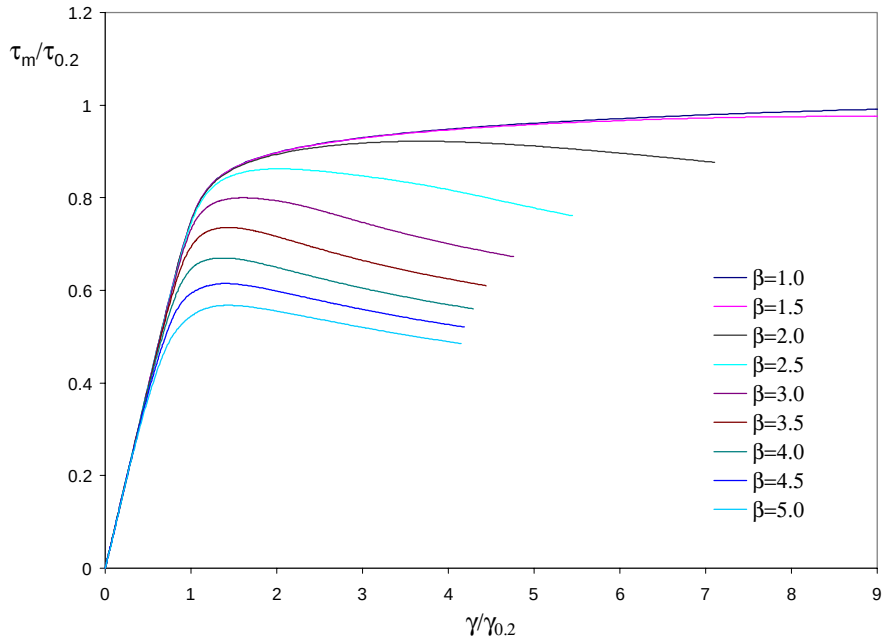

Figure 4.13 : Stress-strain relationships of plates exposed to pure shear loads. The plates are made of alloy 6082-T6. They have straight, simply supported edges and they have not been exposed to welding. The stress-strain curves from plates with the smaller value of the slenderness, β, will have the higher top points.

Figures 4.13-4.14 give examples of stress-strain curves and the critical values of the shear stresses for different values of the axial slenderness, β. The maximum value of the stress-strain curves is called τ_{mu}. This value is either the top point of the curves or the mean shear stress when the normalised shear strain equals 10 times the yield shear strain. The plates are made of alloy 6082-T6, and they have no residual stresses or soft zones. All plates had an aspect ratio, a/b=3.

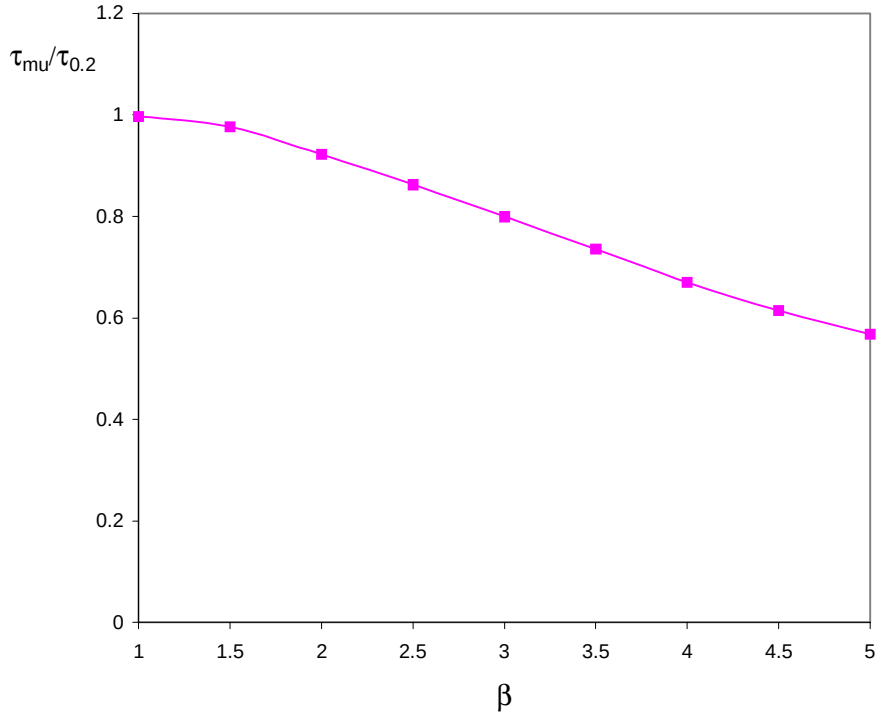

Figure 4.14 : Maximum capacities of plates exposed to pure shear load. The plates are made of alloy 6082-T6. They have straight, simply supported edges and they have not been exposed to welding.

4.7.6 Axial Compression in Combination with Shear Loads

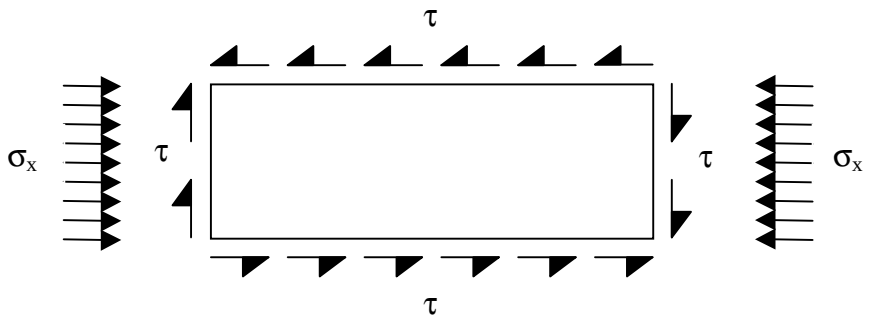

Figure 4.15 : Plates exposed to axial compression in combination with shear loads.

When plates are exposed to the combination of axial compression and shear loads, the shear loads are enforced in the same way as for pure shear loading. The axial forces are added by

imposing an axial force at the mid node of one of the short edges and restraining the mid node at the other short edge from moving in the axial direction.

As for biaxial compression the plates are collapsed with the ratio between the axial stresses and the shear stresses kept constant, and the critical axial stresses and critical shear stresses are normalised with respect to ultimate uniaxial strengths in their respective directions.

$$\tau_m = k \cdot \sigma_{mx} \tag{4.18}$$

$$R_\tau = \frac{\tau_m}{\tau_{mu}} \tag{4.19}$$

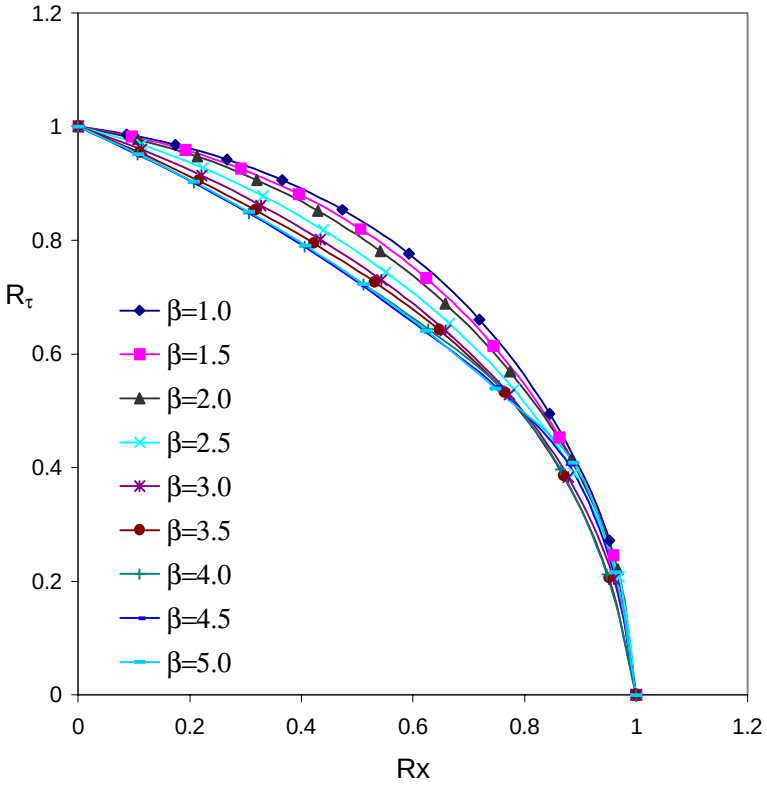

Figure 4.16 : Interaction curves for plates exposed to axial compression in combination with shear loads. The plates are made of alloy 6082-T6. They have straight, simply supported edges and they have not been exposed to welding.

4.7.7 Plate Strip Analyses

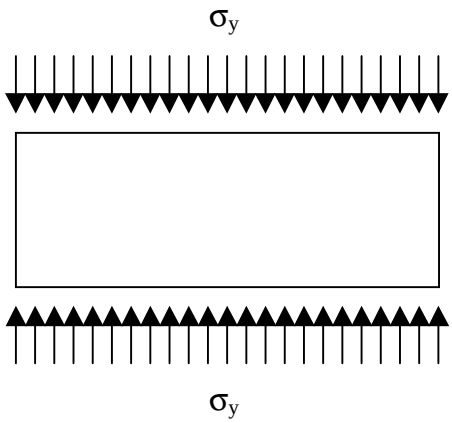

Figure 4.17 :Plate strip analyses of plates

These analyses have been performed for transversally loaded plates. They have been performed by changing the boundary conditions along the short edges of the plate. The nodes did not have to stay in the x-y plane, but was free to move out of the plane.

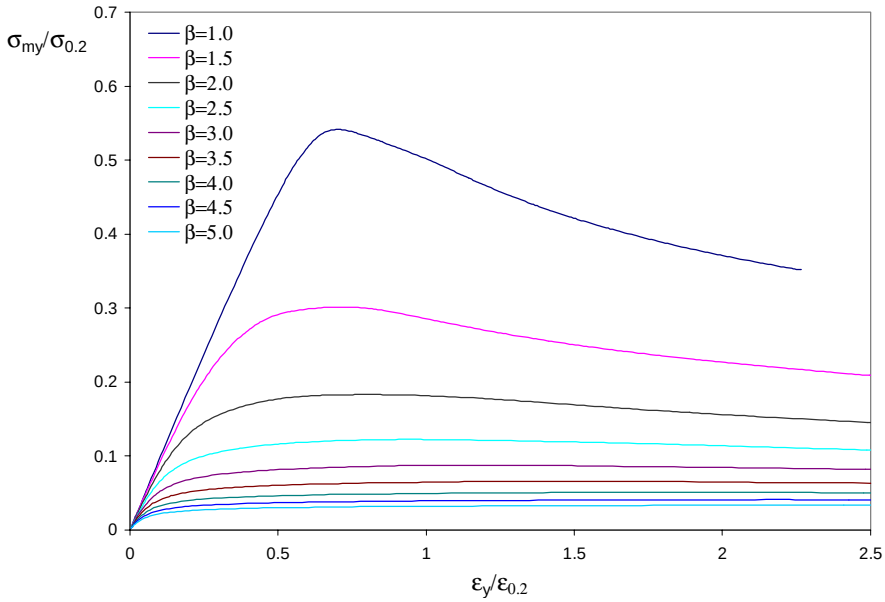

Figure 4.18 : Stress-strain relationships of plate strips with straight, simply supported edges. The plates are made of alloy 6082-T6 and consist of the base material only. The stress-strain curves from plates with the smaller value of the slenderness, β, will have the higher top points.

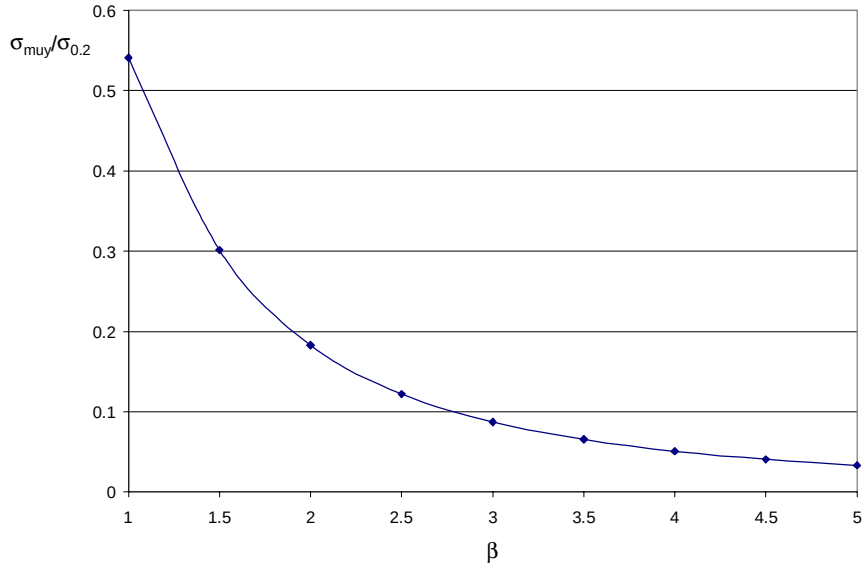

Figure 4.19 : Maximum capacities of plate strips with straight, simply supported edges. The plates are made of alloy 6082-T6 and consist of the base material only.

4.8 Convergence Test

The convergence analyses have been performed for axially and transversally loaded plates with aspect ratio, a/b=3. Both plates consisting of the base material only and plates exposed to heat affected zones along all edges were investigated. The alloy used was 6082-T6, the breadth of the heat affected zones was equal to 25 mm, and the 0.2 percent tensile proof stress in the heat affected zones was equal to half the 0.2 percent tensile proof stress of the base material. The residual stresses in tension were equal to 75 percent of the reduced 0.2 percent tensile proof stress in the heat affected zones.

The results from the element model used in most of the analyses (mesh number 3), were compared with results from a model consisting of four times the number of elements (mesh number 4) and a model consisting of 16 times the number of elements (mesh number 5).

Figure 4.20 shows the results from analyses of axially loaded plates, and Figure 4.21 gives the percentage reduction in buckling capacity as compared to analyses with the most coarse element mesh. The corresponding results for transversally loaded plates are given in Figures 4.22 and 4.23.

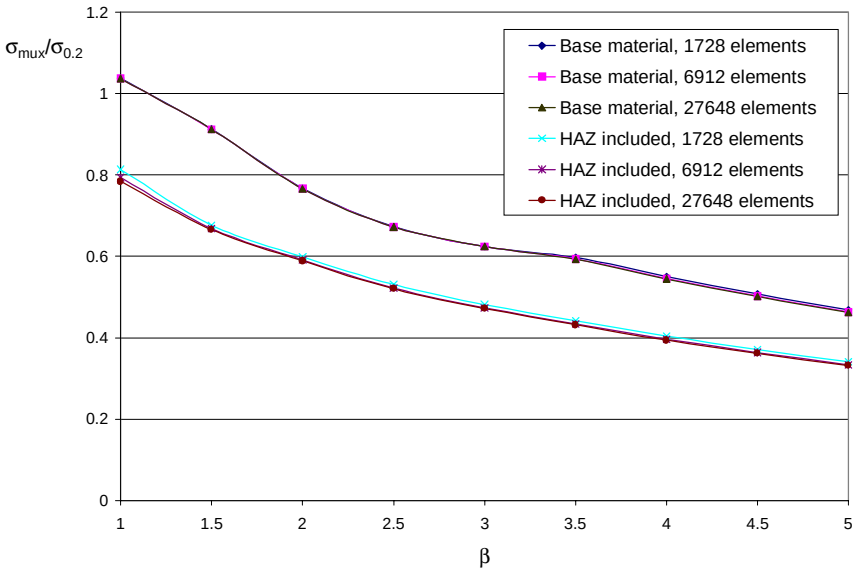

Figure 4.20 : Convergence analyses of axially loaded plates

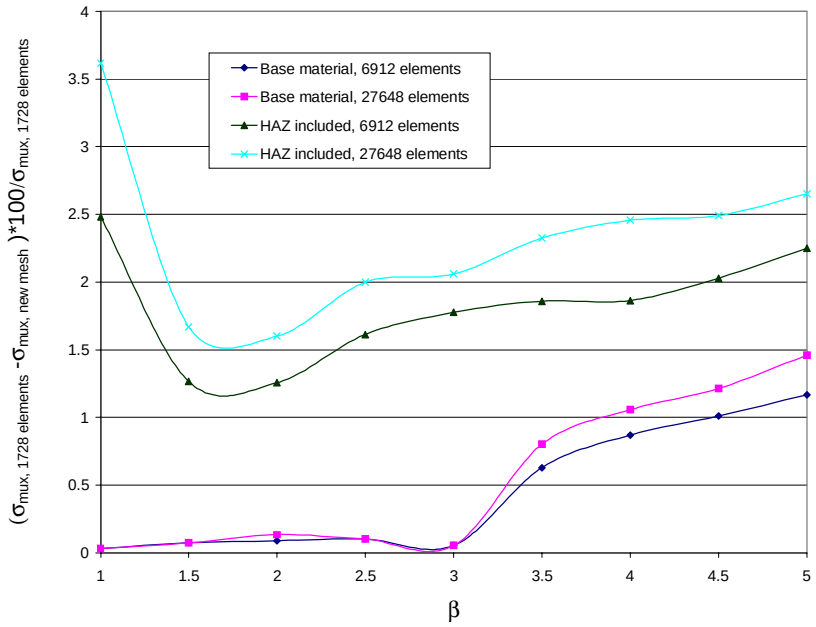

Figure 4.21 : Percentage reduction in axial buckling capacity as compared to analyses with element mesh consisting of 1728 elements

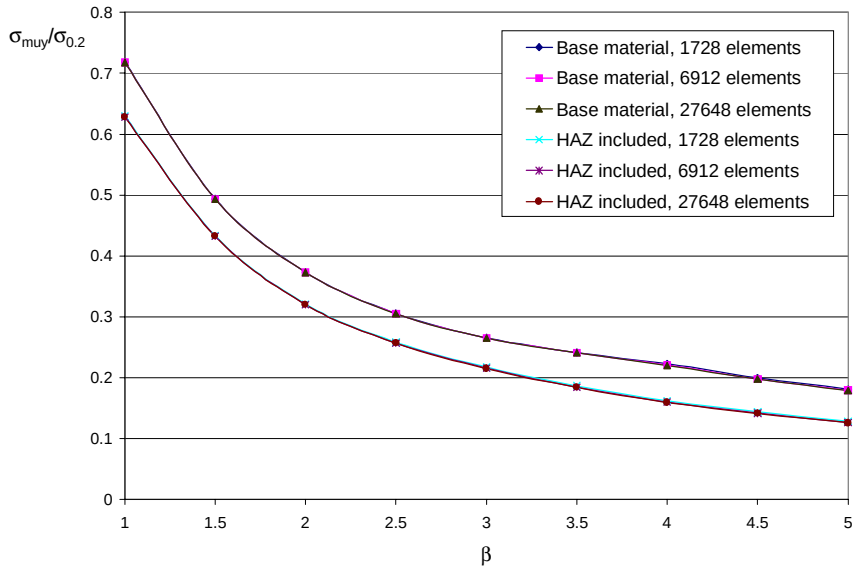

Figure 4.22 : Convergence analyses of transversally loaded plates

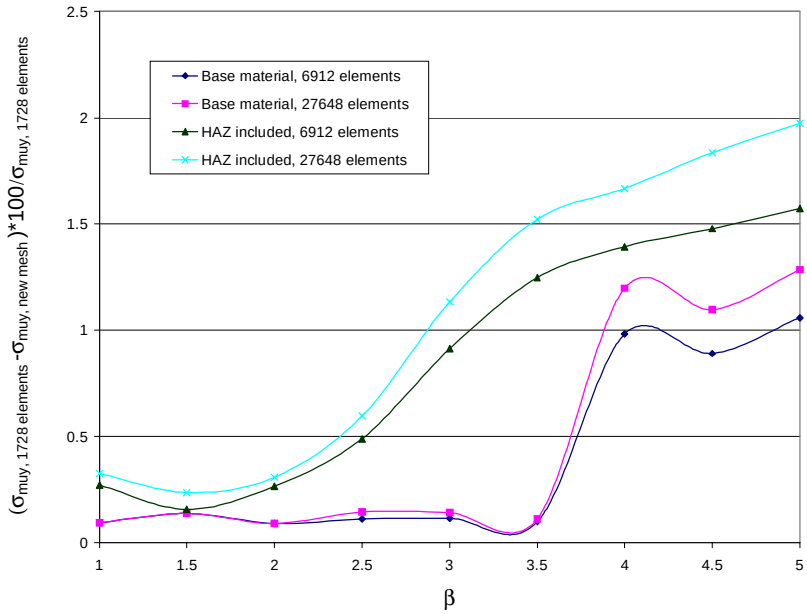

Figure 4.23 : Percentage reduction in transverse buckling capacity as compared to analyses with element mesh consisting of 1728 elements

The percentage reduction in buckling capacity due to finer element meshes is larger for plates with heat affected zones than for plates consisting of the base material only. The reason for this behaviour is that plates exposed to heat affected zones experience local yielding with large strain variations between elements.

Compact, axially loaded plates, for instance, will have local yielding with local failure along loaded edges. The element mesh consisting of 1728 elements only, have two element breadths representing the zone with reduced material parameters. If the number of element

breadths in the zone with reduced material parameters is increased to 4 or 8, the large strains and strain variations are better represented, and most of the artificial increase in stiffness disappears.

Because the analyses are non-linear, both regarding material behaviour and geometry, convergence rate criteria are very difficult to establish. No such attempts have been done by the author, but tabulated values of the buckling capacities are given in Appendix 1; to give the interested reader the best basis for further investigation of the analyses results.

The conclusion that can be drawn from these analyses is that having an element mesh with a characteristic element length of 12.5 mm is sufficient to achieve acceptable accuracy for developing buckling design curves. The largest reduction in buckling capacity due to finer element mesh was 3.6 %, observed for axially loaded plates exposed to heat affected zones and with a slenderness, β=1.0. For β=1.5 - 5.0 the reduction in buckling capacity due to finer element mesh is never larger than 2.7 %.

Chapter 5

Effect of Heat Affected Zones on the Ultimate Capacity

As a matter of form, all the numerical analyses in this chapter, and Chapter 6, have been performed for plates with aspect ratio, a/b=3. Variation of the aspect ratio, a/b, is carried out in Chapter 7 and the following chapters.

5.1 Introduction

The change in the ultimate capacity of aluminium plates due to introduction of soft zones and residual stresses is studied. Residual stresses and soft zones are introduced separately, and they are combined. The value of the residual stresses is varied in parametric studies, and the effect of changing the breadth of the heat affected zones is investigated.

The change in ultimate capacity for different patterns of the heat affected zones and which loading conditions that show the largest change in ultimate capacity due to introduction of heat affected zones are also looked into.

5.2 Axial Loading

5.2.1 Residual Stresses versus Soft Zones

The first phenomena that will be elaborated on, are which effect that is the more important one, residual stresses or soft zones, or do they have to be combined to assure disaster. Aluminium plates have been analysed with residual stresses only and soft zones only in addition to the combined effect.

The residual stresses have their highest value when the reduction of the 0.2 percent tensile proof stress in the heat-affected-zones does not appear, or at least is small, because the residual stresses in tension normally can be found as a percentage of the yield stress of the material that have been exposed to welding. When the residual stresses in tension are large, the residual stresses in compression also have to be large to give zero resultant forces.

5.2.1.1 Residual Stresses Only

Figure 5.1 shows numerical analyses of axially loaded plates that are exposed to residual stresses only. The plates are made of alloy 6082-T6 and have heat affected zones along all edges. The breadth of the zones with residual stresses in tension is always 25 mm. The different percentages given in the figure indicates how large the residual stresses in tension are compared to the yield stress of the base material. 45 % means that the residual stresses in tension are 45 percent of the yield stress of the base material (σ_R^+= 0.45*292 MPa=131.4 MPa).

Figure 5.2 shows the percentage reduction in strength caused by the residual stresses as compared to analyses with no residual stresses. The same results are plotted in Figure A2.1 with the magnitude of the residual stresses along the abscissa. As can be seen from the figures, the presence of residual stresses is without significance for very sturdy plates. Then there is a rapid growth in reduction that reaches it's maximum around β=2. Later the reduction decreases for a local minimum around β=3, and then the reduction increases the more slender becomes and can be as large as 15.3 % for a plate with slenderness β=5.0 and residual stresses equal to the yield stress.

The collapse of very sturdy plates is a crushing phenomenon. The collapse mechanism is yielding far into the plastic range of the stress-strain curves of the materials; this effectively cancels the effect of pre-tensioning due to residual stresses.

The residual stresses in tension are expressed as a fraction of the 0.2% tensile proof stress or yield stress. Keeping the breadths of the zones with residual stresses in tension constant entails the residual stresses in compression to be at the same level. The residual stresses in compression will be at the same level compared to the yield strength of the material, but they will be larger and larger compared to the buckling capacity of the plates the more slender the plates become. The mid part of the plates will be pre-compressed with stresses closer and closer to the values in which the mid parts of the plates buckle out.

The result is that the mid part of the plates buckles out earlier and earlier in the collapse history as the slenderness of the plates is increased, causing a larger and larger relative damage.

Figure A2.1 also indicates that assuming the reduction in buckling capacity to vary linearly with respect to the ratio between the residual stresses in tension and the yield strength of the base material gives a good approximation for all values of the slenderness, β, analysed.

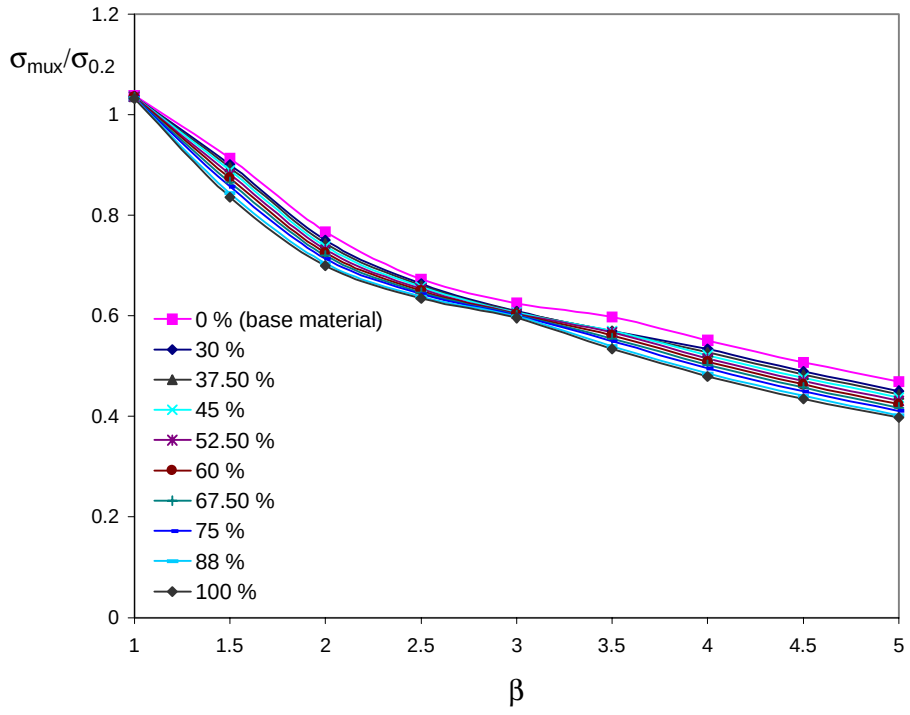

Figure 5.1 : Numerical analyses of plates exposed to residual stresses only. The aluminium alloy is 6082-T6. The percentages given in the figure indicates how large the residual stresses in tension are compared to the yield stress of the base material.

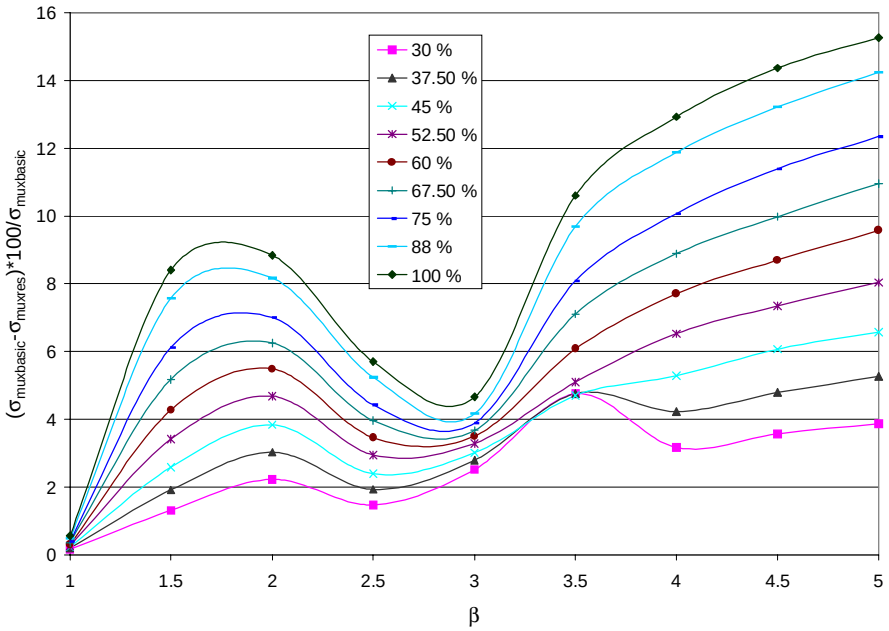

Figure 5.2 : Percentage reduction in strength caused by residual stresses only. The aluminium alloy is 6082-T6. The percentages given in the figure indicates how large the residual stresses in tension are compared to the yield stress of the base material.

5.2.1.2 Soft Zones Only

When a plate is exposed to soft zones only it means that the material in the heat affected zones has a reduced yield stress and knee factor in the Ramberg-Osgood law, but no residual stresses. Figure 5.3 shows numerical analyses of plates exposed to soft zones only. The aluminium alloy used as the reference material is 6082-T6, and the breadth of the soft zones is always 25 mm. The percentage numbers given in the figure indicate how large the yield stresses in the heat affected zones are as compared to the yield stress of the base material. 70 % means that the yield stress in the heat affected zones is 70 percent of the yield stress of the base material ($\sigma_{0.2}^{*}$= 0.70*292 MPa=204.4 MPa).

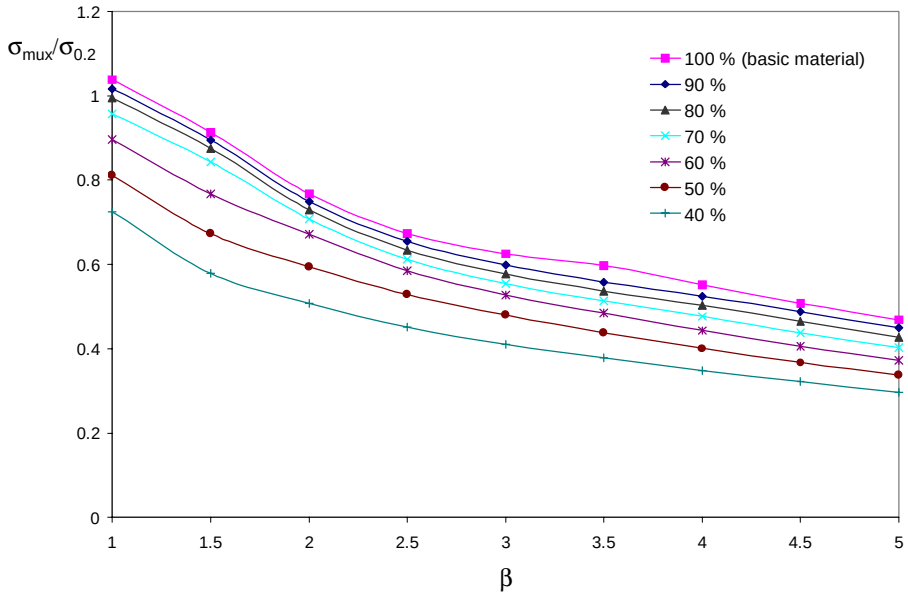

Figure 5.3 : Numerical analyses of plates exposed to soft zones only. The aluminium alloy used as the reference material is 6082-T6. The percentage numbers given in the figure indicate how large the yield stresses in the heat affected zones are as compared to the yield stress of the base material.

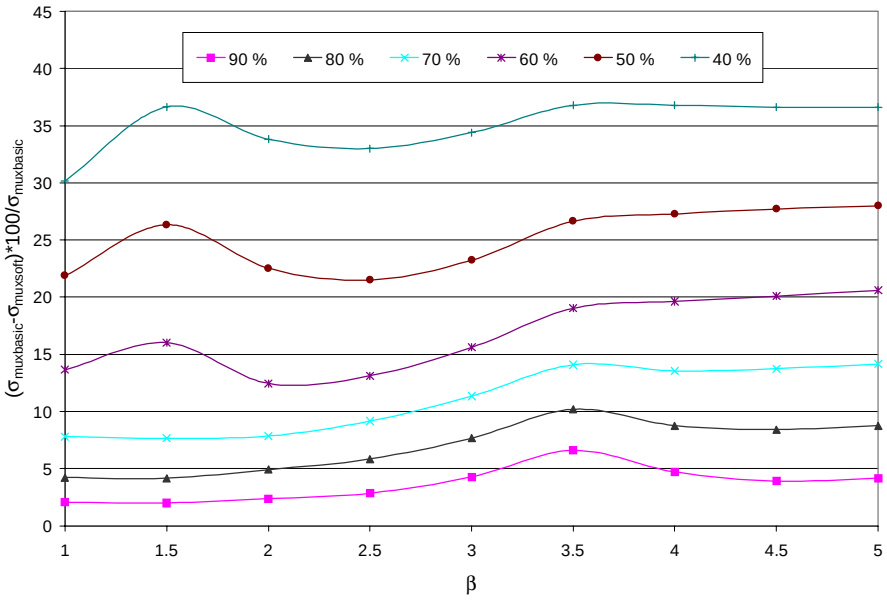

Figure 5.4 : Percentage reduction in strength caused by soft zones only. The aluminium alloy used as the reference material is 6082-T6. The percentage numbers given in the figure indicate how large the yield stresses in the heat affected zones are as compared to the yield stress of the base material.

Figure 5.4 indicates the percentage reduction in strength caused by soft zones as compared to analyses with the base material only. The same results are plotted in Figure A2.2 with the reduction in yield stress along the abscissa.

The reduction in strength is larger for slender plates than sturdy plates, but the variation in buckling capacity due to slenderness is not large, and the reduction in buckling capacity is almost constant for plates with slenderness β=3.5 and higher.

The curvature of the curves in Figure A2.2 also indicates that assuming the reduction in buckling capacity to vary linearly (between a plate having no soft zones and a plate with the chosen ratio between the yield strength in the soft zones and the yield strength of the base material) with respect to the reduction of the yield strength in the soft zones is a conservative assumption. This assumption is more conservative for sturdy plates than slender plates.

5.2.1.3 Combined Effect of Residual Stresses and Soft Zones

When aluminium plates are exposed to the combined effect of residual stresses and soft zones it means that they are exposed to residual stresses and lowered material yield strength in the heat affected zones simultaneously. The residual stresses in tension in all analyses are taken to be equal to 75 percent of the reduced yield strength in the heat affected zones.

Results of analyses for plates exposed to the combined effect of residual stresses and soft zones are shown in Figure 5.5. Aluminium alloy 6082-T6 is used as the reference material. The percentage numbers in the figure indicates the yield strength of the material in the heat affected zones. 60 % means that the yield strength in the heat affected zones is equal to 60 % of the yield strength of the base material ($\sigma_{0.2}^{*}$= 0.60*292 MPa=175.2 MPa). The corresponding value of the residual stresses becomes 75 % of the reduced yield stress (σ_R^{+}= 0.75*0.60*292 MPa=131.4 MPa).

Analyses of plates with no heat affected zones and plates exposed to residual stresses only are shown in the same figure.

Figure 6.6 indicates the percentage reduction in strength caused by the combined effect of residual stresses and soft zones as compared to analyses with the base material only. The same results are plotted in Figure A2.3 with the reduction in yield stress along the abscissa.

Comparing Figure 5.4 and Figure 5.6 leads to an interesting observation: If there is a large difference between the yield strength of the material in the heat affected zones, $\sigma_{0.2}^{*}$, and the yield strength of the base material, $\sigma_{0.2}$, the effect of the yield strength reduction in the heat affected zones is governing while the effect of residual stresses is negligible. Actually the yield strength of the material in the heat affected zones has to be 80% of the yield strength of the base material before the deviations are of practical interest. Ignoring the residual stresses for plates with this reduction of yield stress, or less reduction of yield stress, will be non-conservative.

The main reason why this happens is that the residual stresses are given as a percentage of the yield strengths in the heat affected zones. If the yield strengths in the heat affected zones are small, the residual stresses will be small as well, and without significance.

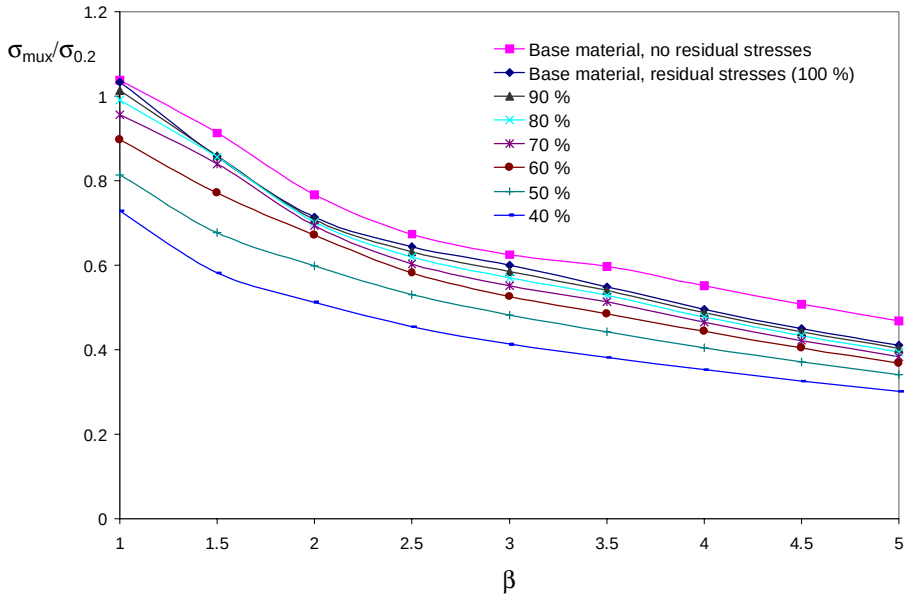

Figure 5.5 : Numerical analyses of plates exposed to the combined effect of residual stresses and soft zones. The aluminium alloy used as the reference material is 6082-T6. The percentage numbers given in the figure indicate how large the yield stresses in the heat affected zones are as compared to the yield stress of the base material.

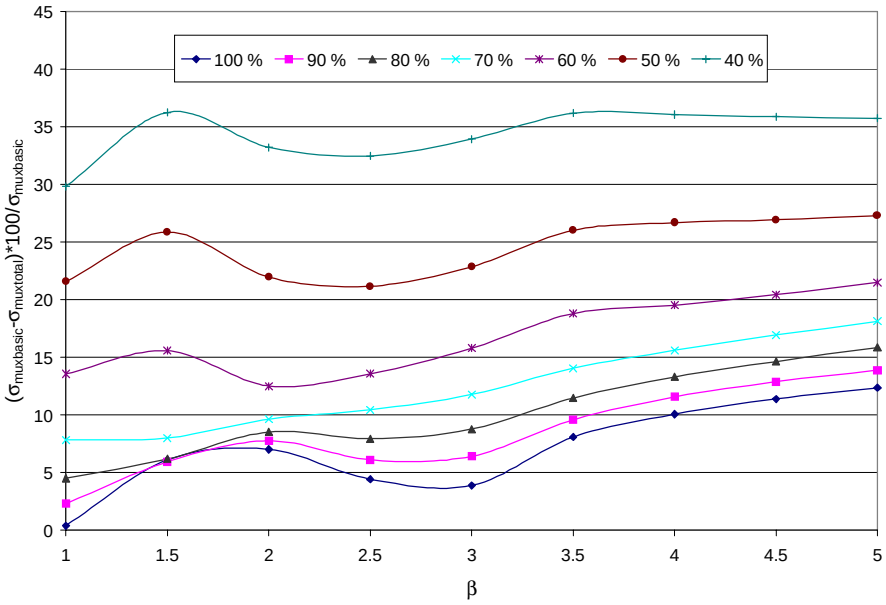

Figure 5.6 : Percentage reduction in strength caused by the combined effect of residual stresses and soft zones. The aluminium alloy used as the reference material is 6082-T6. The percentage numbers given in the figure indicate how large the yield stresses in the heat affected zones are as compared to the yield stress of the base material.

5.2.1.4 Effect of the Width of the Heat Affected Zones

In Table 4.2 the breadths of the heat affected zones according to British Standard 8118 and Eurocode 9 are given, but true zones may deviate from these values. The ultimate strength

has been calculated for plates with different size of the heat affected zones. For a plate with heat affected zones along all edges, the breadth of the heat affected zones has been varied in the range of 0 to 35 mm. Figures 5.7 and 5.8 show results from such analyses. The plates consisted of alloy 6082-T6. In every single analyse all the edges of the plate had the same breadth of the heat-affected-zone. The yield strength in the heat affected zones was equal to 50 % of the yield strength of the base material and the residual stresses in tension were equal to 75 % of the reduced yield strength.

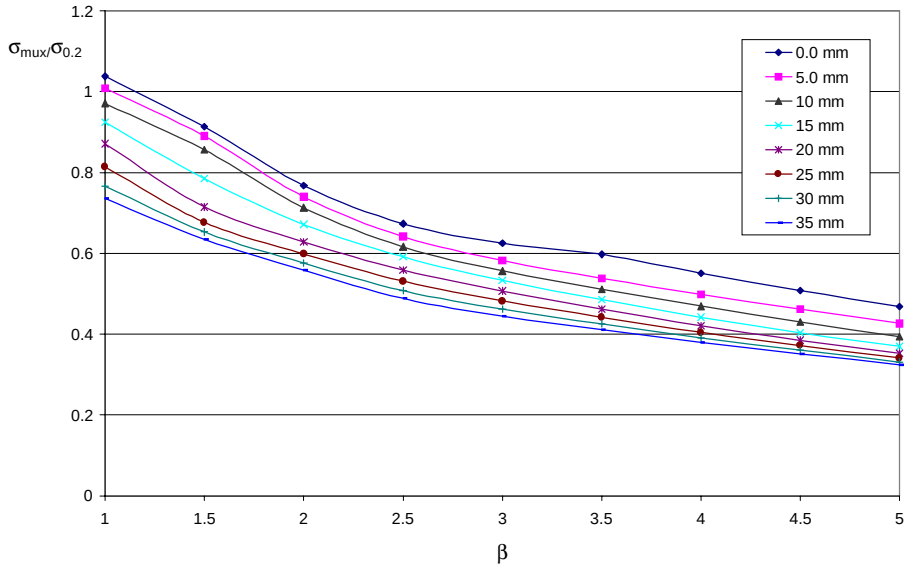

Figure 5.7 : Numerical analyses of plates with different breadths of the heat affected zones. The plates consisted of alloy 6082-T6.

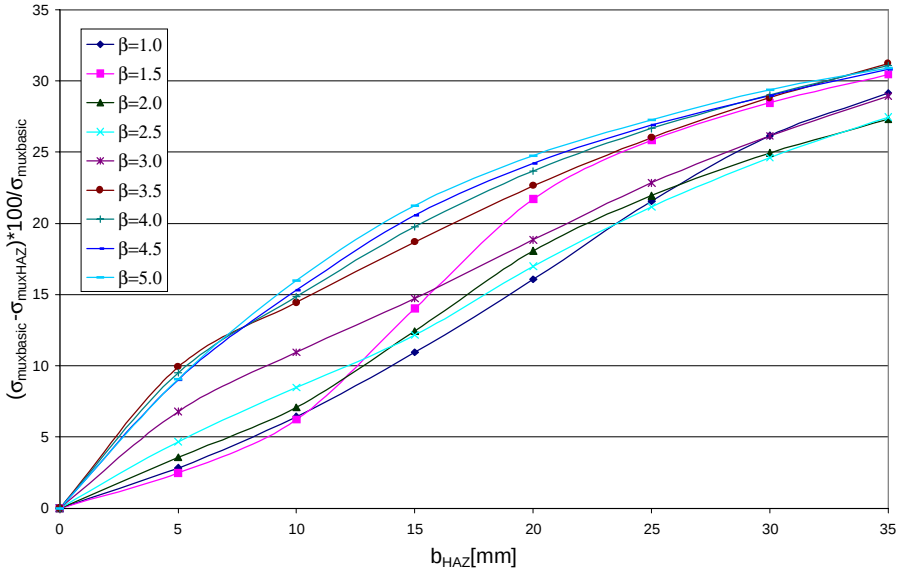

Figure 5.8 : Percentage reduction in strength for plates with different breadths of the heat affected zones. The plates consisted of alloy 6082-T6.

Figures 5.7 and 5.8 illustrate that slender plates have a larger reduction in buckling capacity than compact plates, and that the difference in reduction of buckling capacity decreases as the breadth of the heat affected zones increases.

5.2.2 Different Patterns of the Heat Affected Zones

In these analyses the different patterns of the heat-affected-zones were analysed and their behaviour was compared. The alloy utilised was 6082-T6, and the breadth of a the heat affected zones was always 25 mm. The yield strength in the heat affected zones was set equal to 50 % of the yield strength of the base material and the residual stresses in tension were equal to 75 % of the reduced yield strength.

Figure 5.9 gives results from axially loaded plates. As can be seen from the figure, it is almost no difference in axial buckling capacity if the plates have heat affected zones along all edges, heat affected zones along short edges only or the extruded pattern of the heat affected zones. When the short edges have been affected by welding, there is no part of the plate that can carry axial loads unaffected by reduced material capacities. Most of the load carrying capacity takes place towards the longitudinal edges of the plate. Keeping them unaffected by welding along most of the sides does not help if there are welds at the ends of the longitudinal sides.

Having a heat affected zone in the middle-longitudinal direction is almost without significance for the axial buckling capacity. This is because the stresses towards the middle of the plates in the ultimate load condition are low, and the material does not need to have a high yield strength. For most plates the mid part of the plates buckle before stresses become larger than the reduced yield stress.

Placing a heat affected zone in the middle of the plate, transverse direction, is even more destructive to the axial buckling capacity for slender plates than having heat affected zones along the edges of the plate.

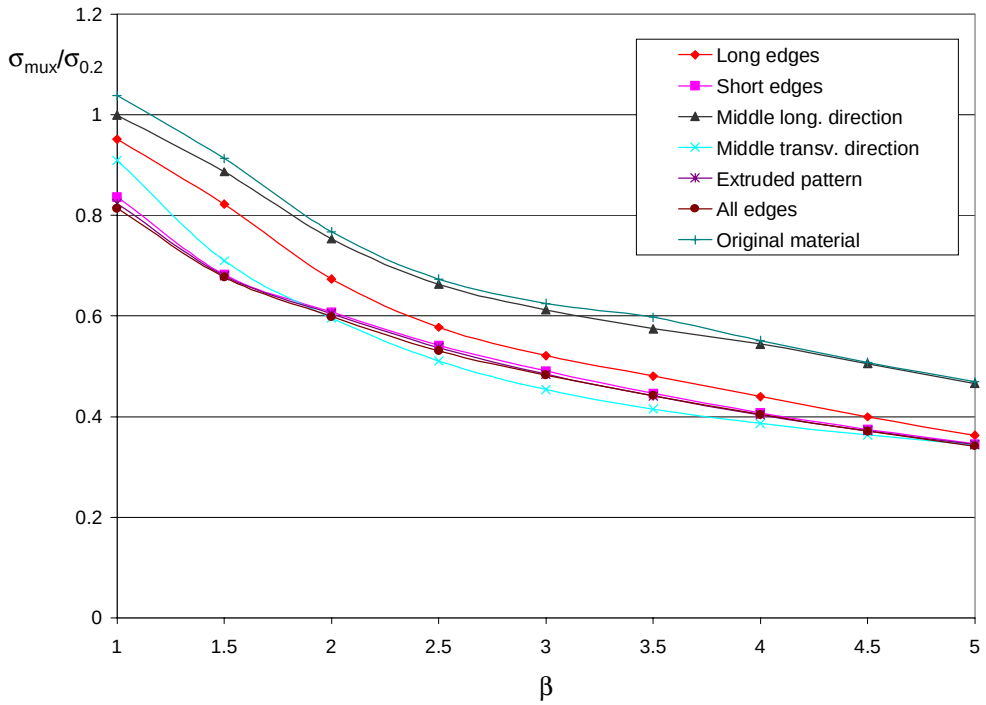

Figure 5.9 : Axial buckling capacity for different patterns of the heat affected zones. The plates consist of alloy 6082-T6.

One may claim that the reduction in load carrying capacity due to the introduction of heat affected zones in the longitudinal direction only can be reasonably well modelled by assuming that the difference in load carrying capacity is equal to the reduction in yield strength between the material unaffected by welding and the material in the heat affected zones times the front area of the heat affected zones, i.e:

$$F_{red} = \left(\sigma_{0.2} - \sigma_{0.2}^{*}\right) \cdot 2b_{HAZ} \cdot t \tag{5.1}$$

The reason for the factor 2 is that there are two heat affected zones, along each of the longitudinal edges.

The corresponding expression for the reduction in average ultimate stress becomes:

$$\sigma_{red} = \left(\sigma_{0.2} - \sigma_{0.2}^{*}\right) \cdot \left(\frac{2b_{HAZ}}{b}\right) \tag{5.2}$$

For the plate considered the reduction will be:

$$\sigma_{red} = (292 - 146) \cdot \left(\frac{2 \cdot 25}{300}\right) = 24.3\,[MPa] \tag{5.3}$$

As can be seen from Table 5.1, the reduction in buckling stress is fairly constant and slightly higher than what was given by Equation 5.3 (the average value is 29.6 MPa). Very slender plates have a higher reduction in buckling capacity than sturdy plates, and the maximum absolute reduction in buckling capacity takes place for slenderness β=3.5.

Table 5.1 : Numerical analyses of axially loaded plates with heat affected zones along longitudinal edges

β [-]	Ultimate capacity of plates consisting of the base material [MPa]	Ultimate capacity of plates with heat affected zones along long edges [MPa]	Difference in ultimate capacity [MPa]	Percentage reduction in ultimate capacity [%]
1.0	303.1	277.8	25.3	8.35
1.5	266.6	240.1	26.5	9.94
2.0	224.1	196.7	27.4	12.2
2.5	196.6	168.6	28.0	14.2
3.0	182.5	152.2	30.3	16.6
3.5	174.5	140.4	34.1	19.5
4.0	160.9	128.4	32.5	20.2
4.5	148.3	116.6	31.7	21.4
5.0	136.9	105.9	31.0	22.6

A conclusion that can be drawn from these analyses is that the reduction in ultimate capacity due to the introduction of heat affected zones along long edges does not vanish if the mean average axial stress for the whole plate is below the reduced yield stress of the material in the heat affected zones. The reason for this is the uneven distribution of axial stresses along the cross section of the plate. The stresses in the parts of the plates that are affected by welding can be higher than the reduced material yield strength although the average stresses are not.

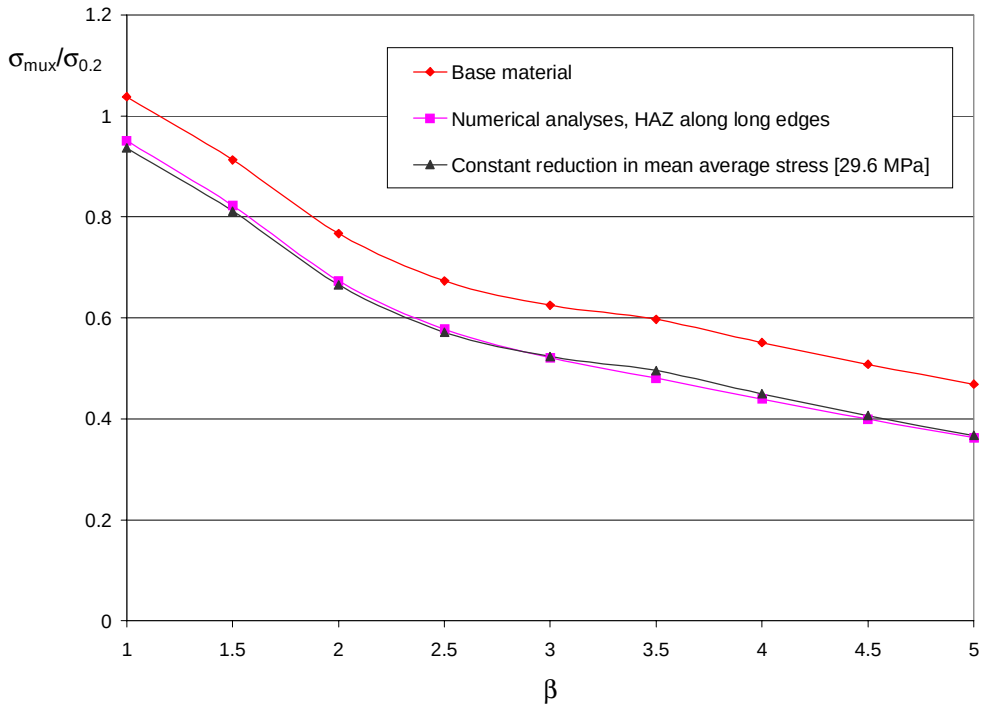

Figure 5.10 : Numerical analyses of axially loaded plates with heat affected zones along longitudinal edges compared with a constant reduction of mean ultimate axial stresses equal to 29.6 MPa. The plates consist of alloy 6082-T6.

Another conclusion from the results in Table 5.1 is that ignoring heat affected zones along long edges results in a much higher percentage error for slender plates than for sturdy plates. For a plate with slenderness β=4.0 the decrease in strength is almost twice as large as when the plate has a slenderness β=2.0.

If the plates have heat affected zones along all edges there is no longer the same absolute reduction in buckling capacity, but the percentage reduction is fairly constant with an average value of 24.5 %.

Table 5.2 : Numerical analyses of plates with heat affected zones along all edges

β [-]	Ultimate capacity of plates consisting of the base material [MPa]	Ultimate capacity of plates with heat affected zones along all edges [MPa]	Difference in ultimate capacity [MPa]	Percentage reduction in ultimate capacity [%]
1.0	303.1	237.7	65.4	21.6
1.5	266.6	197.7	68.9	25.8
2.0	224.1	174.9	49.2	22.0
2.5	196.6	155.0	41.6	21.2
3.0	182.5	140.8	41.7	22.8
3.5	174.5	129.1	45.4	26.0
4.0	160.9	118.0	42.9	26.7
4.5	148.3	108.4	39.9	26.9
5.0	136.9	99.56	37.3	27.3

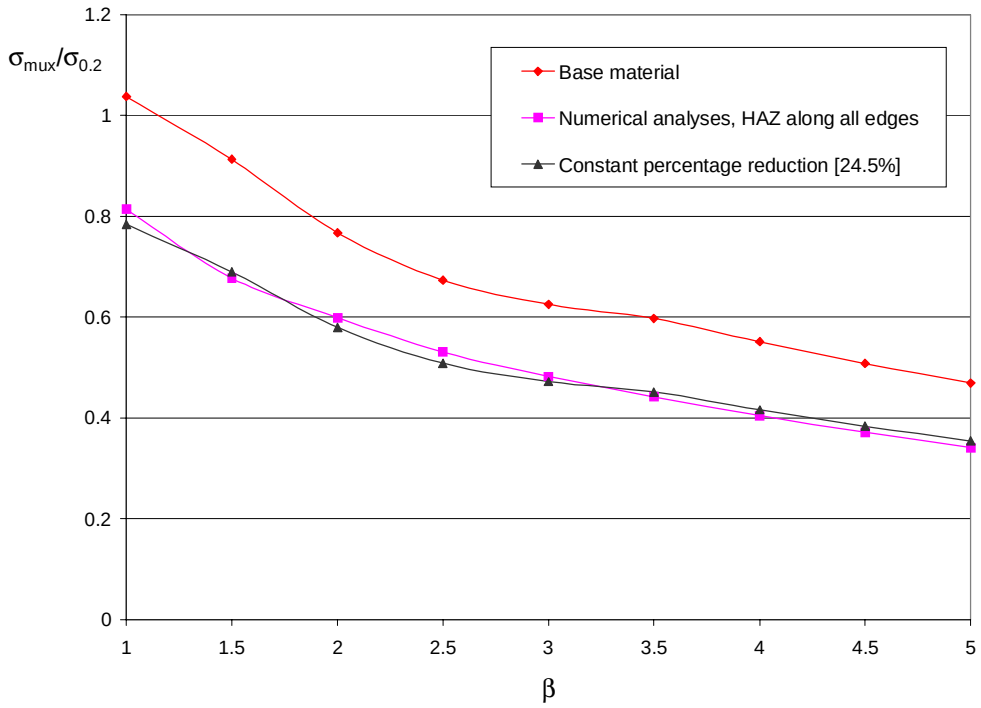

Figure 5.11 : Numerical analyses of axially loaded plates with heat affected zones along all edges compared with a constant percentage reduction of mean axial stress equal to 24.5 %. The plates consist of alloy 6082-T6.

5.3 Transverse loading

5.3.1 Introduction

In order to better understand the ultimate capacity of transversally loaded plates it is useful to have in mind that the load carrying capacity of transversally loaded plates can be handled as a summation of the capacity of a quadratic plate and a plate strip with longitudinal dimensions equal to the difference between the length and the breadth of the plates. This way of regarding the transverse loading capacity is extensively elaborated on in Chapters 7.3 and 10.2.

The way of treating residual stresses and soft zones is equal to the cases with axial loading. Only the combined effect of residual stresses and soft zones is investigated.

5.3.1.1 Combined Effect of Residual Stresses and Soft Zones

Figure 5.12 shows results of numerical analyses of transversally loaded plates that are exposed to the combined effect of residual stresses and soft zones. Analyses of plates with no heat affected zones, and plates with residual stresses only, are shown in the same figure.

The plates are made of alloy 6082-T6 and have heat affected zones along all edges. The breadth of the zones with residual stresses in tension is always 25 mm, and the residual stresses in tension are for all analyses equal to 75 % of the reduced yield strength in the heat affected zones. Figure 5.13 indicates the percentage reduction in strength caused by the combined effect of residual stresses and soft zones as compared to analyses with the base material only.

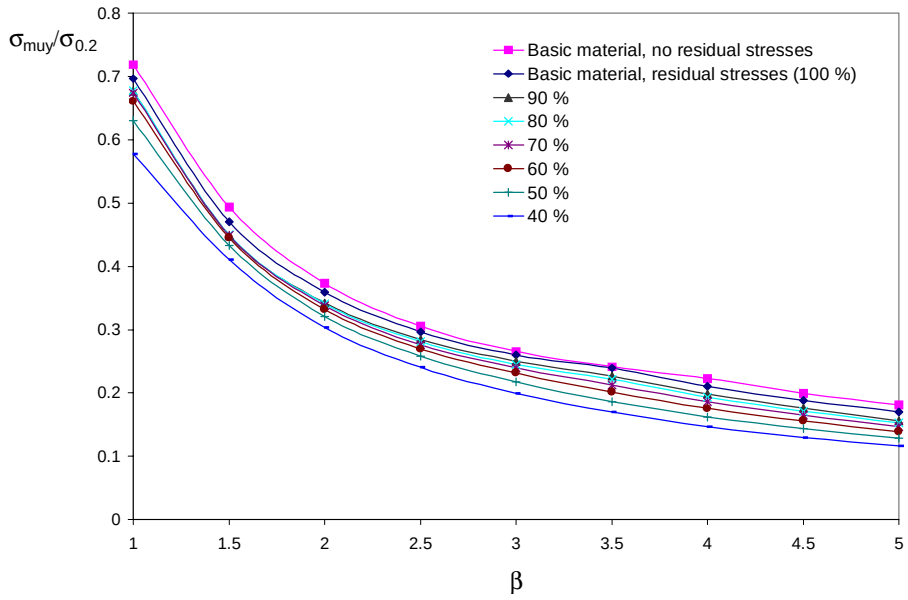

Figure 5.12 : Numerical analyses of transversally loaded plates exposed to the combined effect of residual stresses and soft zones. The plates are made of alloy 6082-T6.

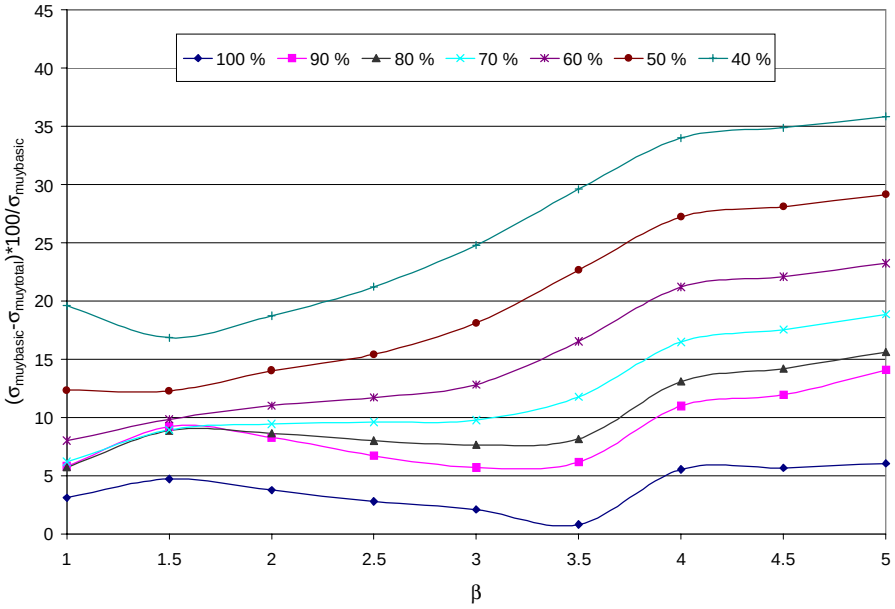

Figure 5.13 : Percentage reduction in strength caused by the combined effect of residual stresses and soft zones. The plates are made of alloy 6082-T6.

The ultimate transverse capacity is less susceptible to the presence of residual stresses than the axial capacity. The reason is that the transverse residual stresses in compression are much smaller.

For the same reduced slenderness,

$$\bar{\lambda} = \sqrt{\frac{\sigma_{0.2}}{\sigma_E}} \tag{5.4}$$

transversally loaded plates are less influenced by heat affected zones when the plates are sturdy, but as the reduced slenderness grows very large, axially and transversally loaded plates tend towards the same percentage reduction in buckling capacity.

The mid-part of sturdy, transversally loaded, plates contributes a larger portion of the total capacity than what is the case for more slender plates. As will be shown in Chapter 5.3.3 the ultimate capacity of the mid portion of the plates, with the behaviour of a plate strip, will not be affected by the heat affected zones (if the plates have heat affected zones along all edges; plates with the extruded pattern of the heat affected zones will be affected). As the plates become more slender, a larger portion of the load carrying capacity takes plates toward the edges of the plates, and the plates become more sensitive to the presence of heat affected zones.

5.3.1.2 Effect of the Size of the Heat Affected Zones

For a plate with heat affected zones along all edges, the breadth of the heat affected zones has been varied from 0 to 35 mm. Figures 5.14-5.15 show results from such analyses. The plates consisted of alloy 6082-T6. In every single analysis all the edges of the plate had the same

breadth of the heat affected zones. The yield strength in the heat affected zones was equal to 50 % of the yield strength of the base material and the residual stresses in tension were equal to 75 % of the reduced yield strength.

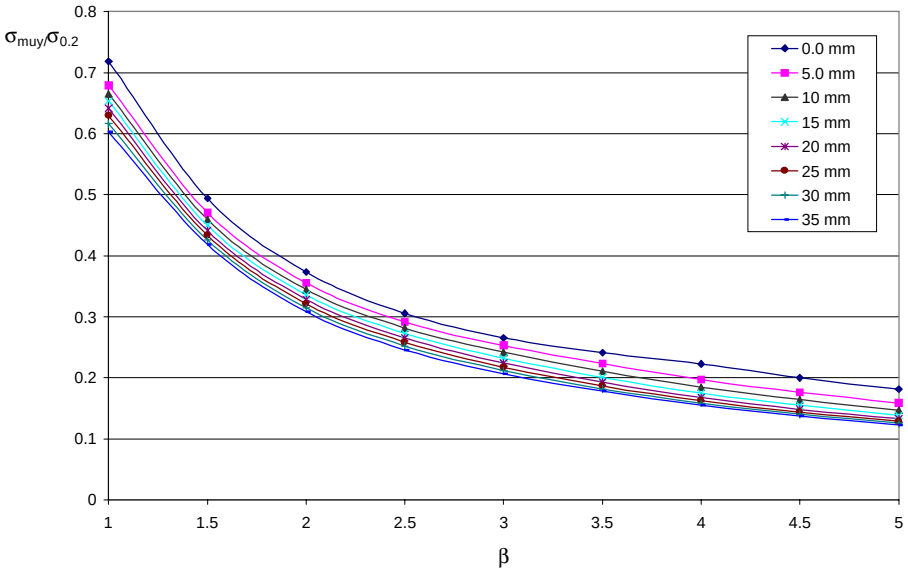

Figure 5.14 : Numerical analyses of plates with different breadths of the heat affected zones. The plates are made of alloy 6082-T6.

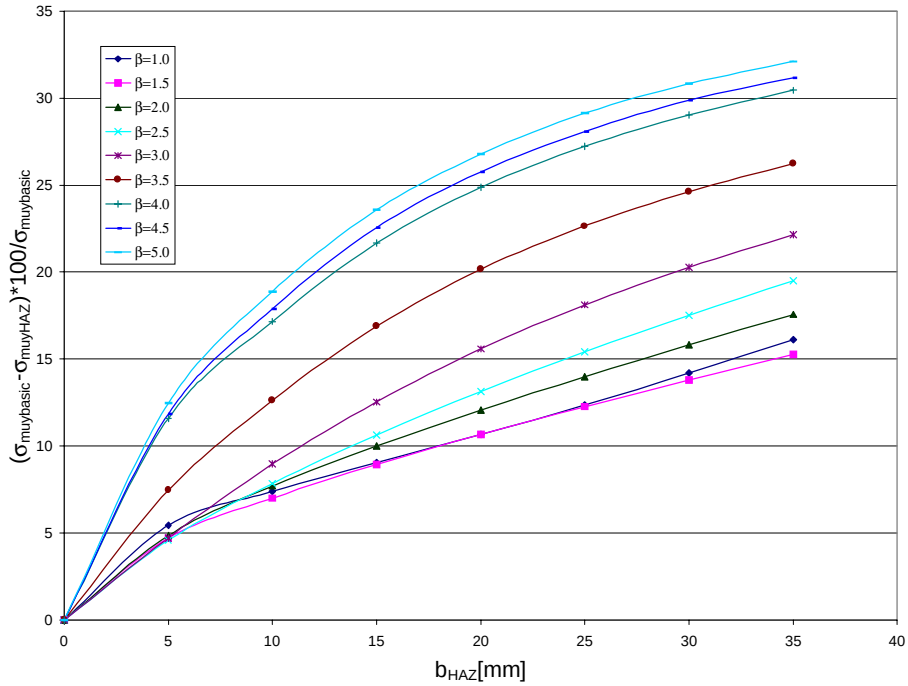

Figure 5.15 : Percentage reduction in strength for plates with different breadths of the heat affected zones. The plates are made of alloy 6082-T6.

As for the axially loaded case slender plates show a larger reduction in buckling capacity than sturdy plates. This is caused by the fact that slender plates carry a relatively larger portion of the load towards the edges of the plate, and for plates with heat affected zones along all edges

it is only in this region that the plates are susceptible to the effect of residual stresses and soft zones (see also Chapter 5.3.3).

5.3.2 Different Patterns of the Heat Affected Zones

Different patterns of the heat affected zones are considered and their effect on the ultimate capacity is compared. The alloy utilised is 6082-T6, and the breadth of all the heat affected zones was always 25 mm. The yield strength in the heat affected zones was equal to 50 % of the yield strength of the base material and the residual stresses in tension were equal to 75 % of the reduced yield strength. Figure 5.16 shows results from analyses of transversally loaded plates.

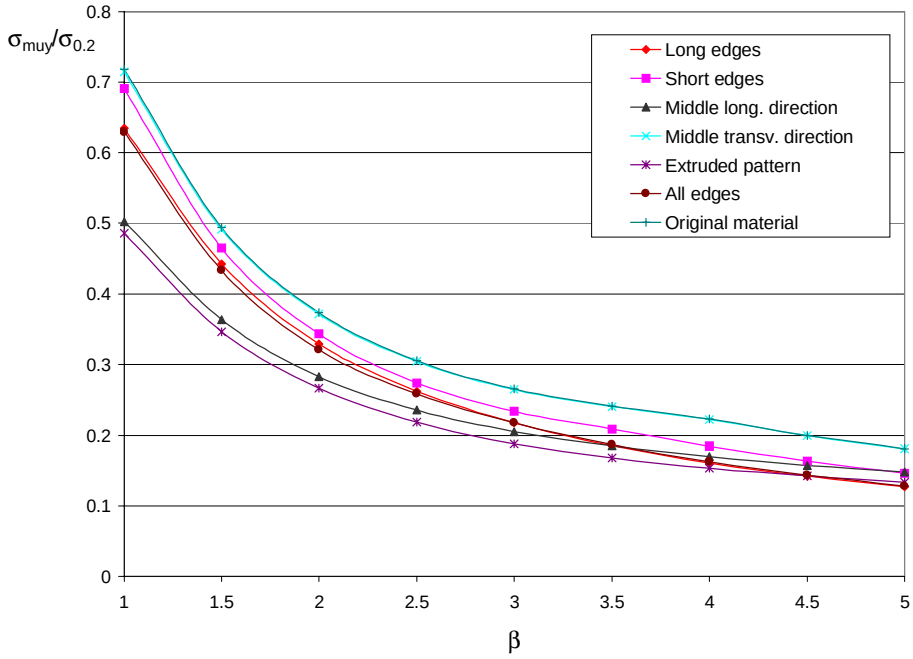

Figure 5.16 : Ultimate capacity of transversely loaded plates for different patterns of the heat affected zones. The plates consists of alloy 6082-T6.

Plates with the extruded pattern of the heat affected zones have the largest reduction in ultimate capacity, followed closely by plates with a heat affected zone in the middle-longitudinal direction. Among the different patterns of the heat affected zones considered (the patterns are given in Figures 2.1-2.6) the mid parts of the plates needed to have a heat affected zone in the middle-longitudinal direction to show any reduction in strength due to heat affected zones (details in Chapter 5.3.3). Plates with the extruded pattern of the heat affected zones and plates with a heat affected zone in the middle-longitudinal direction fulfil this requirement. In addition their heat affected zones make sure that the stresses along the short edges of the plates, that are in the range of the yield stresses, will be affected by the heat affected zones. Because plates with the extruded pattern of the heat affected zones have reduced material parameters along the whole length of the short edges, they will have the largest reduction in strength.

Plates with heat affected zones along all edges and plates with heat affected zones along long edges have almost identical ultimate capacities. The load carrying capacity of the quadratic end parts of the plates is almost identical, because the buckling capacities of quadratic plates with heat affected zones along loaded edges only and quadratic plates with heat affected zones along all edges are about the same. The mid portion of the plates also have the same buckling capacity, identical to a plate strip unaffected by welding.

If the plates have heat affected zones along short edges only the buckling capacity of the parts of plates that are close to the ends of the plates will increase as compared to plates with heat affected zones along longitudinal edges or heat affected zones along all edges. The reason for this is that the reduction in buckling capacity for quadratic plates with heat affected zones along unloaded edges is less than the reduction in buckling capacity for plates with heat affected zones along loaded edges or all edges.

Having a heat affected zone in the middle-transverse direction is harmless for transversally loaded plates. The heat affected zone is placed in a part of the plate with small stresses, and the direction of the heat affected zone makes it impossible to cause reduction in stresses for parts of the plates that are broader than the breadth of the heat affected zone itself.

5.3.3 Plate Strip Analyses

In the plate strip analyses the nodes at the short edges were free to move out of the x-y-plane, but all the nodes at one of the short edges must have the same x-co-ordinate.

Because a plate strip was considered to be the middle part of a plate, plates with no heat affected zones, heat affected zones along long edges and one heat affected zone in the middle-longitudinal direction were analysed. Plate strips with heat affected zones along long edges were believed to represent the middle part of a plate that have heat affected zones along all edges, and plates with a heat affected zone in the middle-longitudinal direction were believed to represent the middle part of plates with the extruded pattern of the heat affected zones.

All plates consisted of alloy 6082-T6, the reduction factor, α, in the heat affected zones was equal to 0.5 and the residual stresses in tension were equal to 75 % of the reduced yield stress. In all the analyses the breadth of the heat affected zones was equal to 25 mm. Figure 5.17 shows results from transversally loaded plate strips and figure 5.18 indicates the percentage reduction in buckling strength as compared to numerical analyses with no heat affected zones.

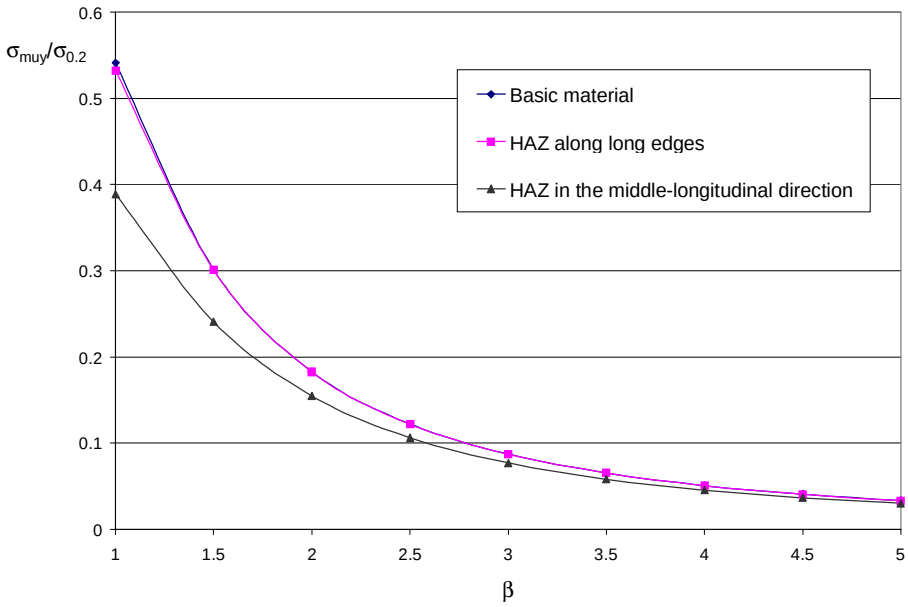

Figure 5.17 : Transverse ultimate capacity for plate strips. The plates consist of alloy 6082-T6, and the 0.2 percent tensile proof stress in the heat affected zones is half the value of the 0.2 percent tensile proof stress of the base material.

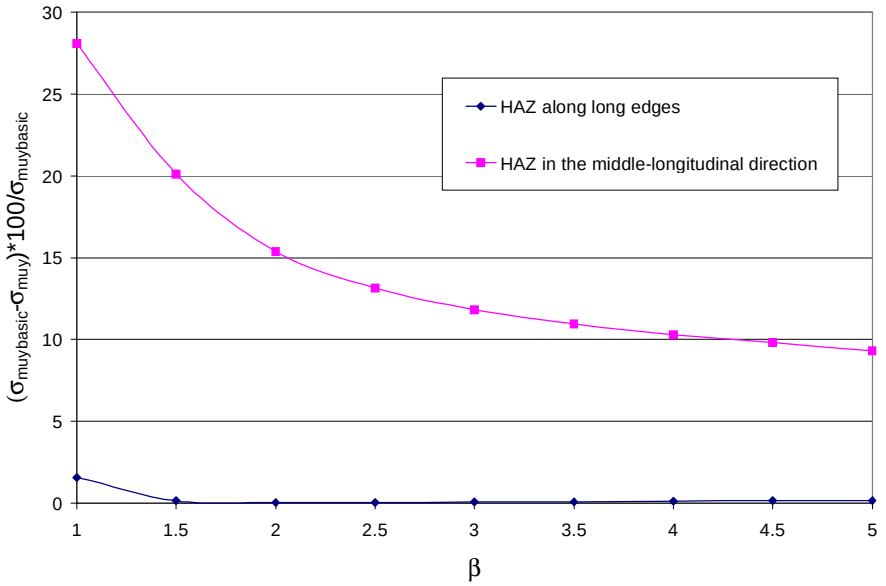

Figure 5.18 : Percentage reduction in ultimate capacity as compared to analyses with plates consisting of the base material only. The plates consist of alloy 6082-T6, and the 0.2 percent tensile proof stress in the heat affected zones is half the value of the 0.2 percent tensile proof stress of the base material.

Plate strips with heat affected zones along long edges are for all practical purposes unaffected by the introduction of the heat affected zones. The largest reduction takes place for β=1.0 and is equal to 1.6 %. This is because bending moments, according to the boundary conditions, at the long edges of the plates are close to zero. Therefore the stresses at the long edges of the

plates never reaches such magnitudes that significant yielding occurs with reduction in ultimate strength, even though the long edges are exposed to heat affected zones.

Introducing a heat affected zone in the middle-longitudinal direction causes a reduction in ultimate strength of 28.1 % for plates with slenderness β=1.0, and the reduction in collapse capacity is significant for all values of the slenderness analysed. The reduction in ultimate strength is never less than 9.3 %. At the middle of the plate the bending moments with resulting bending stresses have their highest values. Placing a heat affected zone is this part of the plates causes additional yielding with loss of strength.

5.4 Biaxial Compression

The main purpose of this chapter is to study the effect of introducing heat affected zones when dealing with biaxial interaction curves. Two different patterns of heat affected zones are considered, heat affected zones along all edges and the extruded pattern of the heat affected zones.

The plates are made of alloy 6082-T6. The reduction factor, α, in the heat affected zones is equal to 0.5, and the residual stresses in tension are equal to 75 % of the reduced yield stress. For all the analyses the breadth of the heat affected zones was set equal to 25 mm.

Only the interaction curves are compared. The differences in uniaxial buckling capacities are discussed in their respective chapters. It should be pointed out that the uniaxial strengths used for normalising may vary slightly from the uniaxial strengths found in chapters dealing with uniaxial capacities only. The is caused by the different eigenmodes used in the analyses (see Chapter 8 for details).

Figures 5.19-5.21 show biaxial interaction curves for plates consisting of the base material only and plates with different patterns of heat affected zones. The shape of the resulting interaction curves for a given slenderness, β, is compared in Figures 5.22-5.30.

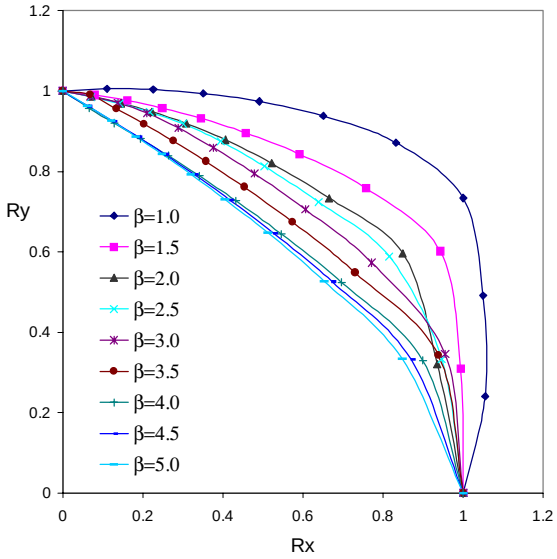

Figure 5.19 : Biaxial interaction curves for plates consisting of the base material only.

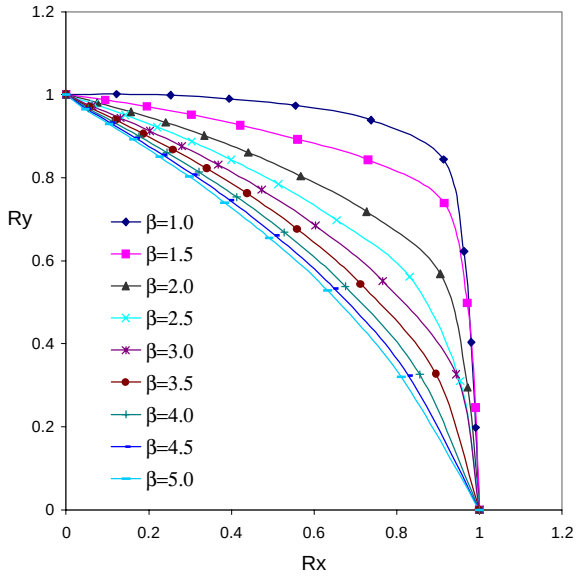

Figure 5.20 : Biaxial interaction curves for plates with HAZ along all edges

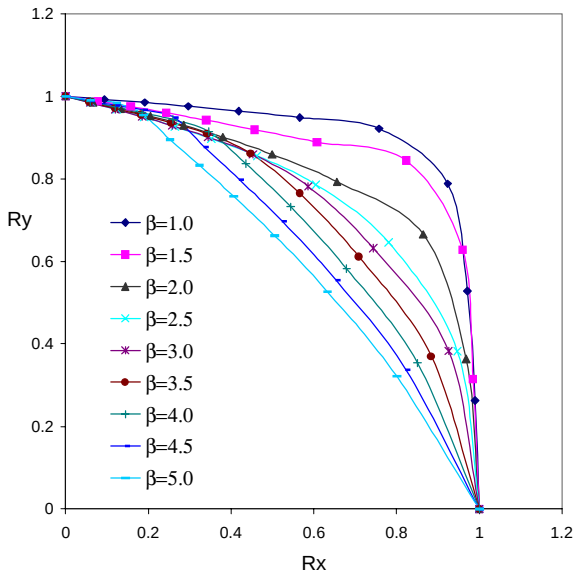

Figure 5.21 : Biaxial interaction curves for plates with the extruded HAZ pattern

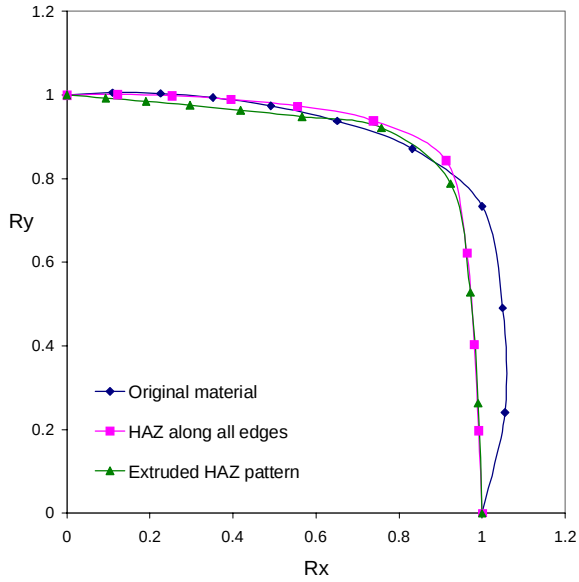

Figure 5.22 : Comparison of biaxial inter-action curves for slenderness β=1.0

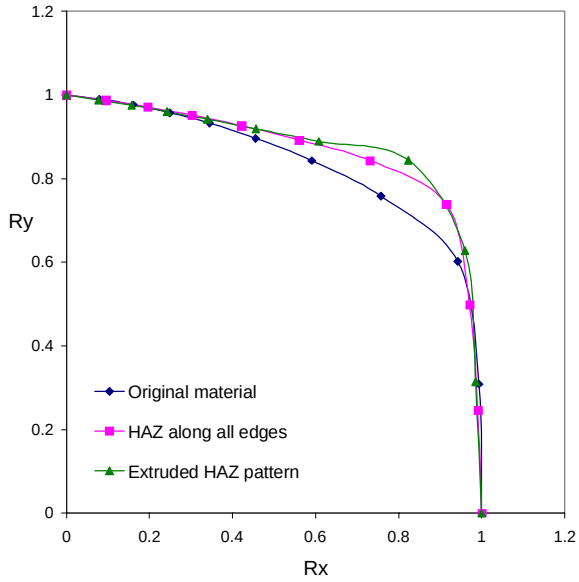

Figure 5.23 : Comparison of biaxial inter-action curves for slenderness β=1.5

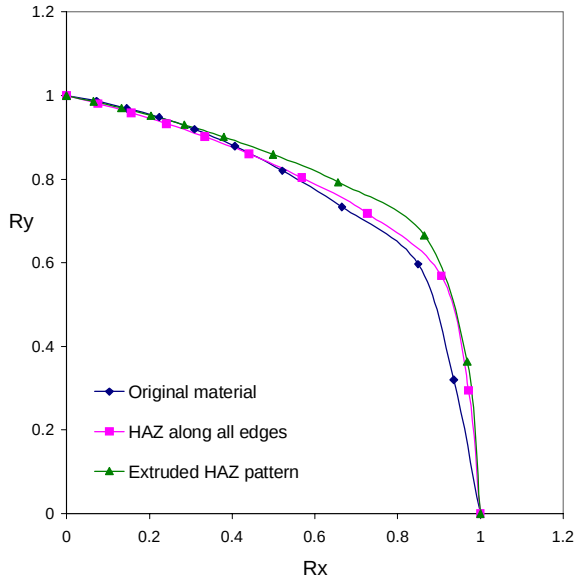

Figure 5.24 : Comparison of biaxial interaction curves for slenderness β=2.0

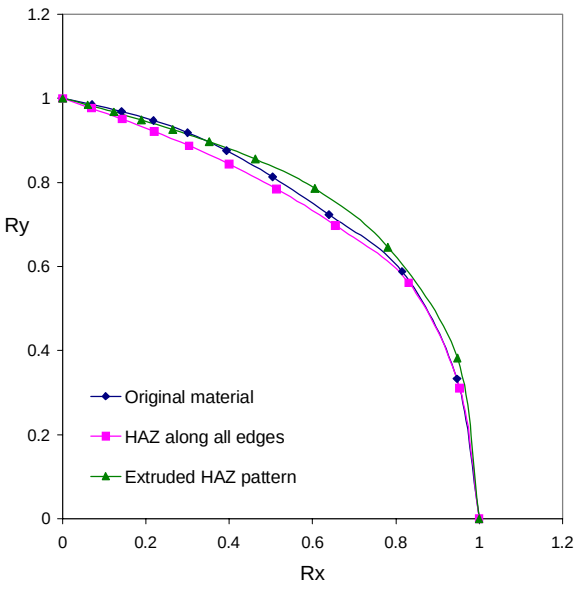

Figure 5.25 : Comparison of biaxial interaction curves for slenderness β=2.5

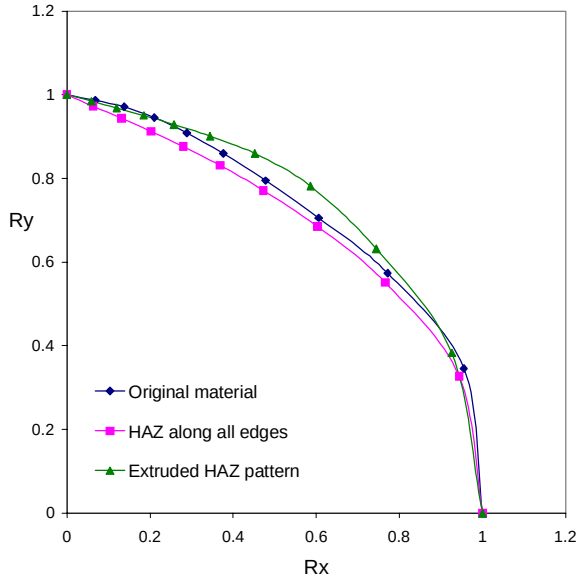

Figure 5.26 : Comparison of biaxial interaction curves for slenderness β=3.0

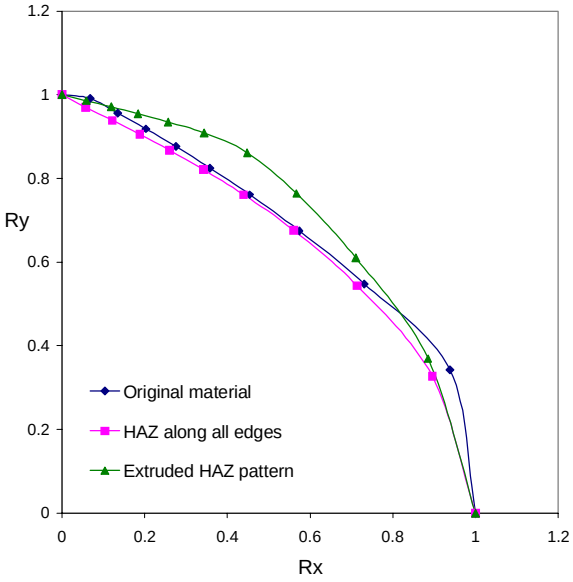

Figure 5.27 : Comparison of biaxial interaction curves for slenderness β=3.5

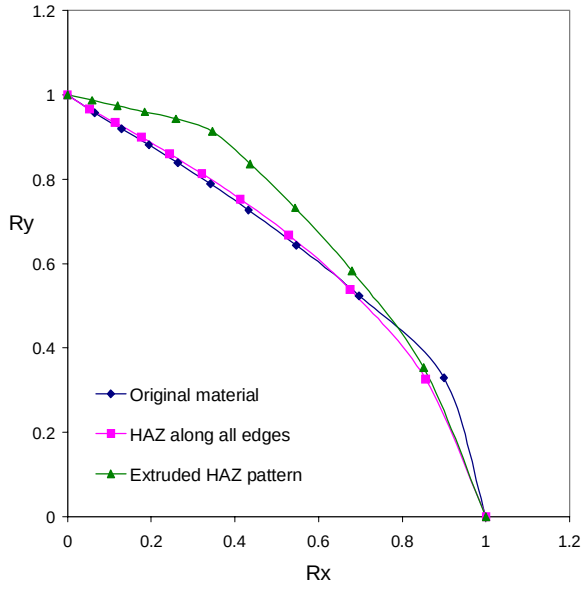

Figure 5.28 : Comparison of biaxial interaction curves for slenderness β=4.0

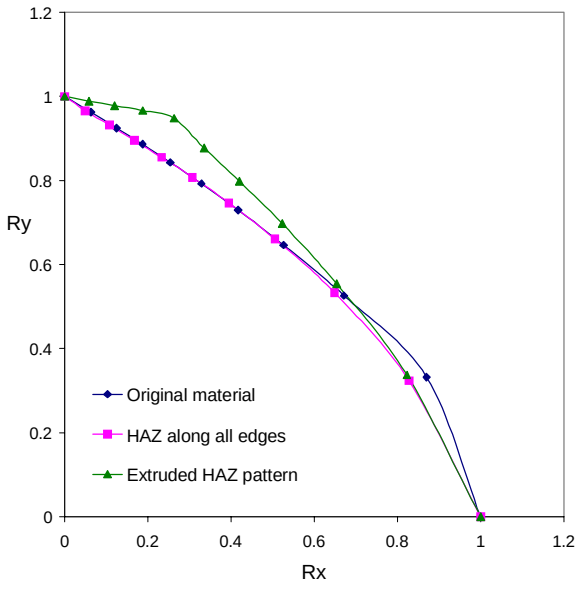

Figure 5.29 : Comparison of biaxial interaction curves for slenderness β=4.5

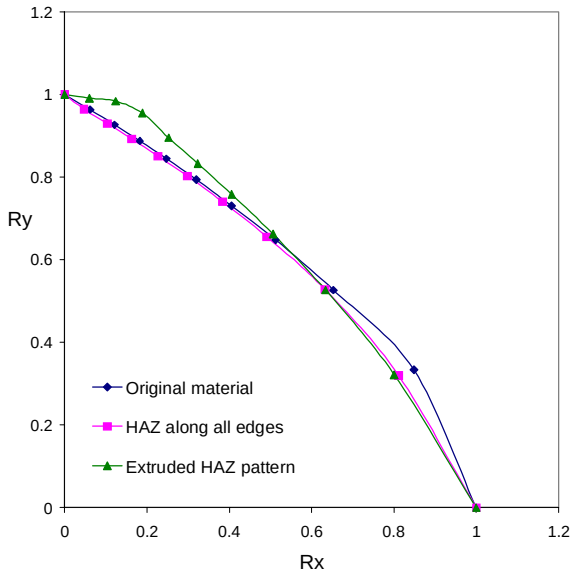

Figure 5.30 : Comparison of biaxial interaction curves for slenderness β=5.0

It is observed that the discrepancies between the interaction curves for the different patterns of the heat affected zones are not large; especially the interaction curves for plates consisting of the base material only and the interaction curves for plates with heat affected zones along all edges are very similar.

Plates with the extruded pattern of the heat affected zones show the weakest interaction, particularly for plates loaded mainly in transverse compression. Much of the transverse collapse capacities are governed by the introduction of a heat affected zone in the middle-longitudinal direction. This heat affected zone has little influence for the axial collapse capacities, making the transverse collapse capacity independent of the axial capacity. As the

axial portion of the loading grows larger the influence of the heat affected zone in longitudinal direction gradually decreases, and the behaviour of the plates with the extruded pattern of the heat affected zones become identical to the behaviour of the plates with heat affected zones along all edges.

5.5 Pure Shear Load

For plates exposed to pure shear loading only plates consisting of the base material and plates with heat affected zones along all edges have been investigated. Numerical analyses of plates made of alloy 6082-T6 are shown in Figure 5.31. Plates with residual stresses only and soft zones only and plates exposed to the combined effect of residual stresses and soft zones have been analysed.

The reduction factor, α, in the heat affected zones was set equal to 0.5, and the residual stresses in the heat affected zones was equal to 75 % of the reduced yield stress. The breadth of the heat affected zones was always 25 mm. Figure 5.32 indicates the reduction in ultimate capacities as compared to analyses with plates consisting of the base material only.

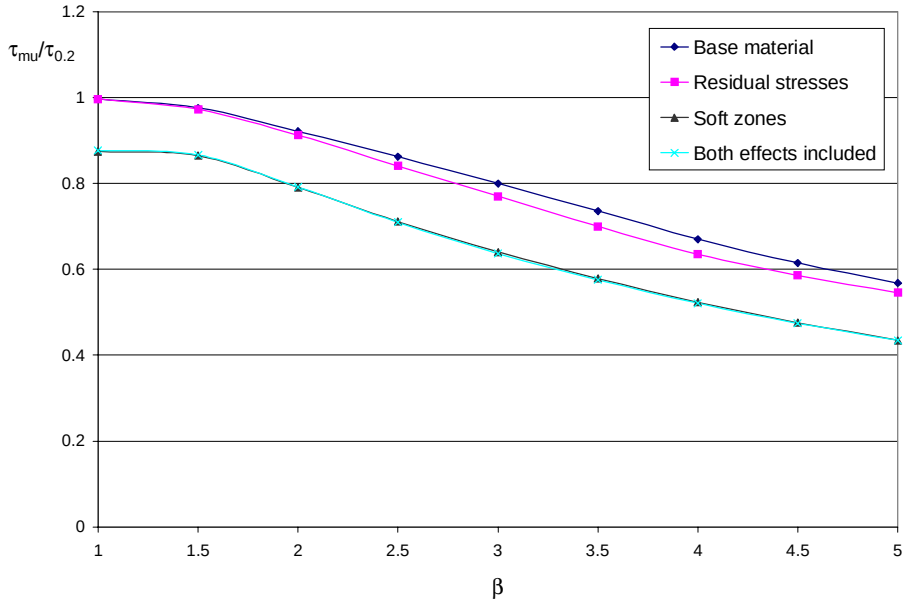

Figure 5.31 : Ultimate capacities of plates made of alloy 6082-T6 exposed to pure shear load

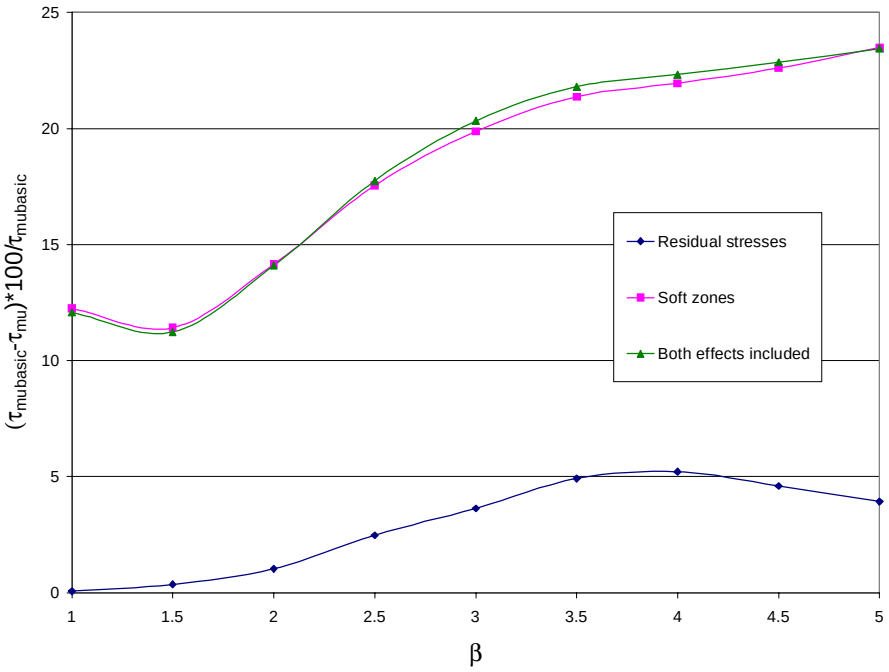

Figure 5.32 : Percentage reduction in shear ultimate capacity for plates exposed to heat affected zones along all edges. The plates are made of alloy 6082-T6.

The residual stresses significantly reduced the shear ultimate capacities for slender plates. Plates with an axial slenderness β=4.0 had a reduction in shear ultimate strength equal to 5.2 %. The collapse capacities for plates exposed to the combined effect of soft zones and residual stresses are dominated by the soft zones.

5.6 Axial Compression in Combination with Shear Loads

Axial compression in combination with shear loads has been studied for plates made of the base material and plates with heat affected zones along all edges. The plates were made of alloy 6082-T6 and had yield stresses in the heat affected zones equal to half the yield stress of the base material. The residual stresses in tension were equal to 75 % of the reduced yield stress in the heat affected zones, and the breadth of the heat affected zones was always 25 mm.

Figures 5.33-5.34 give the interaction curves for plates made of the base material only and plates exposed to the combined effect of residual stresses and soft zones. The interaction curves for the different values of the slenderness, β, are compared in Figures 5.35-5.43.

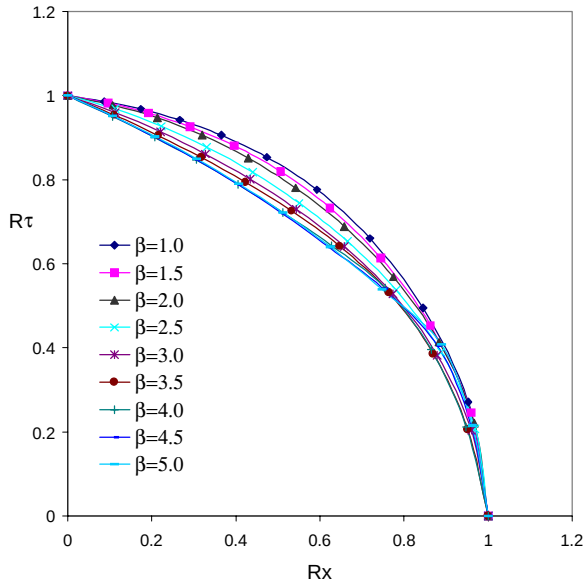

Figure 5.33 : Interaction curves for plates exposed to axial compression in combination with shear loads. The plates are made of the base material only.

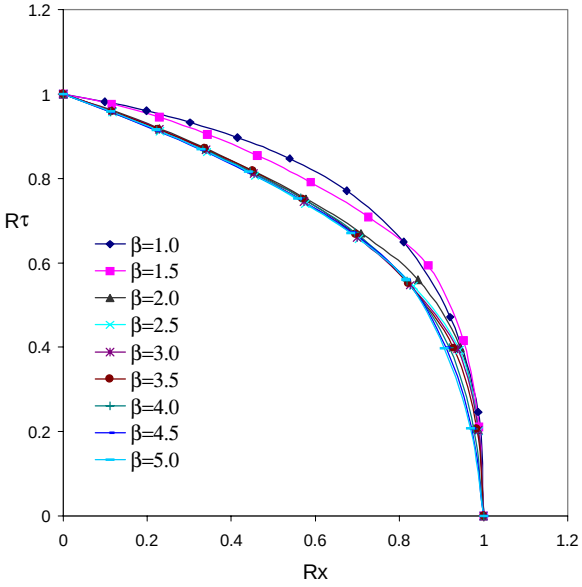

Figure 5.34 : Interaction curves for plates exposed to axial compression in combination with shear loads. The plates have heat affected zones along all edges.

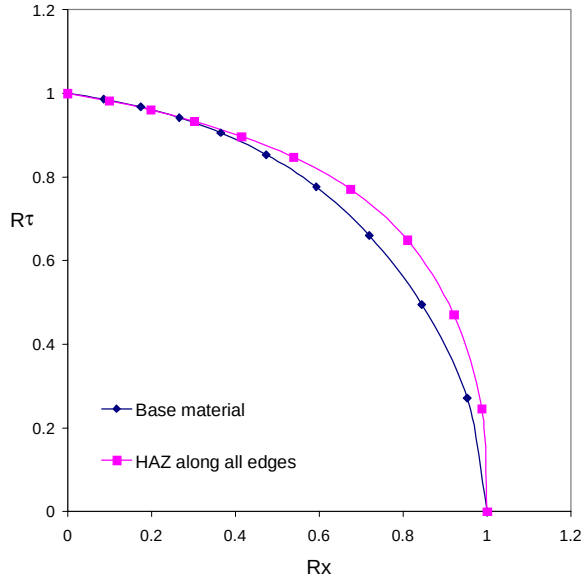

Figure 5.35 : Comparison of interaction curves for slenderness β=1.0

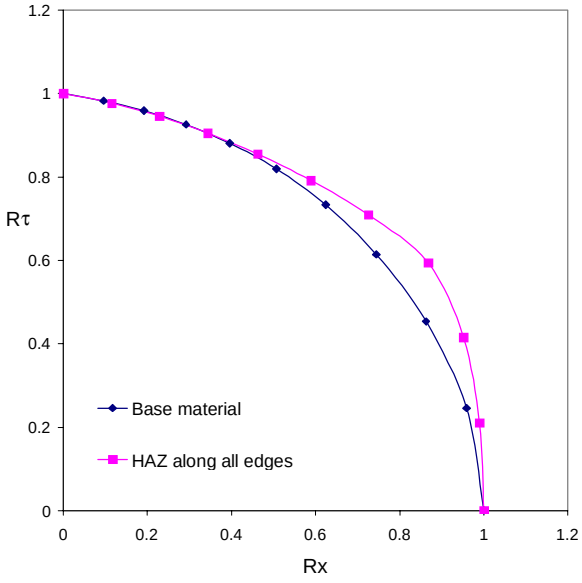

Figure 5.36 : Comparison of interaction curves for slenderness β=1.5

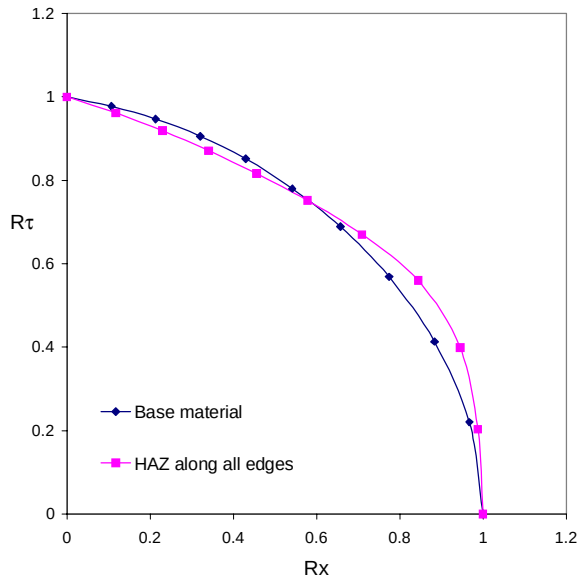

Figure 5.37 : Comparison of interaction curves for slenderness β=2.0

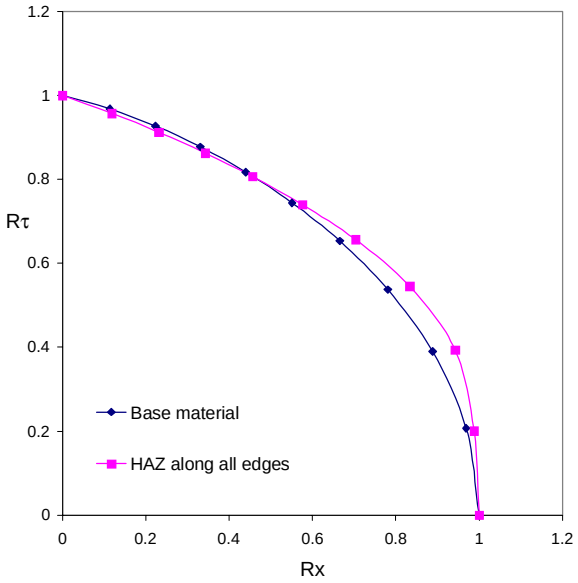

Figure 5.38 : Comparison of interaction curves for slenderness β=2.5

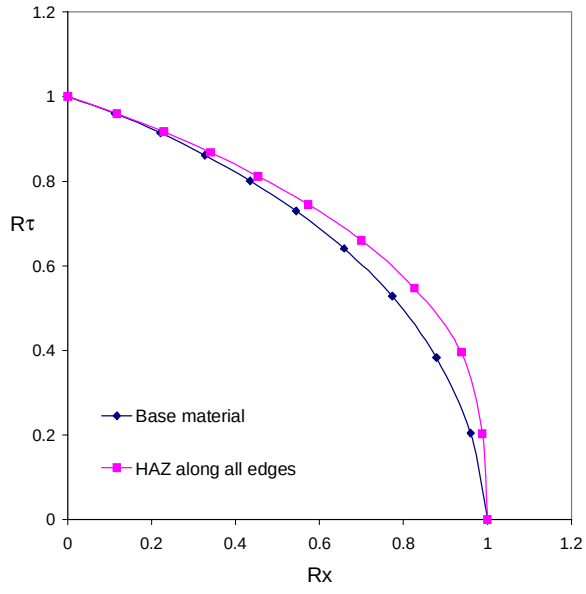

Figure 5.39 : Comparison of interaction curves for slenderness β=3.0

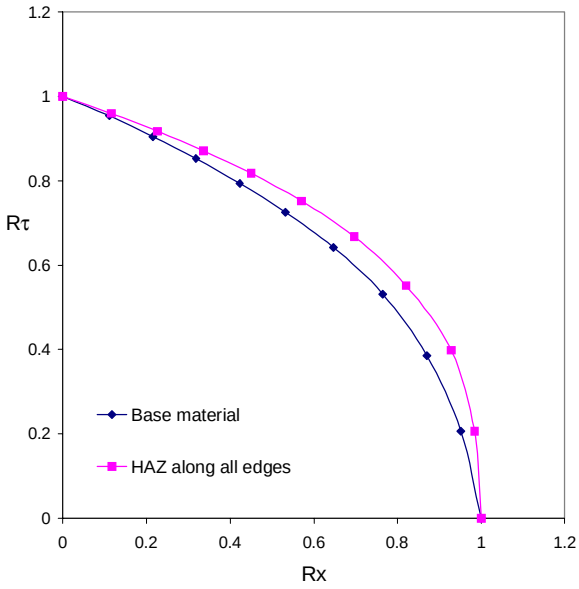

Figure 5.40 : Comparison of interaction curves for slenderness β=3.5

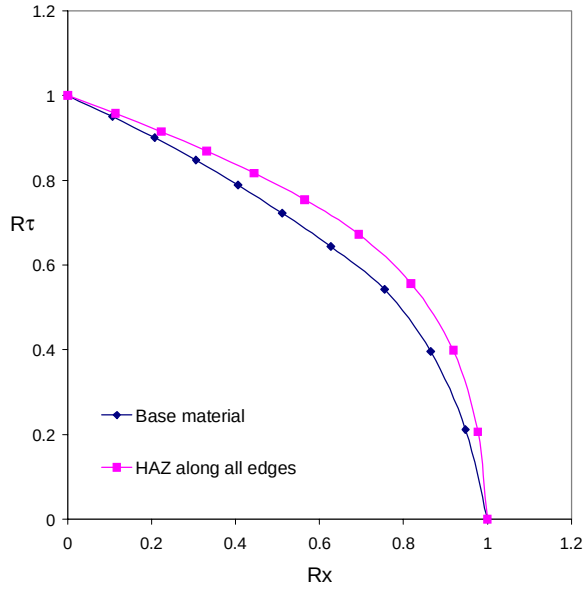

Figure 5.41 : Comparison of interaction curves for slenderness β=4.0

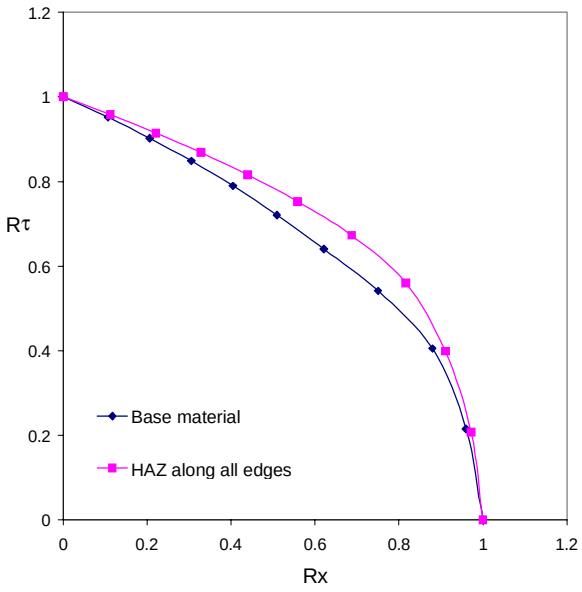

Figure 5.42 : Comparison of interaction curves for slenderness β=4.5

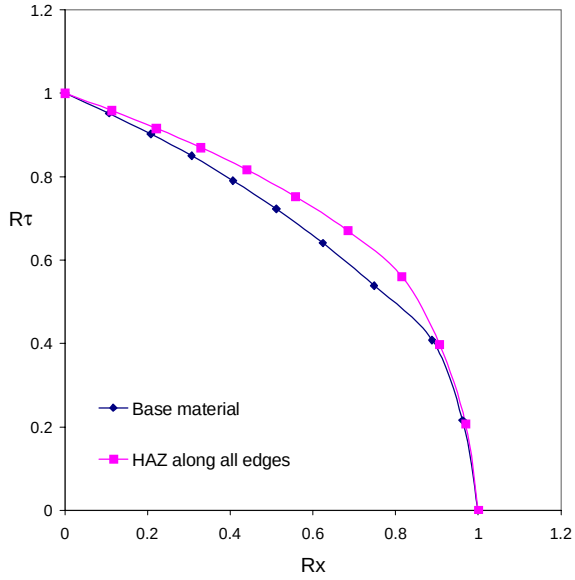

Figure 5.43 : Comparison of interaction curves for slenderness β=5.0

Plates consisting of the base material only show stronger interaction than plates that have been exposed to heat affected zones along all edges. The only exceptions are insignificant differences in the interaction curves for plates loaded mainly by shear loads and having a slenderness, β, equal to 2.0 or 2.5.

Chapter 6

Effect of Boundary Conditions on the Ultimate Capacity

6.1 Introduction

The boundary condition used for most of the analyses in this thesis is straight, simply supported edges (see also Chapter 4.4). This is believed to give a realistic representation for aluminium plates in marine vessels. The boundary condition chosen for most of the analyses is a compromise between the two extremities, free, simply supported edges and straight, clamped edges.

By examining the extreme boundary conditions an interval for which the actual collapse capacities will be found can be established, and one can see where in this interval the ultimate capacities for straight, simply supported edges are located. It is also interesting to study whether introduction of heat affected zones has the same reducing effect independent of boundary conditions, or if the reduction in ultimate capacity vary upon the different boundary conditions.

In this chapter axially loaded plates, transversally loaded plates and plate strips have been exposed to different boundary conditions. Both plates consisting of the base material and plates with heat affected zones along all edges are considered.

6.2 Axial Loading

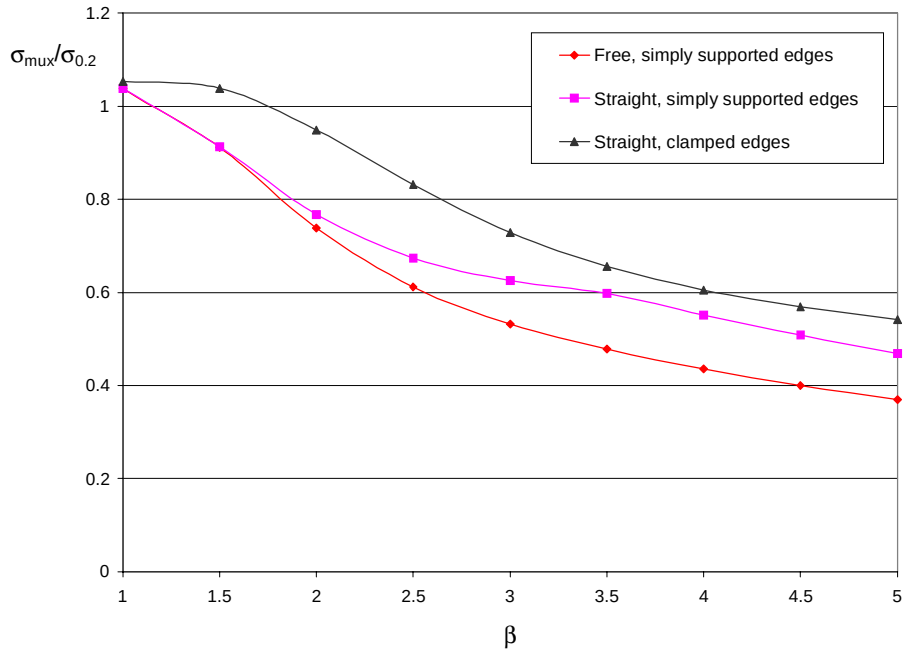

Figure 6.1 : Axial ultimate capacity for plates with different boundary conditions. The plates consist of base material only.

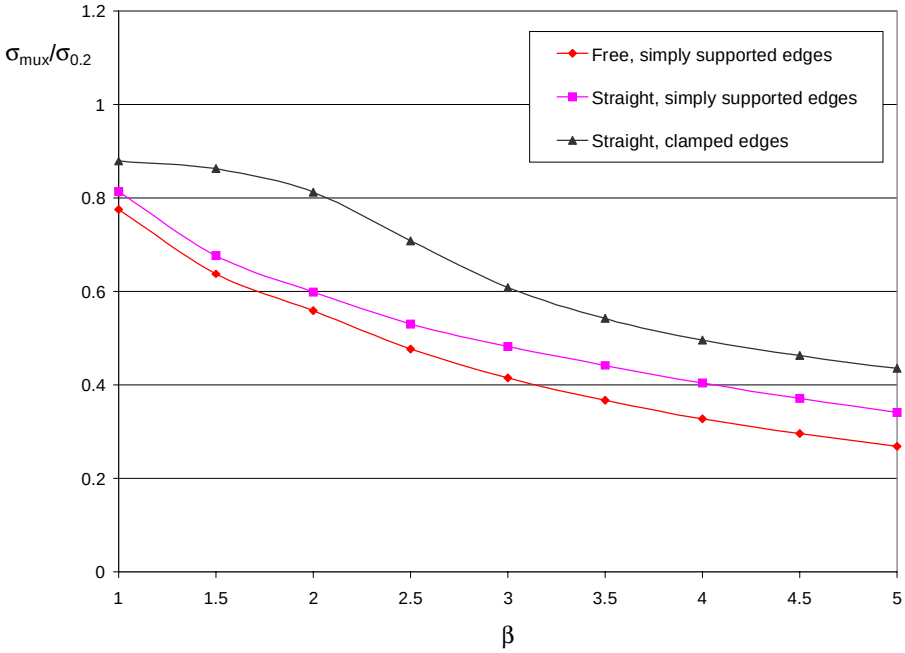

Figure 6.2 : Axial ultimate capacity for plates with different boundary conditions. The plates have heat affected zones along all edges.

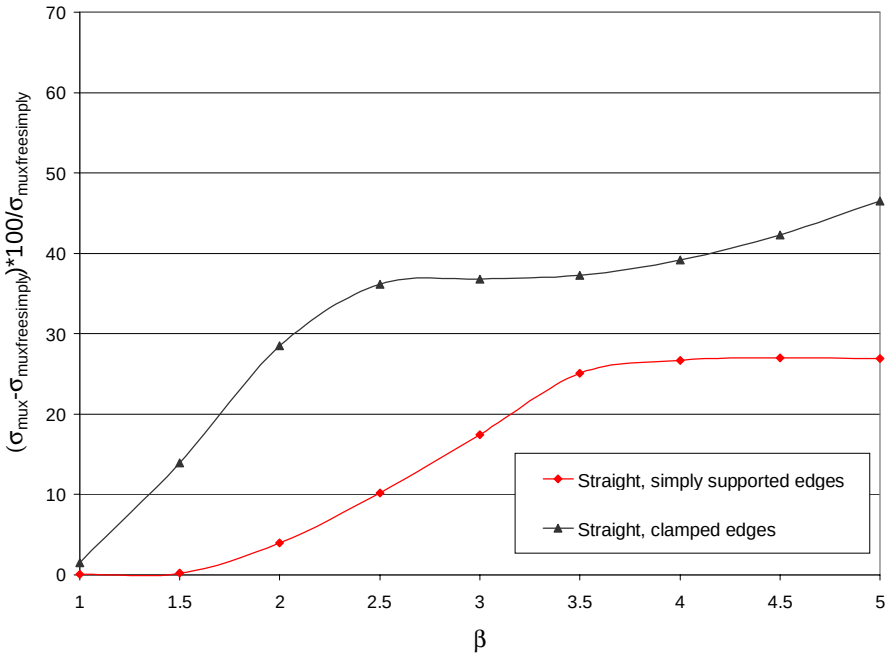

Figure 6.3 : Percentage increase in ultimate capacity as compared to plates with free, simply supported edges. The plates consist of base material only.

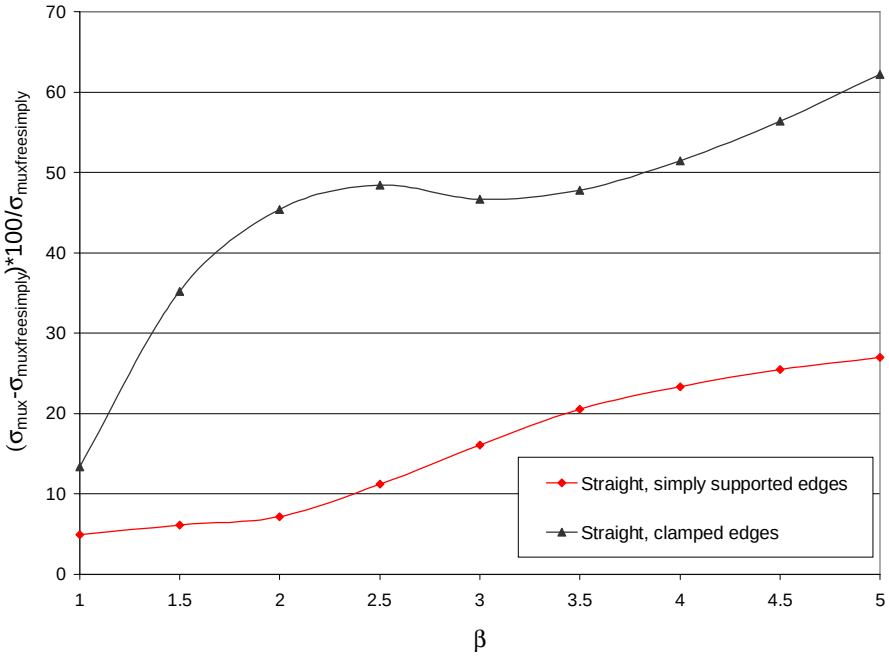

Figure 6.4 : Percentage increase in ultimate capacity as compared to plates with free, simply supported edges. The plates have heat affected zones along all edges.

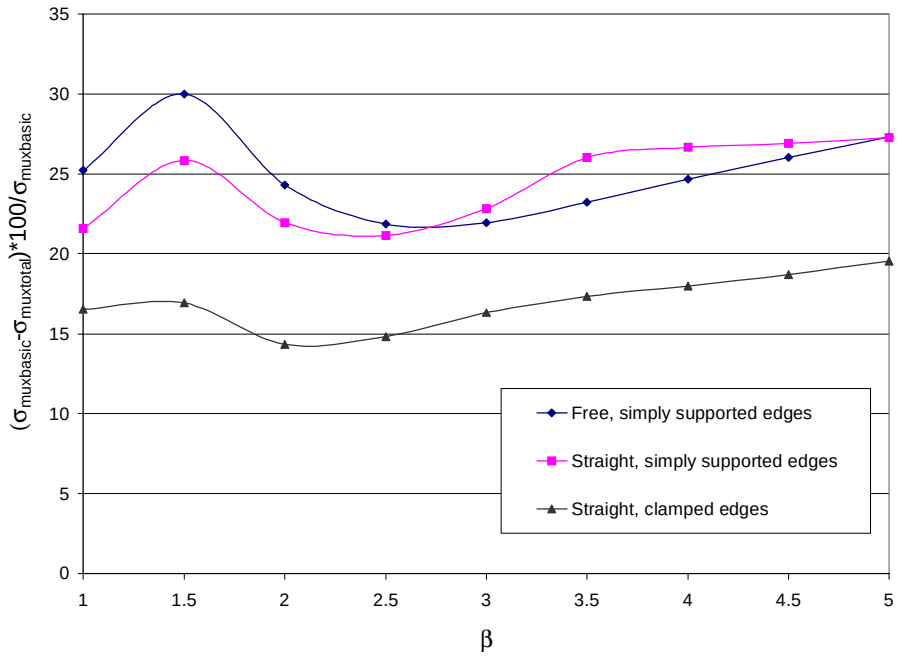

Figure 6.5 : Percentage reduction in ultimate capacity due to the introduction of heat affected zones along all edges for different boundary conditions

The ultimate capacities for axially loaded plates made of alloy 6082-T6 are given in Figures 6.1-6.2. Figure 6.1 shows the results for plates consisting of the base material only, and Figure 6.2 gives the ultimate capacities for plates exposed to heat affected zones along all edges. The increase in collapse capacity as compared to plates with free, simply supported edges is given in Figures 6.3-6.4.

The reductions in ultimate capacities when the plates are exposed to heat affected zones as compared to analyses without heat affected zones are given in Figure 6.5. The curves indicate the percentage reduction for the different boundary conditions analysed.

Changing the boundary conditions from free, simply supported edges to straight, simply supported edges has little effect for sturdy plates. If the plates have no heat affected zones, changing the boundary conditions from free, simply supported edges to straight, simply supported edges has no effect at all. As the plates become more slender the differences in buckling capacities between plates with free, simply supported edges and straight, simply supported edges increase.

Slender plates carry a larger percentage of the ultimate capacity along the longitudinal edges of the plates, and they are easier to deform than more sturdy plates which collapse in more crushing like fashions. Keeping the edges straight assures pure straining along the edges and obstructs geometrical changes close to the edges.

When the boundary conditions are changed from free, simply supported edges to straight, simply supported edges, plates consisting of the base material only and plates with heat affected zones along all edges have very similar increases in strength (the differences between the two curves in Figures 6.3 and 6.4 are never larger than 4.9 %). This is not the case if the boundary conditions are altered from free, simply supported edges to straight, clamped edges. Plates with heat affected zones along all edges have a substantially larger increase in collapse strength than plates consisting of the base material only (the largest difference between the curves in Figures 6.3 and 6.4 is 21.3 %).

An other way to express to observations in the previous paragraph can be found by looking at Figure 6.5. Plates with straight, clamped edges have a substantially less reduction in strength by the introduction of heat affected zones than plates with free, simply supported edges or plates with straight, simply supported edges. Plates with free, simply supported edges and plates with straight, simply supported edges have very similar reductions in ultimate capacity by the introduction of heat affected zones.

6.3 Transverse Loading

Transversally loaded plates are handled in the same way as axially loaded plates. The corresponding ultimate capacities for plates made of alloy 6082-T6 are given in Figures 6.6-6.7. Figure 6.6 shows results for plates consisting of the base material only. Figure 6.7 refers to plates with heat affected zones along all edges. The increase in ultimate capacity as compared to plates with free, simply supported edges is given in Figures 6.8-6.9. The reductions in ultimate capacities when the plates are exposed to heat affected zones as compared to analyses without heat affected zones are given in Figure 6.10.

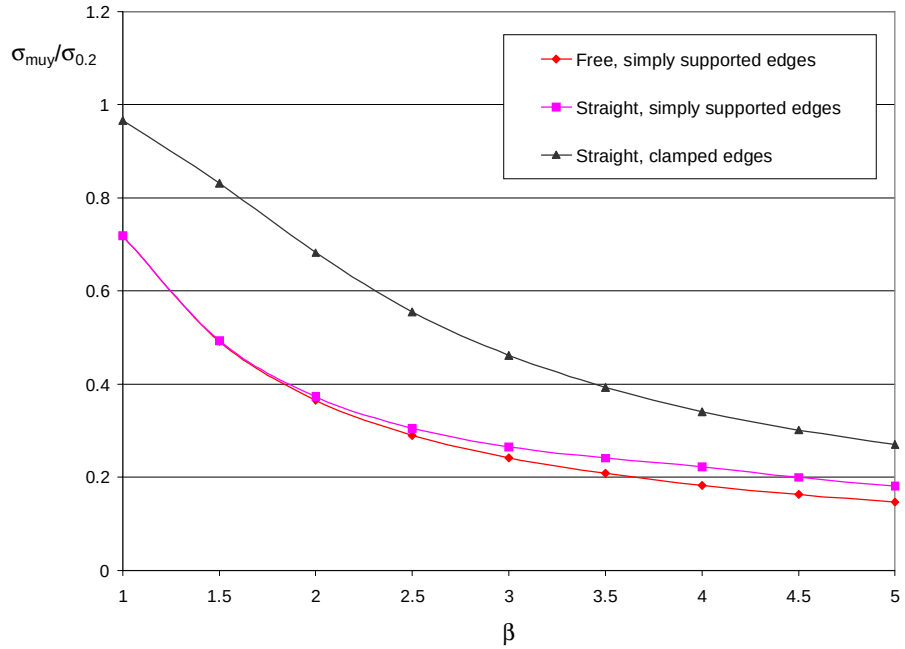

Figure 6.6 : Transverse ultimate capacity for plates with different boundary conditions. The plates consist of base material only.

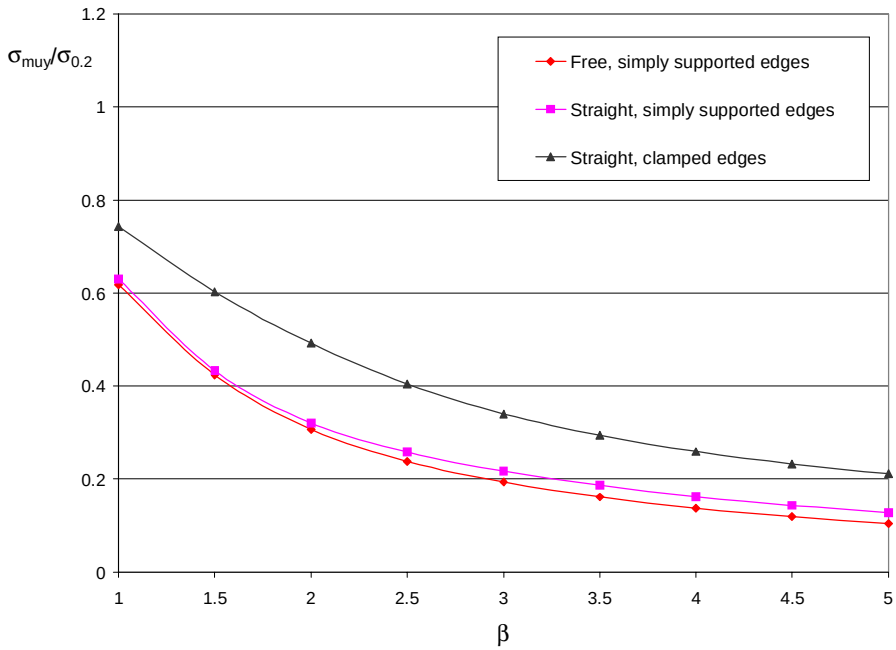

Figure 6.7 : Transverse ultimate capacity for plates with different boundary conditions. The plates have heat affected zones along all edges.

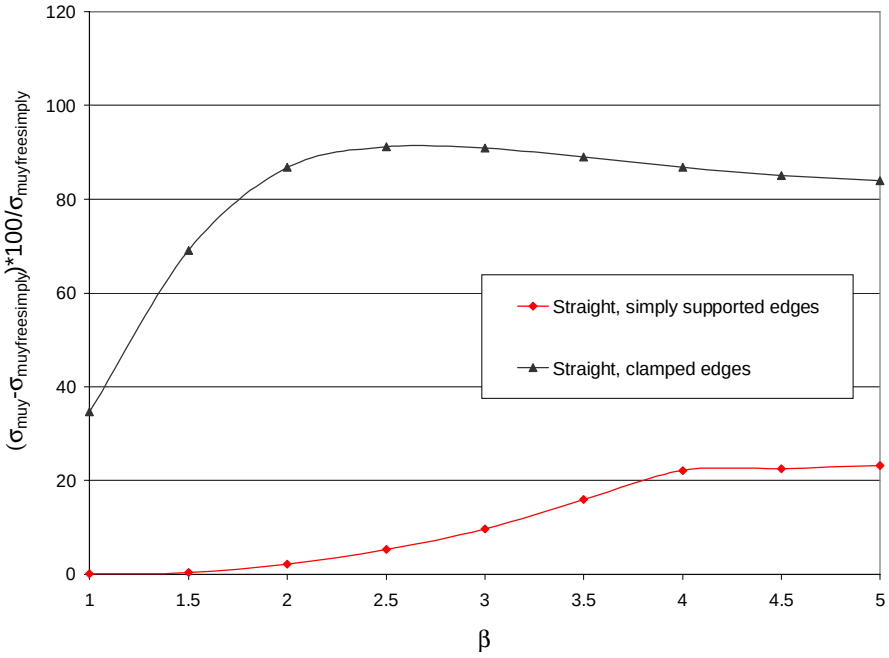

Figure 6.8 : Percentage increase in ultimate capacity as compared to plates with free, simply supported edges. The plates consist of the base material only.

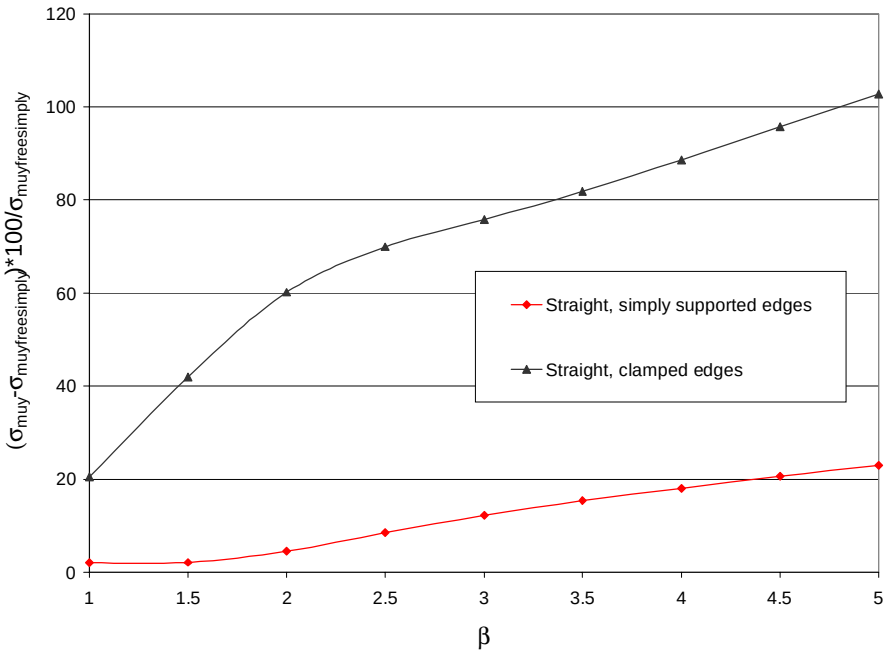

Figure 6.9 : Percentage increase in ultimate capacity as compared to plates with free, simply supported edges. The plates have heat affected zones along all edges.

The reduction in ultimate capacity due to heat affected zones is illustrated in Figure 6.10. The curves indicate the percentage reduction for the different boundary conditions analysed.

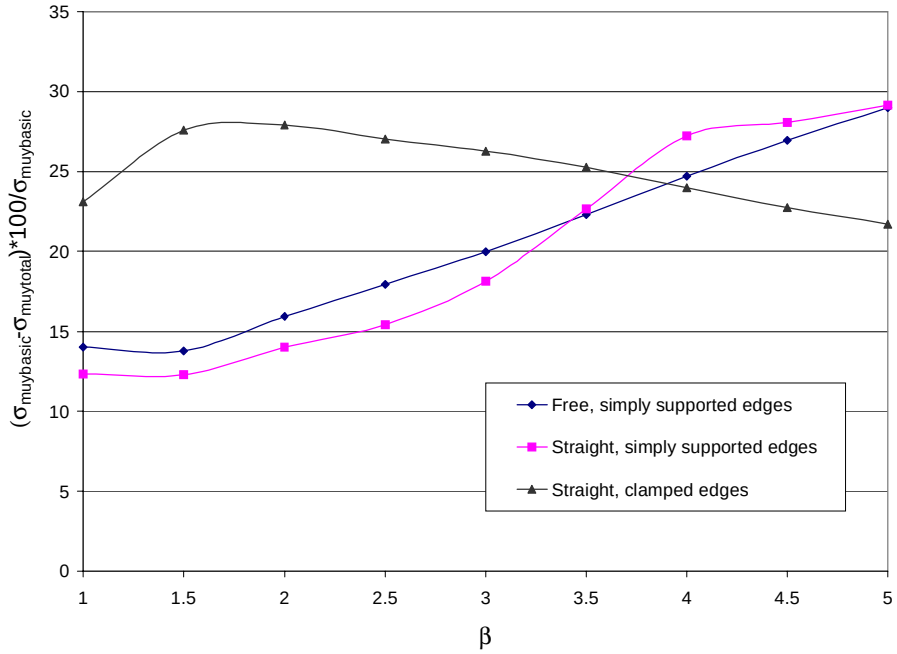

Figure 6.10 : Percentage reduction in ultimate capacity due to the introduction of heat affected zones along all edges for the different boundary conditions analysed

Changing the boundary conditions from free, simply supported edges to straight, simply supported edges does not increase the ultimate capacities as much as for axially loaded plates. The reason is that more of the load carrying takes place in the mid part of the plates. The mid part of the plates, with behaviour equal to a plate strip, are not affected by changing the boundary conditions from free, simply supported edges to straight, simply supported edges at all (details in Chapter 6.4). However, the trend is the same, altering the boundary conditions from free, simply supported edges to straight, simply supported edges has little effect for sturdy plates, but significantly increase the ultimate capacity for slender plates.

As for the axially loaded case; plates with free, simply supported edges and plates with straight, simply supported edges have very similar reductions in ultimate capacity by the introduction of heat affected zones.

Plates with straight, clamped edges have much larger reductions in ultimate capacity due to introduction of heat affected zones along all edges than plates with free, simply supported edges or plates with straight, simply supported edges (the only exceptions are for very slender plates where the reductions in ultimate capacity due to introduction of heat affected zones are about the same for all three boundary conditions studied). These trends are the opposite trends as to what happens in the axially loaded cases. The reason for this behaviour is that the mid parts of the plates, with behaviour similar to a plate strip, have their maximum bending moments in the parts of the plates with heat affected zones (more details in Chapter 6.4).

6.4 Plate Strip Analyses

In the same manner as for transversally loaded plates, the ultimate capacity for plate strips with different boundary conditions are given in Figures 6.11-6.12. The increase in collapse capacity as compared to plates with free, simply supported edges is given in Figures 6.13-6.14. The reductions in ultimate capacities when the plates are exposed to heat affected zones as compared to analyses without heat affected zones are given in Figure 6.15.

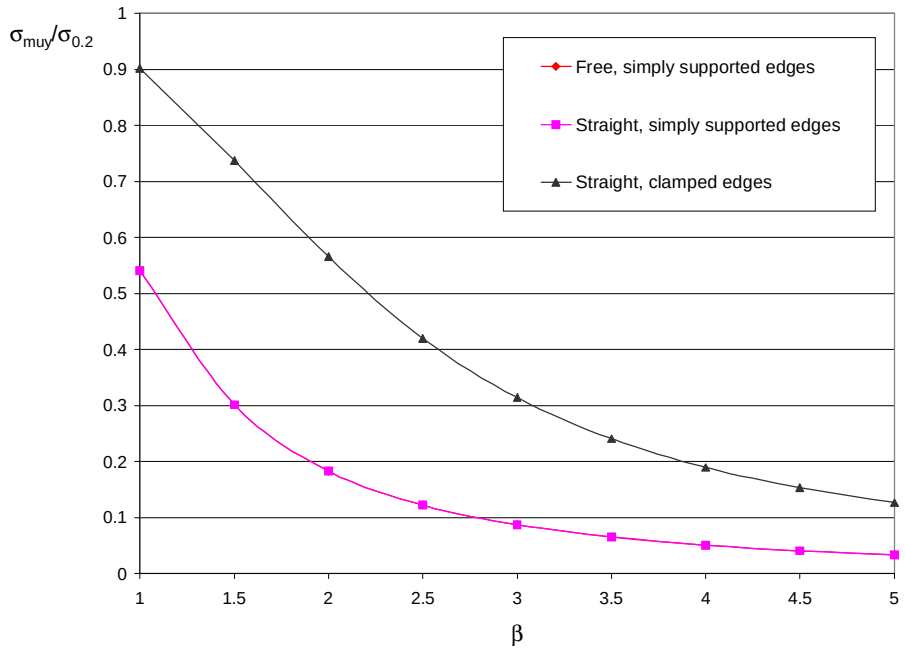

Figure 6.11 : Transverse ultimate capacity for plate strips with different boundary conditions. The plates consist of the base material only.

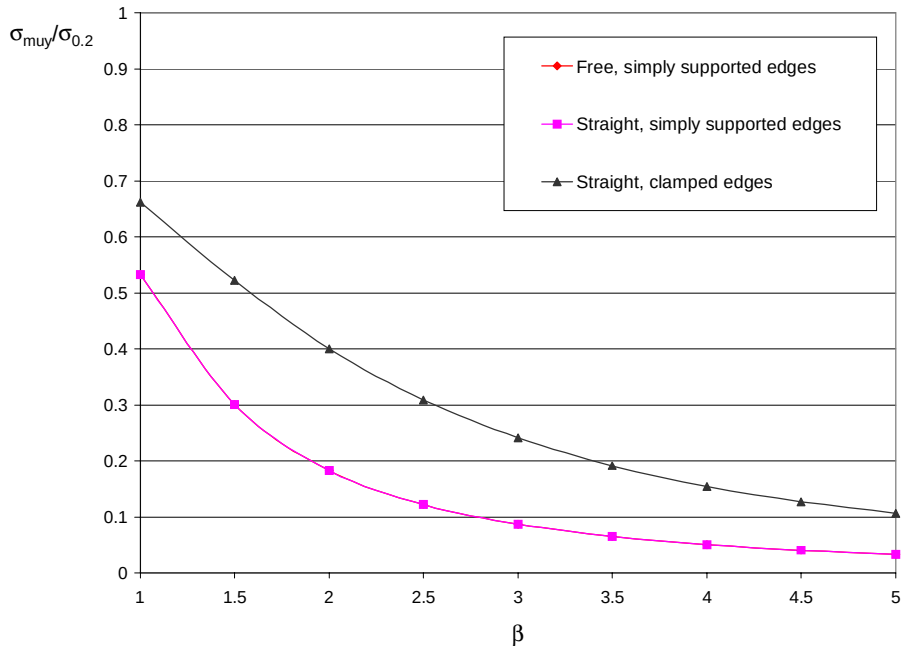

Figure 6.12 : Transverse ultimate capacity for plate strips with different boundary conditions. The plates have heat affected zones along all edges.

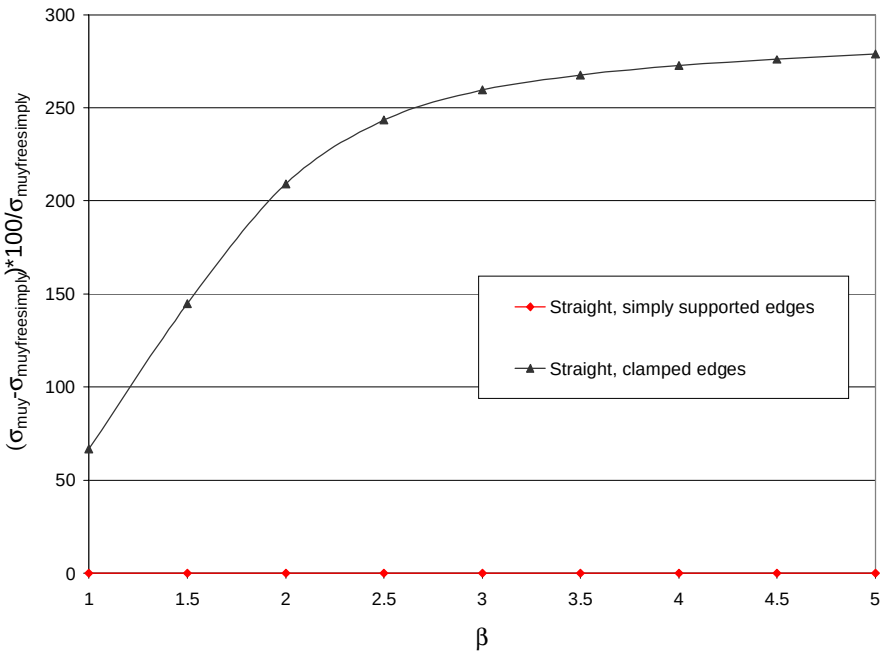

Figure 6.13 : Percentage increase in ultimate capacity as compared to plate strips with free edges. The plates consist of the base material only.

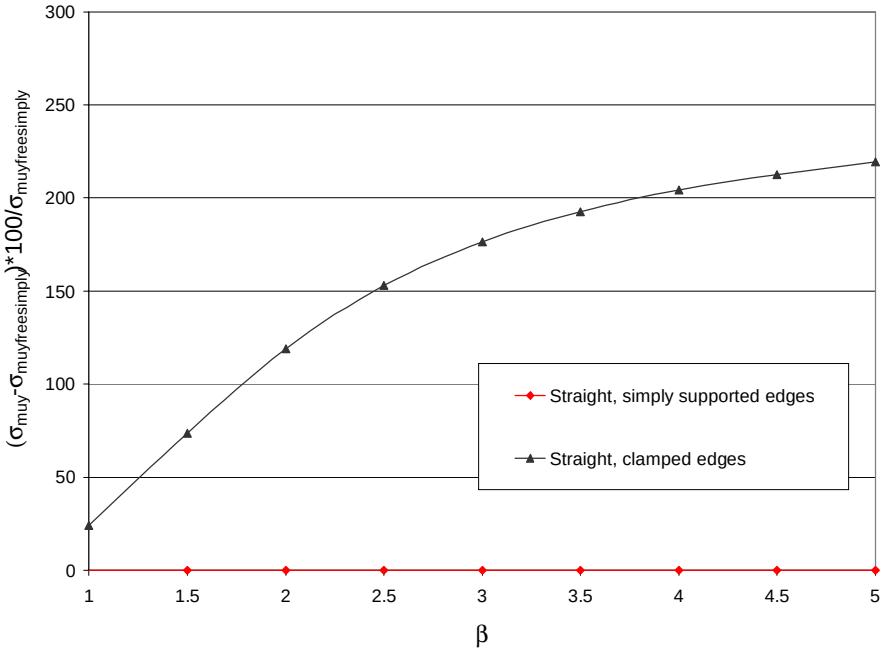

Figure 6.14 : Percentage increase in ultimate capacity as compared to plate strips with free edges. The plates have heat affected zones along all edges.

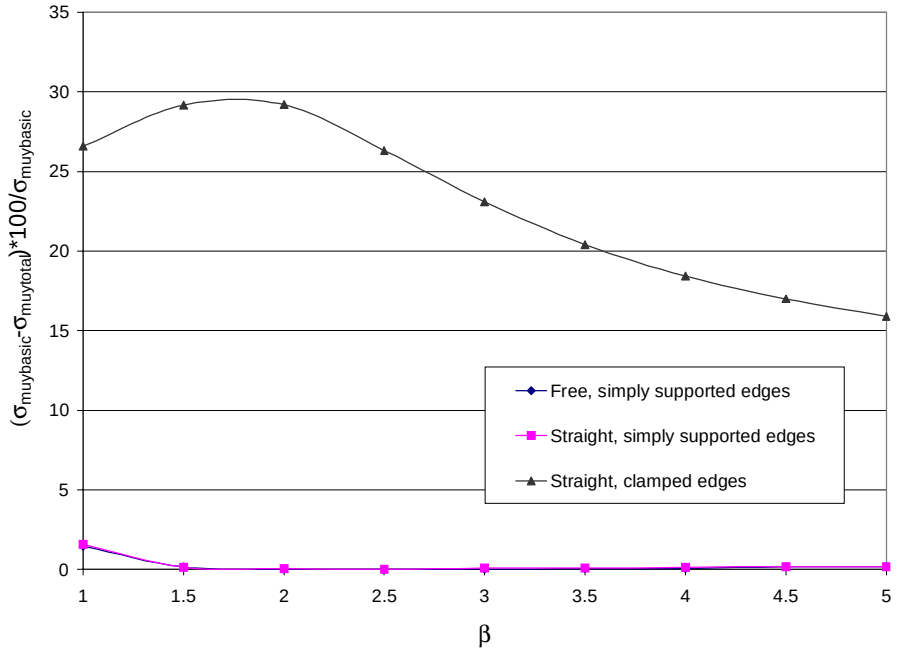

Figure 6.15 : Percentage reduction in ultimate capacity due to the introduction of heat affected zones along all edges for the different boundary conditions analysed

Plate strips with free, simply supported edges and plate strips with straight, simply supported edges have the exact same ultimate capacity and behaviour, and their ultimate capacities do not change when heat affected zones are introduced.

Changing the bending boundary conditions from simply supported edges to clamped edges is identical to reducing the linear buckling length to half it's original value and increasing the linear buckling loads to four times their original values. Even when non-linear material behaviour and non-linear geometry are taken into account, slender plates have an increase in ultimate capacity of more than 200 percent. As the plates become more compact, and collapse of the plates is more dominated by yielding, the increase in strength due to change of boundary conditions diminish.

The ultimate capacity of plates with heat affected zones will be less influenced by change of boundary conditions than plates made of base material. This is due to premature yielding in the heat affected zones.

Chapter 7

Effect of Aspect Ratio on Ultimate Capacity

7.1 Purpose of the Parametric Study

All analyses up to now have been performed for plates with an aspect ratio of ω=a/b=3. The reason for investigating other values of the aspect ratio, ω, is to be able to understand the plate buckling phenomena for all aspect ratios likely to occur. On the basis of this physical understanding design formulas suitable for all aspect ratios, ω, can be developed.

Analyses will be carried out with different load conditions and boundary conditions as well as different patterns of heat affected zones.

7.2 Axial Compression

7.2.1 Basic Analyses and Analyses with Heat Affected Zones

In the first three plots, Figures 7.1-7.3, the patterns of the heat affected zones are kept constant, but the aspect ratio, a/b, is varied. In Figures 7.4-7.5 the aspect ratio, a/b, is kept constant, and the patterns of the heat affected zones are altered.

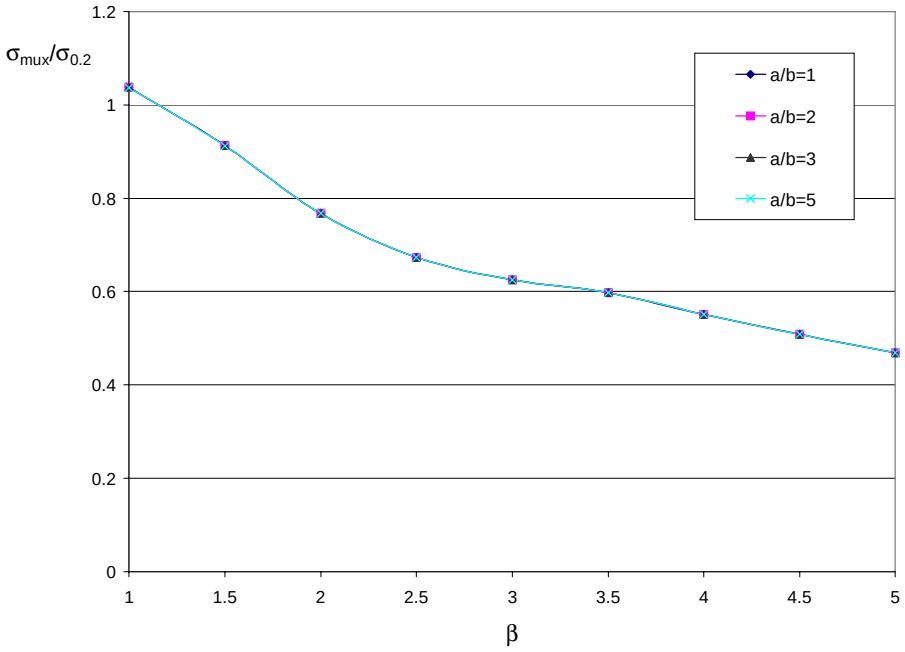

Figure 7.1: Axial ultimate capacity for plates with straight, simply supported edges and different values of the aspect ratio, ω. The plates have no heat affected zones.

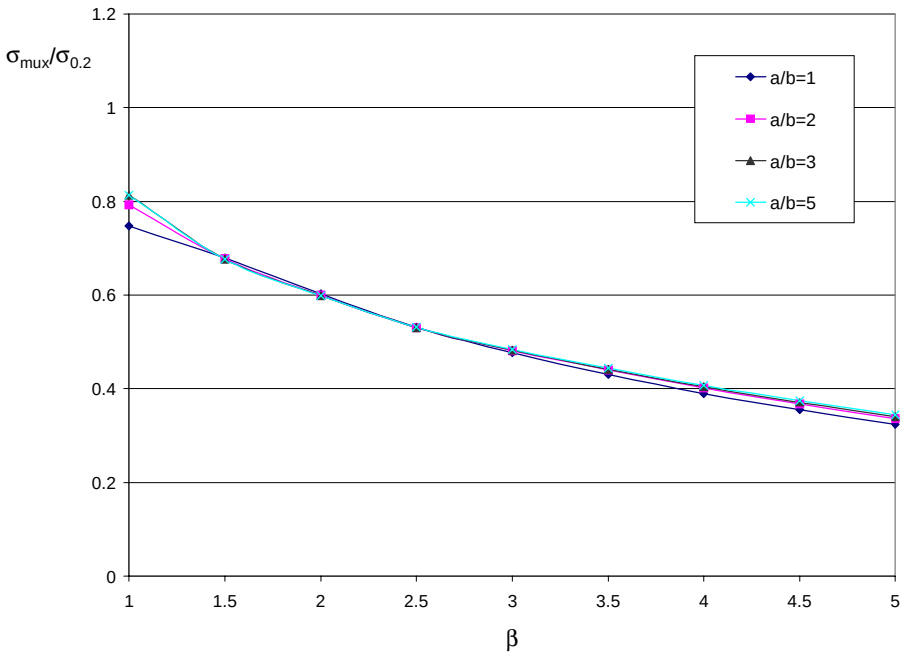

Figure 7.2: Axial ultimate capacity for plates with straight, simply supported edges and different values of the aspect ratio, ω. The plates have heat affected zones along all edges.

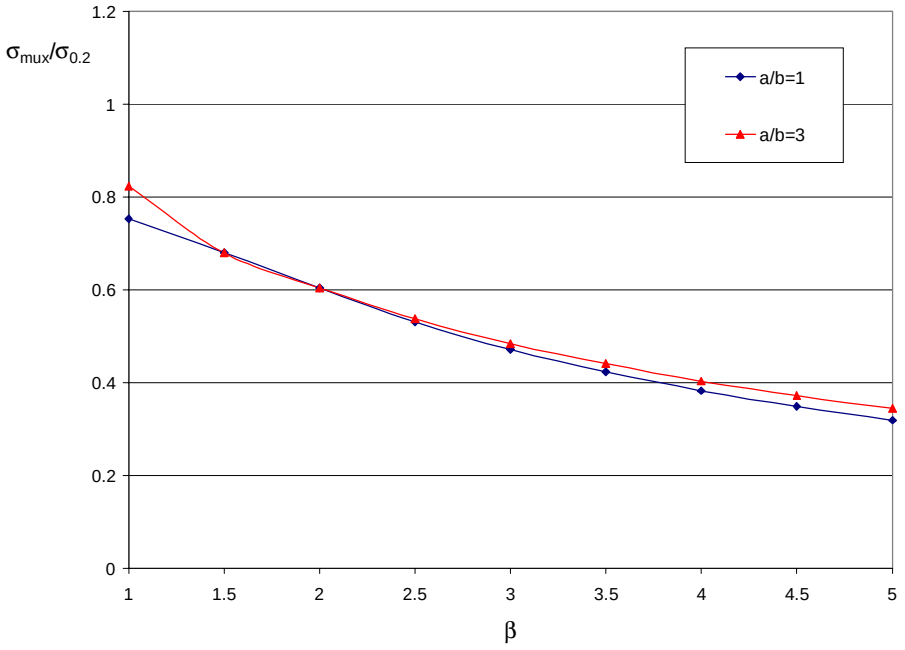

Figure 7.3: Axial ultimate capacity for plates with straight, simply supported edges and different values of the aspect ratio, ω. The plates have the extruded pattern of the heat affected zones.

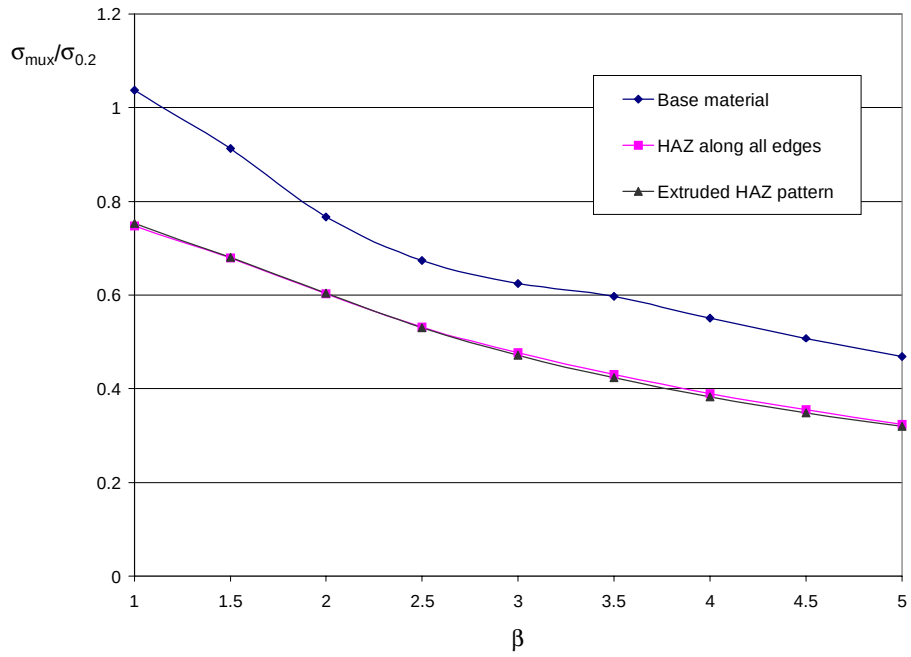

Figure 7.4 : Axial ultimate capacity for plates with straight, simply supported edges and different patterns of the heat affected zones. The aspect ratio, a/b=1.

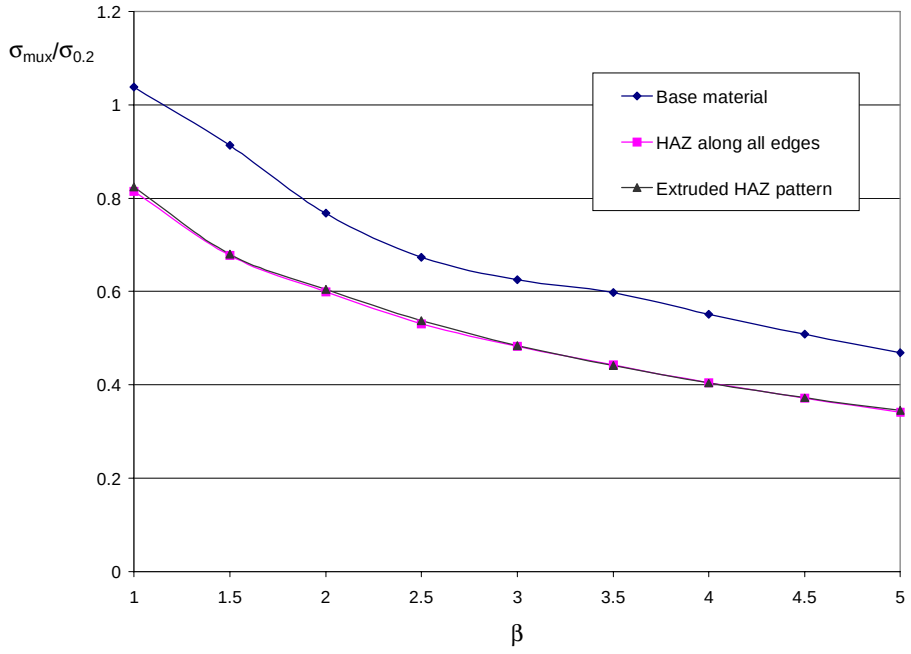

Figure 7.5 : Axial ultimate capacity for plates with straight, simply supported edges and different patterns of the heat affected zones. The aspect ratio, a/b=3.

If the plates consist of the base material only, the axial ultimate capacity is identical for all values of the aspect ratio, a/b. This is as expected, in view of the relevant buckling modes.

Introducing heat affected zones along all edges of the plates is more critical for plates with aspect ratio, a/b=1. Although plates with aspect ratio, a/b=1, show lower axial ultimate

capacity than plates with higher aspect ratios, the differences observed are not very large. The lower ultimate capacity is believed to be caused by the fact that plates with aspect ratio, a/b=1, have heat affected zones at both loaded edges of a single half wave buckling mode. For higher values of the aspect ratio, a/b, the number of heat affected zones along the loaded edges of the single half waves of the relevant buckling mode is restricted to either one or zero.

Plates with the extruded pattern of the heat affected zones show the exact same trend, and the trend is believed to be caused by the same effect. Plates with aspect ratio, a/b=1, have heat affected zones at both loaded edges of a single half wave.

The results shown in Figures 7.4 and 7.5 also confirm that the axial ultimate capacities for plates with heat affected zones along all edges, and plates with the extruded pattern of the heat affected zones, are almost identical, not only for plates with aspect ratio, a/b=3, but for other values of the aspect ratio, a/b, as well.

7.2.2 Alternative Boundary Conditions

In the previous section results for rectangular plates with straight, simply supported edges are given, considering base material only and two different patterns of heat affected zones. In this section plates with free, simply supported edges and straight, clamped edges are considered. Plates consisting of the base material only and plates with heat affected zones along all edges are investigated. The results are plotted in Figures 7.6-7.11.

In the first four plots, the boundary conditions are kept constant, and the aspect ratio, a/b, is varied. In the following two plots the aspect ratio, a/b, is kept constant and the boundary conditions are varied.

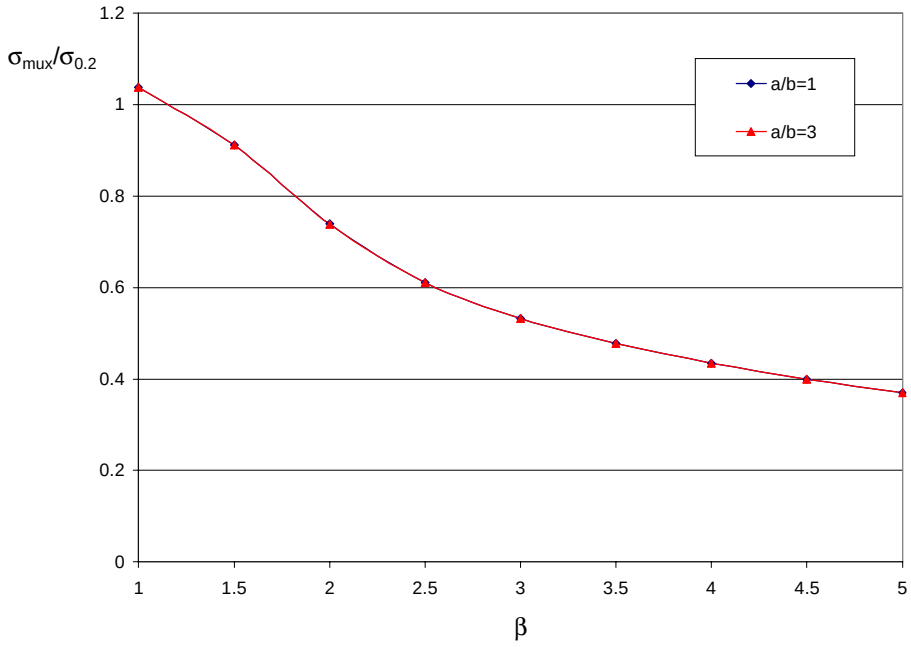

Figure 7.6 : Axial ultimate capacity of plates with free, simply supported edges. The plates consist of the base material only.

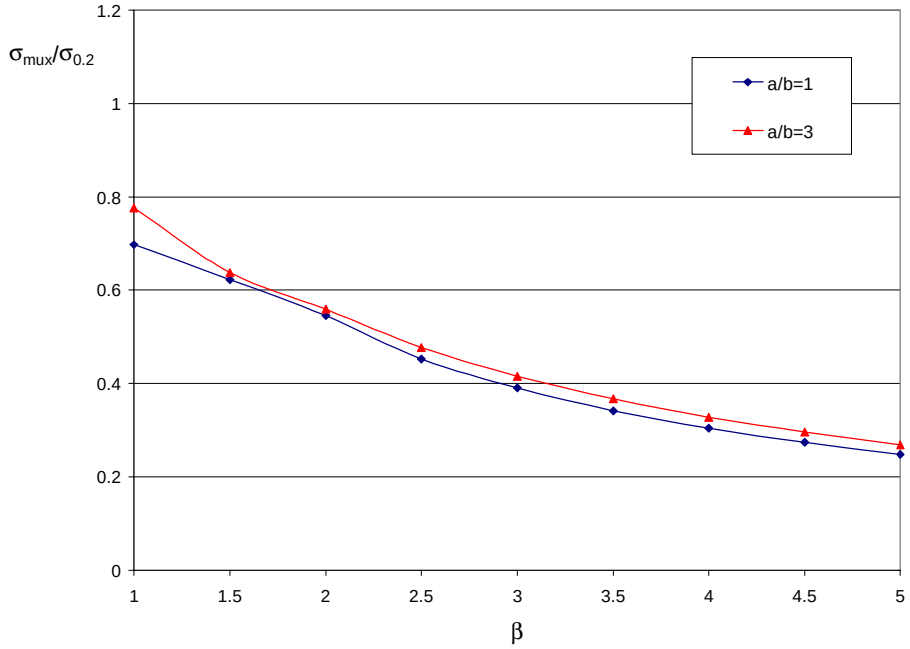

Figure 7.7 : Axial ultimate capacity of plates with free, simply supported edges. The plates have heat affected zones along all edges.

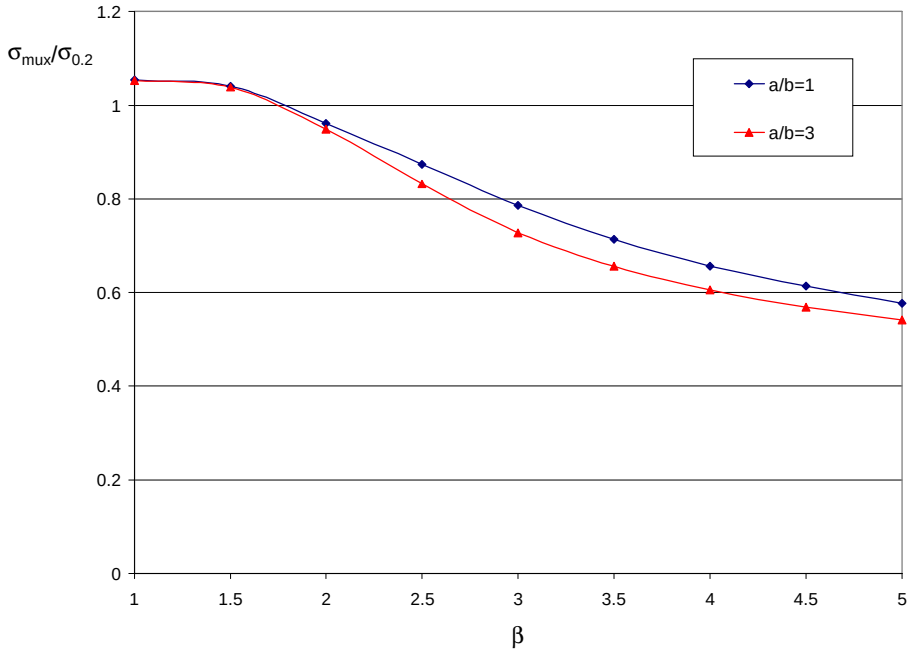

Figure 7.8 : Axial ultimate capacity of plates with straight, clamped edges. The plates consist of the base material only.

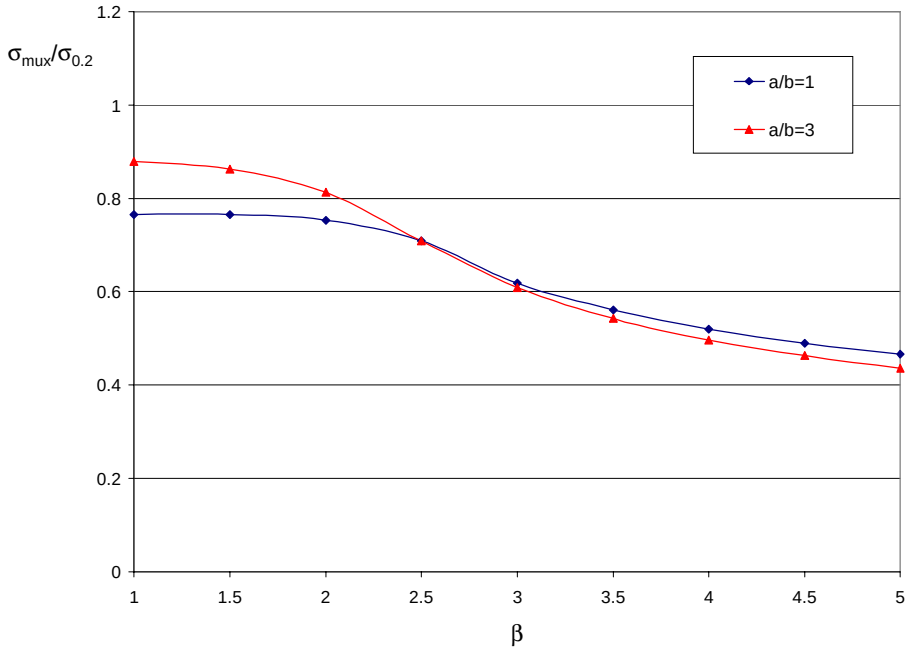

Figure 7.9 : Axial ultimate capacity of plates with straight, clamped edges. The plates have heat affected zones along all edges.

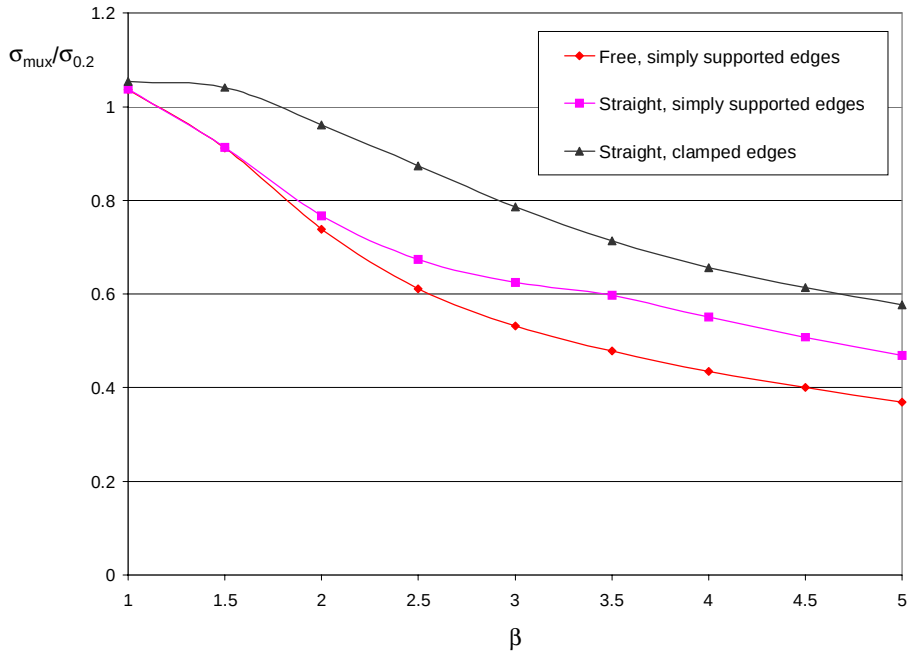

Figure 7.10 : Axial ultimate capacities for plates with aspect ratio, a/b=1. The plates consist of the base material only.

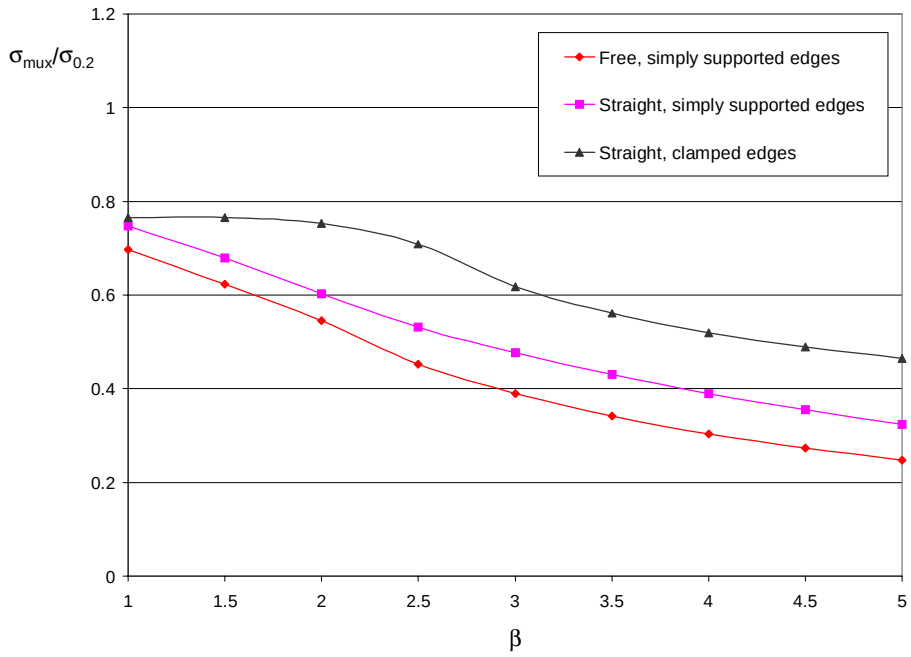

Figure 7.11 : Axial ultimate capacities for plates with aspect ratio, a/b=1. The plates have heat affected zones along all edges.

The axial ultimate capacity for plates consisting of the base material only and with free, simply supported edges, are identical for all values of the aspect ratio, a/b. This is the same behaviour as for plates with straight, simply supported edges. If the plates are exposed to heat affected zones along all edges, plates with aspect ratio, a/b=1, have the lower ultimate capacity. The additional loss in collapse strength is believed to be caused by the fact that plates with aspect ratio, a/b=1, have heat affected zones along all four edges of a single half wave buckling mode. Also this behaviour is the same as for plates with straight, simply supported edges.

Plates with straight, clamped edges and no heat affected zones, show a higher ultimate capacity for plates with aspect ratio, a/b=1, than plates with other values of the aspect ratio. The reason for this behaviour is that plates with aspect ratio, a/b=1, have clamped bending boundary conditions along all four edges of a single half wave. For plates with higher values of the aspect ratio, a/b, the clamped bending boundary conditions along imaginary edges of a single half wave buckling mode are restricted to either two or three edges.

Introducing heat affected zones makes things more complicated. Plates with an aspect ratio of a/b=1, have the advantage of having clamped bending boundary conditions along all four edges of a single half wave, but they have the disadvantage of having heat affected zones along all four edges of a single half wave.

For compact plates, with collapse dominated by yielding, the presence of heat affected zones along all four edges of a single half wave is the dominating effect, and plates with aspect ratio, a/b=1, have the lowest ultimate capacities. As the plates become more slender, the advantage of having clamped bending boundary conditions along all four edges of a single half wave is more crucial, and plates with aspect ratio, a/b=1, regain the highest ultimate capacity.

7.3 Transverse Compression

7.3.1 Basic Cases

For plates subjected to transverse compression the number of load cases needs to be reduced to get manageable results. This is done by assuming that the transverse ultimate capacity of rectangular aluminium plates can be described as the weighted sum of the ultimate capacity of a square plate and the transverse ultimate capacity of an infinitely long plate.

$$\frac{\sigma_{muy}}{\sigma_{0.2}} = \frac{1}{\omega}\left(\frac{\sigma_{muy}}{\sigma_{0.2}}\right)_{\substack{\text{square}\\\text{plate}}} + \left(1-\frac{1}{\omega}\right)\left(\frac{\sigma_{muy}}{\sigma_{0.2}}\right)_{\substack{plate\\strip}} \tag{7.1}$$

or

$$\frac{\sigma_{muy}}{\sigma_{0.2}} = \frac{b}{a}\left(\frac{\sigma_{muy}}{\sigma_{0.2}}\right)_{\substack{\text{square}\\\text{plate}}} + \left(1-\frac{b}{a}\right)\left(\frac{\sigma_{muy}}{\sigma_{0.2}}\right)_{\substack{plate\\strip}} \tag{7.2}$$

The transverse ultimate capacity of an infinitely long plate is expected to be equal to the transverse ultimate capacity of a plate strip. The assumptions made in Equations 7.1 and 7.2 were introduced by Valsgård (1979). In order to find the transverse collapse capacity of a plate with a given aspect ratio, ω, one simply has to combine the axial collapse curves for square plates with transverse plate strip curves by the use of Equation 7.2.

The pattern of the heat affected zones is asymmetrical for plates with the extruded HAZ pattern. The square plates have to be loaded transversally to give the correct "axial" capacity. Figure 7.12 shows the results for quadratic plates loaded transversally. As can be seen from this figure, plates with heat affected zones along all edges and plates with the extruded pattern of the heat affected zones no longer have the same capacity.

Due to the heat affected zone in the middle of the plate, perpendicular to the loading direction, plates with the extruded pattern of the heat affected zones have lower ultimate capacities than plates with heat affected zones along all edges. The heat affected zone in the middle of the plates is placed in the parts of the plates with the largest bending moments causing maximum reduction in ultimate capacity.

Transverse ultimate capacities, obtained by numerical analyses of plates with different aspect ratios, a/b, can now be compared with results found by the use of Equation 7.2. Figures 7.13-7.15 show the results for transversally loaded plates made of the base material only, and two patterns of heat affected zones. The results found by the use of Equation 7.2 are presented as design values in the figures.

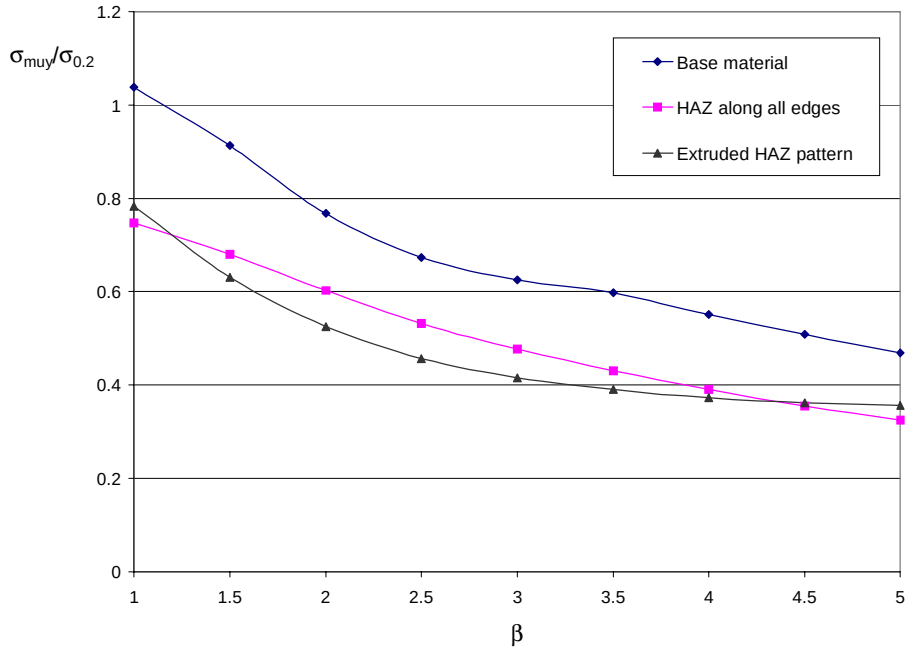

Figure 7.12 : Transverse ultimate capacity of quadratic plates (aspect ratio, a/b=1)

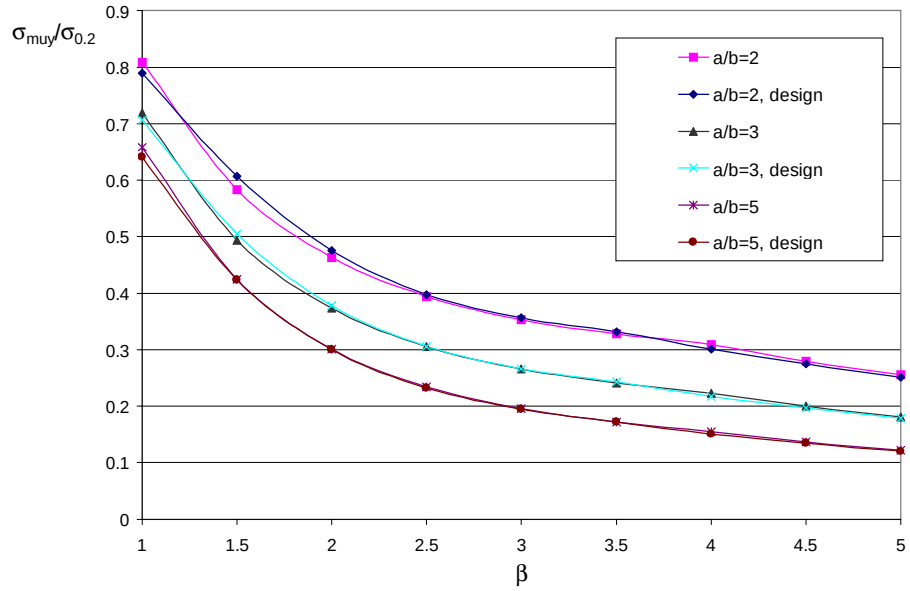

Figure 7.13 : Transverse ultimate capacities of plates with different aspect ratios, a/b. The results from numerical analyses are compared with the capacitiy found by use of Equation 7.2. The plates consist of the base material only.

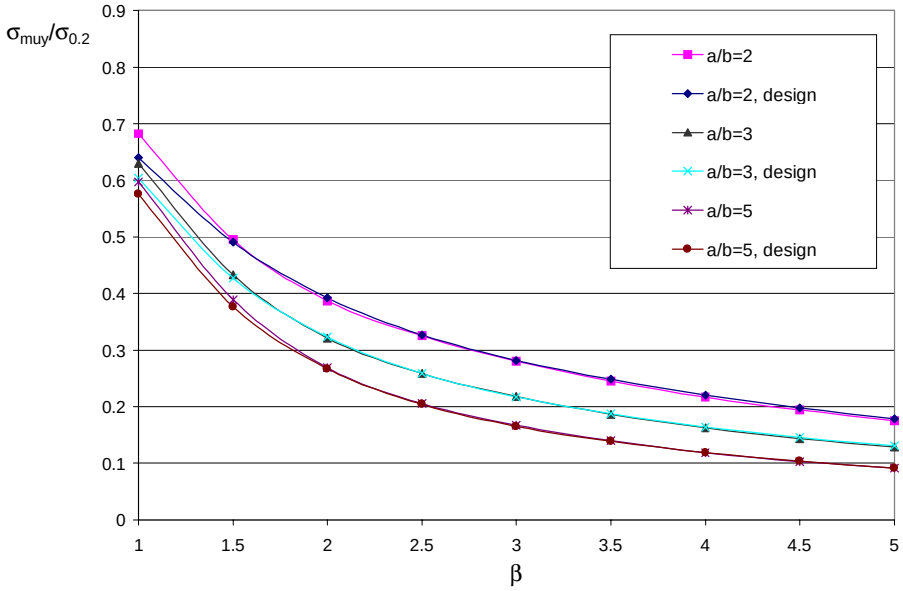

Figure 7.14 : Transverse ultimate capacities of plates with different aspect ratios, a/b. The results from numerical analyses are compared with the capacity found by use of Equation 7.2. The plates have heat affected zones along all edges.

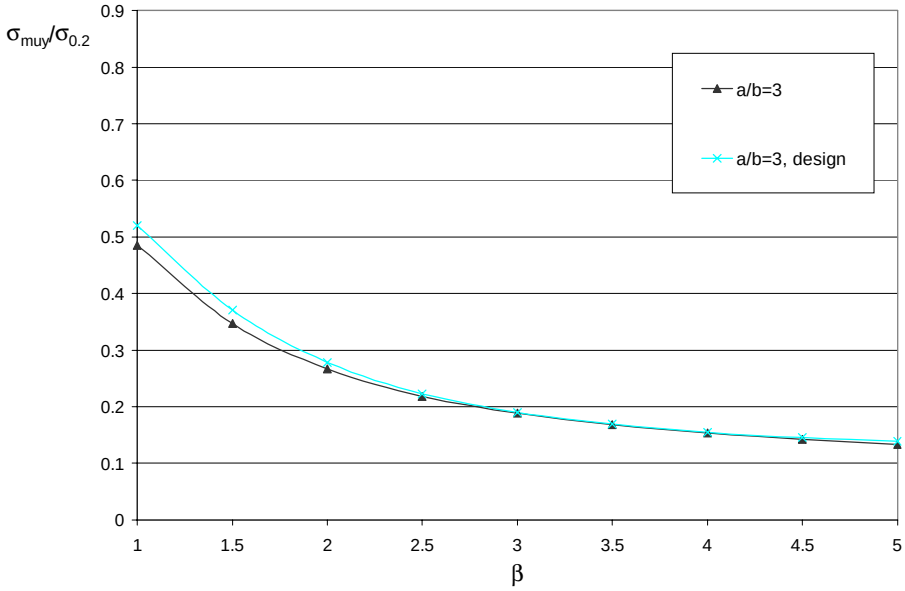

Figure 7.15 : Transverse ultimate capacities of plates with aspect ratio, a/b=3. The results from numerical analyses are compared with the capacity found by use of Equation 7.2. The plates have the extruded pattern of the heat affected zones.

If the plates have no heat affected zones, the results obtained by numerical simulations of plates with the actual aspect ratio and the results obtained by the use of Equation 7.2 are almost identical. For plates with slenderness, β=1.0, and heat affected zones along all edges of the plates, the results obtained by the use of Equation 7.2 seem to be a little less than the values obtained by the numerical simulations. For all other values of the slenderness, β, the deviations between numerical simulations and Equation 7.2 are insignificant.

Plates with the extruded pattern of the heat affected zones have only been analysed for aspect ratios, a/b=1 and a/b=3. Sturdy plates show the opposite trend as compared to plates with heat affected zones along all edges. Equation 7.2 predicts ultimate capacities that are a little too high as compared to numerical analyses.

For all patterns of the heat affected zones, aspect ratios, and values of the slenderness, β, analysed, there was no indication that Equation 7.2 is unsuitable for design purposes. However, depending on the patterns of the heat affected zones, the right collapse curve for the square plate capacity and the right collapse curve for the plate strip capacity have to be chosen.

7.3.2 Changing Boundary Conditions

It has now been documented that Equation 7.2 is very well suited if the edges of the plates are straight, simply supported. The question then is whether Equation 7.2 also can be used for other boundary conditions.

To answer this question numerical analyses of plates with both free, simply supported edges and straight, clamped edges have been performed. The collapse curves for plates with aspect ratio, a/b=3, have been compared with results obtained by the use of Equation 7.2. The results can be found in Figures 7.16-7.19.

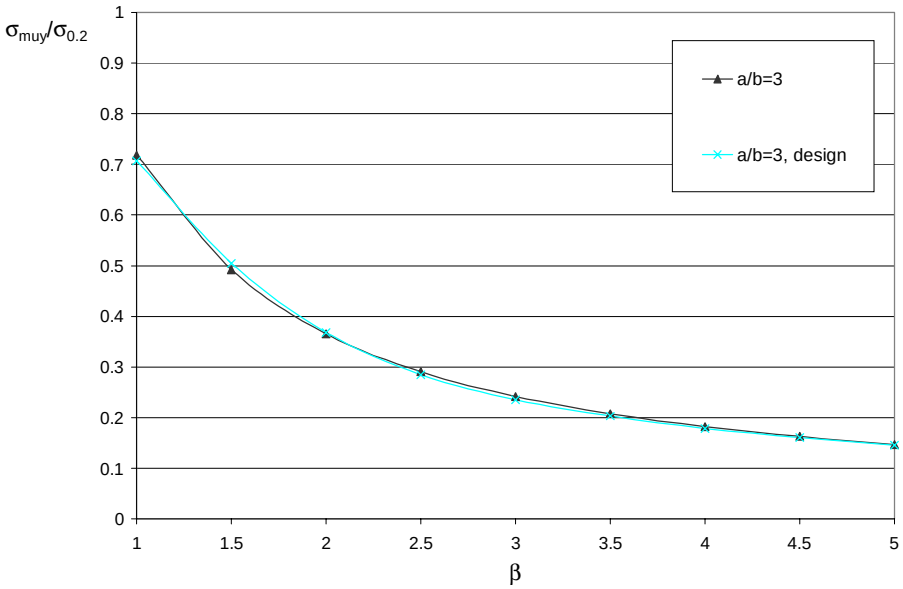

Figure 7.16 : Transverse ultimate capacity of plates with free, simply supported edges and aspect ratio, ω=3, compared with ultimate capacity obtained by Equation 7.2. The plates have no heat affected zones.

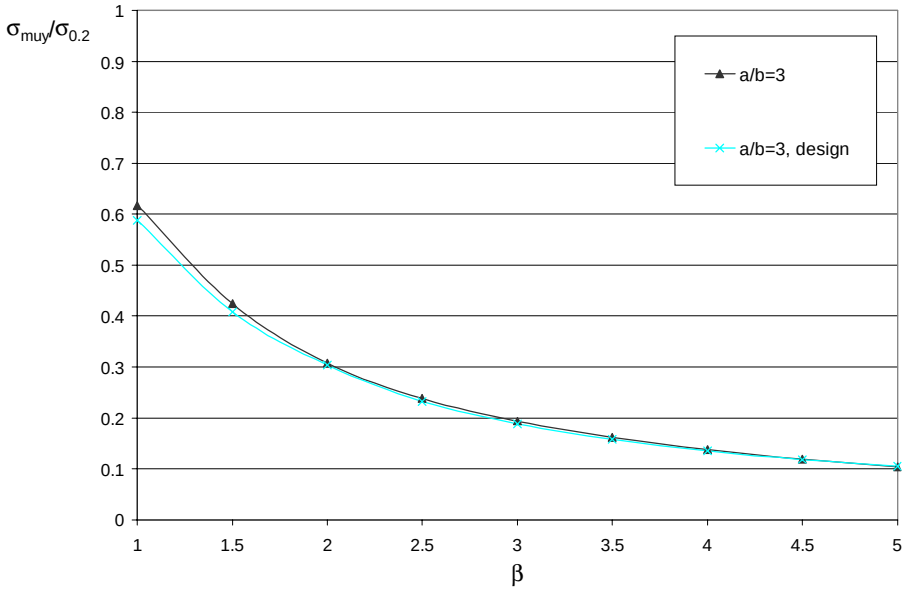

Figure 7.17 : Transverse ultimate capacity of plates with free, simply supported edges and aspect ratio, ω=3, compared with ultimate capacity obtained by Equation 7.2. The plates have heat affected zones along all edges.

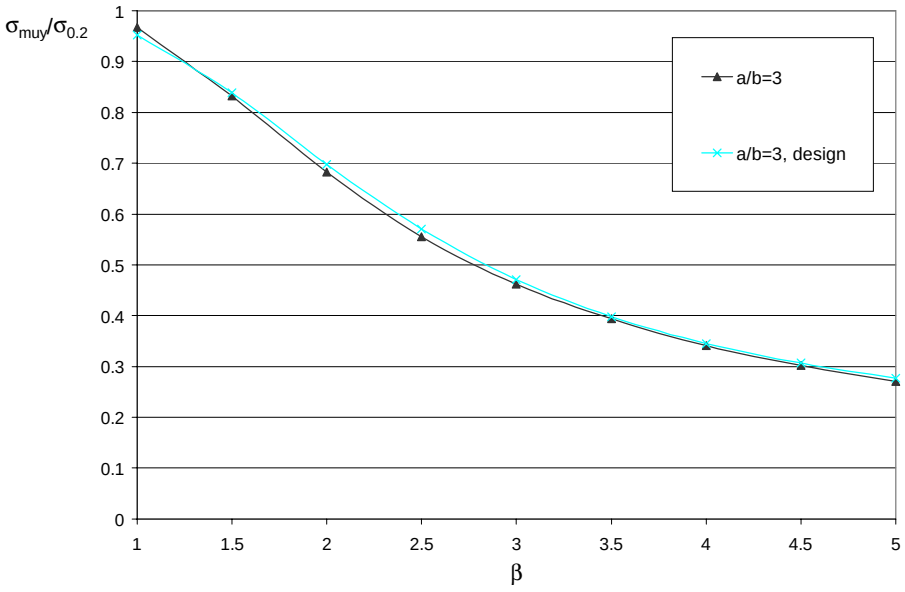

Figure 7.18 : Transverse ultimate capacity of plates with straight, clamped edges and aspect ratio, ω=3, compared with ultimate capacity obtained by Equation 7.2. The plates have no heat affected zones.

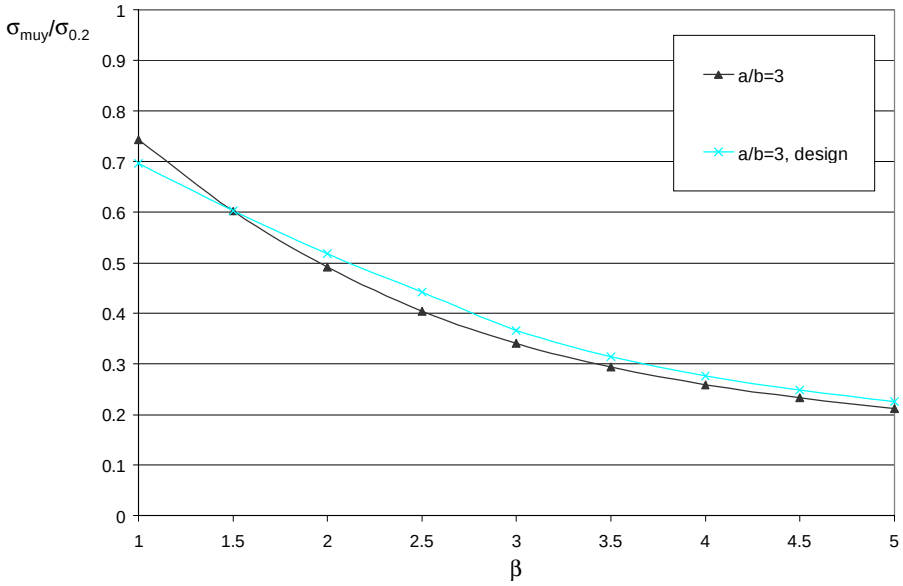

Figure 7.19 : Transverse ultimate capacity of plates with straight, clamped edges and aspect ratio, ω=3, compared with ultimate capacity obtained by Equation 7.2. The plates have heat affected zones along all edges.

The largest discrepancies between the collapse capacity obtained by numerical analyses of plates with aspect ratio, a/b=3, and results found by use of Equation 7.2, occurred if the plates had straight, clamped edges and were exposed to heat affected zones along all edges. The biggest difference took place for slenderness, β=2.5. Using Equation 7.2 over-estimated the strength of the plate by 9.3 %.

Although discrepancies between numerical analyses and results obtained by the use of Equation 7.2 were observed for plates exposed to heat affected zones along all edges, using Equation 7.2 seems to be a reasonable choice as design method. Adequate collapse curves for the square plate capacity and the plate strip capacity, however, need to be chosen for the relevant case.

7.4 Biaxial Compression

7.4.1 Interaction Curves for Plates with Different Slenderness for Given Aspect Ratio

Plates made of alloy 6082-T6 have been investigated in biaxial compression for aspects ratios, a/b, equal to 1, 2, 3 and 5. For all these aspect ratio values the plates have been analysed considering plates of base material only and plates having heat affected zones along all edges. Plates with aspect ratio, a/b=3, have also been investigated with the extruded pattern of the heat affected zones (see Chapter 5.4). Figures 7.20-7.27 show the biaxial interaction curves for the different aspect ratios.

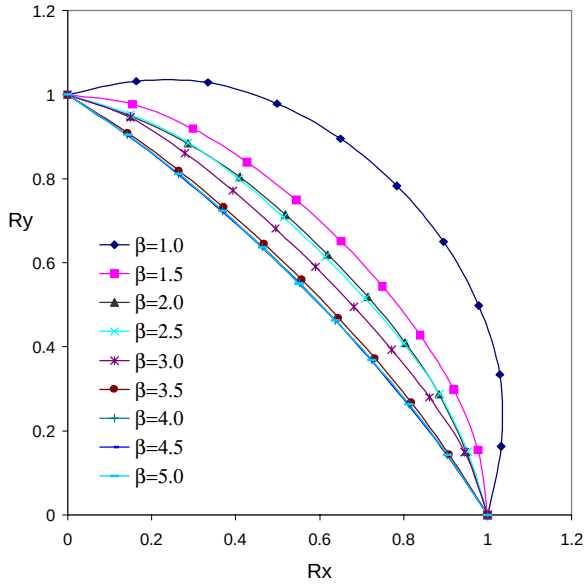

Figure 7.20 : Biaxial interaction curves for plates with aspect ratio, a/b=1. The plates are made of base material.

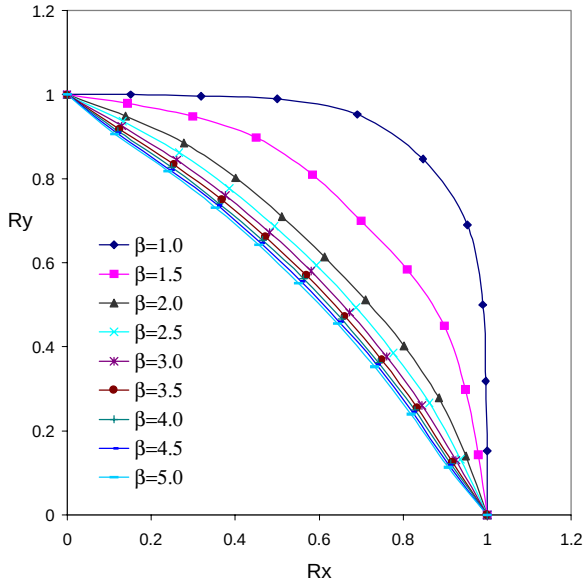

Figure 7.21 : Biaxial interaction curves for plates with aspect ratio, a/b=1. The plates have heat affected zones along all edges.

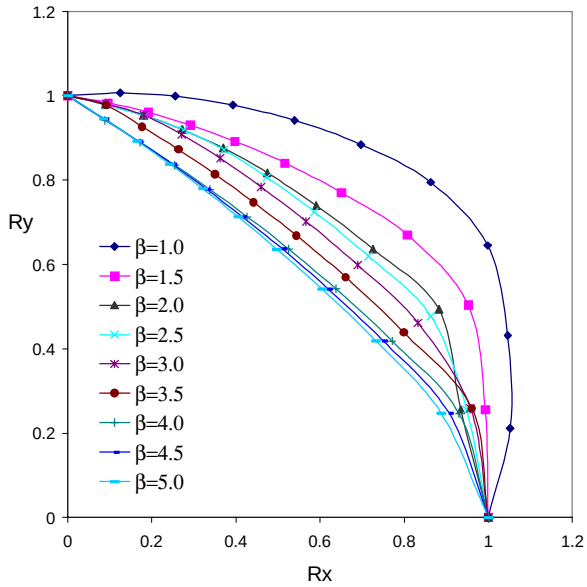

Figure 7.22 : Biaxial interaction curves for plates with aspect ratio, a/b=2. The plates are made of base material.

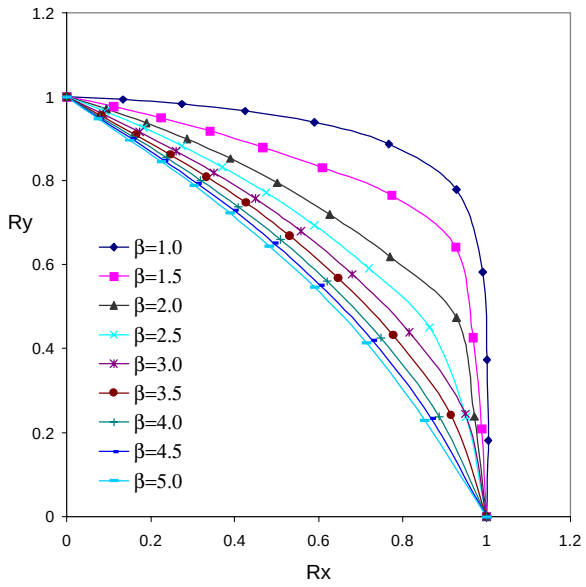

Figure 7.23 : Biaxial interaction curves for plates with aspect ratio, a/b=2. The plates have heat affected zones along all edges.

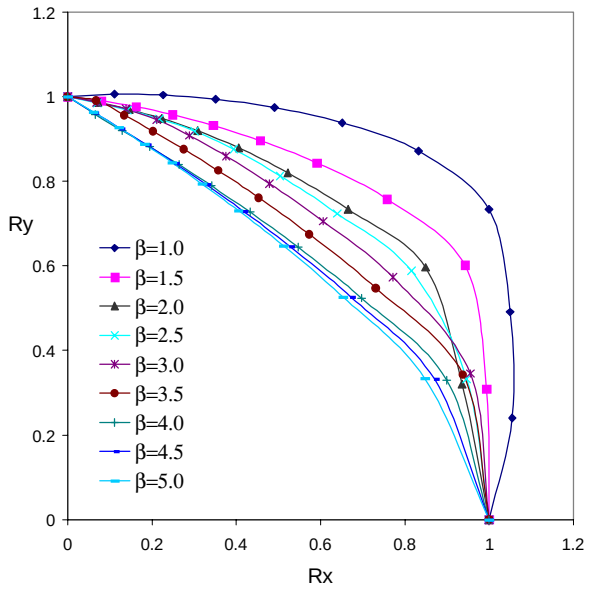

Figure 7.24 : Biaxial interaction curves for plates with aspect ratio, a/b=3. The plates are made of base material.

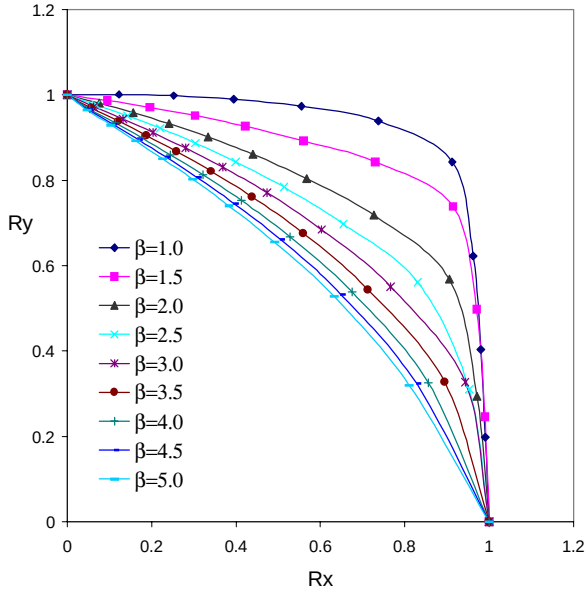

Figure 7.25 : Biaxial interaction curves for plates with aspect ratio, a/b=3. The plates have heat affected zones along all edges.

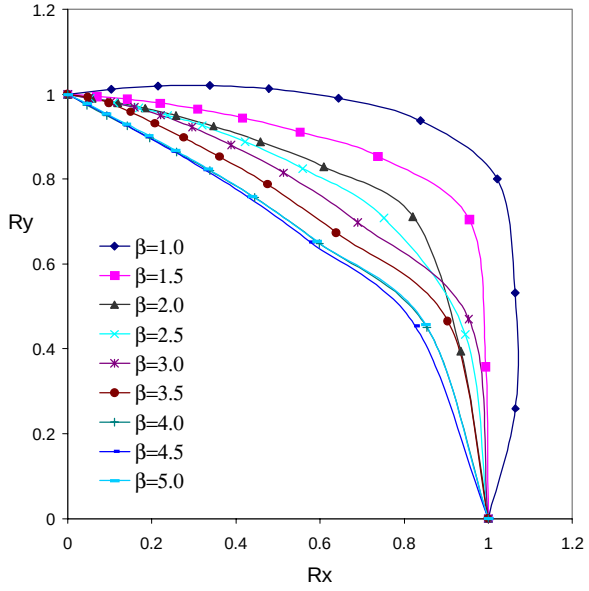

Figure 7.26 : Biaxial interaction curves for plates with aspect ratio, a/b=5. The plates are made of base material.

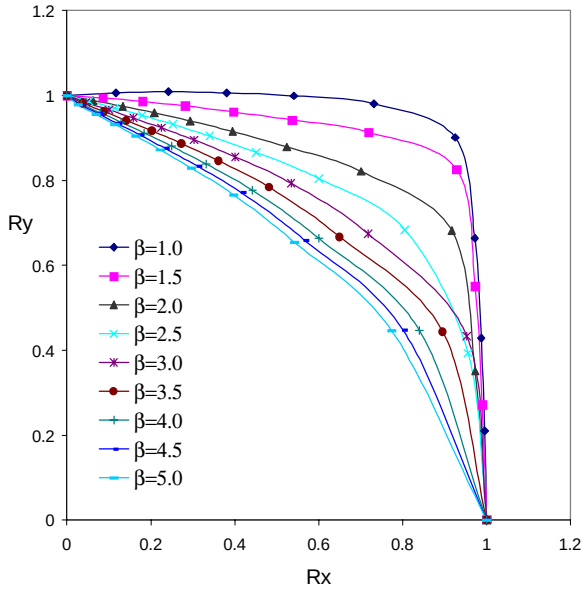

Figure 7.27 : Biaxial interaction curves for plates with aspect ratio, a/b=5. The plates have heat affected zones along all edges.

The biaxial collapse curves plotted in Figures 7.20-7.27 are very difficult to compare by just looking at the different plots. The plots in the next chapters clarify the differences in biaxial interaction behaviour. Differences caused by varying plate slenderness, β, aspect ratio, a/b, and patterns of the heat affected zones are examined.

7.4.2 Interaction Curves for Plates with Different Aspect Ratios for a Given Slenderness

In Figures 7.28-7.36 the biaxial interaction curves for plates with different aspect ratios, a/b, have been combined. Curves for plates with a given slenderness, β, have been plotted separately. The plates are made of the base material only. Figures 7.37-7.45 show the same results for plates with heat affected zones along all edges.

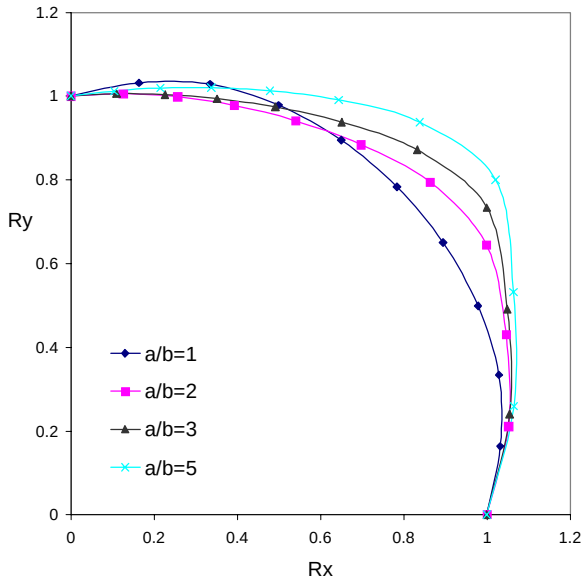

Figure 7.28 : Biaxial interaction curves for plates with slenderness β=1.0. The plates are made of base material.

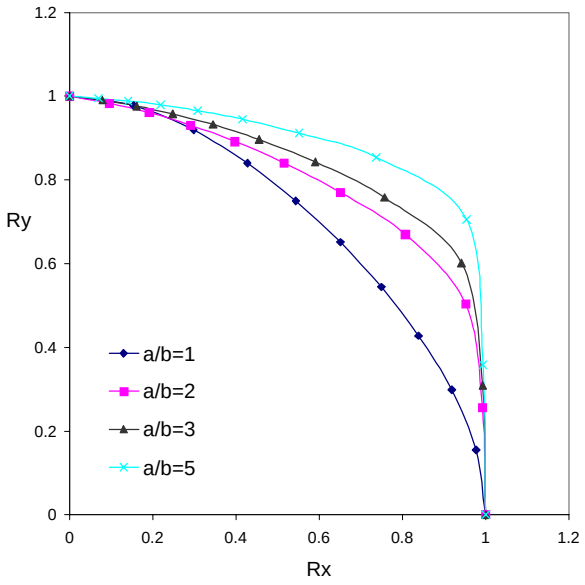

Figure 7.29 : Biaxial interaction curves for plates with slenderness β=1.5. The plates are made of base material.

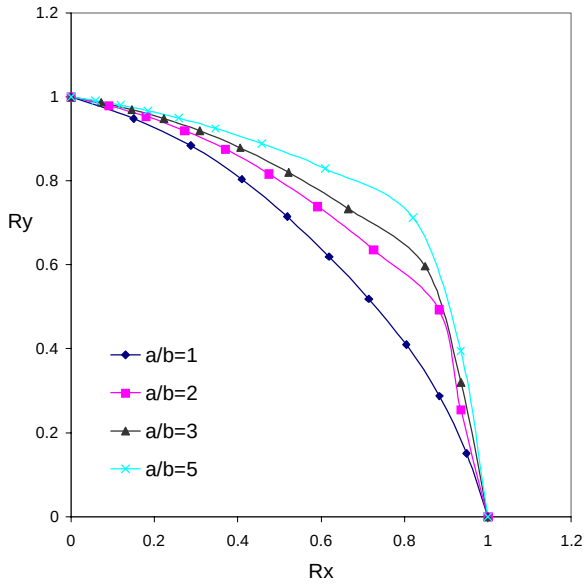

Figure 7.30 : Biaxial interaction curves for plates with slenderness β=2.0. The plates are made of base material.

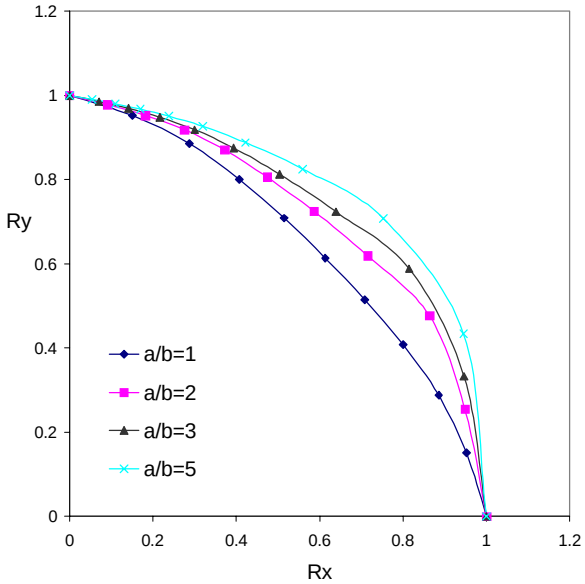

Figure 7.31 : Biaxial interaction curves for plates with slenderness β=2.5. The plates are made of base material.

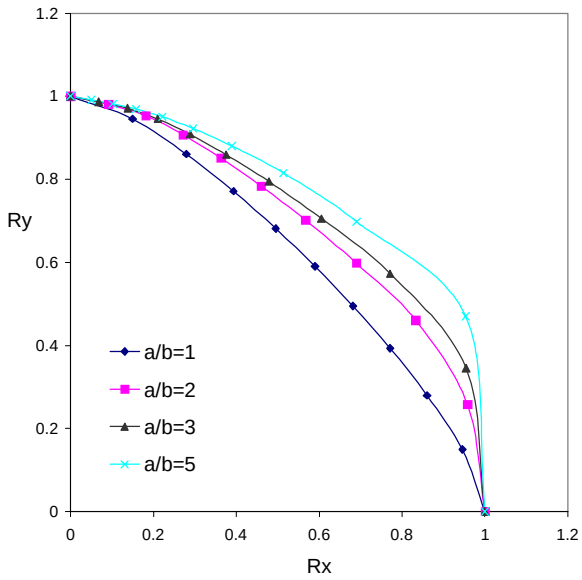

Figure 7.32 : Biaxial interaction curves for plates with slenderness β=3.0. The plates are made of base material.

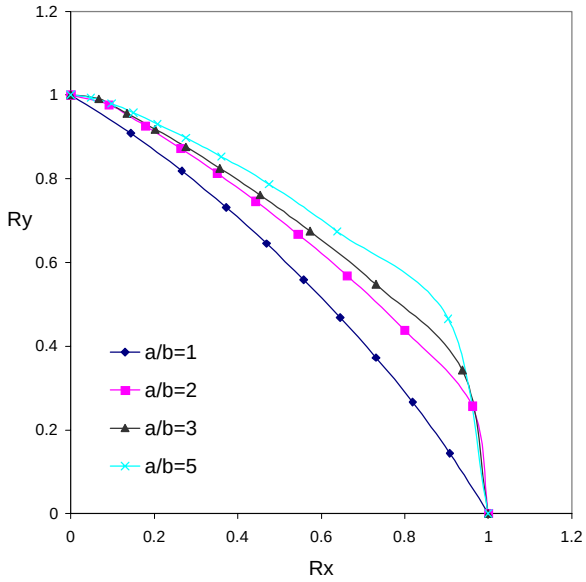

Figure 7.33 : Biaxial interaction curves for plates with slenderness β=3.5. The plates are made of base material.

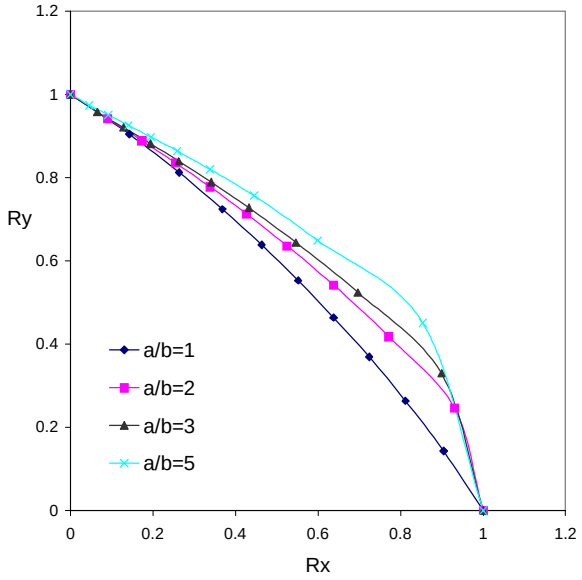

Figure 7.34 : Biaxial interaction curves for plates with slenderness β=4.0. The plates are made of base material.

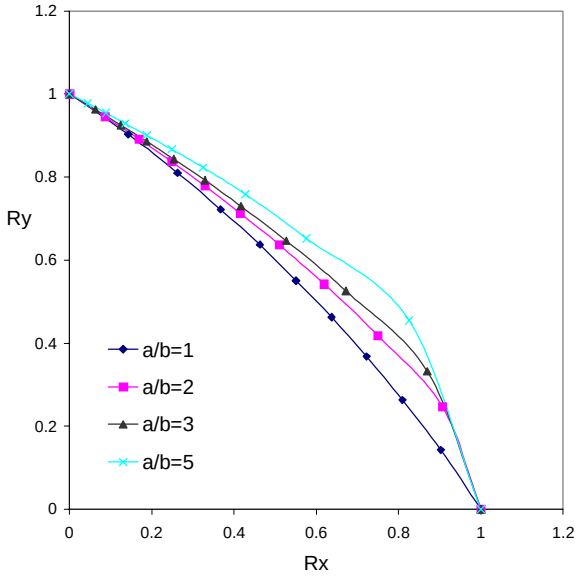

Figure 7.35 : Biaxial interaction curves for plates with slenderness β=4.5. The plates are made of base material.

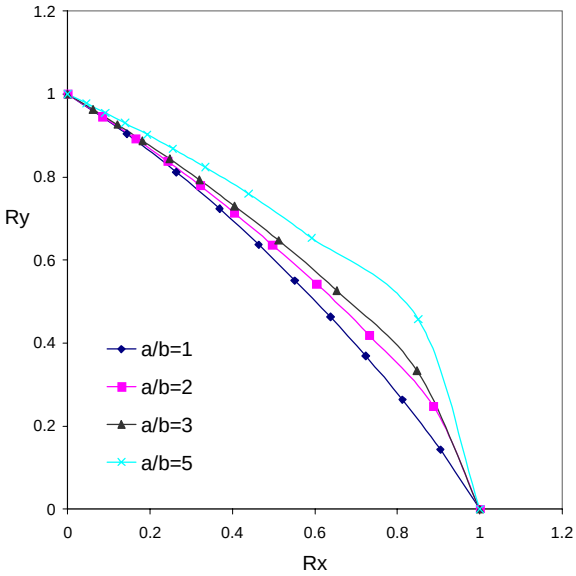

Figure 7.36 : Biaxial interaction curves for plates with slenderness β=5.0. The plates are made of base material.

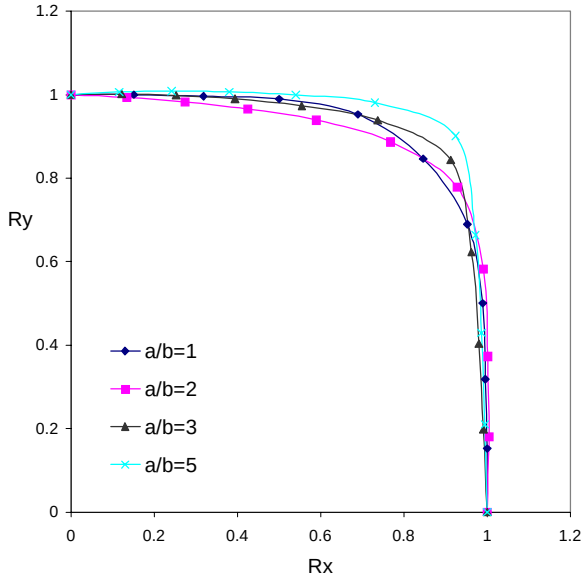

Figure 7.37 : Biaxial interaction curves for plates with slenderness β=1.0. The plates have heat affected zones along all edges.

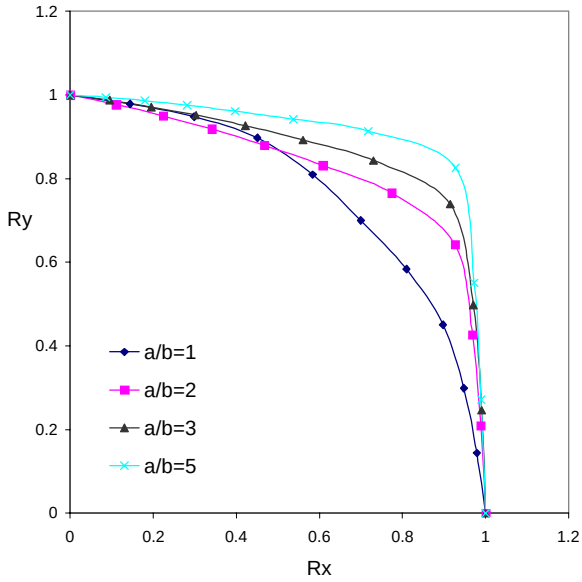

Figure 7.38 : Biaxial interaction curves for plates with slenderness β=1.5. The plates have heat affected zones along all edges.

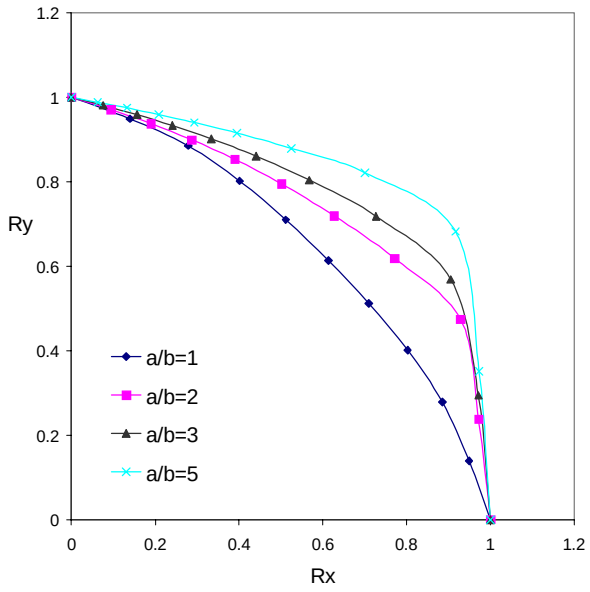

Figure 7.39 : Biaxial interaction curves for plates with slenderness β=2.0. The plates have heat affected zones along all edges.

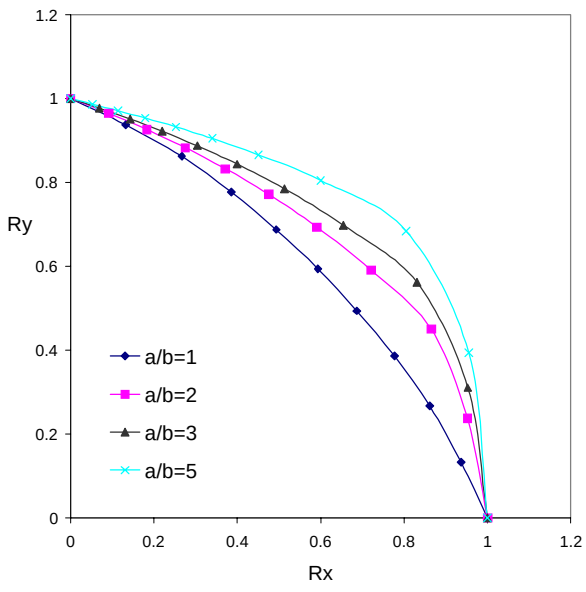

Figure 7.40 : Biaxial interaction curves for plates with slenderness β=2.5. The plates have heat affected zones along all edges.

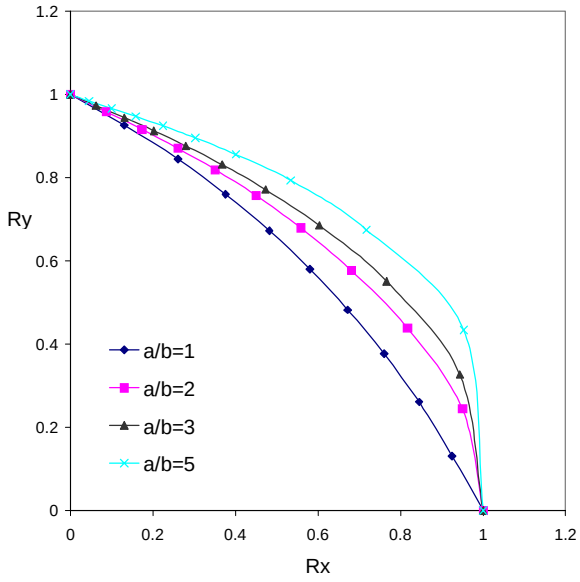

Figure 7.41 : Biaxial interaction curves for plates with slenderness β=3.0. The plates have heat affected zones along all edges.

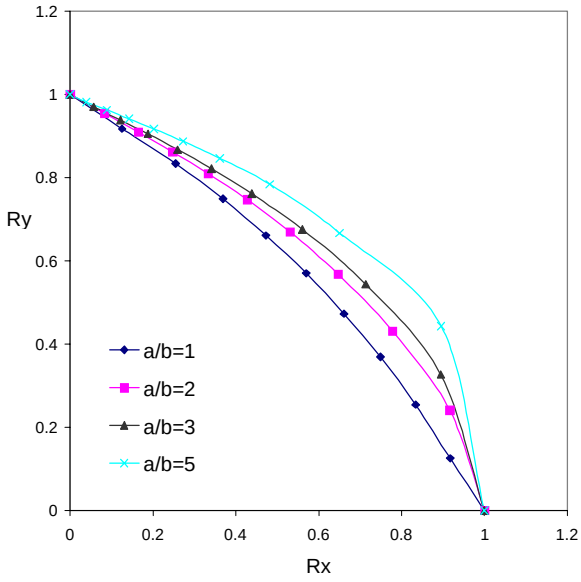

Figure 7.42 : Biaxial interaction curves for plates with slenderness β=3.5. The plates have heat affected zones along all edges.

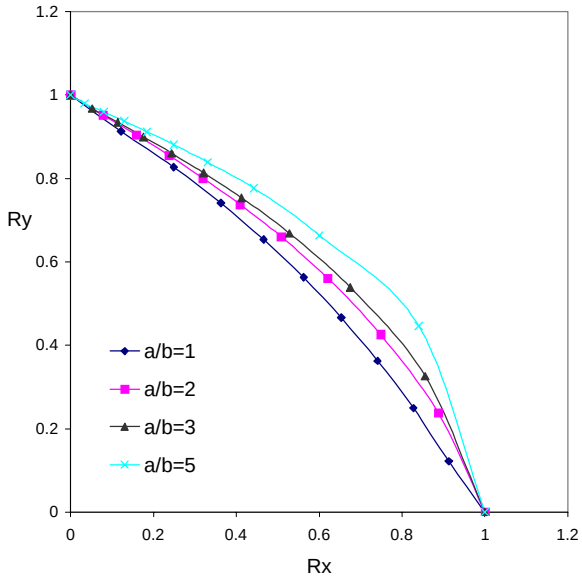

Figure 7.43 : Biaxial interaction curves for plates with slenderness β=4.0. The plates have heat affected zones along all edges.

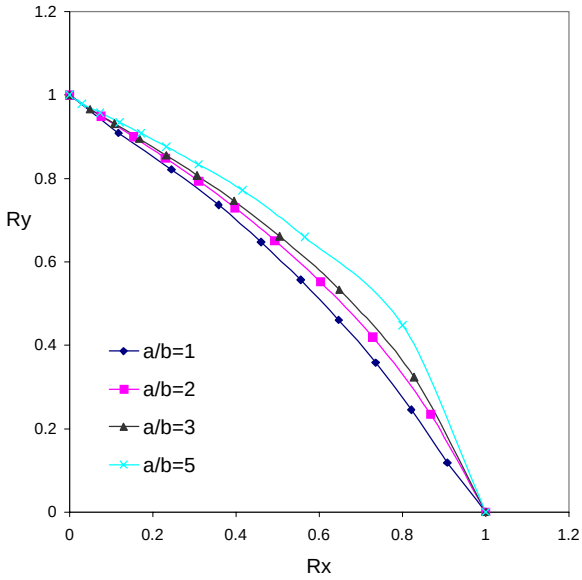

Figure 7.44 : Biaxial interaction curves for plates with slenderness β=4.5. The plates have heat affected zones along all edges.

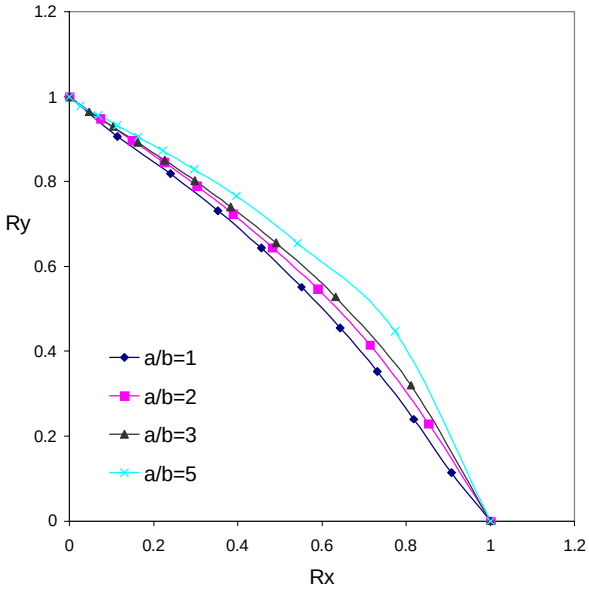

Figure 7.45 : Biaxial interaction curves for plates with slenderness β=5.0. The plates have heat affected zones along all edges.

7.4.3 Interaction Curves for Different HAZ Patterns for Given Aspect Ratio and Slenderness

For each plate slenderness, β, the biaxial curve for plates consisting of the base material only is plotted together with the curve from analyses with plates having heat affected zones along all edges. Plates with aspect ratio, a/b=3, is covered in Chapter 5.4.

7.4.3.1 a/b=1

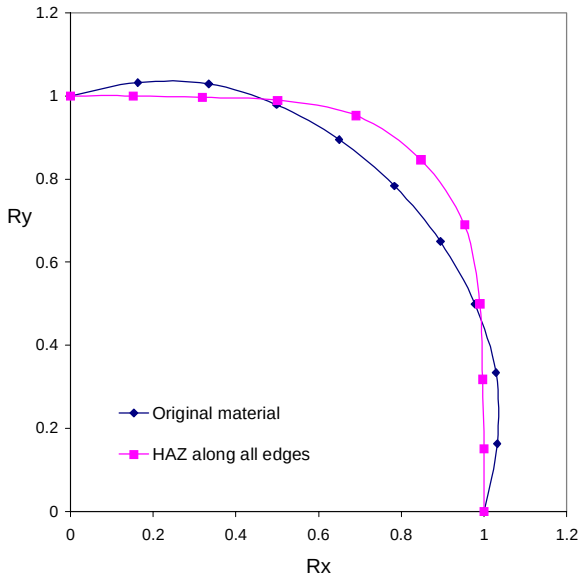

Figure 7.46 : Comparison of biaxial interaction curves for slenderness β=1.0

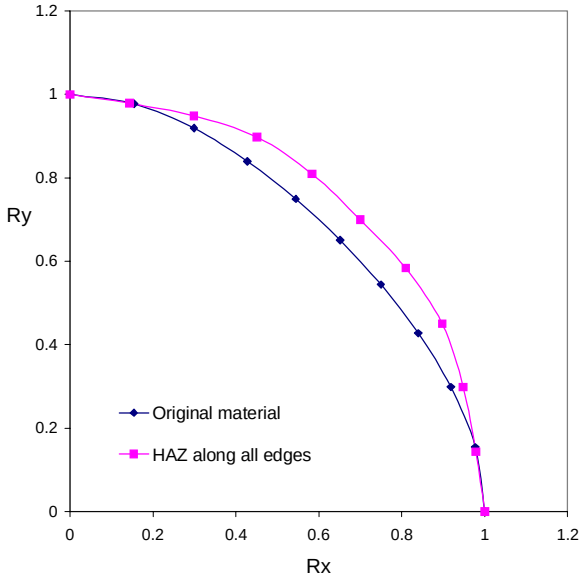

Figure 7.47 : Comparison of biaxial interaction curves for slenderness β=1.5

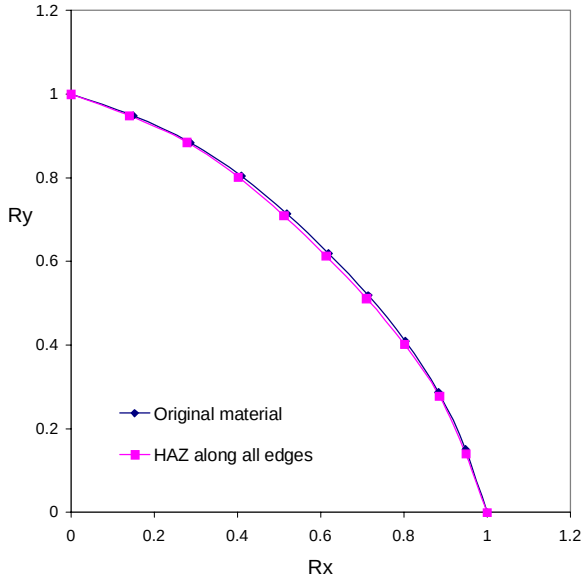

Figure 7.48 : Comparison of biaxial interaction curves for slenderness β=2.0

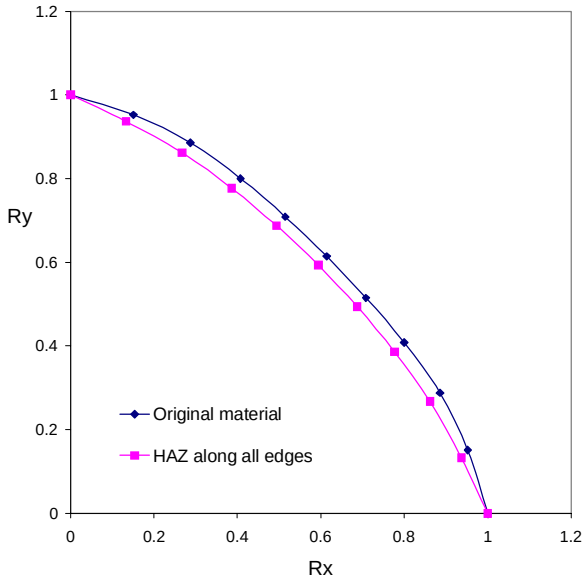

Figure 7.49 : Comparison of biaxial interaction curves for slenderness β=2.5

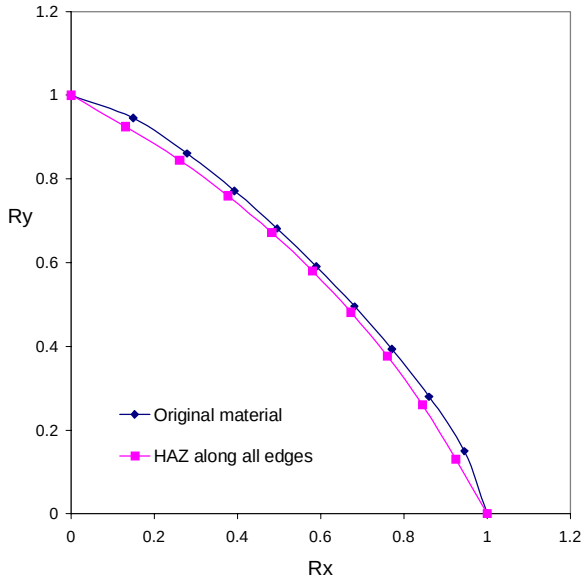

Figure 7.50 : Comparison of biaxial interaction curves for slenderness β=3.0

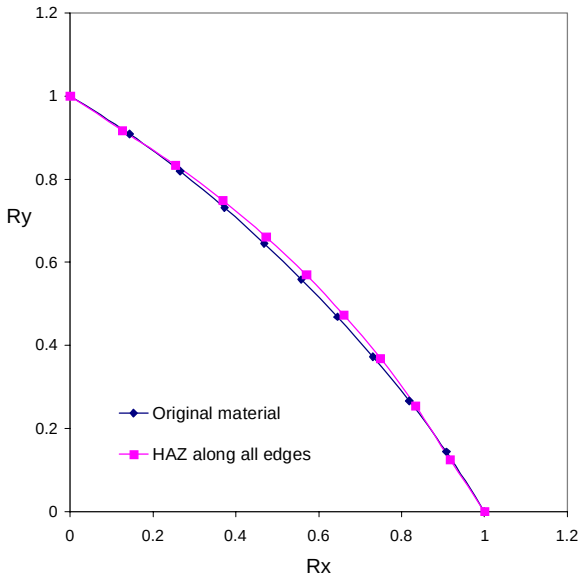

Figure 7.51 : Comparison of biaxial interaction curves for slenderness β=3.5

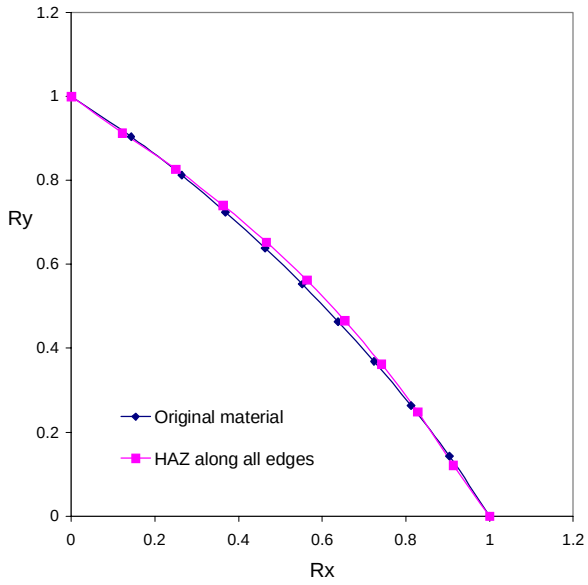

Figure 7.52 : Comparison of biaxial interaction curves for slenderness β=4.0

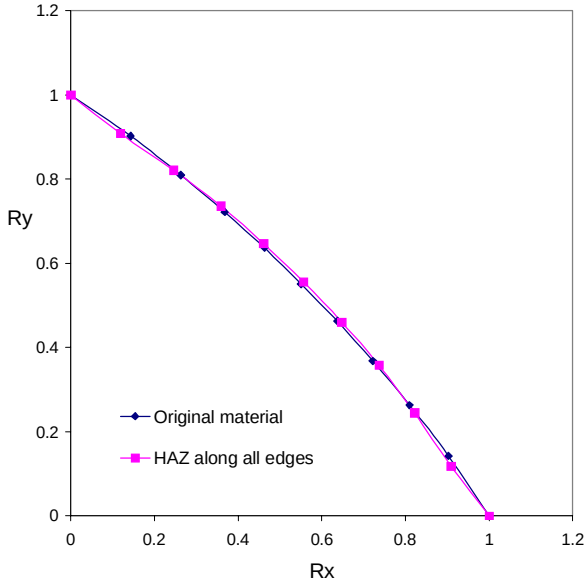

Figure 7.53 : Comparison of biaxial interaction curves for slenderness β=4.5

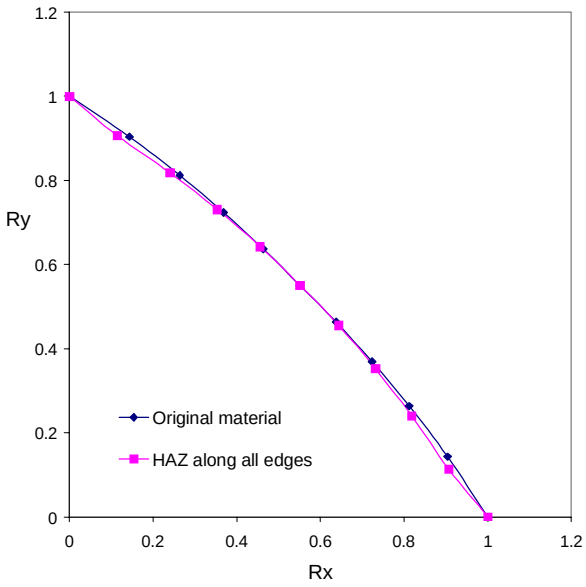

Figure 7.54 : Comparison of biaxial interaction curves for slenderness β=5.0

7.4.3.2 a/b=2

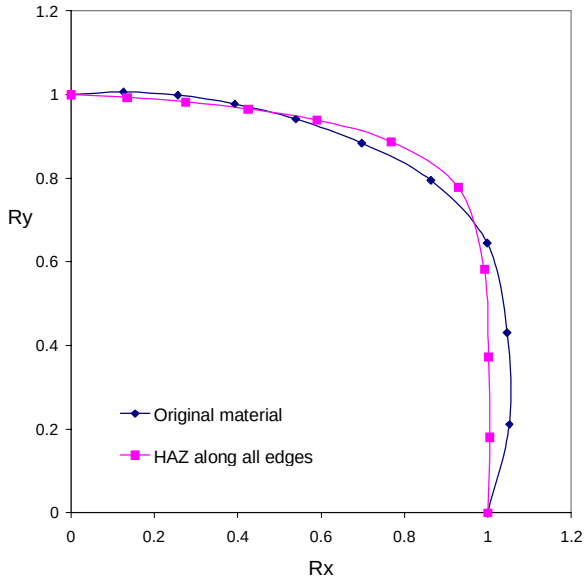

Figure 7.55 : Comparison of biaxial interaction curves for slenderness β=1.0

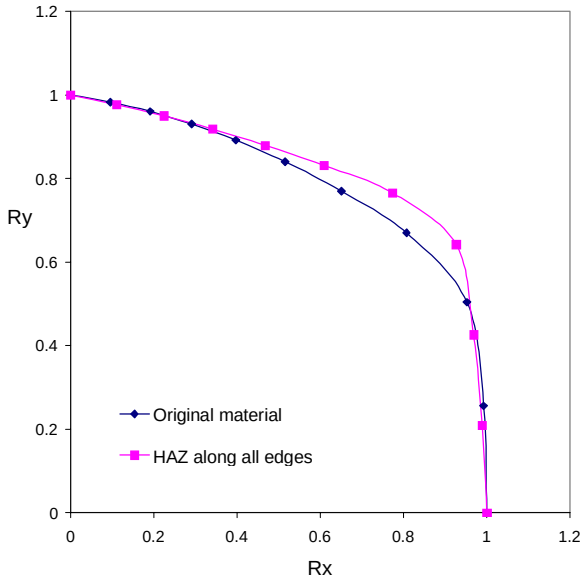

Figure 7.56 : Comparison of biaxial interaction curves for slenderness β=1.5

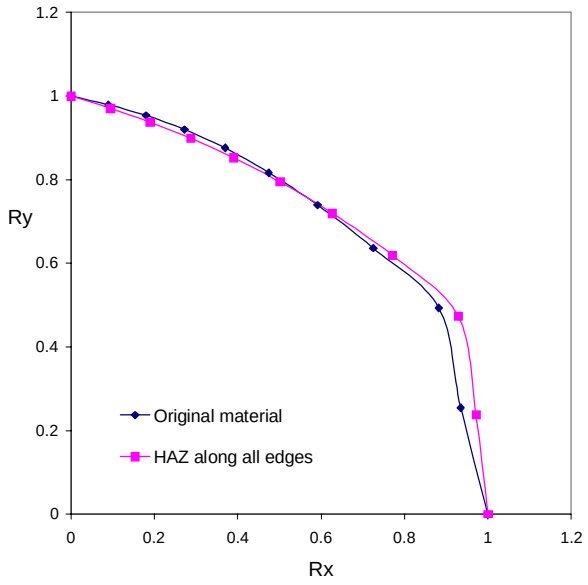

Figure 7.57 : Comparison of biaxial interaction curves for slenderness β=2.0

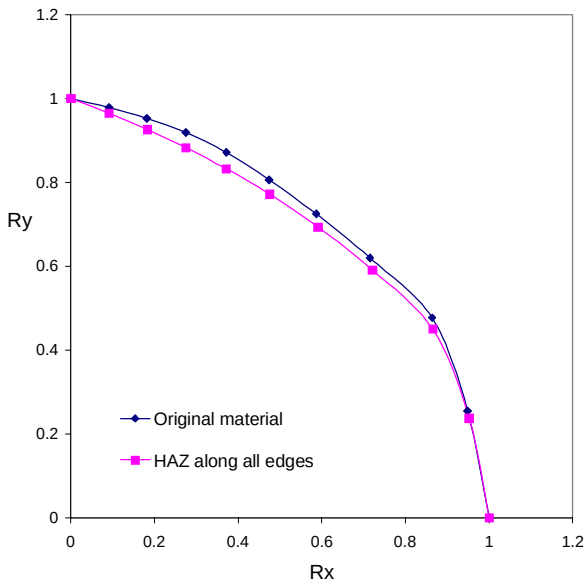

Figure 7.58 : Comparison of biaxial interaction curves for slenderness β=2.5

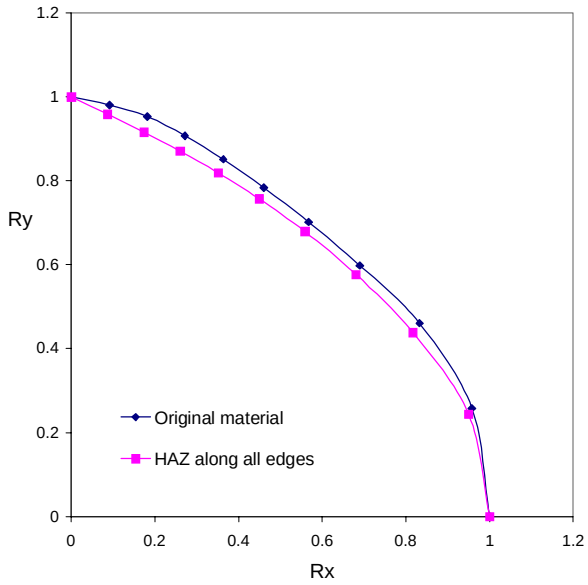

Figure 7.59 : Comparison of biaxial interaction curves for slenderness β=3.0

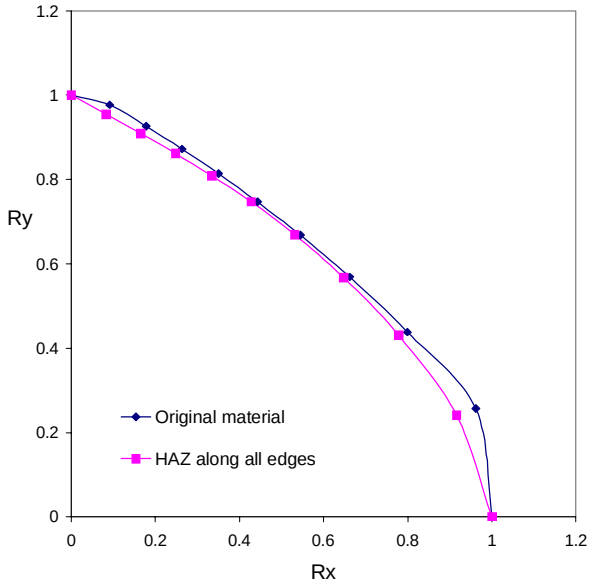

Figure 7.60 : Comparison of biaxial interaction curves for slenderness β=3.5

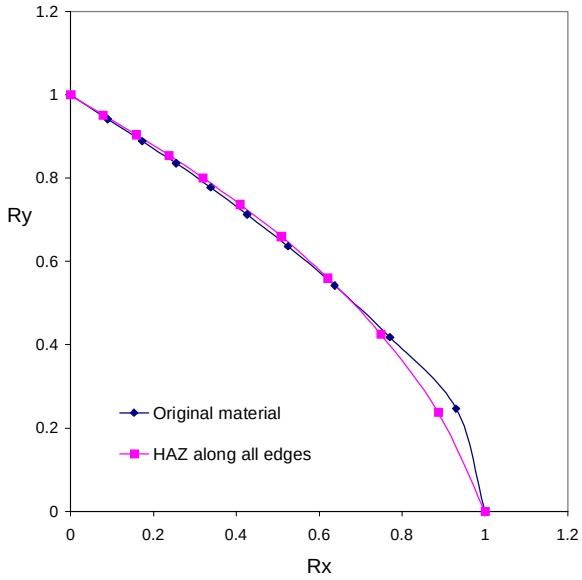

Figure 7.61 : Comparison of biaxial interaction curves for slenderness β=4.0

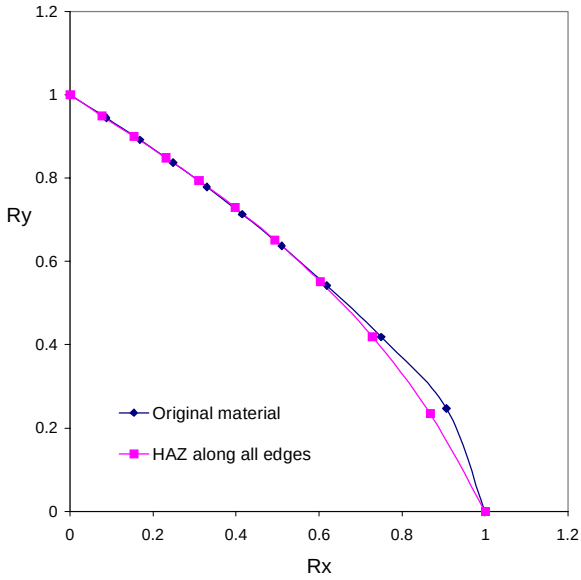

Figure 7.62 : Comparison of biaxial interaction curves for slenderness β=4.5

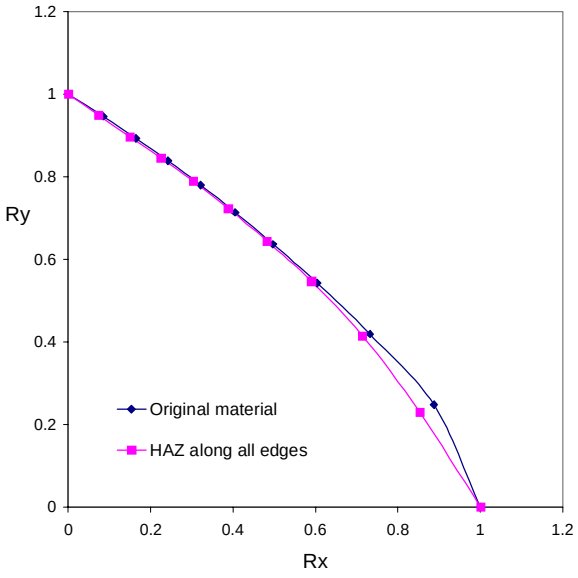

Figure 7.63 : Comparison of biaxial interaction curves for slenderness β=5.0

7.4.3.3 a/b=5

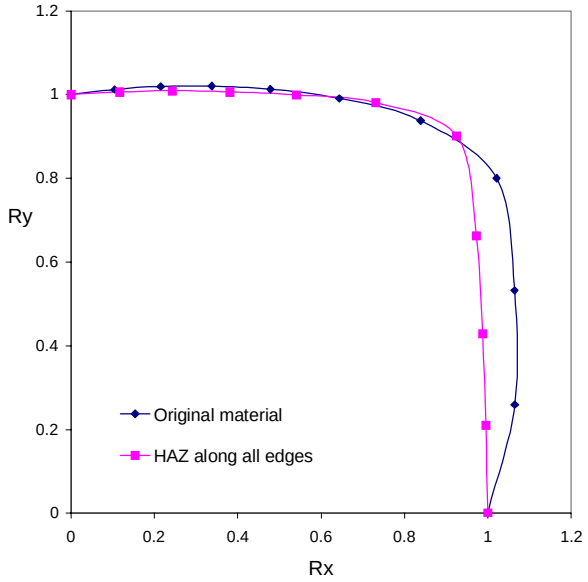

Figure 7.64 : Comparison of biaxial interaction curves for slenderness β=1.0

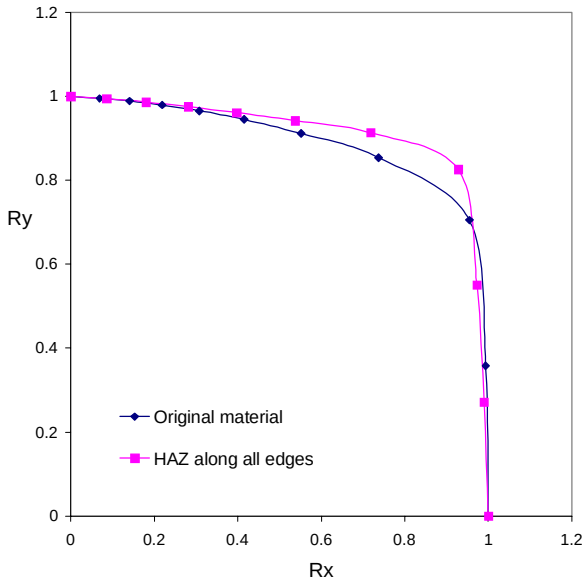

Figure 7.65 : Comparison of biaxial interaction curves for slenderness β=1.5

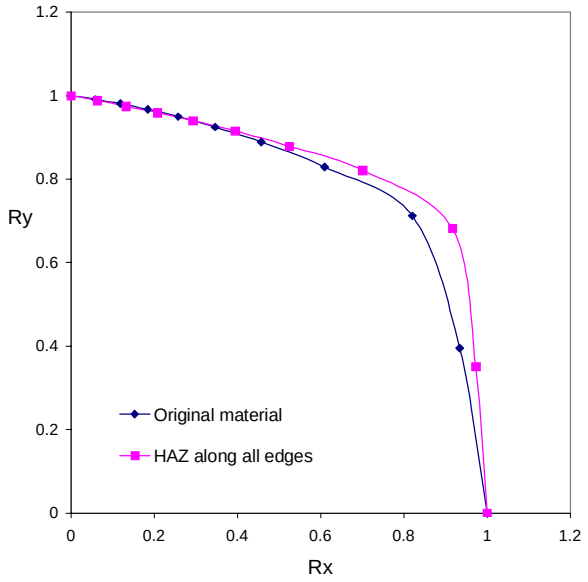

Figure 7.66 : Comparison of biaxial interaction curves for slenderness β=2.0

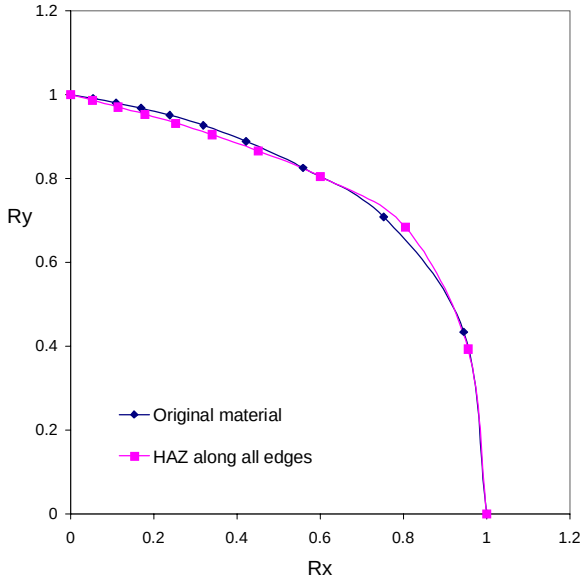

Figure 7.67 : Comparison of biaxial interaction curves for slenderness β=2.5

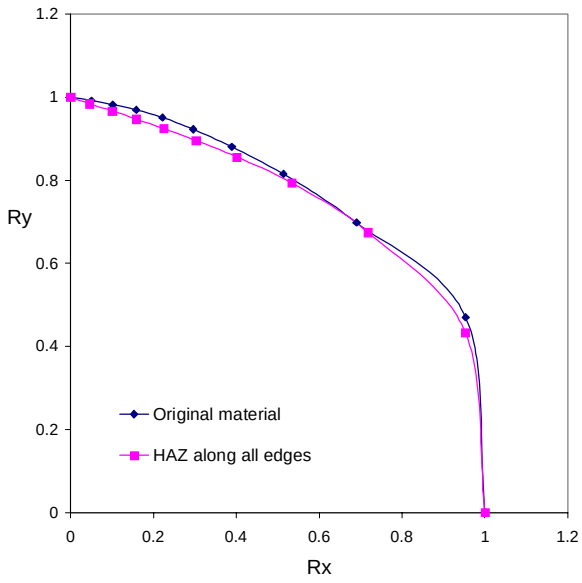

Figure 7.68 : Comparison of biaxial interaction curves for slenderness β=3.0

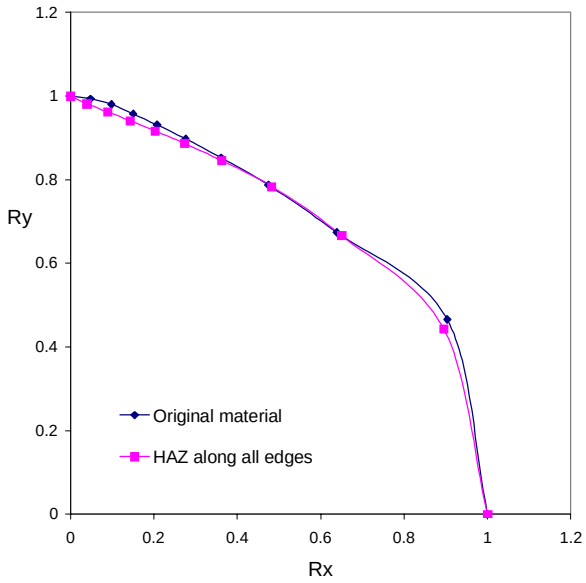

Figure 7.69 : Comparison of biaxial interaction curves for slenderness β=3.5

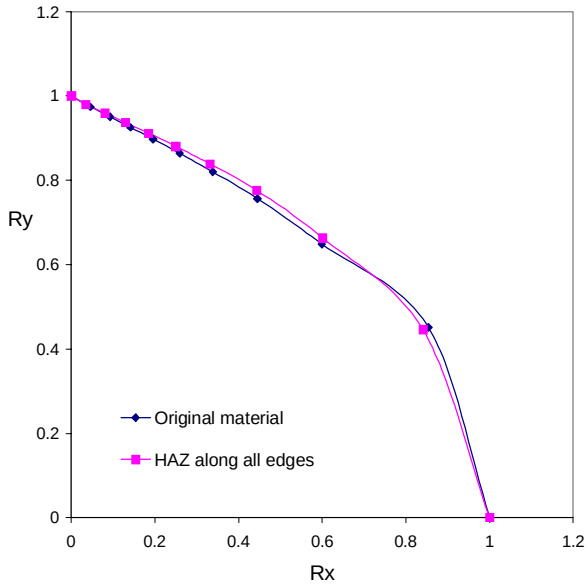

Figure 7.70 : Comparison of biaxial interaction curves for slenderness β=4.0

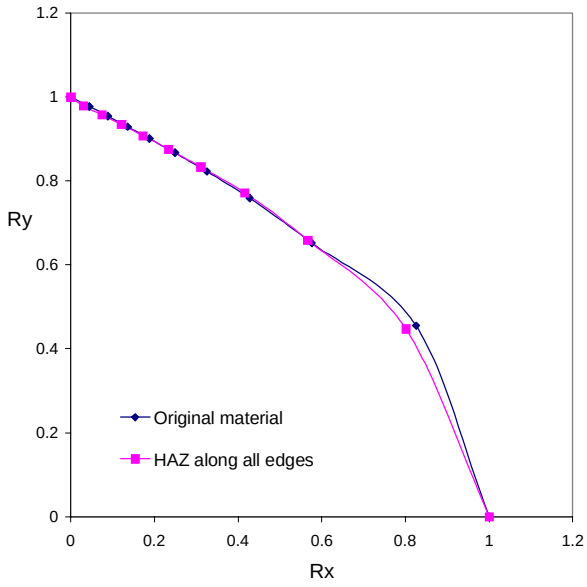

Figure 7.71 : Comparison of biaxial interaction curves for slenderness β=4.5

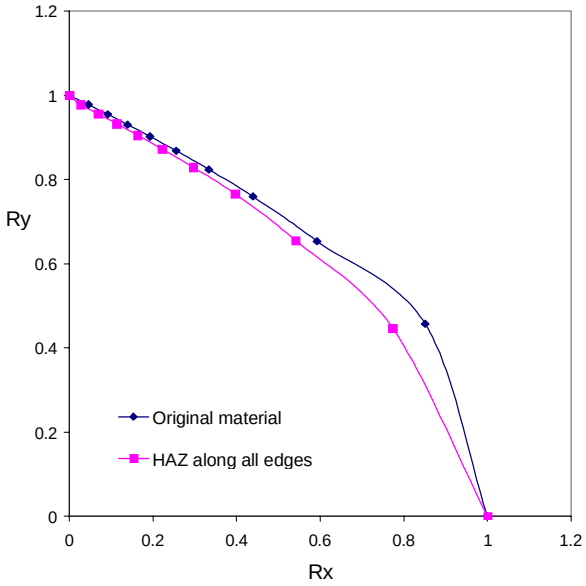

Figure 7.72 : Comparison of biaxial interaction curves for slenderness β=5.0

Plates with aspect ratio, a/b=1, show stronger interaction (the stronger the interaction is the closer the interaction is to linear interaction) than plates with higher values of the aspect ratio, a/b. There is also a larger difference in the shape of the biaxial interaction curves if the aspect ratio is altered from a/b=1 to a/b=2 than if the aspect ratio is altered between other two neighbouring integer values.

One reason for this behaviour is that plates with aspect ratio, a/b=1, have the same critical initial deflection pattern for all loading conditions, one half wave in both longitudinal and transverse direction. For other values of the aspect ratio, a/b, the initial deflection patterns giving the lowest ultimate capacities will vary depending on the loading condition.

This only explains a part of the variation in the shapes of the biaxial interaction curves as the aspect ratio, a/b, is altered. Assuming the slenderness, β, to be constant, the axial ultimate capacity will also be constant for all values of the aspect ratio, a/b. The transverse ultimate capacity, on the other hand, will be lower and lower, as the value of the aspect ratio, a/b, increases. The same relative transverse load utilisation will result in a lower and lower absolute force. As transverse forces become lower and lower they will have less and less influence on the axial ultimate capacity; allowing the same axial utilisation to have a higher transverse utilisation.

Because there is a bigger change in transverse buckling capacities as the aspect ratio, a/b, is changed from a/b=1 to a/b=2, than between any other neighbouring integer values, the alteration in the shape of the biaxial interaction curves will also be larger if the aspect ratio, a/b, is changed from a/b=1 to a/b=2, than between any other neighbouring integer values.

If the plates become extremely sturdy, the biaxial interaction curves are limited by the Hencky-von Mises ellipse, independent of the aspect ratio, a/b. Very slender plates will be limited by linear interaction, independent of the aspect ratio, a/b. This explains why the biaxial interaction curves gradually coincide as the slenderness, β, increases, and why the interaction curves gradually coincide if β becomes extremely small.

As have already been mentioned in Chapter 5.4 there are no large discrepancies in the biaxial interaction curves if the plates are exposed to heat affected zones or not. Most of the differences take place for compact plates. Plates consisting of the base material only seem to have a little stronger interaction, but there are no general trends and the differences in shapes are not very large.

Much of the same arguments described previously can be used. For the biaxial interaction curves to be different, the relationship between the axial and transverse buckling capacities needs to be different for plates having the same slenderness, β, and the same aspect ratio, a/b. This is observed in Chapter 5.4. Plates with heat affected zones along all edges and plates with the extruded pattern of the heat affected zones have the same axial capacity, but plates with the extruded pattern of the heat affected zones have weaker transverse capacitiy. The axial loading is less influenced, and the interaction becomes weaker.

Introducing heat affected zones along all edges of a plate lower both the axial capacities and the transverse capacities of the plates, but the lowering is done in such a fashion that the relationship between axial and transverse loads is kept fairly constant. This may be explained by looking at the reductions in axial and transverse capacities. If the aspect ratio, a/b=1, the axial and transverse capacities are identical and the relationship between them is equal to unity, both before and after the introduction of heat affected zones.

For plates with higher values of the aspect ratio, a/b, the reduction in axial capacity is a little larger than the reduction in transverse capacity, but this effect is not large enough to significantly alter the relationship between axial and transverse ultimate capacity.

Chapter 8

Effect of Initial Deflections on Ultimate Capacity

8.1 General

In this chapter the effects of altering the initial deflection amplitude and the initial deflection pattern of axially and transversally loaded plates are studied.

In the analyses so far, plates exposed to axial loading or transverse loading have been given their respective linear eigenmodes as initial deflection patterns (the details can be found in Chapter 4.5). In this chapter axial and transverse collapse analyses with the initial deflection patterns used in the biaxial analyses, have been carried out, and the results compared with collapse analyses with the linear elastic eigenmodes used as the initial deflection patterns.

To study the sensitivity of aluminium plates to the value of the maximum initial deflection amplitude, parametric studies where the maximum initial deflection amplitude is varied have been performed.

The sensitivity of plates to change in initial deflection amplitude and initial deflection pattern has been studied for plates consisting of the base material only and plates with heat affected zones along all edges.

8.2 Effect of Initial Deflection Amplitude

8.2.1 Axial Compression

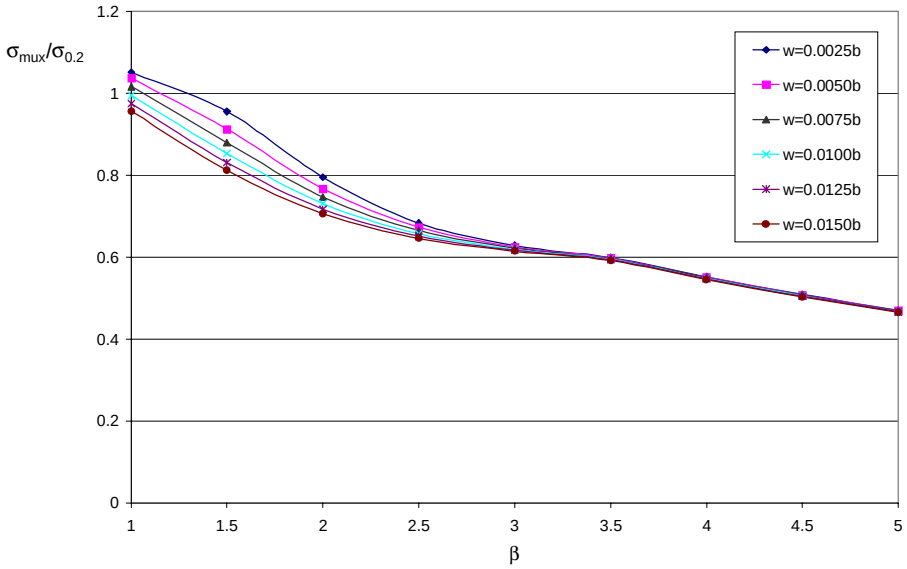

Figure 8.1 : Axial ultimate capacities for different maximum values of the initial out of plane deflection, w. The plates are made of the base material only. Aspect ratio, a/b=3.

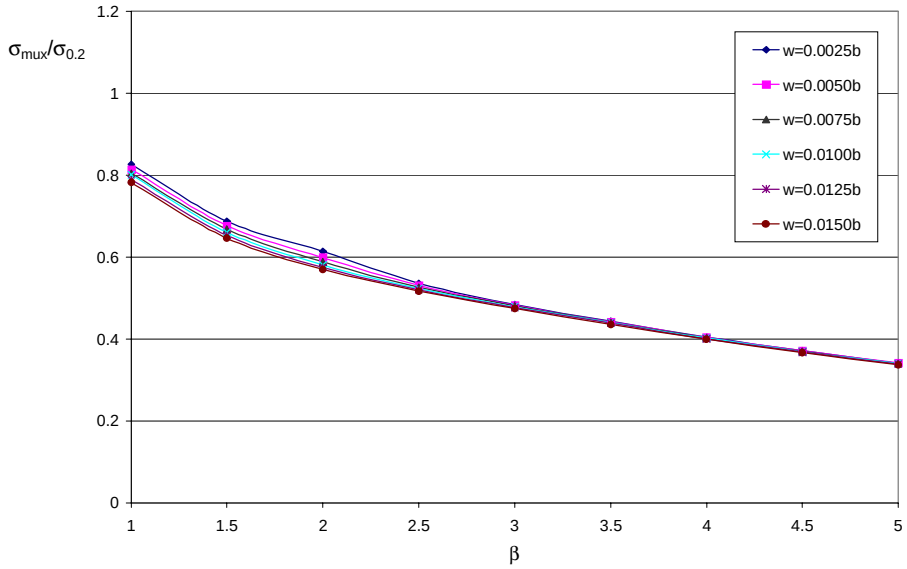

Figure 8.2 : Axial ultimate capacities for different maximum values of the initial out of plane deflection, w. The plates have heat affected zones along all edges. Aspect ratio, a/b=3.

Figures 8.1 and 8.2 give the axial ultimate capacities for different maximum levels of the initial out of plane deflection, w. In Figure 8.1 the plates consist of the base material only, and in Figure 8.2 the plates have heat affected zones along all edges. Curves showing the percentage reduction in strength as compared to analyses with the smallest value of the maximum initial out of plane deflection, w, are given in Appendix 3.

8.2.2 Transverse Compression

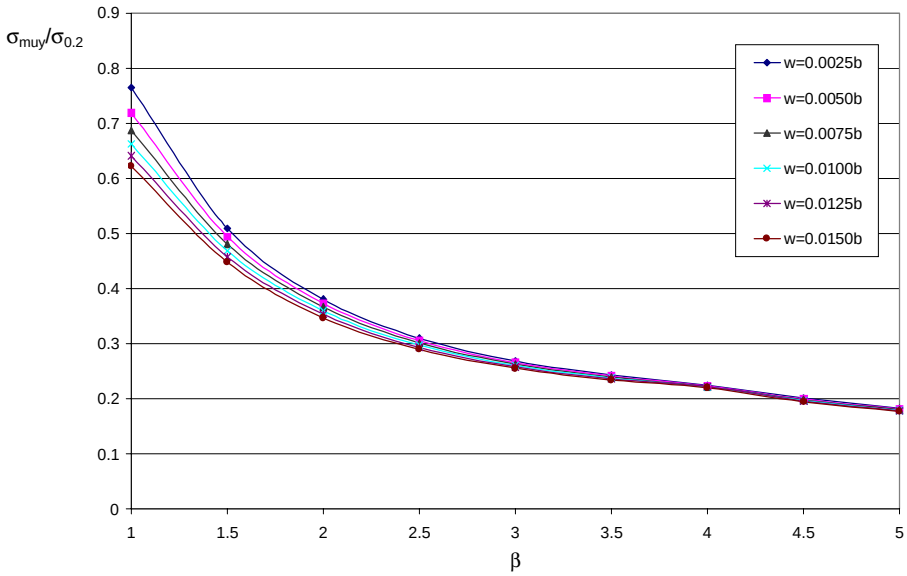

Figure 8.3 : Transverse ultimate capacities for different maximum values of the initial out of plane deflection, w. The plates are made of the base material only. Aspect ratio, a/b=3.

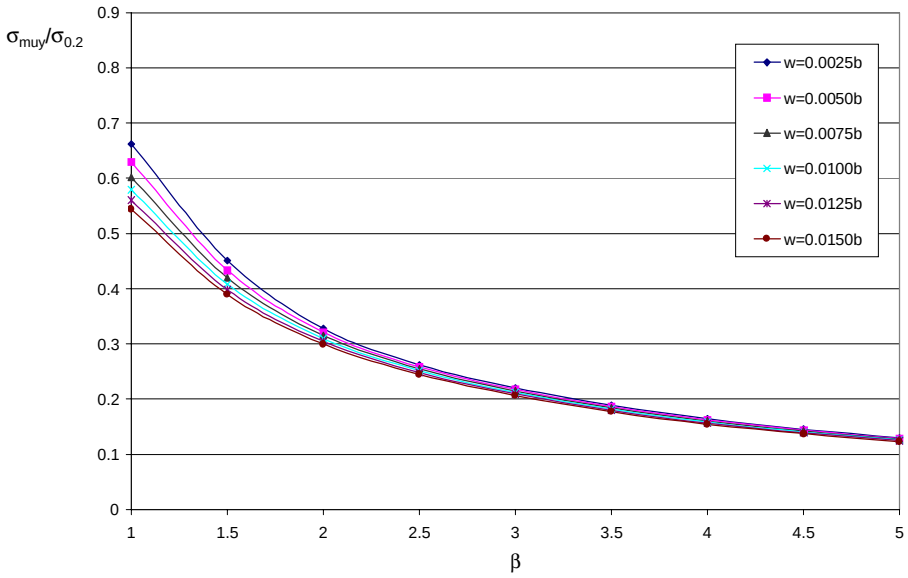

Figure 8.4 : Transverse ultimate capacities for different maximum values of the initial out of plane deflection, w. The plates have heat affected zones along all edges. Aspect ratio, a/b=3.

Figures 9.3 and 9.4 show the transverse ultimate capacities for different maximum levels of the initial out of plane deflection, w. Figure 9.3 gives the results for plates consisting of the base material only, and Figure 9.4 gives the results for plates with heat affected zones along all edges. Curves showing the percentage reduction in strength as compared to analyses with the smallest value of the maximum initial out of plane deflection, w, are given in Appendix 3.

8.2.3 Discussion

When plates are given initial imperfections, there is no longer a bifurcation problem, but a limit point problem. Due to the presence of initial imperfections, the plates start to deflect immediately. When the deflections become sufficiently large, areas with plasticity are gradually created. For slender plates the formation of regions with plasticity takes place for larger deflections than more sturdy plates. When the deflection due to external loads needs to be large before plasticity occurs, the initial value of the imperfection becomes less important.

The before mentioned behaviour, with increasing sensitivity to initial deformations the more compact the plates become, continues until the plates become so compact that collapse occurs by crushing; and the importance of initial imperfections gradually disappears.

For axially loaded plates with slenderness, β, less than 3.0, the presence of heat affected zones seems to lower the importance of maximum initial deflection amplitudes. The collapse mechanism for those plates are local failure at the loaded edges, and this collapse mechanism is believed to be more unaffected by the values of the initial deflections.

8.3 Effect of Initial Deflection Pattern

For pure axial loading and pure transverse loading the linear elastic eigenmodes for simply supported edges are chosen as the initial deflection patterns. Using the linear elastic eigenmodes is believed to give low ultimate capacities, but will they always give the lowest ultimate capacities?

In experiments on aluminium plates done by Mofflin (see Mofflin, 1983, page 3.31) he concluded "that the ultimate load cannot be particularly sensitive to wavelength". Mofflin did experiments on the ultimate capacity of plates with different values of the slenderness, β, and no particular wavelength seemed to dominate the post buckling shape, but he observed a shortening of the preferred wavelength as the plates become extremely compact ($\beta<0.6$).

To check the sensitivity of the plates to variations in the initial deflection patterns, axial and transverse collapse analyses with the initial deflection patterns used in the biaxial analyses (formulas in Chapter 4.5), have been carried out, and the results compared with collapse analyses with the linear elastic eigenmodes used as the initial deflection patterns.

8.3.1 Axial Loading

Figure 9.5 and 9.6 show results of axially loaded plates with aspect ratio, a/b=3. The curves for other aspect ratios, a/b, are given in Appendix 4.

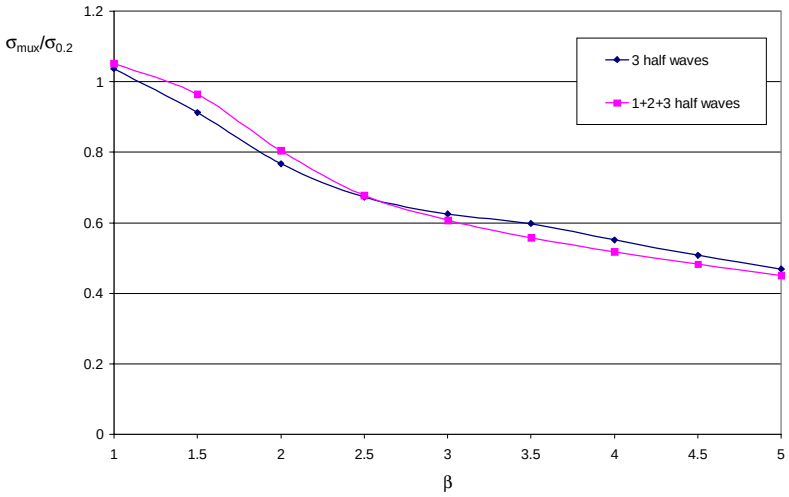

Figure 8.5 : Axial ultimate capacity obtained by using the linear elastic eigenmode, compared with ultimate capacity obtained by using the initial deflection pattern employed in the biaxial analyses. The plates have no heat affected zones, and the aspect ratio, a/b=3.

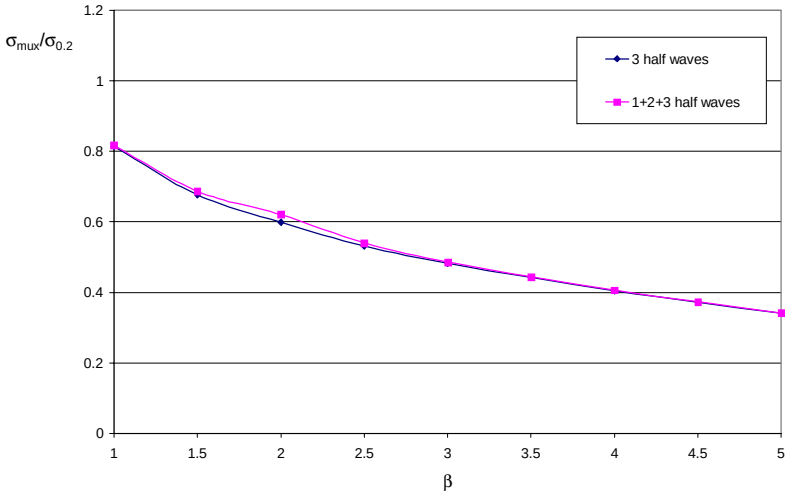

Figure 8.6 : Axial ultimate capacity obtained by using the linear elastic eigenmode, compared with ultimate capacity obtained by using the initial deflection pattern employed in the biaxial analyses. The plates have heat affected zones along all edges, and the aspect ratio, a/b=3.

8.3.2 Transverse Loading

Figure 9.7 and 9.8 show results of transversally loaded plates with aspect ratio, a/b=3. The curves for other aspect ratios, a/b, are given in Appendix 4.

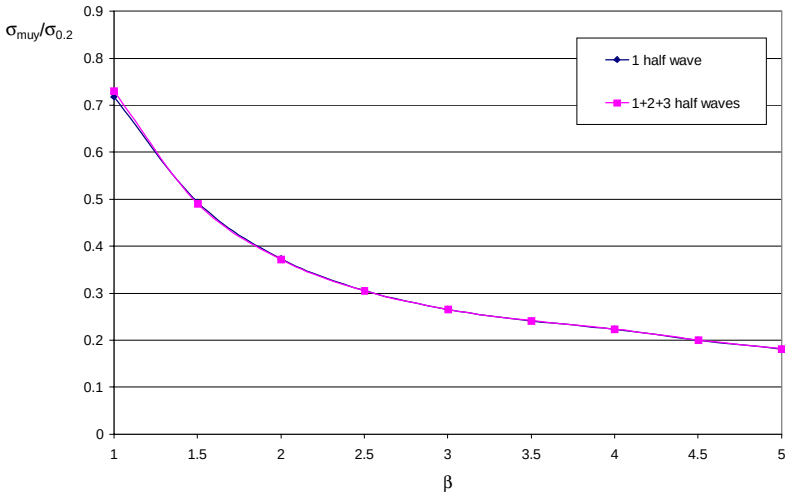

Figure 8.7 : Transverse ultimate capacity obtained by using the linear elastic eigenmode, compared with ultimate capacity obtained by using the initial deflection pattern employed in the biaxial analyses. The plates have no heat affected zones, and the aspect ratio, a/b=3.

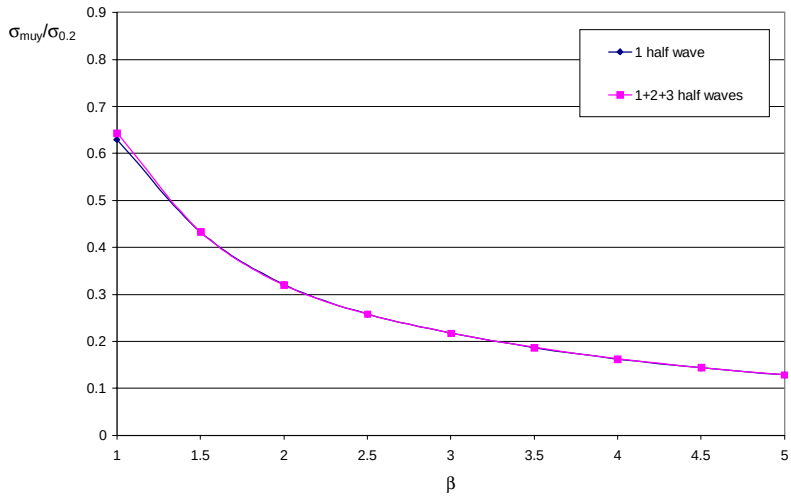

Figure 8.8 : Transverse ultimate capacity obtained by using the linear elastic eigenmode, compared with ultimate capacity obtained by using the initial deflection pattern employed in the biaxial analyses. The plates have heat affected zones along all edges, and the aspect ratio, a/b=3.

8.3.3 Discussion

As long as the loading is transverse, no peculiar behaviour is observed. Plates with the elastic eigenmode (one half wave in both longitudinal and transverse direction) have the lowest ultimate capacities for all plates analysed. Introducing heat affected zones along all edges does not change this behaviour. The increase in ultimate capacity if the initial deflection pattern is altered from the linear elastic buckling mode to the initial deflection pattern used for biaxial analyses, is negligible.

If the plates have heat affected zones along all edges, axially loaded plates show the same behaviour as transversally loaded plates. Compact plates with the biaxial initial deflection pattern have slightly higher ultimate capacity than plates with the initial deflection pattern equal to the linear eigenmodes.

On the other hand, if the axially loaded plates consist of the base material only, slender plates with the biaxial initial deflection pattern have lower ultimate capacity than plates with the linear eigenmode as the initial deflection pattern. The author has difficulties explaining this phenomenon, that occurs for all values of the aspect ratio, a/b.

One possible explanation can be found by looking at the collapse mechanisms. Plates exposed to the biaxial initial deflection patterns collapse with a large deflection at the mid part of the plate in on of the out-of-plane directions, and only small deflections in the opposite direction. The deflection in the middle part of the plate has a much higher value for the same overall axial strain than the equally valued deflections observed for plates with the linear elastic eigenmodes as the initial deflection patterns.

The much higher deflections at the mid part of the plate create a much higher out of plane curvature with much more abrupt geometry changes between the different parts of the plates

Taking into account the fact that most of the load carrying takes place towards the longitudinal edges of the plate, an effective transfer of the longitudinal stresses is prevented by the abrupt geometry changes. The higher out of plane curvature also results in higher bending moments at the mid part of the plate with reduced capability to carry longitudinal stresses.

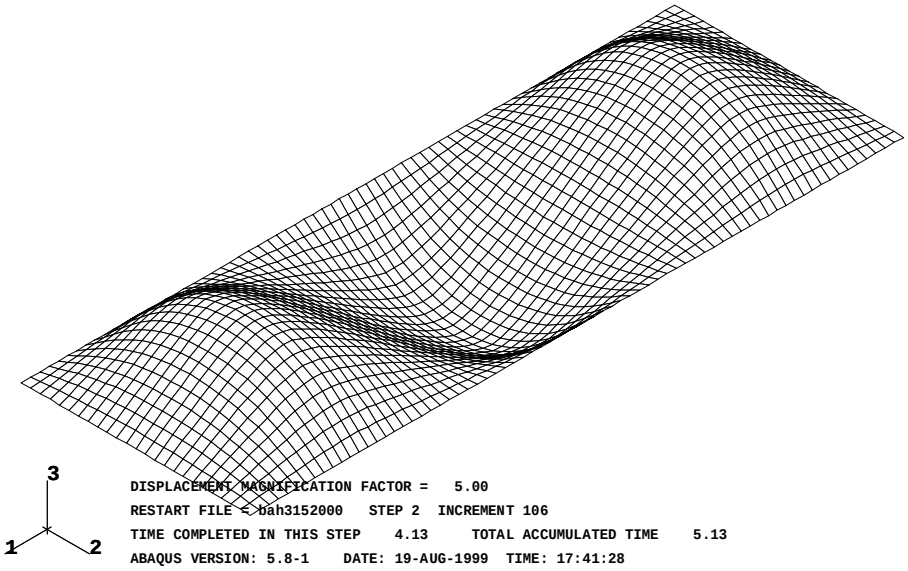

Figure 8.9 : Collapse machanism for axially loaded plate with initial deflection pattern equal to the linear elastic eigenmode. The plate has no heat affected zones. The aspect ratio, a/b=3.

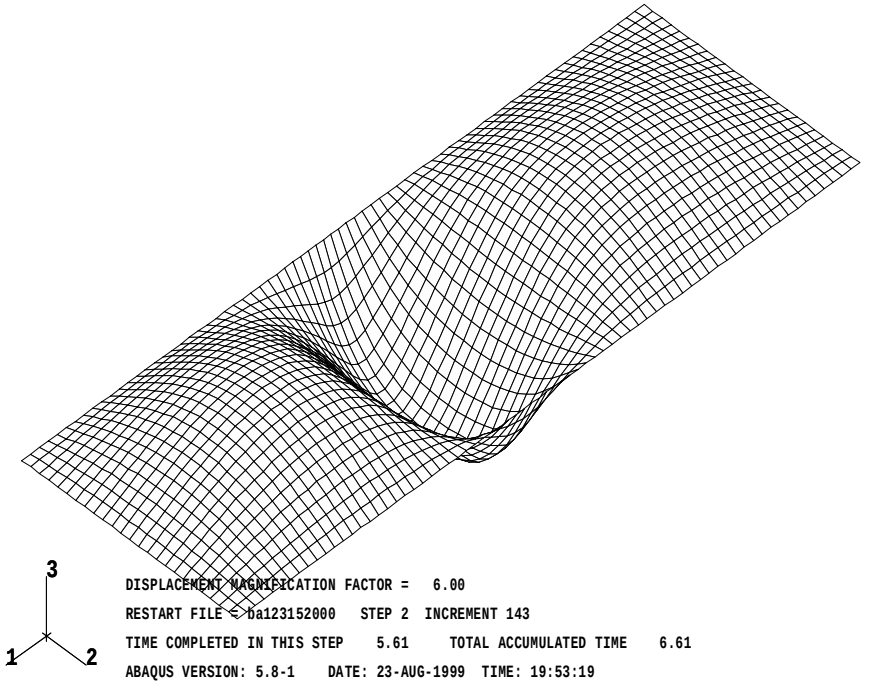

Figure 8.10 : Collapse machanism for axially loaded plate with the biaxial initial deflection pattern. The plate has no heat affected zones. The aspect ratio, a/b=3.

Chapter 9

Effect of Material Properties on Ultimate Capacity

9.1 Introduction

So far all analyses have been performed for alloy 6082-T6. The material properties in the heat affected zones have been altered in parametric studies, but the material properties in the parts of the plates not affected by welding have not been varied. These parts constitute the major parts of the plates. Aluminium alloys have a huge variation in material characteristics. It is therefore interesting to investigate the behaviour of plates made of other alloys.

The materials given in Table 2.5 are believed to represent a high, medium and low utilisation of aluminium alloy (Mofflin, 1983). The axial, transverse and biaxial collapse curves for these three different alloys have been investigated and compared. The goal is to find a unified way of presenting the collapse results, that is, an appearance which is as similar as possible for the different aluminium alloys investigated.

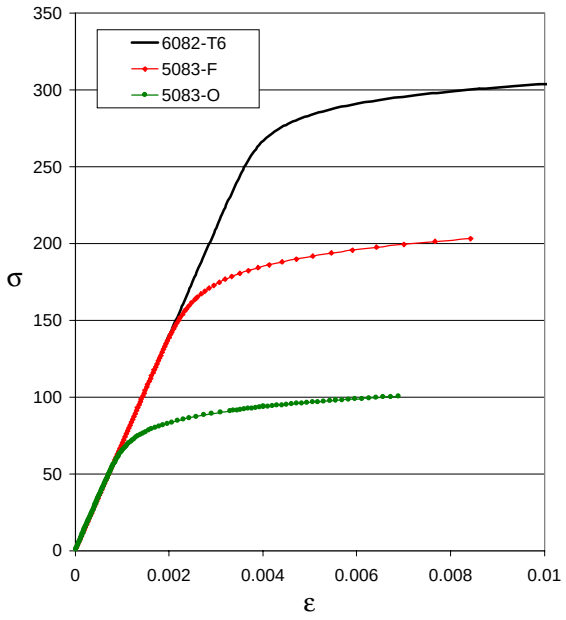

Figure 9.1 : Stress-strain curves for the different aluminium alloys investigated

9.2 Normalising Results

9.2 .1 Axial Loading

The stresses, σ_{elpl}, corresponding to equal elastic and plastic strain are believed to be better suited as normalising stresses. For the more commonly used normalising stress, the 0.2 percent tensile proof stresses, or $\sigma_{0.2}$, the elastic strain vary depending on aluminium alloy considered, while the plastic permanent strain is kept constant. When using the strain

corresponding to equal elastic and plastic strain, both the elastic part of the strain and the plastic part of the strain is varied for the different alloys investigated. The points obtained, are believed to be in a more similar part of the utilisation of the different aluminium alloys.

Table 9.1 compares $\sigma_{0.2}$ and σ_{elpl} for the different alloys analysed. Because the plastic part of the strain is constant when calculating the 0.2 percent tensile proof stress, high utilised aluminium alloys have to increase the stress to obtained the stress making the elastic part of the strain equal to the plastic part of the strain, while low utilised aluminium alloys must reduce the stress as compared to the 0.2 percent tensile proof stress.

Table 9.1 : Comparison of the 0.2 percent tensile proof stress and the stress corresponding to equal elastic and plastic strain for the different aluminium alloys used in the analyses

Alloy	$\sigma_{0.2}$	σ_{elpl}
6082-T6	292	300.71
5083-F	190	194.19
5083-O	91	86.75

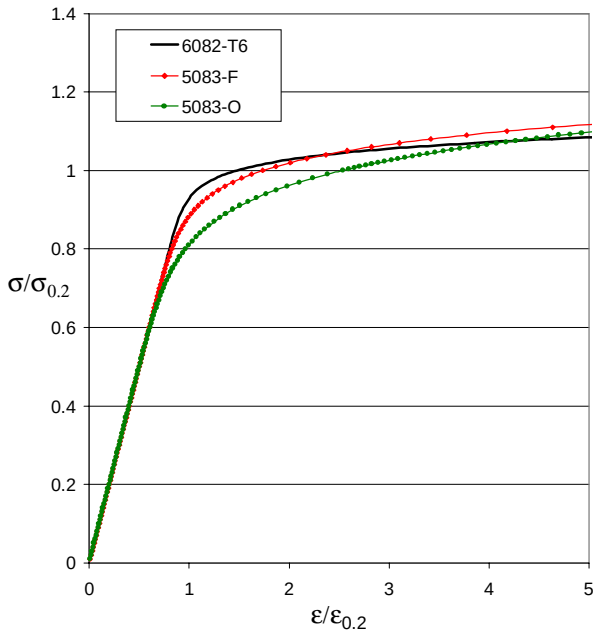

Figure 9.2 : Stress-strain curves for the different aluminium alloys investigated. The curves have been normalised with the 0.2 percent tensile proof stress.

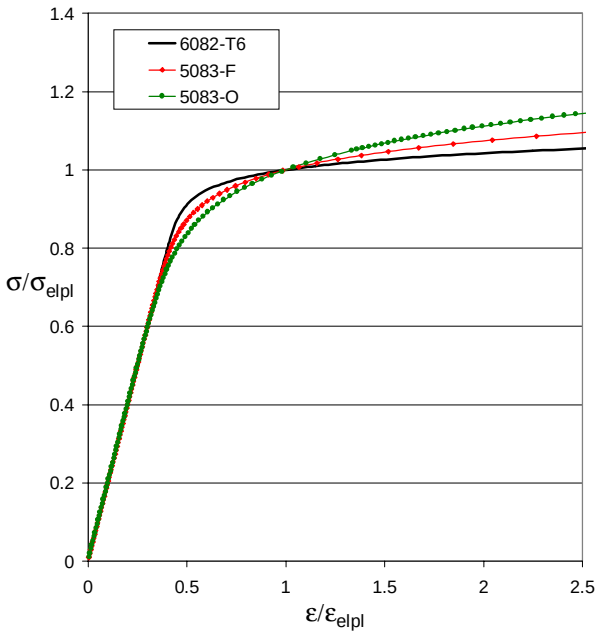

Figure 9.3 : Stress-strain curves for the different aluminium alloys investigated. The curves have been normalised with the stress corresponding to equal elastic and plastic strain.

Figure 9.4 shows the axial ultimate capacities for the different alloys analysed. The ultimate capacities have been normalised with respect to the 0.2 % tensile proof stresses. In Figure 9.5 the same axial ultimate capacities have been normalised with the stress corresponding to equal elastic and plastic strain.

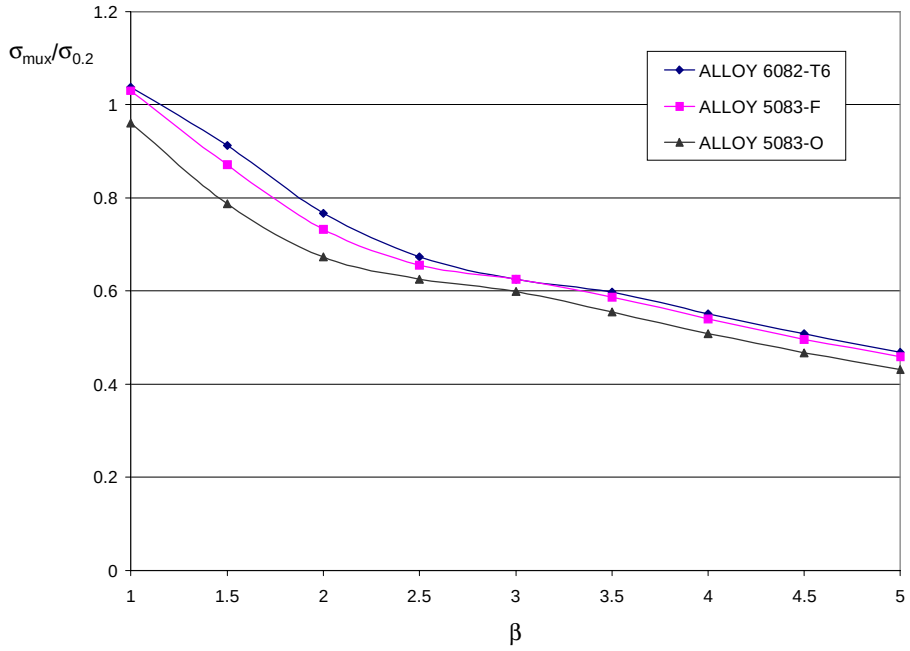

Figure 9.4 : Axial ultimate capacities of different aluminium alloys. The plates consist of the base material only, and their ultimate capacities have been normalised with the 0.2 percent tensile proof stress.

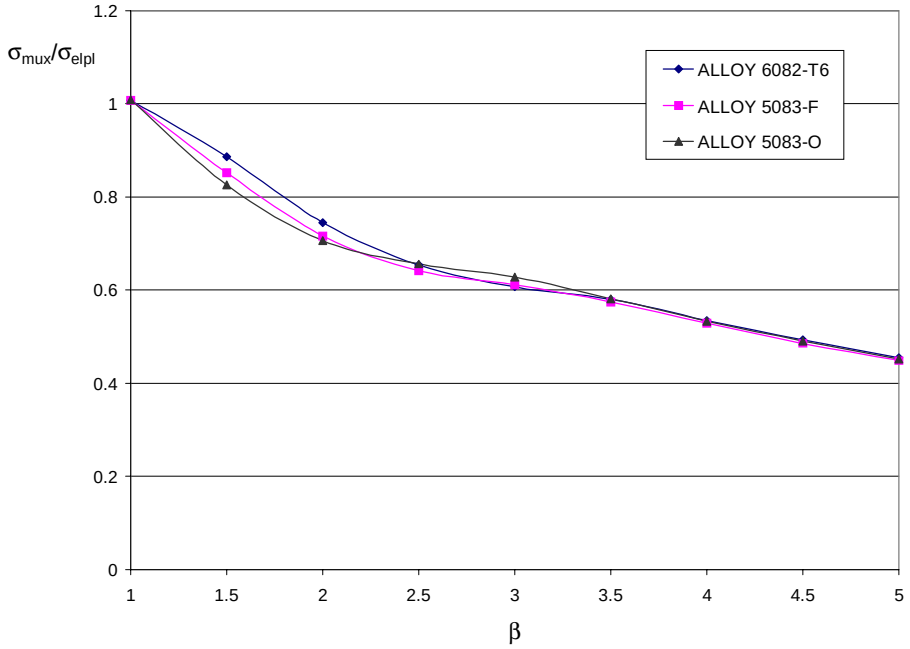

Figure 9.5 : Axial ultimate capacities of different aluminium alloys. The plates consist of the base material only, and their ultimate capacities have been normalised with the stress corresponding to equal elastic and plastic strain.

Comparing Figures 9.4 and 9.5 one can see that normalising the different axial ultimate capacities with respect to the stress corresponding to equal elastic and plastic strain makes the different collapse curves very similar. One single curve can be established to represent the

axial ultimate capacities for all the different aluminium alloys analysed. This is not the case if one uses the 0.2 percent tensile proof stress as the normalising stress.

Figures 9.6 and 9.7 give axial ultimate capacities of plates exposed to heat affected zones along all edges. In Figure 9.6 the plates have a 10 percent reduction of the yield strength in the heat affected zones, and in Figure 9.7 the plates have a 50 percent reduction of the yield strength in the heat affected zones. The ultimate capacities are normalised with respect to the stresses giving equal elastic and plastic strain.

The 50 percent reduction of the yield strength in the heat affected zones is realistic for alloy 6082-T6, but for alloys 5083-F and 5083-O such a large reduction in yield strength in the heat affected zones is introduced for the purpose of studying sensitivity.

Curves with the ultimate capacities normalised with the 0.2 percent tensile proof stress are given in Appendix 5.

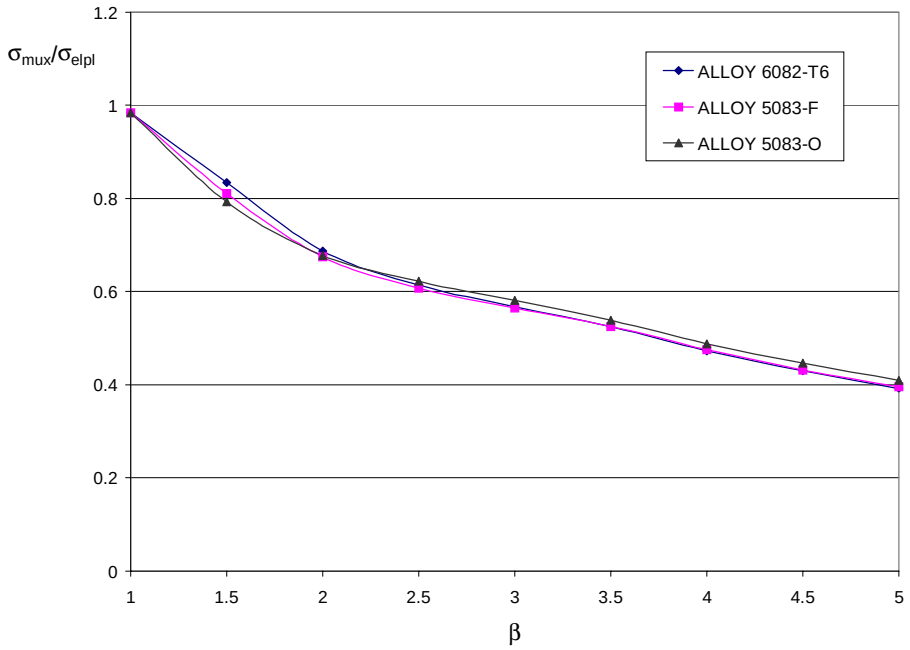

Figure 9.6 : Axial ultimate capacities of different aluminium alloys. The plates have heat affected zones along all edges. The reduction in yield strength in the heat affected zones is 10 percent.

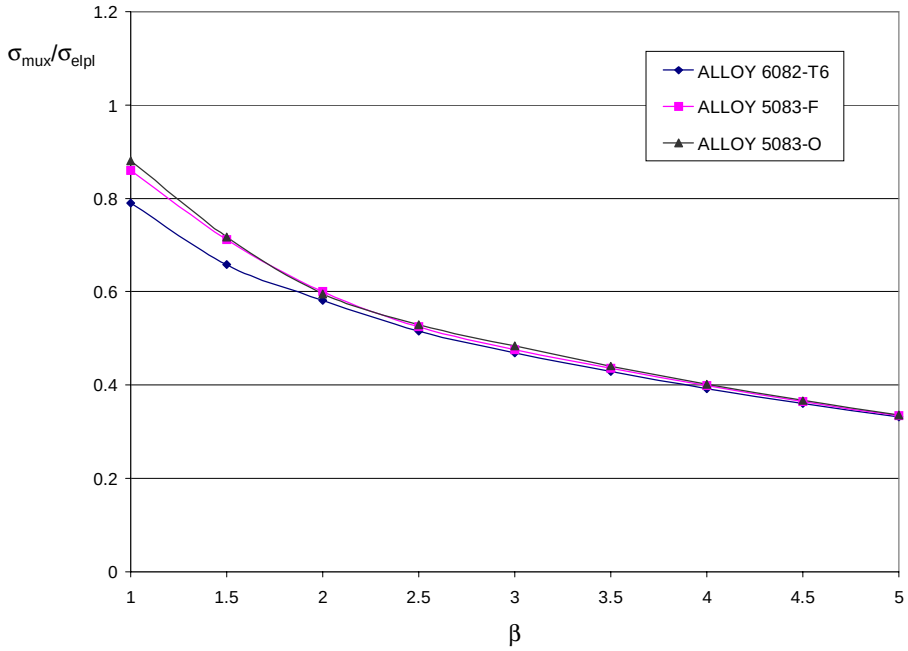

Figure 9.7 : Axial ultimate capacities of different aluminium alloys. The plates have heat affected zones along all edges. The reduction in yield strength in the heat affected zones is 50 percent.

Normalising the ultimate capacities with the stress corresponding to equal elastic and plastic strain makes the collapse curves for the different aluminium alloys analysed look very similar also when they are exposed to heat affected zones. For compact plates (β=1.0, 1.5 and 2.0) plates having the higher utilised aluminium alloys start out with the higher ultimate capacities, but as the reduction of yield strength in the heat affected zones increases, they end out with the lower ultimate capacities. The reason for this behaviour is the local collapse mechanism at the plate ends.

The plates experience excessive yielding with utilisation of the material far into the plastic region. Highly utilised aluminium alloys have a more gentle slope of the stress-strain curve far into the plastic region than lower utilised aluminium alloys and experience less residual strength as the strains grow large.

9.2.2 Transverse Loading

The ultimate capacities of plates loaded transversally have also been normalised with the stress corresponding to equal elastic and plastic strain. Figures 9.8, 9.9 and 9.10 show the results for plates consisting of the base material only and plates exposed to 10 and 50 percent reduction of the yield stress in the heat affected zones.

Curves with the ultimate capacities normalised with the 0.2 percent tensile proof stress are given in Appendix 5.

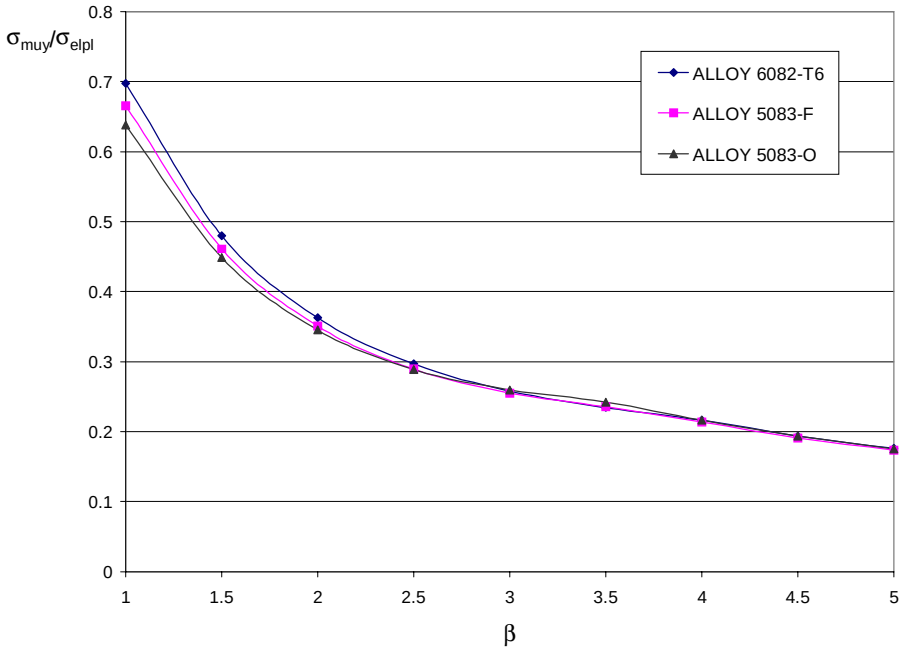

Figure 9.8 : Transverse ultimate capacity of different aluminium alloys. The plates consist of the base material only, and their ultimate capacity has been normalised with the stress corresponding to equal elastic and plastic strain. Aspect ratio, a/b=3.

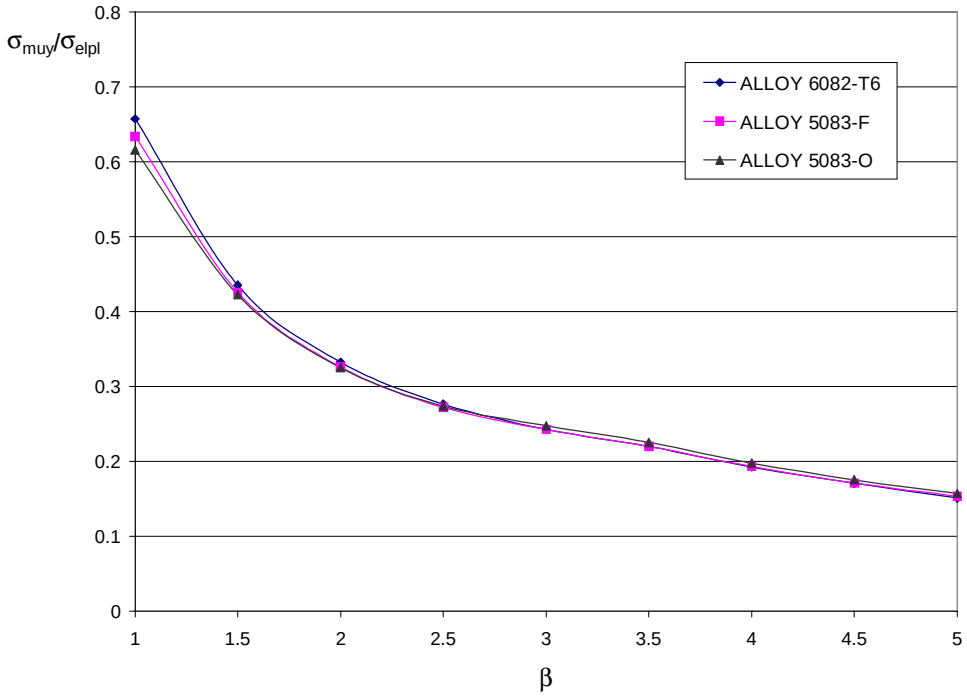

Figure 9.9 : Transverse ultimate capacity of different aluminium alloys. The plates have heat affected zones along all edges, and their ultimate capacity has been normalised with the stress corresponding to equal elastic and plastic strain. The reduction in yield strength in the heat affected zones is 10 percent. Aspect ratio, a/b=3.

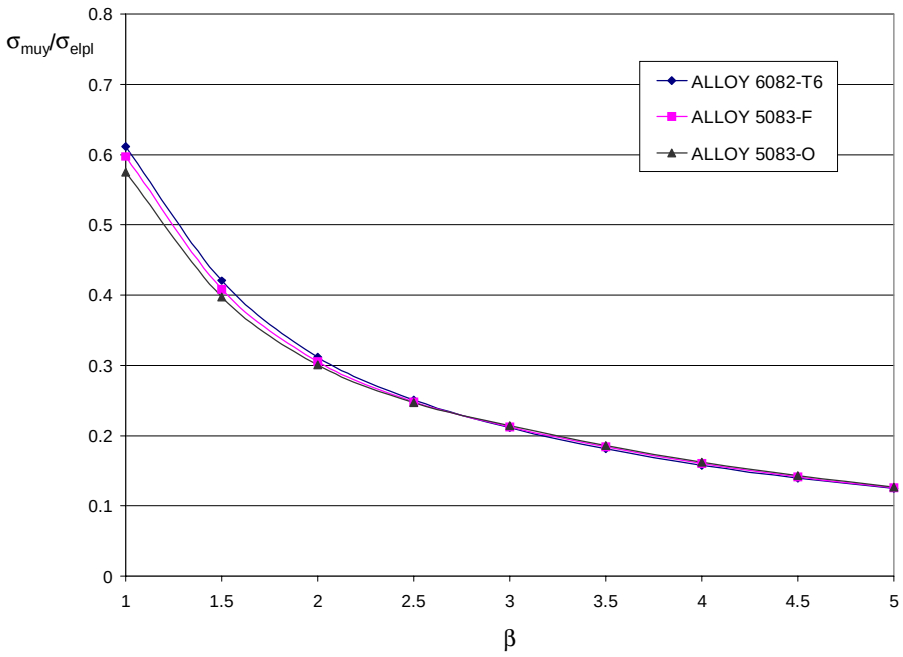

Figure 9.10 : Transverse ultimate capacity of different aluminium alloys. The plates have heat affected zones along all edges, and their ultimate capacity has been normalised with the stress corresponding to equal elastic and plastic strain. The reduction in yield strength in the heat affected zones is 50 percent. Aspect ratio, a/b=3.

Normalising the collapse curves with the stress corresponding to equal elastic and plastic strain gives an even better fit for transversally loaded plates with aspect ratio, a/b=3, than what was the case for axially loaded plates. The biggest discrepancies occurs for the most compact plates.

9.2.3 Plate Strip Analyses

Curves with the buckling capacities normalised with the 0.2 percent tensile proof stress are given in Appendix 5. Only plates consisting of the base material only have been investigated.

For slender plates there is an almost exact agreement between the different aluminium alloys, but when the collapse mechanisms are more dominated by yielding, the more higher utilised aluminium alloys show larger relative ultimate capacities. The main reason for this behaviour is believed to be caused by the sharper knee factor, n, in the Ramberg Osgood law.

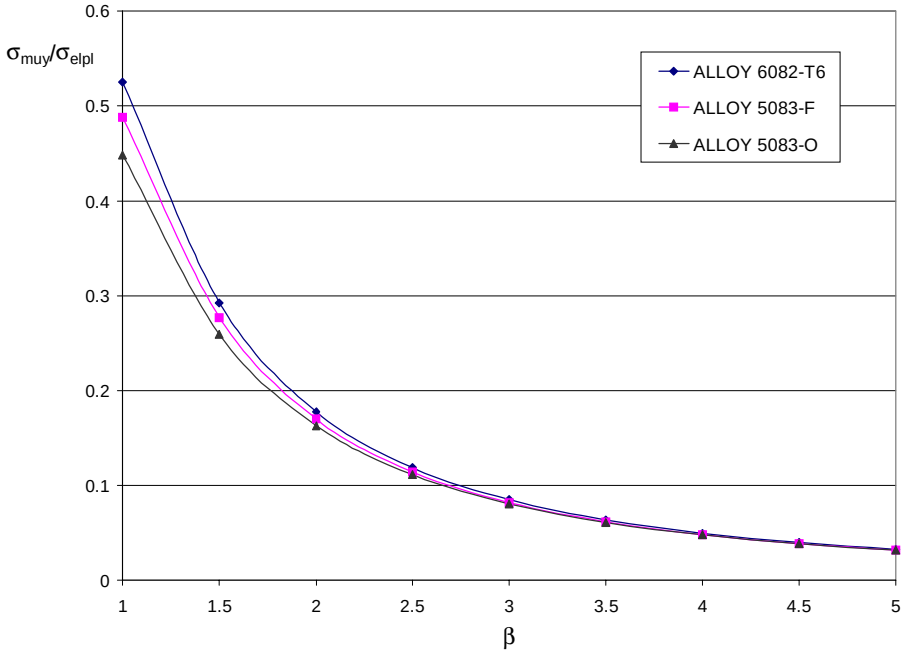

Figure 9.11 : Plate strip analyses of plates made of different aluminium alloys. The plates consist of the base material only, and their ultimate capacity has been normalised with the stress corresponding to equal elastic and plastic strain.

9.2.4 Biaxial Loading

The purpose of this section is to investigate whether there is any difference in the shape of the biaxial interaction curves for the different alloys.

In this section interaction curves for different alloys are presented for plates with given slenderness, β. First results for plates made of base material and then for plates with heat affected zones along all edges, are presented. Plots with only one alloy, but all values of the slenderness, β, in the same figure are given in Appendix 5.

9.2.4.1 Base Material

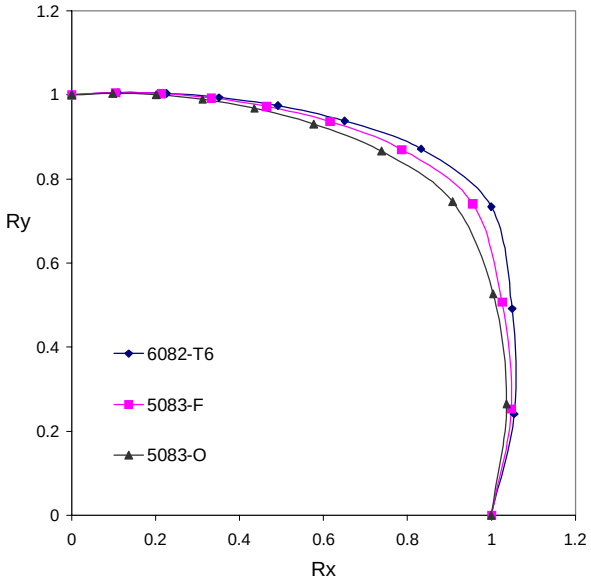

Figure 9.12 : Interaction curves for β=1.0

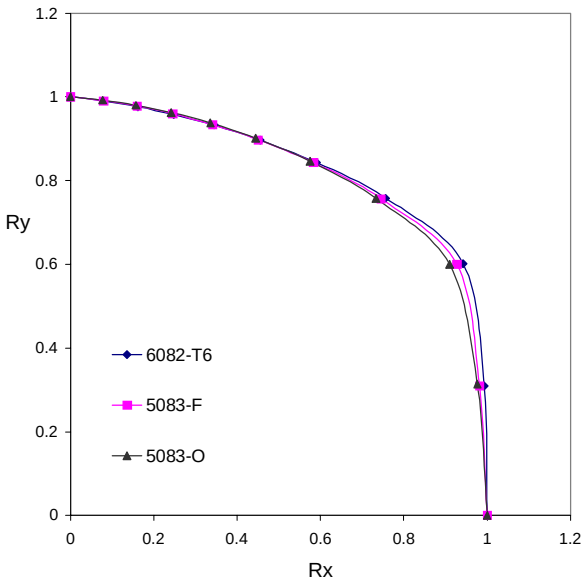

Figure 9.13 : Interaction curves for β=1.5

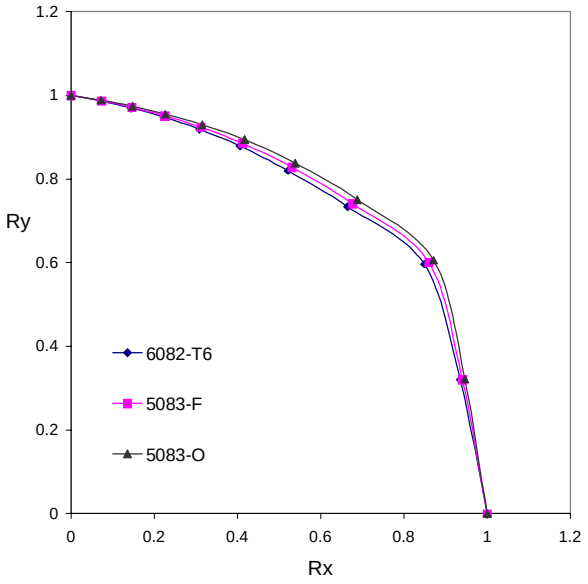

Figure 9.14 : Interaction curves for β=2.0

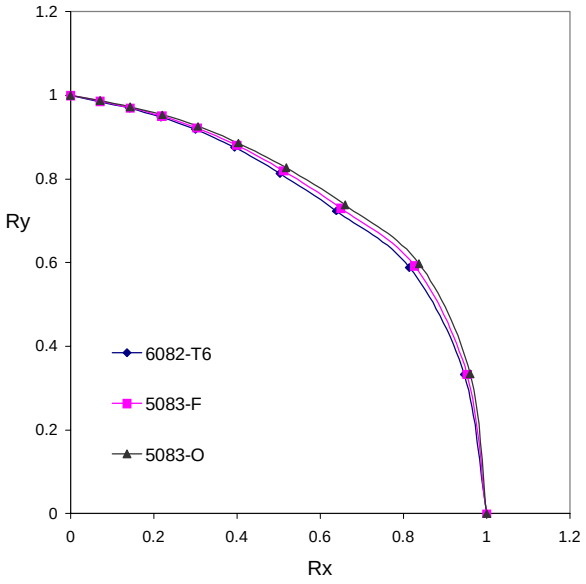

Figure 9.15 : Interaction curves for β=2.5

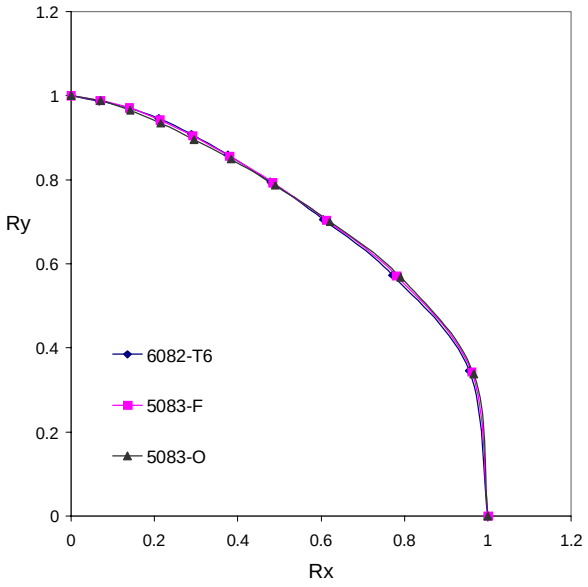

Figure 9.16 : Interaction curves for β=3.0

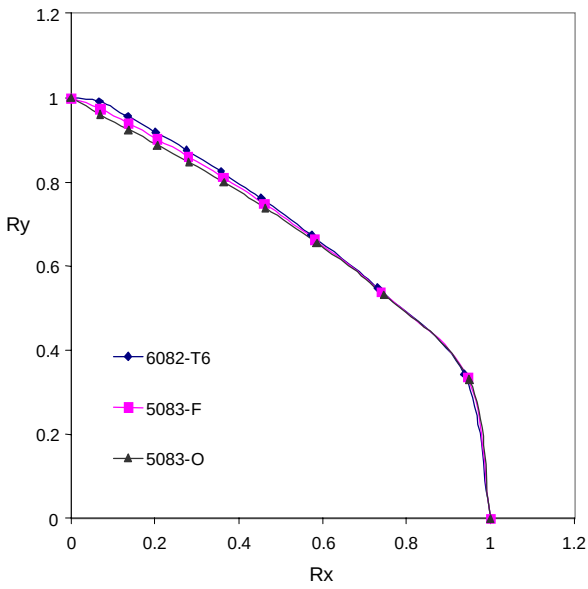

Figure 9.17 : Interaction curves for β=3.5

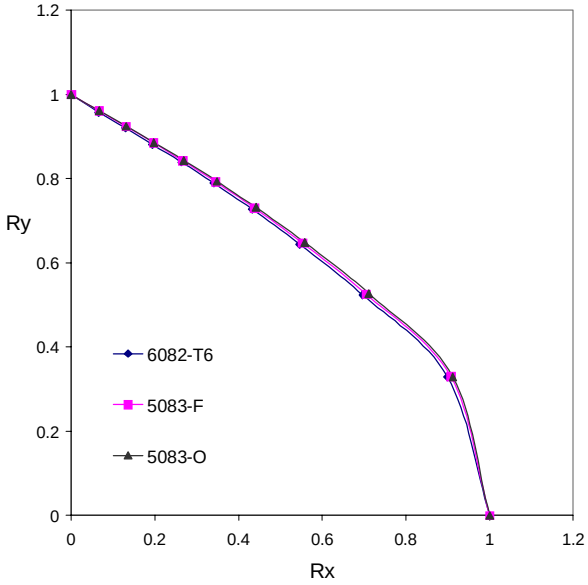

Figure 9.18 : Interaction curves for β=4.0

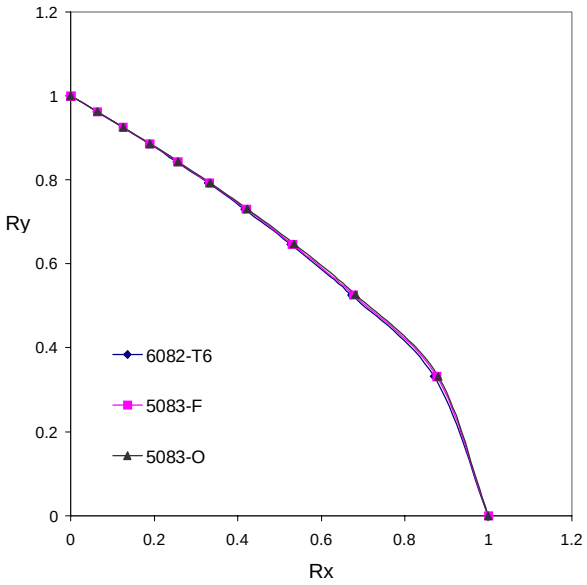

Figure 9.19 : Interaction curves for β=4.5

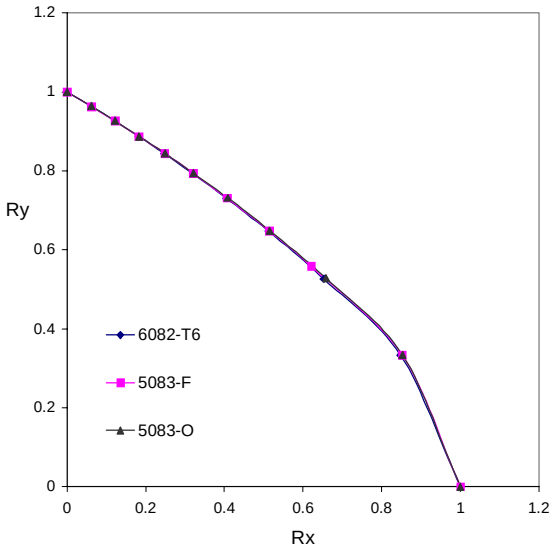

Figure 9.20 : Interaction curves for β=5.0

9.2.4.2 Heat Affected Zones along All Edges

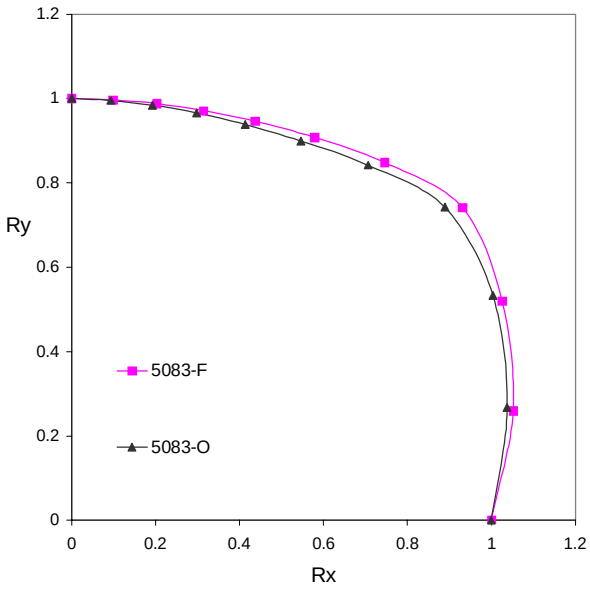

Figure 9.21 : Interaction curves for β=1.0

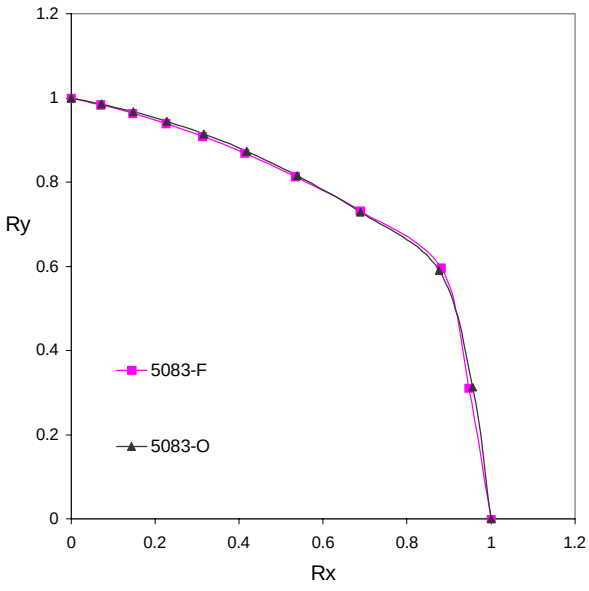

Figure 9.22 : Interaction curves for β=1.5

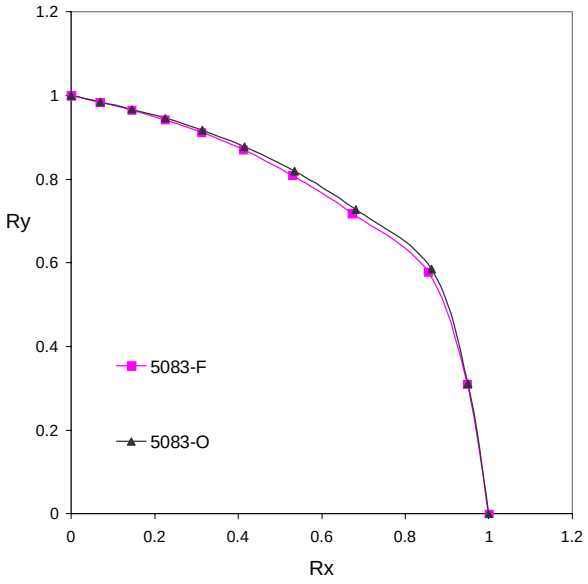

Figure 9.23 : Interaction curves for β=2.0

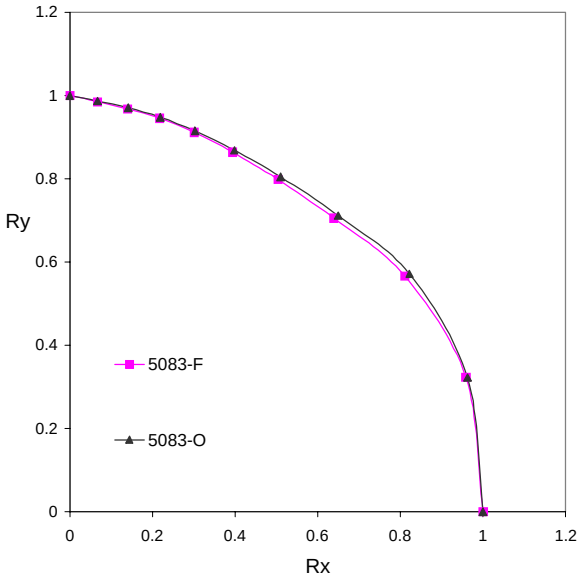

Figure 9.24 : Interaction curves for β=2.5

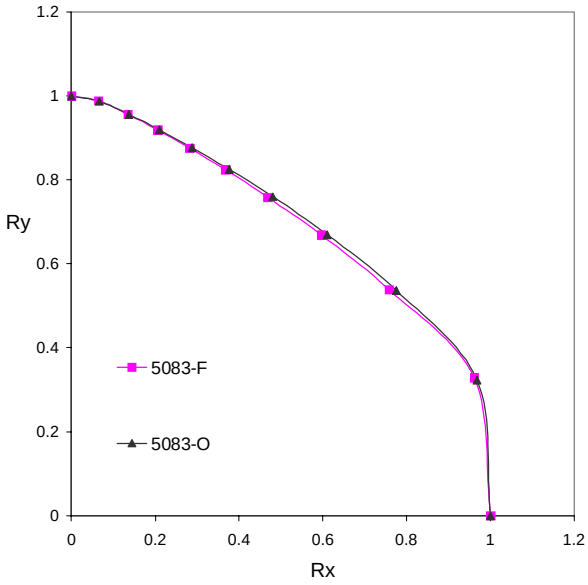

Figure 9.25 : Interaction curves for β=3.0

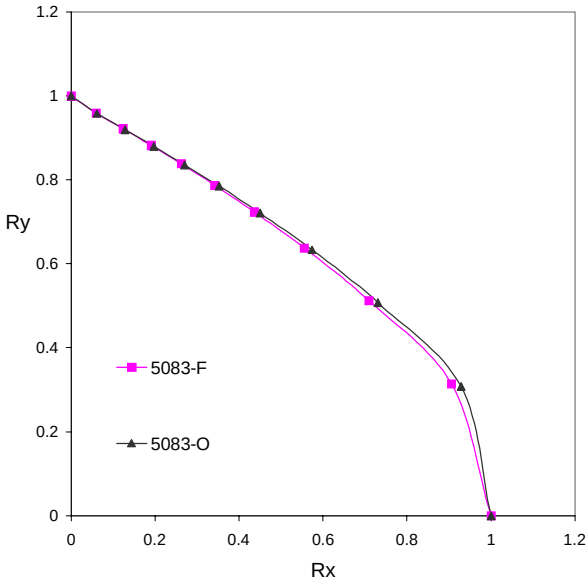

Figure 9.26 : Interaction curves for β=3.5

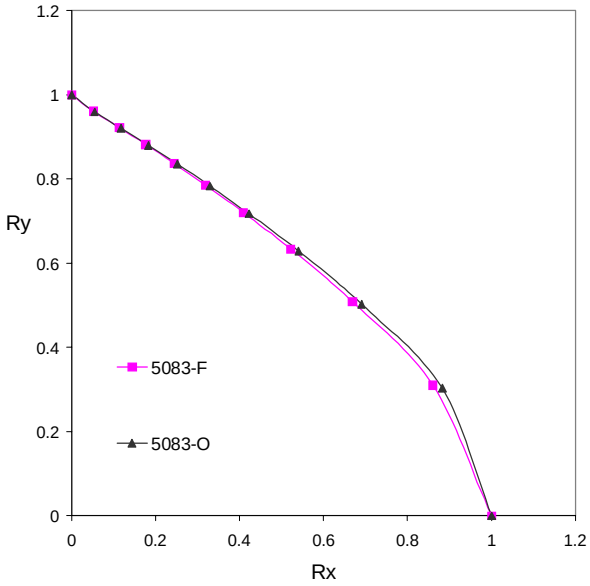

Figure 9.27 : Interaction curves for β=4.0

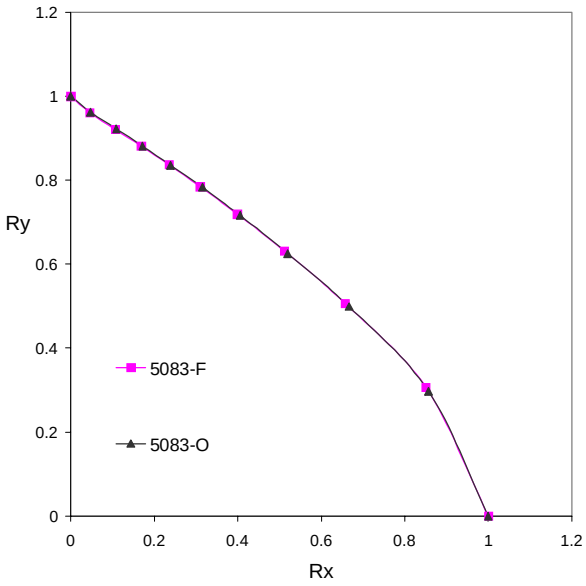

Figure 9.28 : Interaction curves for β=4.5

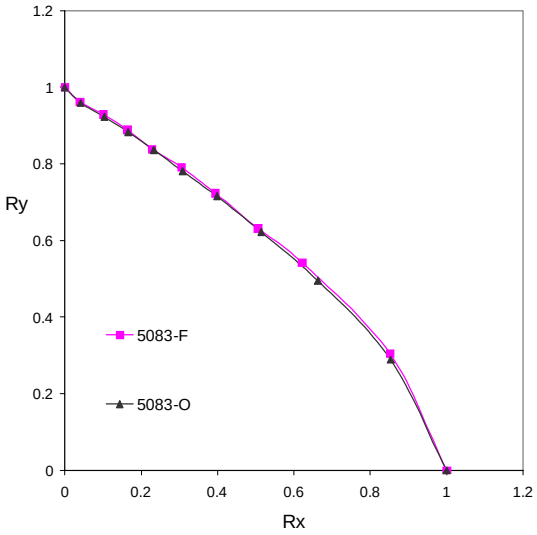

Figure 9.29 : Interaction curves for β=5.0

No significant differences in biaxial interaction curves are observed. The two main parameters influencing the shapes of the biaxial interaction curves are the slenderness, β, and the aspect ratio, a/b. As long as these parameters are kept constant there will be no significant differences in the shape of the biaxial interaction curves.

9.3 Effect of Aspect Ratio, ω=a/b

In Chapter 7 it was found that the axial ultimate capacity for plates without heat affected zones were the same for all values of the aspect ratio, a/b. Moreover, it was demonstrated that the transverse ultimate capacity can be established by combining the ultimate capacity of a

aquare plate and a plate strip. In this chapter it will be investigated whether these findings also hold for the other two alloys.

9.3.1 Axial Loading

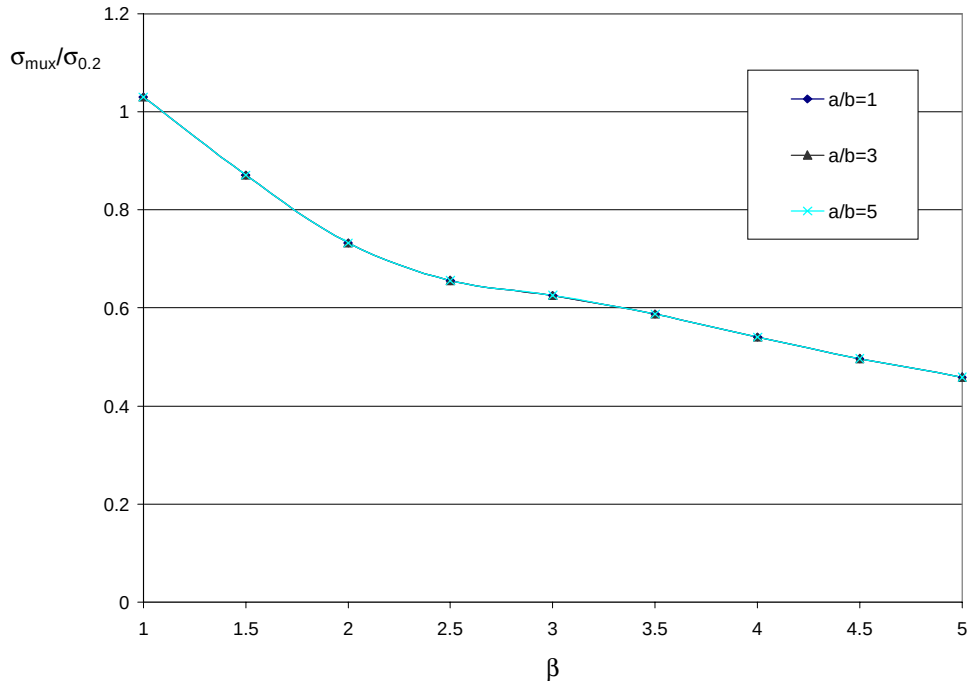

Figure 9.30 : Axial ultimate capacitiy of plates with different aspect ratios, a/b. The plates consist of alloy 5083-F and have no heat affected zones.

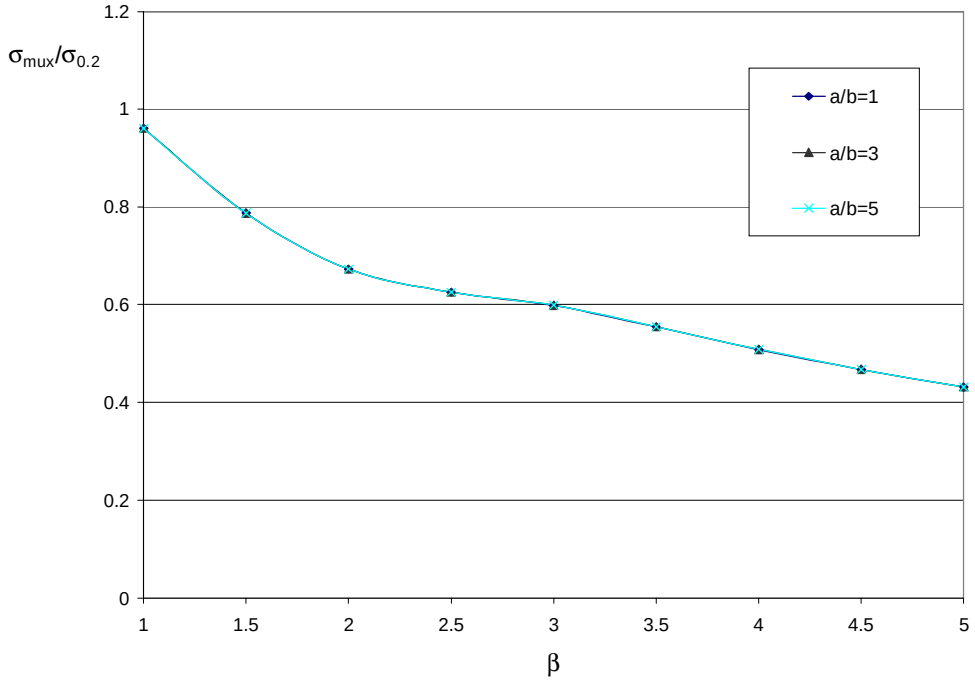

Figure 9.31 : Axial ultimate capacity of plates with different aspect ratios. The plates consist of alloy 5083-O and have no heat affected zones.

9.3.2 Transverse Loading

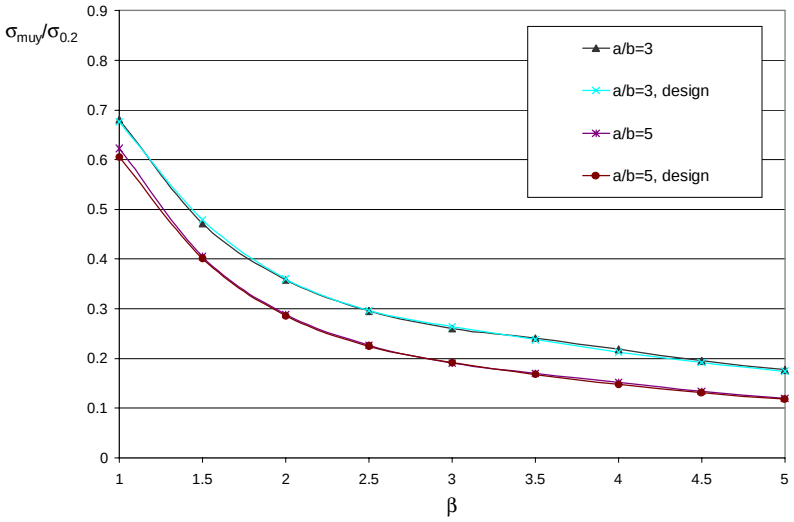

Figure 9.32 : Transverse ultimate capacity of plates with different aspect ratios, a/b. The results from numerical analyses of plates with the actual aspect ratio, a/b, are compared with the capacity found by the use of Equation 7.2. The plates consist of alloy 5083-F and have no heat affected zones.

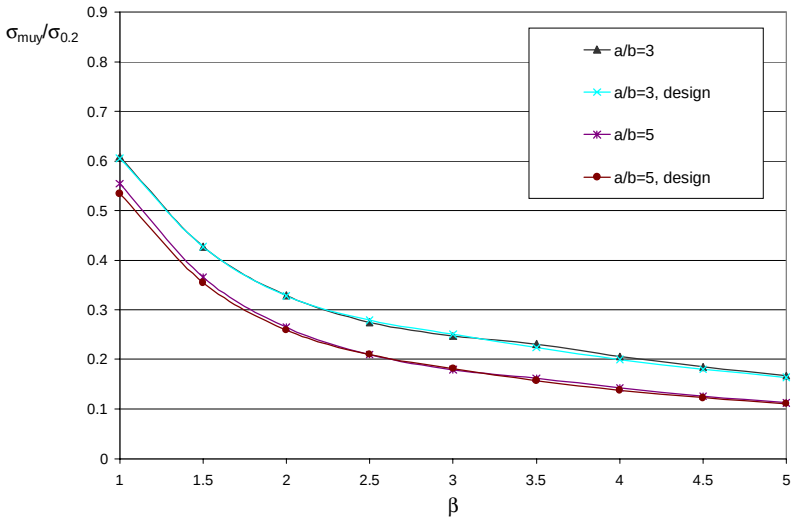

Figure 9.33 : Transverse ultimate capacitiy of plates with different aspect ratios, a/b. The results from numerical analyses of plates with the actual aspect ratio, a/b, are compared with the capacity found by the use of Equation 7.2. The plates consist of alloy 5083-O and have no heat affected zones.

Plates with straight, simply supported edges and consisting of the base material only, have the exact same axial ultimate capacity for all aspect ratios, a/b, investigated. This statement holds not only for alloy 6082-T6, but for alloy 5083-F and alloy 5083-O as well.

Equation 7.2 is well suited for describing the transverse ultimate capacity of plates with straight, simply supported edges and consisting of the base material only. It can be used for all aluminium alloys investigated. Plates with heat affected zones have not been investigated.

Chapter 10

Design Formulas

10.1 Axial Compression

A design equation suitable for determining the collapse capacity of axially loaded aluminium plates with straight, simply supported edges is developed.

The ultimate capacities of aluminium plates consisting of the base material are found by choosing the lowest axial ultimate capacity for the different values of the slenderness, β, chosen from the initial deflection patterns, aspect ratios, a/b, and aluminium alloys that give the lowest ultimate capacities. The capacities found are used as a basis for developing an equation describing the ultimate capacity of plates consisting of the base material.

The same line of action is used for creating an equation expressing the ultimate capacity for plates exposed to heat affected zones; with a breadth of the heat affected zones equal to 25 mm and the yield strength in the heat affected zones equal to half the value of the yield strength of the base material.

The axial ultimate capacity for other breadths of the heat affected zones, and other ratios between the yield strength of the aluminium alloy in the heat affected zones and the yield strength of the base material is then developed. The axial ultimate capacity is assumed to vary linearly both with the breadth of the heat affected zones and the ratio between the yield strength of the aluminium alloy in the heat affected zones and the yield strength of the base material.

The curves are normalised with the stress corresponding to equal elastic and plastic strain. All maximum initial deflection amplitudes are equal to 0.005b. Due to customary access to computer programming the equations chosen for curve fitting are picked out on the basis of their ability to reproduce the numerical results with a minimum of deviation.

10.1.1 Ultimate Strength Formula for Plates Consisting of the Base Material

For a particular aluminium alloy the collapse capacities are identical for all values of the aspect ratio, a/b, if the plates consists of the base material only, but they vary depending on the initial deflection pattern.

The basis for the proposed design curve is to use the lowest axial ultimate capacity for the different values of the slenderness, β; chosen from the initial deflection patterns, aspect ratios, a/b, and aluminium alloys that give the lowest ultimate capacity.

A curve giving an almost identical fit to the lowest ultimate capacities can be written as:

$$\frac{\sigma_{\text{mux}}}{\sigma_{\text{elpl}}} = 1.562 - 1.426\, e^{-0.9403\,\beta^{-0.8616}} \qquad (10.1)$$

The collapse capacities used as basis for the curve development are given in Table 10.1, and Figure 10.1 shows the fit between the numerical data and the curve obtained.

Table 10.1 : Ultimate capacities used as basis for the proposed design formula

Slenderness, β [-]	$\frac{\sigma_{mux}}{\sigma_{elpl}}$	Aspect ratio a/b	Eigenmode	Aluminium alloy
1.0	1.008	1	Axial	6082-T6
1.5	0.8260	1	Axial	5083-O
2.0	0.7062	1	Axial	5083-O
2.5	0.6337	3	Biaxial	5083-O
3.0	0.5755	3	Biaxial	5083-O
3.5	0.5304	3	Biaxial	5083-F
4.0	0.4927	3	Biaxial	5083-F
4.5	0.4589	3	Biaxial	5083-F
5.0	0.4301	3	Biaxial	5083-F

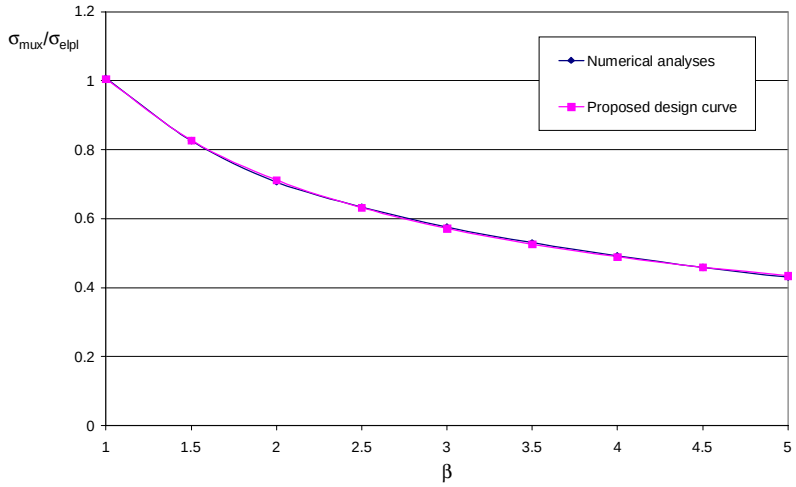

Figure 10.1 : Comparison of the proposed design curve and results from numerical analyses.

10.1.2 Ultimate Strength Formula for Plates with Heat Affected Zones

For plates with heat affected zones, the ultimate capacity will vary with the aspect ratio, a/b. The aspect ratio, a/b=1, gives the lowest ultimate capacity and is used as basis for curve fitting. There is for all practical purposes no difference in ultimate capacity for plates with heat affected zones along all edges and plates with the extruded pattern of the heat affected zones, but the lowest capacities for a given slenderness, β, are used as basis for design. The data are given in Table 10.2.

A curve giving an almost identical fit to the lowest ultimate capacities for plates with a breadth of the heat affected zones equal to 25 mm and $\sigma_{0.2}^{*}=0.5\sigma_{0.2}$, can be written as:

$$\frac{\sigma_{mux}}{\sigma_{elpl}} = 0.7495 - 0.7036\, e^{-3.387\,\beta^{-1.224}} \qquad (10.2)$$

Figure 10.2 shows the fit between the numerical data and the curve obtained.

Table 10.2 : Ultimate capacities used as basis for the proposed design formula

Slenderness, β [-]	$\frac{\sigma_{mux}}{\sigma_{elpl}}$	HAZ pattern	Aluminium alloy
1.0	0.7256	HAZ along all edges	6082-T6
1.5	0.6601	HAZ along all edges	6082-T6
2.0	0.5849	HAZ along all edges	6082-T6
2.5	0.5151	Extruded HAZ Pattern	6082-T6
3.0	0.4576	Extruded HAZ Pattern	6082-T6
3.5	0.4114	Extruded HAZ Pattern	6082-T6
4.0	0.3718	Extruded HAZ Pattern	6082-T6
4.5	0.3385	Extruded HAZ Pattern	6082-T6
5.0	0.3100	Extruded HAZ Pattern	6082-T6

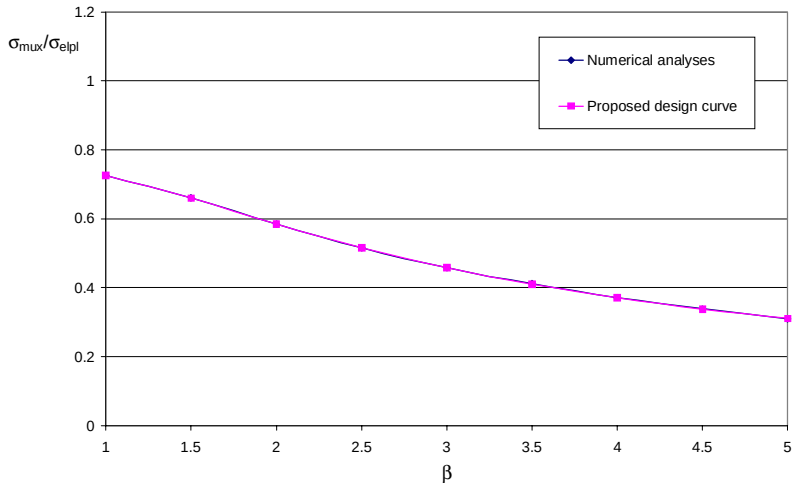

Figure 10.2 : Comparison of the proposed design curve and results from numerical analyses.

10.1.3 Design Formula for Plates with Different Extensions of HAZ

Two design formulas for axially loaded plates have now been established, namely, one formula for plates with no heat affected zones and one formula for plates with 25 mm extension of the heat affected zones and the 0.2 percent tensile proof stress in the heat affected zones equal to half the yield stress of the base material.

Based on the results in Chapter 6 the reduction of the ultimate capacity can be assumed to vary linearly with the breadth of the heat affected zones along loaded edges. The reduction of the ultimate capacity can also be assumed to vary linearly with the ratio between the yield

strength of the aluminium alloy in the heat affected zones and the yield strength of the base material.

The last assumption holds if the yield strength of the material in the heat affected zones is less than 90 percent of the yield strength of the base material. If the yield strength of the material in the heat affected zones is larger than 90 percent of the yield strength of the base material, the residual stresses alone will cause a reduction of ultimate capacity approximately equal to the capacity of a plate with yield strength of the material in the heat affected zones equal to 90 percent of the base material. Plates have to be unwelded to take full advantage of the curve for plates with no heat affected zones.

Assuming linear variation both regarding the breadth of the heat affected zones and the ratio between the yield strength of the material in the heat affected zones and the base material, Equations 10.1 and 10.2 can be combined to give:

$$\begin{aligned}\frac{\sigma_{mux}}{\sigma_{elpl}} &= (1-K)\left(\frac{\sigma_{mux}}{\sigma_{elpl}}\right)_{\substack{Base\\material}} + K\left(\frac{\sigma_{mux}}{\sigma_{elpl}}\right)_{\substack{Heat\ affected\\zones}} \\ &= \left(\frac{\sigma_{mux}}{\sigma_{elpl}}\right)_{\substack{Base\\material}} - K\left[\left(\frac{\sigma_{mux}}{\sigma_{elpl}}\right)_{\substack{Base\\material}} - \left(\frac{\sigma_{mux}}{\sigma_{elpl}}\right)_{\substack{Heat\ affected\\zones}}\right]\end{aligned} \tag{10.3}$$

$$K = \frac{b_{HAZ}}{25}\cdot 2\cdot\left(1-\frac{\sigma_{0.2}^{*}}{\sigma_{0.2}}\right) \tag{10.4}$$

$$\begin{aligned}\frac{\sigma_{mux}}{\sigma_{elpl}} &= 1.562 - 1.426e^{-0.9403\beta^{-0.8616}} \\ &\quad - \frac{b_{HAZ}}{25}\cdot 2\cdot\left(1-\frac{\sigma_{0.2}^{*}}{\sigma_{0.2}}\right)\left[1.562 - 1.426e^{-0.9403\beta^{-0.8616}} - \left(0.7495 - 0.7036e^{-3.387\beta^{-1.224}}\right)\right]\end{aligned} \tag{10.5}$$

or

$$\begin{aligned}\frac{\sigma_{mux}}{\sigma_{elpl}} &= 1.562 - 1.426e^{-0.9403\beta^{-0.8616}} \\ &\quad - b_{HAZ}\left(1-\frac{\sigma_{0.2}^{*}}{\sigma_{0.2}}\right)\left(0.06500 - 0.1142e^{-0.9403\beta^{-0.8616}} + 0.05629e^{-3.387\beta^{-1.224}}\right)\end{aligned} \tag{10.6}$$

where b_{HAZ} is given in mm.

The above equation is believed to give the axial ultimate capacity for all values of the breadth of the heat affected zones along loaded edges and all ratios between the yield stress of the material in the heat affected zones and the base material. It is important to note that $\sigma_{0.2}^{*}$ for

welded plates can not be set larger than $0.9\sigma_{0.2}$, because of the effect of the residual stresses that are present. Figure 10.3 shows design curves for plates with a breadth of the heat affected zones equal to 25 mm and different reductions of yield strength in the heat affected zones (the curve with $\sigma_{0.2}^{*}/\sigma_{0.2}=1.0$ can only be used for plates that have not been welded, the design values for welded plates cannot exceed the values given in the curve with $\sigma_{0.2}^{*}/\sigma_{0.2}=0.9$).

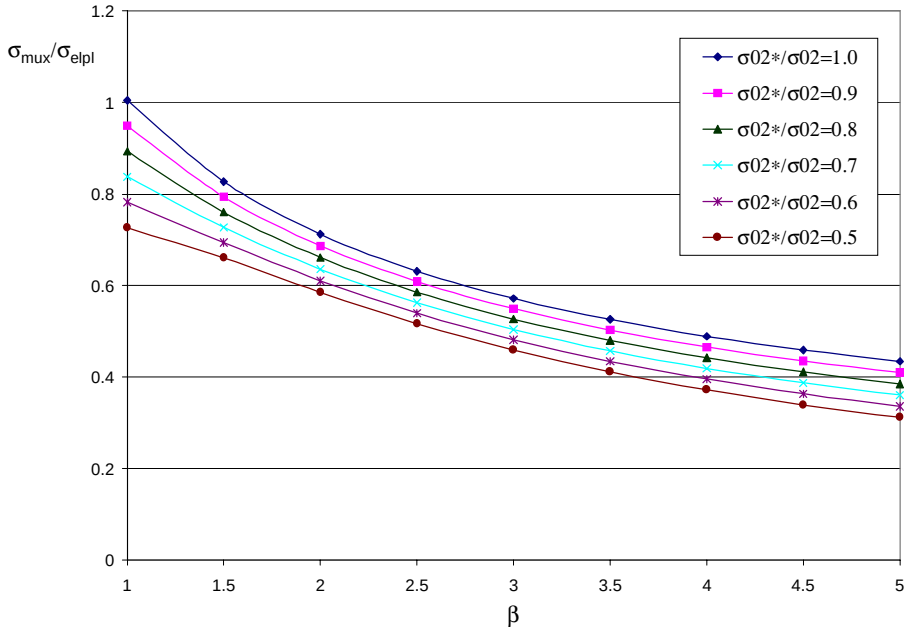

Figure 10.3 : Design curves for the axial ultimate strength of plates with a breadth of the heat affected zones along the loaded edges equal to 25 mm.

10.2 Transverse Compression

10.2.1 Basic Considerations

The problem with transverse compression is that one has to find a way to handle the different aspect ratios that occur. As have been elaborated on in Chapter 7.3, an adequate way of finding transverse ultimate capacities of aluminium plates is to divide the load carrying capacity into two parts:

$$\frac{\sigma_{muy}}{\sigma_{elpl}} = \frac{b}{a}\left(\frac{\sigma_{muy}}{\sigma_{elpl}}\right)_{\substack{\text{square}\\\text{plate}}} + \left(1-\frac{b}{a}\right)\left(\frac{\sigma_{muy}}{\sigma_{elpl}}\right)_{\substack{plate\\strip}} \tag{10.7}$$

For transverse compression two equations will be proposed, one equation suitable for plates with heat affected zones along all edges and one equation for plates with the extruded pattern of the heat affected zones. The equation for plates with the extruded pattern of the heat affected zones is the most conservative one and can also be used for plates with heat affected zones along all edges.

10.2.2 Design Formula for Plates with Heat Affected Zones along All Edges

Due to symmetry, the quadratic plate capacity part can be taken directly from the equation for axially loaded plates (Equation 10.6).
The plate strip part of the equation need no correction for heat affected zones. The plate strip collapse data for alloy 5083-O have been chosen as basis for the curve fitting because plates made of alloy 5083-O have the lowest plate strip ultimate capacities (details in Chapters 5.3.3 and 9.2.2). The data used are given in Table 10.3, and a curve giving an almost identical fit to the data used is described by Equation 10.8.

$$\frac{\sigma_{muy}}{\sigma_{elpl}} = 0.6629 - 0.6581\, e^{-1.119\beta^{-2.026}} \qquad (10.8)$$

Table 10.3 : Ultimate capacities used as basis for the proposed design formula

Slender-ness β[-]	1.0	1.5	2.0	2.5	3.0	3.5	4.0	4.5	5.0
$\frac{\sigma_{muy}}{\sigma_{elpl}}$	0.4485	0.2590	0.1630	0.1111	0.08050	0.06086	0.04762	0.03838	0.03160

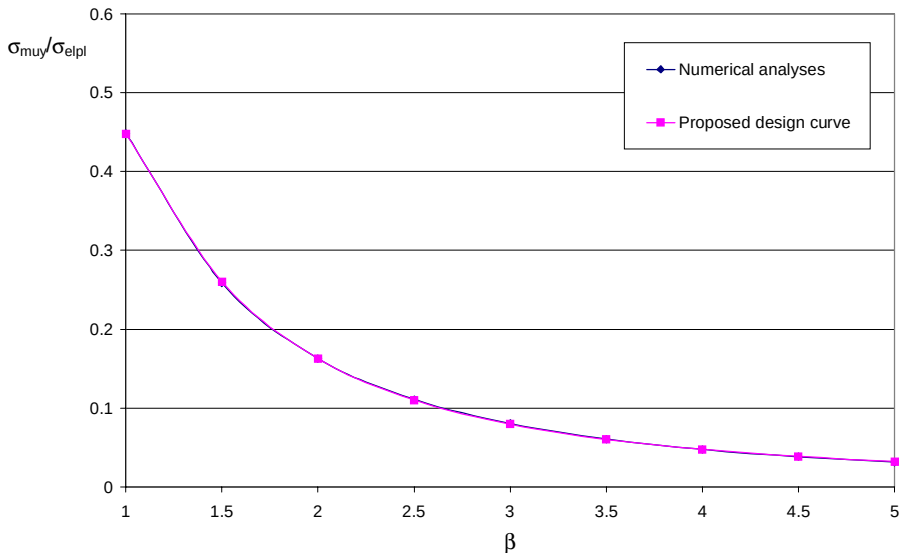

Figure 10.4 : Comparison of the proposed design curve and results from numerical analyses.

Combining Equation 10.6 with Equation 10.8 by the use of Equation 10.7 gives:

$$\frac{\sigma_{muy}}{\sigma_{elpl}} = \frac{b}{a}\left(1.562 - 1.426\, e^{-0.9403\,\beta^{-0.8616}}\right)$$
$$-\left(\frac{b}{a}\right) b_{HAZ}\left(1-\frac{\sigma^{*}_{0.2}}{\sigma_{0.2}}\right)\left(0.06500 - 0.1142\, e^{-0.9403\,\beta^{-0.8616}} + 0.05629\, e^{-3.387\,\beta^{-1.224}}\right) \qquad (10.9)$$
$$+\left(1-\frac{b}{a}\right)\left(0.6629 - 0.6581\, e^{-1.119\,\beta^{-2.026}}\right)$$

Figure 10.5 shows design curves for plates with a breadth of the heat affected zones equal to 25 mm and different reductions of yield strength in the heat affected zones. The design curve for plates without reductions of the yield strength in the heat affected zones ($\sigma_{0.2}^{*}/\sigma_{0.2}$=1.0) can only be used for plates that have not been welded.

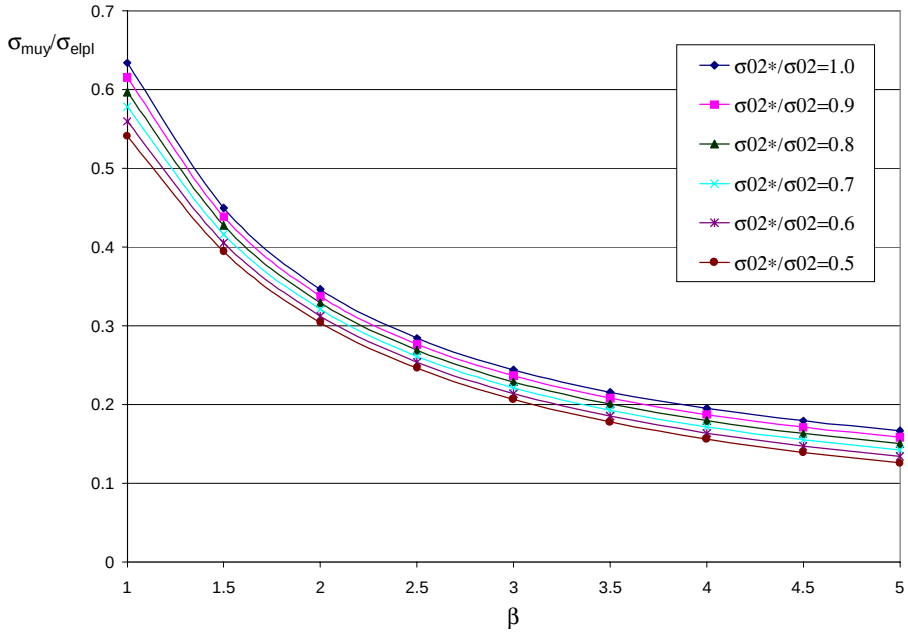

Figure 10.5 : Transverse design curves for a breadth of the heat affected zones equal to 25 mm and aspect ratio, a/b=3.

10.2.3 Design Formula for Plates with the Extruded Pattern of the Heat Affected Zones

Both the square plate part and the plate strip part of the equation need to be altered when the patterns of the heat affected zones is changed form heat affected zones along all edges to the extruded HAZ pattern.

Square plates loaded transversally have a lower ultimate capacity if they are exposed to the extruded pattern of the heat affected zones than if they are exposed to heat affected zones along all edges (see Chapter 7.3.1), and plate strips with a heat affected zone in the middle-longitudinal direction have a lower ultimate capacity than plate strips with heat affected zones along long edges (see Chapter 5.3.3).

10.2.3.1 Ultimate Strength Formula for Square Plate

By similar line of action as for plates with heat affected zones along all edges, the equation for the ultimate capacity of plates with the breadth of the heat affected zones equal to 25 mm and $\sigma_{0.2}^{*}=0.5\sigma_{0.2}$ becomes:

$$\frac{\sigma_{muy}}{\sigma_{elpl}} = 0.8173 - 0.5080\, e^{-2.187\,\beta^{-2.145}} \qquad (10.10)$$

The collapse capacities used as basis for the curve development are given in Table 10.4, and Figure 10.6 shows the fit between the numerical data and the curve obtained.

Table 10.4 : Ultimate capacities used as basis for the proposed design formula

Slenderness, β [-]	$\frac{\sigma_{muy}}{\sigma_{elpl}}$	Aluminium Alloy
1.0	0.7605	6082-T6
1.5	0.6125	6082-T6
2.0	0.5101	6082-T6
2.5	0.4436	6082-T6
3.0	0.4034	6082-T6
3.5	0.3784	6082-T6
4.0	0.3615	6082-T6
4.5	0.3508	6082-T6
5.0	0.3462	6082-T6

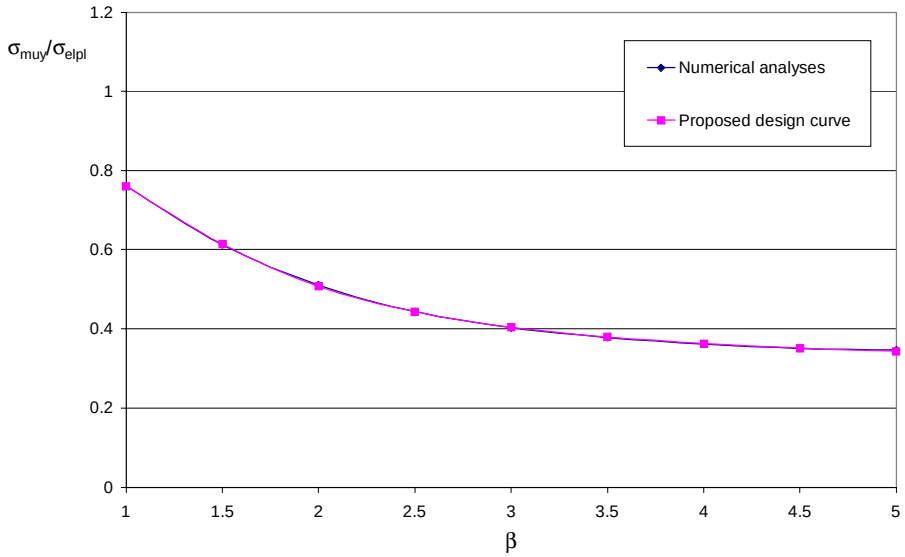

Figure 10.6 : Comparison of the proposed design curve and results from numerical analyses

Combining Equations 10.1 and 10.10 by the use of Equation 10.3 gives:

$$\frac{\sigma_{muy}}{\sigma_{elpl}} = 1.562 - 1.426e^{-0.9403\beta^{-0.8616}} - \frac{b_{HAZ}}{25} \cdot 2 \cdot \left(1 - \frac{\sigma_{0.2}^{*}}{\sigma_{0.2}}\right)\left[1.562 - 1.426e^{-0.9403\beta^{-0.8616}} - \left(0.8173 - 0.5080e^{-2.187\beta^{-2.145}}\right)\right] \quad (10.11)$$

$$\frac{\sigma_{muy}}{\sigma_{elpl}} = 1.562 - 1.426e^{-0.9403\beta^{-0.8616}} - b_{HAZ}\left(1 - \frac{\sigma_{0.2}^{*}}{\sigma_{0.2}}\right)\left(0.05958 - 0.1141e^{-0.9403\beta^{-0.8616}} + 0.04064e^{-2.187\beta^{-2.145}}\right) \quad (10.12)$$

10.2.3.2 Ultimate Strength Formula for Plate Strip

The equation for plate strips with the breadth of the heat affected zone equal to 25 mm and $\sigma_{0.2}^{*}=0.5\sigma_{0.2}$ becomes:

$$\frac{\sigma_{muy}}{\sigma_{elpl}} = 0.5037 - 0.5023e^{-1.384\beta^{-1.976}} \quad (10.13)$$

The collapse capacities used as basis for the curve development are given in Table 10.5, and Figure 10.7 shows the fit between the numerical data and the curve obtained.

Table 10.5 : Buckling capacities used as basis for the proposed design formula

Slenderness, β [-]	$\frac{\sigma_{muy}}{\sigma_{elpl}}$	Aluminium Alloy
1.0	0.3778	6082-T6
1.5	0.2338	6082-T6
2.0	0.1503	6082-T6
2.5	0.1031	6082-T6
3.0	0.07479	6082-T6
3.5	0.05670	6082-T6
4.0	0.04429	6082-T6
4.5	0.03575	6082-T6
5.0	0.02942	6082-T6

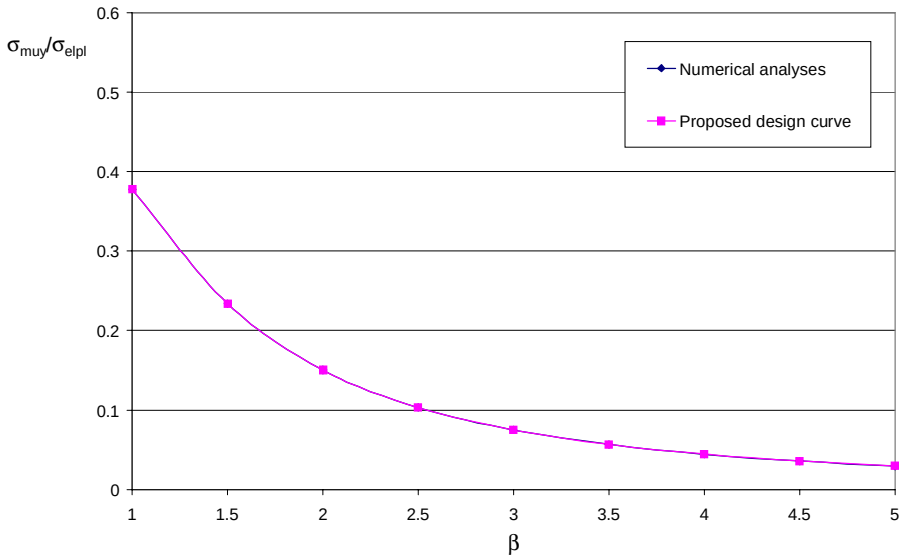

Figure 10.7 : Comparison of the proposed design curve and results from numerical analyses

Combining Equations 10.8 and 10.13 by the use of Equation 10.3 gives:

$$\frac{\sigma_{muy}}{\sigma_{elpl}} = 0.6629 - 0.6581 e^{-1.119\beta^{-2.026}} - \frac{b_{HAZ}}{25mm} \cdot 2 \cdot \left(1 - \frac{\sigma^*_{0.2}}{\sigma_{0.2}}\right)\left[0.6629 - 0.6581 e^{-1.119\beta^{-2.026}} - \left(0.5037 - 0.5023 e^{-1.384\beta^{-1.976}}\right)\right] \quad (10.14)$$

$$\frac{\sigma_{muy}}{\sigma_{elpl}} = 0.6629 - 0.6581\, e^{-1.119\beta^{-2.026}} - b_{HAZ}\left(1 - \frac{\sigma^*_{0.2}}{\sigma_{0.2}}\right)\left(0.01274 - 0.05265 e^{-1.119\beta^{-2.026}} + 0.04018 e^{-1.384\beta^{-1.976}}\right) \quad (10.15)$$

10.2.3.3 Design Formula for Plates with Different Extensions of HAZ

Finally, using Equations 10.12 and 10.15 in conjunction with Equation 10.7 gives:

$$\frac{\sigma_{muy}}{\sigma_{elpl}} = \frac{b}{a}\left(1.562 - 1.426e^{-0.9403\beta^{-0.8616}}\right)$$
$$-\left(\frac{b}{a}\right)b_{HAZ}\left(1-\frac{\sigma^{*}_{0.2}}{\sigma_{0.2}}\right)\left(0.05958 - 0.1141e^{-0.9403\beta^{-0.8616}} + 0.04064e^{-2.187\beta^{-2.145}}\right)$$
$$+\left(1-\frac{b}{a}\right)\left(0.6629 - 0.6581\,e^{-1.119\beta^{-2.026}}\right) \qquad (10.16)$$
$$-\left(1-\frac{b}{a}\right)b_{HAZ}\left(1-\frac{\sigma^{*}_{0.2}}{\sigma_{0.2}}\right)\left(0.01274 - 0.05265e^{-1.119\beta^{-2.026}} + 0.04018e^{-1.384\beta^{-1.976}}\right)$$

Figure 10.8 shows design curves for plates with a breadth of the heat affected zones equal to 25 mm and different reductions of yield strength in the heat affected zones. The design curve for plates without reductions of the yield strength in the heat affected zones ($\sigma_{0.2}^{*}/\sigma_{0.2}$=1.0) can only be used for plates that have not been welded.

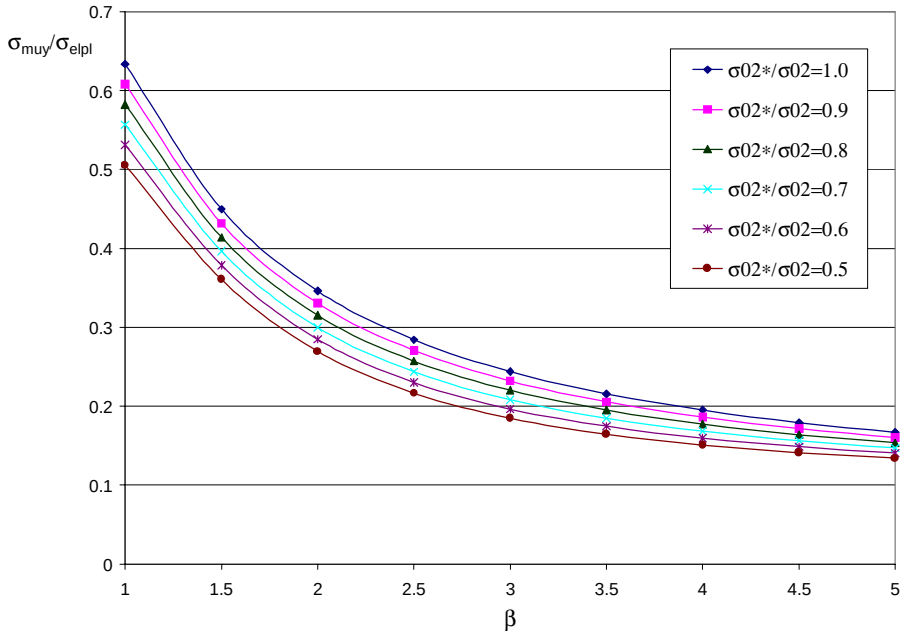

Figure 10.8 : Design curves for the transverse ultimate strength for plates with a breadth of the heat affected zones equal to 25 mm and aspect ratio, a/b=3.

10.3 Biaxial Compression

10.3.1 General Considerations

A separate set of biaxial interaction curves has been proposed for each aspect ratio, a/b. For each aspect ratio, a/b, and slenderness value, β, the curve giving the most conservative interaction has been chosen as basis for design, independently of the pattern of the heat affected zones (base material, HAZ along all edges or extruded HAZ pattern). Only interaction curves for alloy 6082-T6 have been used as basis for design, but as have been shown in Chapter 10, other aluminium alloys do have nearly identical biaxial interaction

curves. The interaction curves used as basis for design curve development are given in Table 10.6.

Table 10.6 : Interaction curves used as basis for design

Aspect ratio, a/b=1									
β	1.0	1.5	2.0	2.5	3.0	3.5	4.0	4.5	5.0
HAZ pattern	Base material	Base material	All edges	All edges	All edges	Base material	Base material	Base material	Base material
Aspect ratio, a/b=2									
β	1.0	1.5	2.0	2.5	3.0	3.5	4.0	4.5	5.0
HAZ pattern	All edges	Base material	Base material	All edges	All edges	All edges	All edges	All edges	All edges
Aspect ratio, a/b=3									
β	1.0	1.5	2.0	2.5	3.0	3.5	4.0	4.5	5.0
HAZ pattern	Extruded	Base material	Base material	All edges	All edges	All edges	All edges	All edges	All edges
Aspect ratio, a/b=5									
β	1.0	1.5	2.0	2.5	3.0	3.5	4.0	4.5	5.0
HAZ pattern	All edges	Base material	Base material	Base material	All edges	All edges	All edges	All edges	All edges

10.3.2 Interaction Curves for Different Aspect Ratios

Equation 10.17 can be used to describe the interaction curves for all aspect ratios. The exponent, γ, is the same for all values of the aspect ratio, a/b, but vary with the different values of the slenderness, β. The exponent, ξ, vary both with aspect ratio, a/b, and slenderness, β. Table 10.7 shows the equations for the exponents γ and ξ.

$$R_x^{\gamma} + R_y^{\xi} = 1 \tag{10.17}$$

In Figures 10.9-10.16 the biaxial interaction curves used as basis for design are plotted together with the proposed design curves. Curves comparing each individual interaction curve used as basis for design with each individual design curve are quoted in Appendix 6.

Table 10.7 : Equations for design curve exponents

Aspect ratio, a/b	**γ**	**ξ**
1	$\frac{1.181}{1-2.320e^{-1.380\beta}}$ (10.18)	$\frac{1.181}{1-2.320e^{-1.380\beta}}$ (10.19)
2	$\frac{1.181}{1-2.320e^{-1.380\beta}}$ (10.18)	$\frac{1}{0.2009+0.3460\ln(\beta)}$ (10.20)
3	$\frac{1.181}{1-2.320e^{-1.380\beta}}$ (10.18)	$4.017-2.842e^{-7.967\beta^{-2.850}}$ (10.21)
5	$\frac{1.181}{1-2.320e^{-1.380\beta}}$ (10.18)	$\frac{1}{0.1120\beta+0.004107\beta^2-0.004987}$ (10.22)

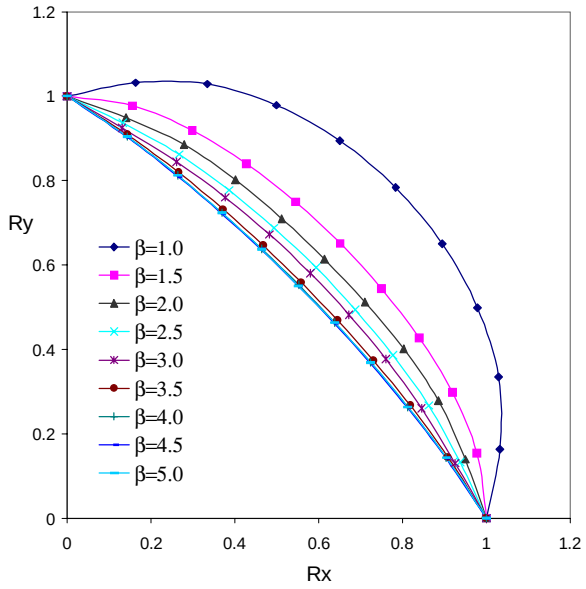

Figure 10.9 : Interaction curves used as basis for design. Aspect ratio, a/b=1.

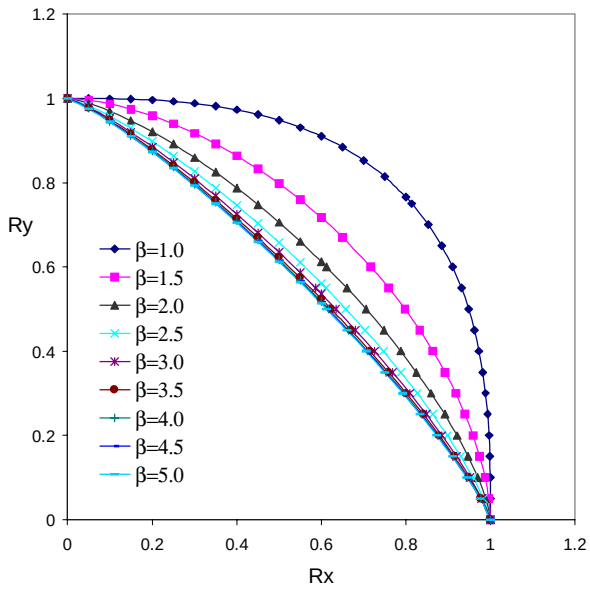

Figure 10.10 : Proposed design curves for aspect ratio, a/b=1.

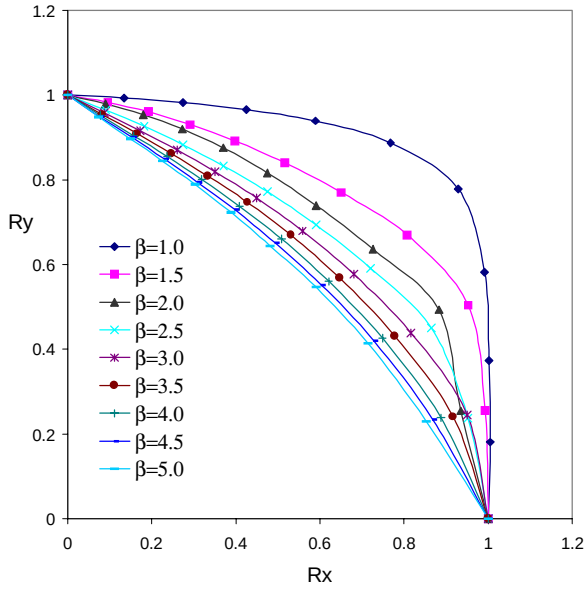

Figure 10.11 : Interaction curves used as basis for design. Aspect ratio, a/b=2.

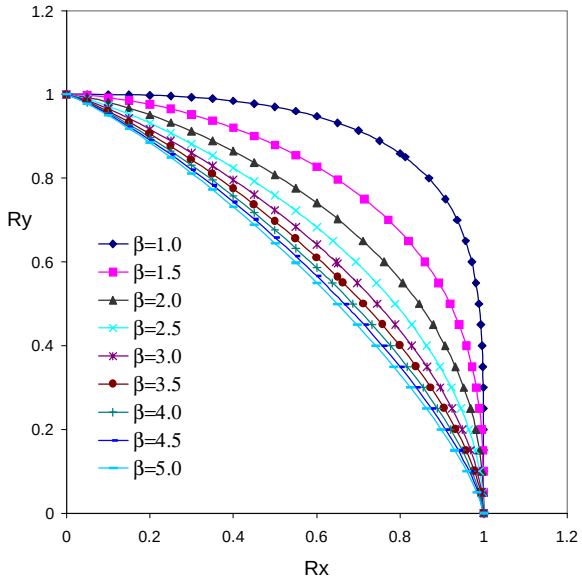

Figure 10.12 : Proposed design curves for aspect ratio, a/b=2.

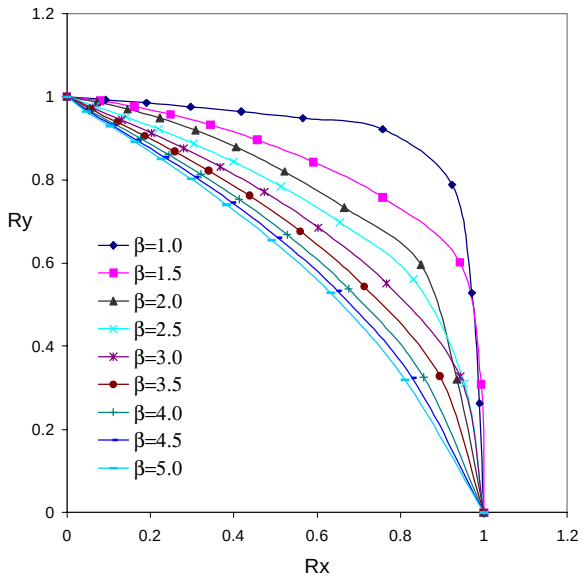

Figure 10.13 : Interaction curves used as basis for design. Aspect ratio, a/b=3.

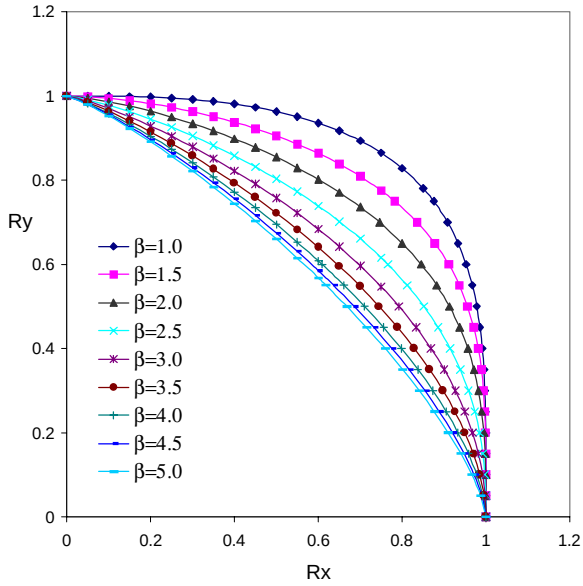

Figure 10.14 : Proposed design curves for aspect ratio, a/b=3.

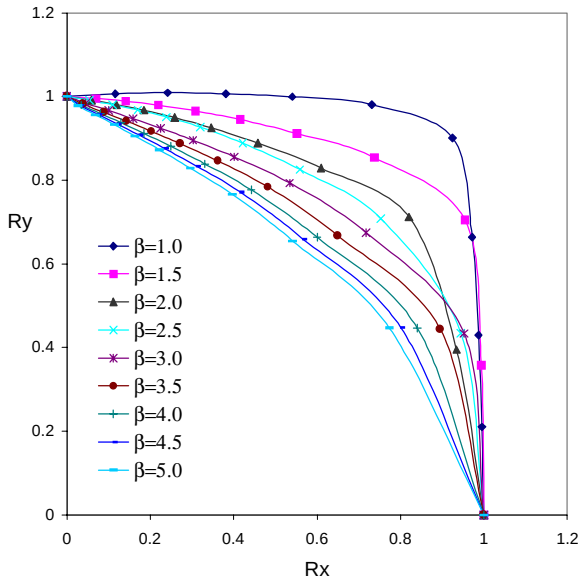

Figure 10.15 : Interaction curves used as basis for design. Aspect ratio, a/b=5.

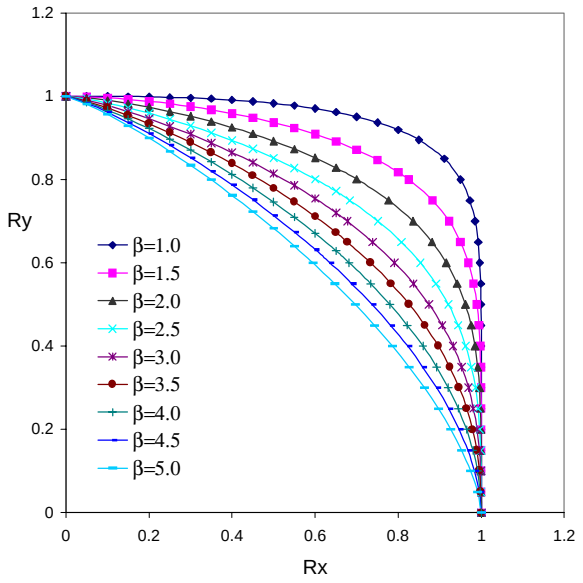

Figure 10.16 : Proposed design curves for aspect ratio, a/b=5.

10.3.3 Linear Interpolation

Developing individual interaction formulas for all aspect ratio values investigated may seem a little circumstantial, but with modern computer programming this will be no problem for practical use.

As have been elaborated on in Chapter 7.4, using linear interpolation between interaction curves with aspect ratio, a/b=1, and higher values of the aspect ratio, will be conservative.

The interaction curves for aspect ratio, a/b=1, and aspect ratio, a/b=5, can be selected. To determine interaction capacities for intermediate values of the aspect ratio, linear interpolation can be applied.

10.4 Pure Shear Loads

10.4.1 Ultimate Strength Formula for Plates Consisting of the Base Material

Plates loaded in shear have only been investigated for an aspect ratio of a/b=3. The proposed design formula should be used with caution for other aspect ratios, a/b.

A curve giving an almost identical fit to the ultimate capacities for the different values of the slenderness, β, can be written as:

$$\frac{\tau_{mu}}{\tau_{elpl}} = 0.9725 - 1.200\, e^{-5.840\,\beta^{-1.071}} \qquad (10.23)$$

The collapse capacities used as basis for the curve development are given in Table 10.8, and Figure 10.17 shows the fit between the numerical data and the curve obtained.

Table 10.8 : Ultimate capacities used as basis for the proposed design formula

Slender-ness β[-]	1.0	1.5	2.0	2.5	3.0	3.5	4.0	4.5	5.0
$\frac{\tau_{mu}}{\tau_{elpl}}$	0.9682	0.9481	0.8951	0.8375	0.7764	0.7148	0.6509	0.5967	0.5514

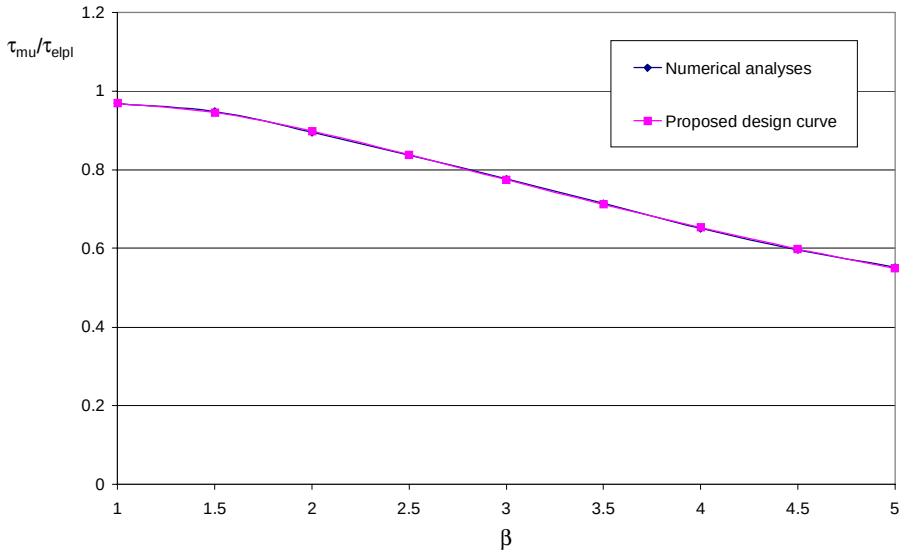

Figure 10.17 : Comparison of the proposed design curve and results from numerical analyses.

10.4.2 Ultimate Strength Formula for Plates with Heat Affected Zones

A curve giving an almost identical fit to the ultimate capacities for plates with a breadth of the heat affected zones equal to 25 mm and $\sigma_{0.2}^{*}=0.5\sigma_{0.2}$, can be written as:

$$\frac{\tau_{mu}}{\tau_{elpl}} = 0.8564 - 0.6603 e^{-6.732\,\beta^{-1.715}} \qquad (10.24)$$

The data used are given in Table 10.9, and Figure 10.18 shows the fit between the numerical data and the curve obtained.

Table 10.9 : Ultimate capacities used as basis for the proposed design formula

Slender-ness β[-]	1.0	1.5	2.0	2.5	3.0	3.5	4.0	4.5	5.0
$\frac{\tau_{mu}}{\tau_{elpl}}$	0.8513	0.8415	0.7689	0.6889	0.6186	0.5589	0.5055	0.4603	0.4221

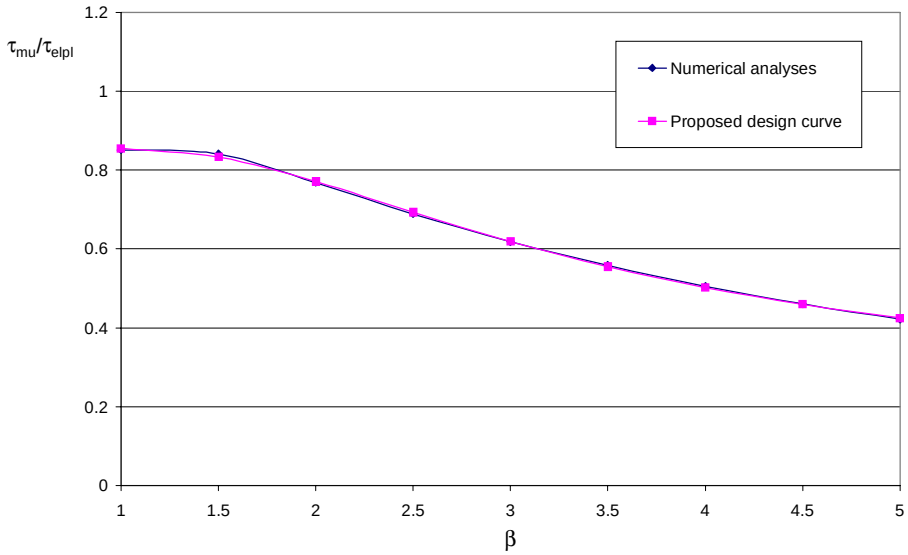

Figure 10.18 : Comparison of the proposed design curve and results from numerical analyses.

10.4.3 Design Formula for Plates with Different Extensions of HAZ

The development of the design formula is based on the same assumptions as were made for axially loaded and transversally loaded plates. The reduction in ultimate capacity is assumed to vary linearly both with the breadth of the heat affected zones and with the ratio between the yield strength of the aluminium alloy in the heat affected zones and the yield strength of the base material. A design equation covering all breadths of the heat affected zones and all ratios between the yield strength in the heat affected zones and the yield strength of the base material can then be written as:

$$\frac{\tau_{mu}}{\tau_{elpl}} = (1-K)\left(\frac{\tau_{mu}}{\tau_{elpl}}\right)_{\substack{Base\\material}} + K\left(\frac{\tau_{mu}}{\tau_{elpl}}\right)_{\substack{Heat\ affected\\zones}}$$
$$= \left(\frac{\tau_{mu}}{\tau_{elpl}}\right)_{\substack{Base\\material}} - K\left[\left(\frac{\tau_{mu}}{\tau_{elpl}}\right)_{\substack{Base\\material}} - \left(\frac{\tau_{mu}}{\tau_{elpl}}\right)_{\substack{Heat\ affected\\zones}}\right] \tag{10.25}$$

$$K = \frac{b_{HAZ}}{25\ mm}\cdot 2\cdot\left(1-\frac{\sigma^{*}_{0.2}}{\sigma_{0.2}}\right) \tag{10.26}$$

$$\frac{\tau_{mu}}{\tau_{elpl}} = 0.9725 - 1.200e^{-5.840\beta^{-1.071}}$$
$$-\frac{b_{HAZ}}{25mm}\cdot 2\cdot\left(1-\frac{\sigma^{*}_{0.2}}{\sigma_{0.2}}\right)\left[0.9725-1.200e^{-5.840\beta^{-1.071}} - \left(0.8564-0.6603e^{-6.732\beta^{-1.715}}\right)\right] \tag{10.27}$$

or

$$\frac{\tau_{mu}}{\tau_{elpl}} = 0.9725 - 1.200\,e^{-5.840\beta^{-1.071}}$$
$$-b_{HAZ}\cdot\left(1-\frac{\sigma^{*}_{0.2}}{\sigma_{0.2}}\right)\left[0.009288-0.09600\,e^{-5.840\beta^{-1.071}} + 0.05282\,e^{-6.732\beta^{-1.715}}\right] \tag{10.28}$$

This equation is illustrated in Figure 10.19 for b_{HAZ}=25 mm. For welded plates $\sigma_{0.2}^{*}$ can not be larger than $0.9\sigma_{0.2}$, because one has to account for the residual stresses that are present.

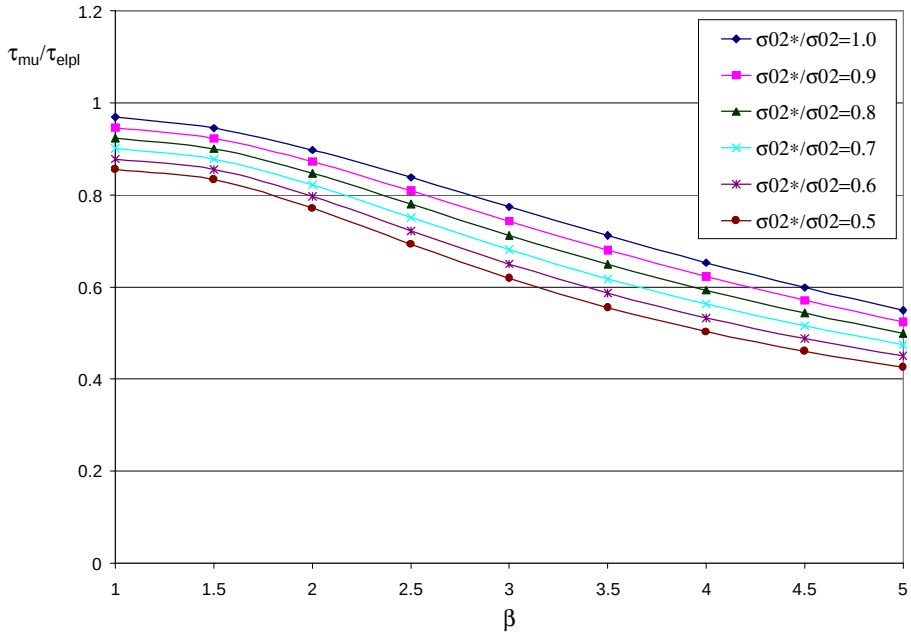

Figure 10.19 : Shear design curves for a breadth of the heat affected zones equal to 25 mm

10.5 Axial Compression in Combination with Shear Loads

10.5.1 Design Formula for Plates with an Aspect Ratio of a/b=3

The interaction curves for plates made of the base material only show more conservative interaction than the interaction curves for plates with heat affected zones along all edges. The only exception is for plates with slenderness β=2.0 and β=2.5, and where the plates are mainly exposed to shear loading (large values of Rτ and low values of Rx); but the reduction in capacity for plates with slenderness β=2.0 is believed to be insignificant, and for plates with slenderness β=2.5 it is hardly visible (details in Chapter 5.6).

Interaction curves for plates consisting of the base material only are used as basis for design formula. The proposed design formula is as follows:

$$R_x^{\gamma} + R_{\tau}^{1.94} = 1 \tag{10.29}$$

$$\gamma = \frac{0.02585 + 1.742\beta^{-4.372}}{0.02379 + \beta^{-4.372}} \tag{10.30}$$

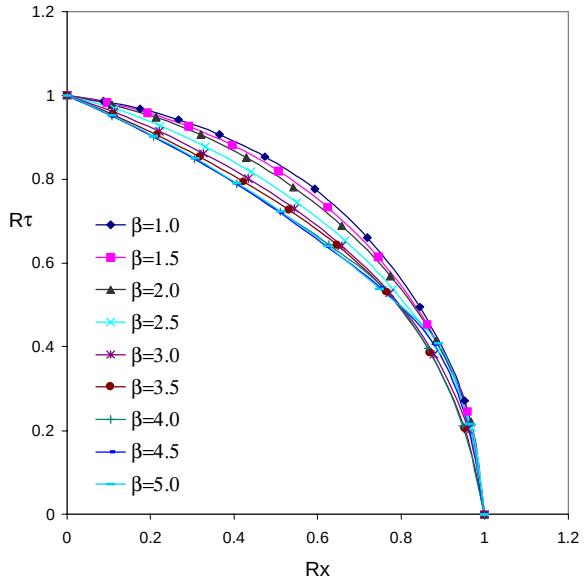

Figure 10.20 : Interaction curves used as basis for design formula (interaction curves for plates without heat affected zones).

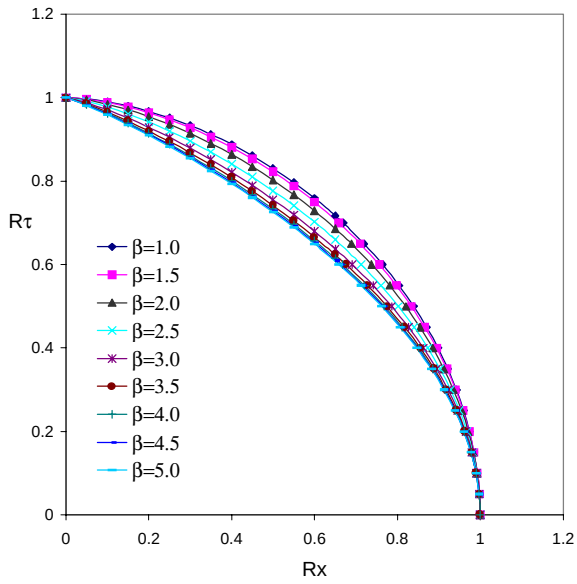

Figure 10.21 : Proposed design curves

Chapter 11

Comparison of Proposed Design Formulations with Existing Codes

11.1 Introduction

The design codes chosen for comparison are: Eurocode 9 (1998), Lloyd's Register of Shipping (1996), Det Norske Veritas Classification AS (1996) and Det Norske Veritas Classification AS (1995). In the following sections these design codes are referred to as Eurocode 9, Lloyd's, DNV HSLC and DNV 30.1, respectively.

DNV 30.1 is a design code meant for steel structures, but it has features interesting for the design of aluminium plates and is herein transformed to a code for aluminium structures by introducing yield stresses and elastic modulus relevant for aluminium alloys.

Most design codes will not allow the mean average stresses to exceed the value of the 0.2 percent tensile proof stress of the material in the parts of the plates with heat affected zones. In the design codes (for instance DNV HSLC and Lloyd's) where this is particularly taken into account, reductions are carried out. For the other design rules such reductions are left out in then design code comparison. If, for instance, parts of DNV 30.1 should be employed for design of aluminium structures, restricting the mean average stresses to the values of the 0.2 percent tensile proof stresses in the heat affected zones may seem like a reasonable restriction.

Most aluminium alloys have substantial residual capacity beyond the 0.2 percent tensile proof stress, so as long as the stresses stay below the 0.2 percent tensile proof stress, this will be a conservative requirement. On the other hand, this have to be a local yielding check. If the design formulas take advantage of post buckling capacities, with uneven distribution of stresses over the breadth of the plates, the local stresses may be way beyond the 0.2 percent tensile proof stress in the heat affected zones, although the mean average stresses are not. Some of the formulas in DNV 30.1, take advantage of post buckling strength with uneven distributions of yield stresses over the breadth of the plate.

The design formulas proposed by the author take full advantage of all residual strength in the stress-strain curves of the different alloys. This may lead to very large local strains challenging the limits of fracture. The problem of finding the limits of fracture has not been looked into by the author. On the other hand, restricting the local strains to be below the 0.2 percent tensile proof stress in the heat affected zones, will be very conservative.

11.2 Axial Compression

Lloyd's and DNV HSLC are based on linear elastic buckling with a Johnson-Ostenfeld correction (details in Section 3.2.1). The curves are normalised with the 0.2 % tensile proof stress, and to account for heat affected zones the mean axial buckling stress, σ_{mux}, has to be lower than the reduced yield stress of the material after welding.

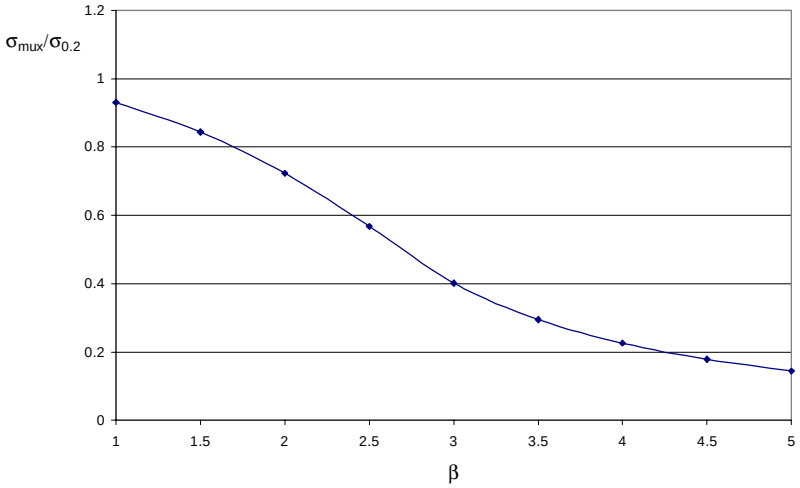

Figure 11.1 : Linear elastic buckling with Johnson-Ostenfeld correction, used in Lloyd's and DNV HSLC

If the 0.2 percent tensile proof stress is used as the normalising stress, aluminium plates made of highly utilised aluminium alloys (heat treated and cold worked alloys) show a larger relative strength (higher ultimate load for the same slenderness, β) than aluminium alloys with low utilisation (details in Chapter 9). Due to the introduction of residual stresses plates that have been welded will have an additional reduction in strength.

In Eurocode 9 these effects are accounted for to form three separate collapse curves: heat treated, unwelded; heat treated, welded or non heat treated, unwelded; and non heat treated, welded. In addition there is a reduction because of soft zones. Only soft zones along unloaded (long) edges are considered and no reduction is made if the mean axial stress, σ_{mux}, is below the yield strength of the material affected by welding.

Assuming the elastic modulus, E, to be equal to 70000 N/mm^2, the three different collapse curves in Eurocode 9 can be written as:

$$\frac{\sigma_{mux}}{\sigma_{0.2}} = \frac{1.912}{\beta} - \frac{0.7857}{\beta^2} \tag{11.1}$$

$$\frac{\sigma_{mux}}{\sigma_{0.2}} = \frac{1.733}{\beta} - \frac{0.7071}{\beta^2} \tag{11.2}$$

$$\frac{\sigma_{mux}}{\sigma_{0.2}} = \frac{1.494}{\beta} - \frac{0.5357}{\beta^2} \tag{11.3}$$

and are shown in Figure 11.2.

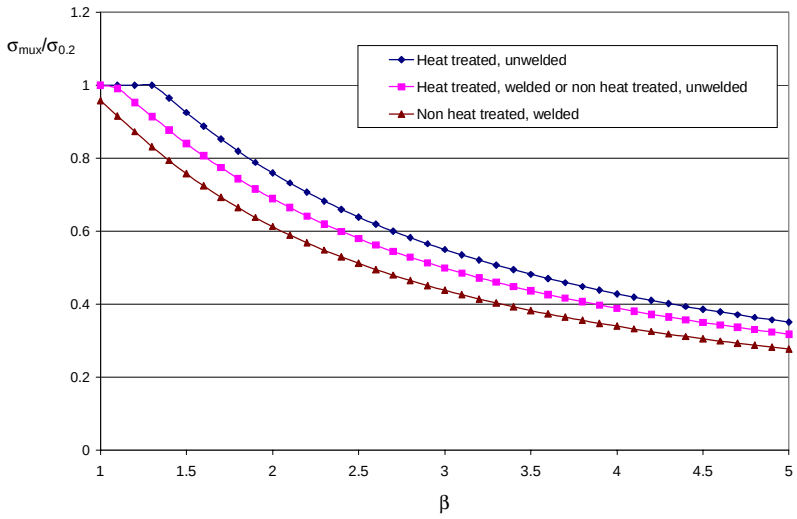

Figure 11.2 : Axial buckling curves given in Eurocode 9

DNV 30.1 has three different curves, one for the serviceability limit state (SLS), one for the ultimate limit state (ULS) and one for the effective flange of a stiffened panel. To be able to use these curves the yield stress of steel has been replaced by the 0.2 % tensile proof stress. Since DNV 30.1 is a code for steel structures, no effects of soft zones are considered, but the effective flange curve accounts for reasonable values of residual stresses that will be present in a steel structure.

DNV 30.1, SLS

$$\frac{\sigma_{mux}}{\sigma_{0.2}} = \frac{1}{\sqrt{1+\bar{\lambda}^4}} \qquad (11.4)$$

DNV 30.1, ULS

$$\frac{\sigma_{mux}}{\sigma_{0.2}} = \frac{1}{\sqrt{1+\bar{\lambda}^4}} \quad \text{if} \quad \bar{\lambda} \le 1.0 \qquad (11.5)$$

$$\frac{\sigma_{mux}}{\sigma_{0.2}} = \frac{1}{\bar{\lambda}\sqrt{2}} \quad \text{if} \quad 1.0 < \bar{\lambda} \le 5 \qquad (11.6)$$

DNV 30.1, Effective Flange

$$\frac{\sigma_{mux}}{\sigma_{0.2}} = \frac{1.8}{\beta} - \frac{0.8}{\beta^2} \qquad (11.7)$$

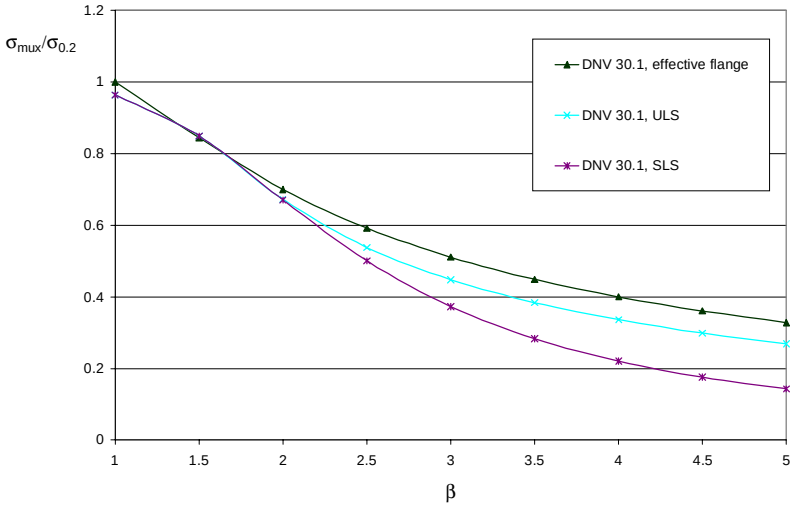

Figure 11.3 : Buckling curves given in DNV 30.1

The comparison of the different design curves will be limited to two cases. The first example is a plate made of a non heat treated alloy that have been welded (b_{HAZ}=25 mm), but with no reduction in yield strength in the heat affected zones. For convenience the stress corresponding to equal elastic and plastic strain, σ_{elpl}, is chosen to be equal to the 0.2 percent tensile proof stress, $\sigma_{0.2}$. Since the effective flange formula represents an upper bound for the formulas given in DNV 30.1, it is chosen as the curve for comparison. The different design curves are compared in Figure 11.4.

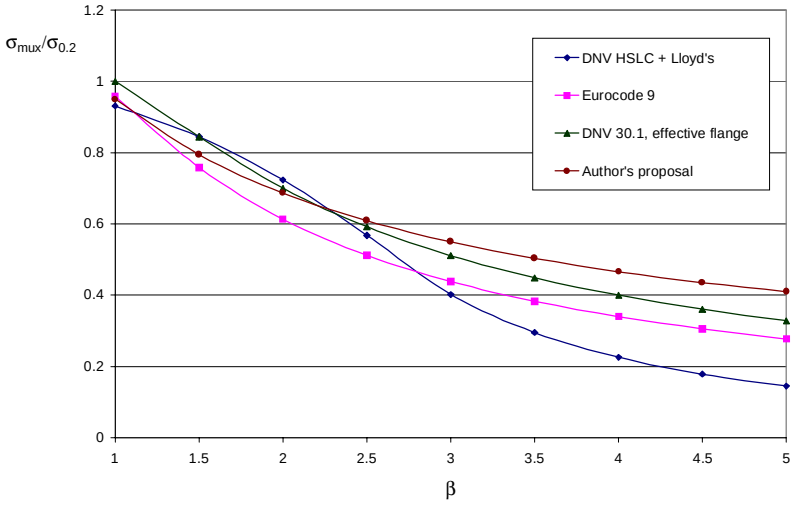

Figure 11.4 : Comparison of proposed design formula with different design codes for a non-heat treated alloy that have been welded, but without any reduction in yield strength due to welding.

The second example is a plate made of a heat treated alloy that have been welded. The length of the plate is a=900 mm and the breadth of the plate is b=300mm. The plate has heat affected zones along all edges, and the breadth of the heat affected zones is 25 mm. The 0.2 percent tensile proof stress in the heat affected zones is half the value of the 0.2 percent

tensile proof stress of the base material (292 MPa). The comparison of the different design curves is given in Figure 11.5.

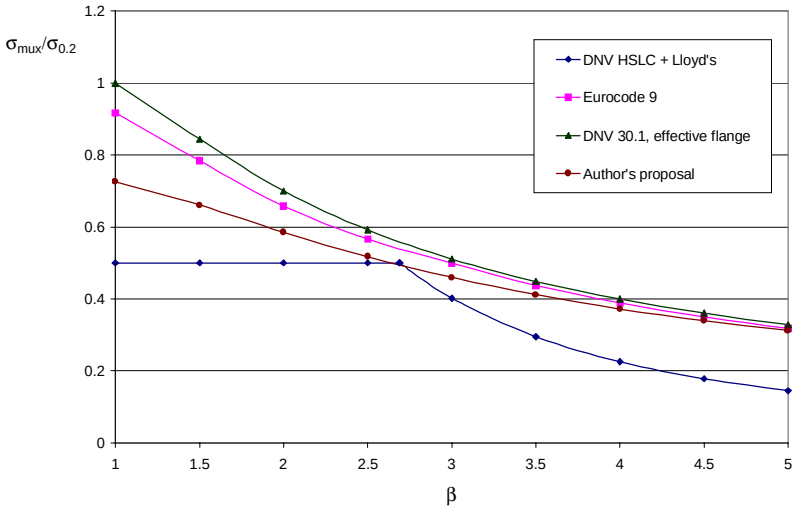

Figure 11.5 : Comparison with different design codes for a heat treated alloy that have been welded. The plate has heat affected zones along all edges and the breadth of the heat affected zones is 25 mm. The 0.2 percent tensile proof stress in the heat affected zones is half the value of the 0.2 percent tensile proof stress of the base material.

If the plates have no reduction in the 0.2 percent tensile proof stress due to welding, Eurocode 9 and the proposed design curve predict the same collapse capacities for the most sturdy plates. The ultimate capacity of the most slender plates, on the other hand, is 32.4 percent smaller according to Eurocode 9.

If the plates have a 50 percent reduction in the 0.2 percent tensile proof stress due to welding, the situation is the opposite. Eurocode 9 and the proposed design curve predicts almost the same ultimate capacity for the most slender plates. For the most sturdy plates Eurocode 9 gives a ultimate capacity that is 26.2 percent higher than the values of the proposed design curve.

The design curve proposed in this thesis takes full advantage of all non-linear residual strength, but have a much larger reduction due to the introduction of reduced yield strength in the heat affected zones.

Plates with heat affected zones along all edges, or with the extruded pattern of the heat affected zones, have a larger reduction in ultimate capacity than plates with heat affected zones along long edges only; but as have been thoroughly elaborated on in Chapter 5.2.2, the reduction in ultimate capacity due to the introduction of heat affected zones along long edges does not vanish if the mean average axial stress for the whole plate is below the yield stress of the material in the heat affected zones.

If all non-linear residual capacity has been taken advantage of, the reduction in ultimate capacity due to introduction of heat affected zones along long edges could be modelled by the same absolute reduction in average ultimate stress. The reason for this was the uneven

distribution of axial stresses along the cross section of the plate. The stresses in the parts of the plate that were affected by welding was higher than the reduced material strength in the heat affected zones although the average stresses were not.

Eurocode 9 only considers reduction in ultimate capacity due to heat affected zones along long edges. This reduction in ultimate capacity only takes place if the mean average axial stress of the whole plate is larger than the reduced yield stress in the heat affected zones; and only in the parts of the plates that are affected by welding. In the author's opinion this line of action will be acceptable if the axial stresses are evenly distributed along the whole breadth of the plate, and continue to be evenly distributed after the introduction of heat affected zones, with the same value of the axial stresses in the parts of the plates not affected by welding.

One way to achieve an even distribution of axial stresses across the whole breadth of the plate is to keep the stresses below the proportional limit, or Euler load, but the design formulas given in Eurocode 9 will not always fulfil this condition, especially not for very slender plates.

The results in Chapter 5.2.2 show the largest reductions in ultimate capacity due to the introduction of heat affected zones along long edges for very slender plates. Eurocode 9 has no reduction in ultimate capacity for very slender plates exposed to heat affected zones along long edges.

Despite this way of treating the introduction of heat affected zones, it is only for compact plates with heat affected zones along all edges, or with the extruded pattern of the heat affected zones, and with a large reduction of the 0.2 percent tensile proof stress in the heat affected zones, that Eurocode 9 predicts considerably higher ultimate capacities than what is found by numerical analyses.

The comparison of the proposed design curve with DNV HSLC and Lloyd's reveals that using linear elastic buckling with Johnson Ostenfeld correction is very conservative for slender plates and the degree of conservatism becomes larger and larger the more slender the plates become. If the reduction in yield stress in the heat affected zones is as large as 50 percent, DNV HSLC and Lloyd's will be conservative for all slenderness values as compared to the proposed design curve, but for smaller reduction in yield strength in the heat affected zones things are a little more difficult to follow.

In Appendix 7 the ultimate capacity predicted by the proposed design formula and ultimate capacities taken from DNV HSLC and Lloyd's are compared for different reductions of the yield stress in the heat affected zones. For slenderness, β=1.5, 2.0 and 2.5, the capacity implied by DNV HSLC can become non-conservative as compared to values given by the proposed design formula, and the values of the non-conservatism can be as large as 9.4 percent.

The DNV 30.1 effective flange curve can be used to predict the ultimate capacity for plates without reduction of yield strength in the heat affected zones, though slightly over-estimating the ultimate capacity for compact plates. For plates with a 50 percent reduction of yield strength in the heat affected zones the DNV 30.1 effective flange formula over-estimates the ultimate capacity for all values of the slenderness, β. For plates with slenderness, β=5.0, the over-prediction is insignificant, but for slenderness, β=1.0, the over-prediction is as large as 37.7 percent as compared to the proposed design curve.

11.3 Transverse Compression

Eurocode 9 does not have relevant design curves for transverse compression of plates, and is not considered .

DNV HSLC and Lloyd's both use linear elastic buckling with a Johnson Ostenfeld correction; but an additional exploitation due to rotational restraint from stiffeners is allowed. The augmentation in strength is the same for all values of the slenderness, β, but it varies from 5 percent for flatbars to 30 percent depending on design rule and type of stiffeners. In the following, curves from DNV HSLC and Lloyd's are treated together and the additional exploitation due to rotational restraint from stiffeners is ignored.

The design equations (Eq. 11.4-11.6) for the serviceability limit state and ultimate limit state given in DNV 30.1 can also be applied for transverse loading. The equation giving the transverse ultimate capacity in the effective flange formulation uses the same approach as have been utilised in this dissertation. The transverse ultimate capacity of a plate is a weighted sum of the capacity of a square plate and a plate strip.

$$\frac{\sigma_{muy}}{\sigma_{0.2}} = \frac{b}{a}\left(\frac{\sigma_{muy}}{\sigma_{0.2}}\right)_{\substack{\text{square}\\ \text{plate}}} + \left(1-\frac{b}{a}\right)\left(\frac{\sigma_{muy}}{\sigma_{0.2}}\right)_{\substack{plate\\ strip}} \tag{11.8}$$

$$\frac{\sigma_{muy}}{\sigma_{0.2}} = \frac{b}{a}\left(\frac{1.8}{\beta}-\frac{0.8}{\beta^2}\right)+0.1\left(1-\frac{b}{a}\right)\left(1+\frac{1}{\beta^2}\right)^2 \tag{11.9}$$

The contribution from the square plate is identical to the formula used to determine the axial capacity of plates (and is discussed in Chapter 11.2).

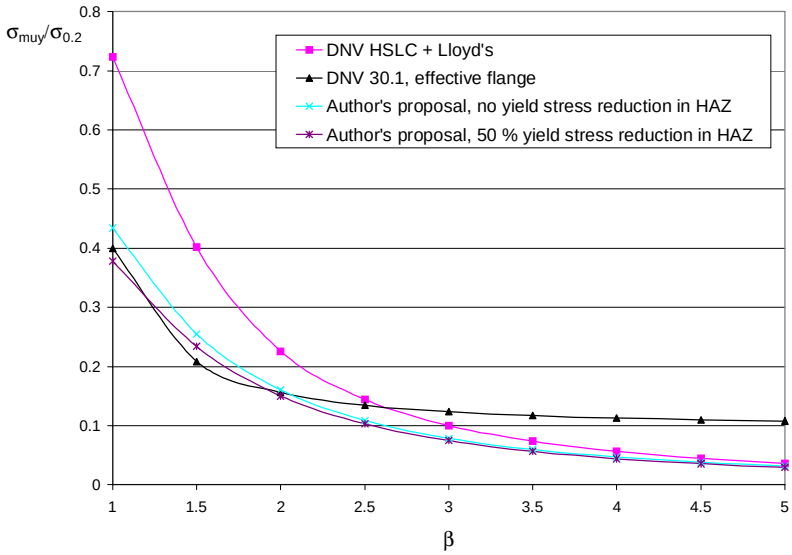

Figure 11.6 : Comparison of the plate strip capacity given by DNV 30.1 effective flange formulation, linear elastic buckling with Johnson Ostenfeld correction (DNV HSLC + Lloyd's) and the proposed design formulas. This case corresponds to an infinitely large aspect ratio.

In Figure 11.6 the plate strip part of the effective flange formulation in DNV 30.1 is compared with the plate strip capacities found in this dissertation and plate strip capacitiy given by linear elastic buckling with a Johnson Ostenfeld correction (DNV HSLC + Lloyd's). The plate strip capacities for plates with heat affected zones, are taken from plate strips with heat affected zones in the middle-longitudinal direction. The breadth of the heat affected zones is 25 mm.

The different design codes can now be compared with the proposed design formulas for different values of the aspect ratio, a/b. The DNV HSLC + Lloyd's collapse curves are written for plates without reduction in yield strength due to welding, and the curves determined "Author's proposal" refer to the transverse ultimate capacitiy for extruded plates with the breadth of the heat affected zones equal to 25 mm.

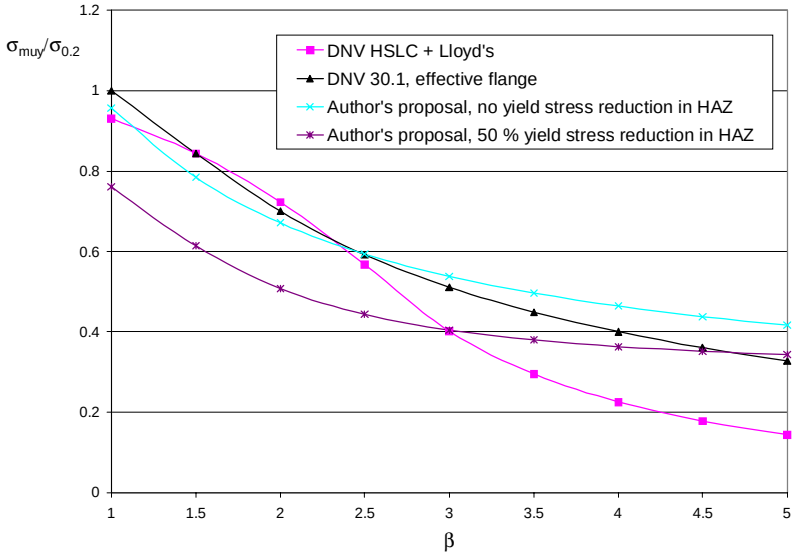

Figure 11.7 : Comparison with transverse ultimate capacity from different design codes. Aspect ratio, a/b=1.

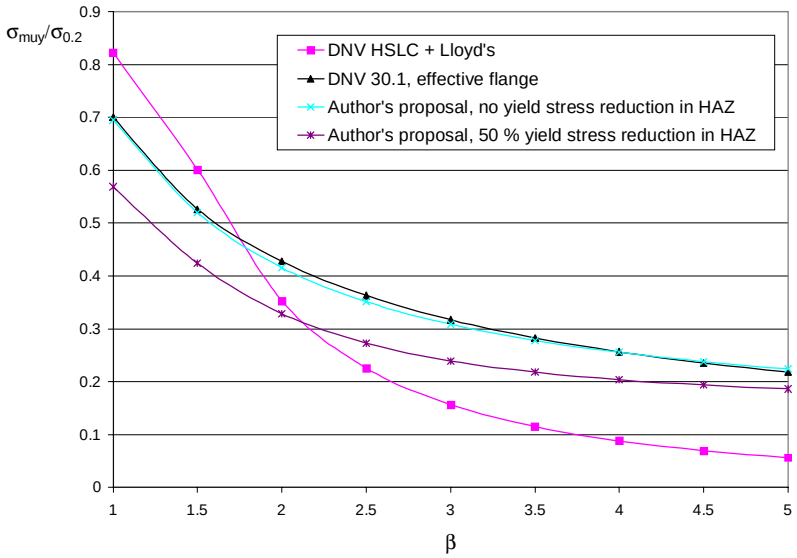

Figure 11.8 : Comparison with transverse ultimate capacity from different design codes. Aspect ratio, a/b=2.

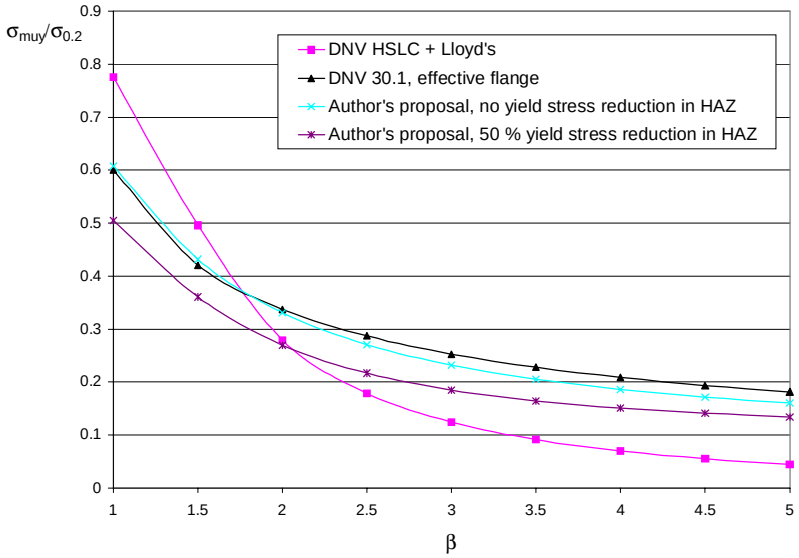

Figure 11.9 : Comparison with transverse ultimate capacitiy from different design codes. Aspect ratio, a/b=3.

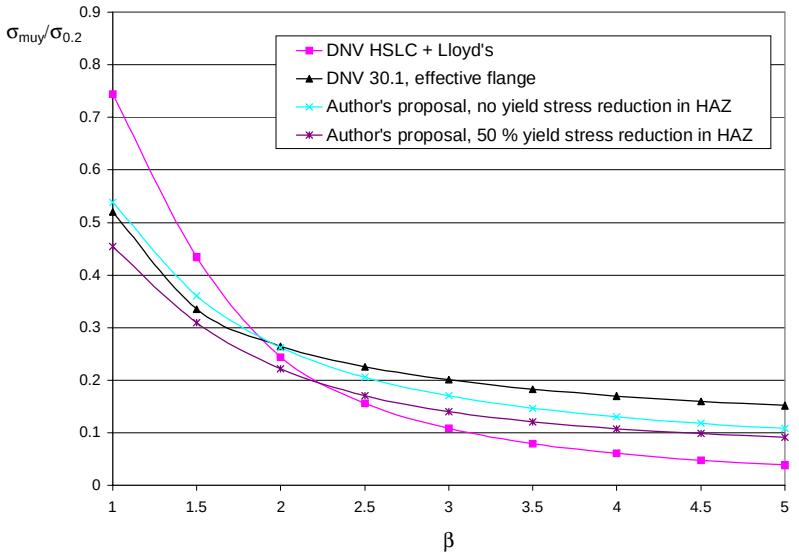

Figure 11.10 : Comparison with transverse ultimate capacity from different design codes. Aspect ratio, a/b=5.

Figures 11.6 and 11.7 represent the limiting cases with respect to aspect ratio. Using linear elastic buckling with Johnson Ostenfeld correction drastically over-estimates the transverse ultimate capacity for sturdy plate strips. The ultimate capacity for square sturdy plates, on the other hand, shows good agreement with the proposed design curve; if the plates do not have reduced yield stress in the heat affected zones due to welding. The result is that the higher the aspect ratio, a/b, becomes, the larger the overestimation of the ultimate capacities given by linear elastic buckling with Johnson Ostenfeld correction is, as compared to the proposed design curves.

For slender plates the situation is the opposite. The plate strip capacity given by linear elastic buckling shows a good agreement with plate strip capacities in the proposed design formulas while the ultimate capacity for square plates is underestimated by using linear elastic buckling as compared to the proposed design formulas. The conclusion is that linear elastic buckling underestimates the transverse ultimate capacity of slender plates as compared to the proposed design formulas, but the differences between results from linear elastic buckling and the proposed design formulas decreases as the aspect ratio, a/b, increases.

The DNV 30.1 effective flange formulation may be compared with results from the proposed design curve for plates without reduction of yield strength in the heat affected zones, as follows.

The plate strip capacity for sturdy plates is lower than the plate strip capacity from the proposed design curve (maximum deviation is 18.3 % for β=1.5). For large β's the plate strip part of the design equation in DNV 30.1 implies ultimate capacity that is more than twice the ultimate capacity found by the proposed design curve. This is non-conservative.

The contribution from the square plate in the design equation shows the opposite tendency. DNV 30.1 predicts the largest ultimate capacities for sturdy plates, and the proposed design formula gives the highest ultimate capacity for slender plates.

The discrepancies in the different contributions of the design equations equal each other out in such a way that plates with an aspect ratio, a/b=2, get almost an identical ultimate capacitiey irrespective of choice of design equation. For aspect ratio, a/b=3, the accordance between the two design proposals is still good enough that both of them can be used for practical design purposes, but if the aspect ratio, a/b, becomes as large as 5, the DNV 30.1 effective flange formulation will over-estimate the ultimate capacity of slender plates.

For plates exposed to heat affected zones, the situation is more perspicuous. Even though the differences between other design curves and the proposed design curves decreases as the aspect ratio, a/b, increases, only linear elastic buckling with Johnson Ostenfeld correction (DNV HSLC + Lloyd's) can, for selected values of the slenderness, β (preferentially slender plates), be used as basis for design. DNV 30.1 effective flange formulation over-estimates the ultimate capacity for all values of the slenderness, β, and all values of the aspect ratio, a/b, larger than one.

11.4 Biaxial Compression

Eurocode 9 does not have relevant design curves for biaxial compression, and is consequently not considered.

In this chapter only the shapes of the interaction curves are considered. The differences in the uniaxial capacities are discussed in their respective chapters (Chapters 11.2 and 11.3).

The biaxial interaction curves in Lloyd's do have different shapes dependent on the value of the aspect ratio, a/b. Five different curves are proposed, corresponding to a/b=1.0, 1.6, 2.0, 3.0 and ∞. They are reproduced in Figure 11.11. One interaction curve, suitable for all values of the aspect ratio, a/b, is given as a formula. It suggests linear interaction. This is

identical to the biaxial interaction curve for aspect ratio, a/b=1, given in the plot. The biaxial interaction curves given in Lloyd's are not dependent on the slenderness, β.

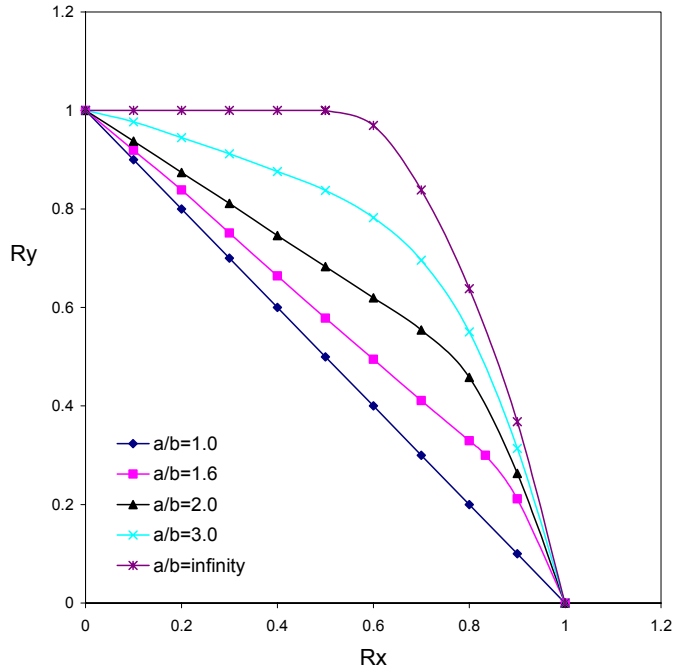

Figure 11.11 : Biaxial interaction curves given in Lloyd's, independent of β.

The biaxial interaction curves provided by DNV HSLC are dependent both on slenderness and aspect ratio. Concerning the aspect ratio dependence one distinguishes between plates with aspect ratios, 1.0<a/b<1.5, and plates with aspect ratios, 1.5≤a/b<8. The slenderness dependence is also separated into the same two intervals.

The slenderness dependence is relatively moderate, but it is opposite in nature for plates with aspect ratio, a/b<1.5, and plates with aspect ratio, a/b>1.5. Plates with aspect ratio, a/b<1.5, show stronger interaction the more slender the plates become, while plates with aspect ratio, a/b>1.5 have the opposite trend, the more compact the plates become, the stronger the interaction.

The aspect ratio dependency is more pronounced with stronger interaction for plates with aspect ratio, a/b<1.5, than plates with aspect ratio, a/b>1.5.

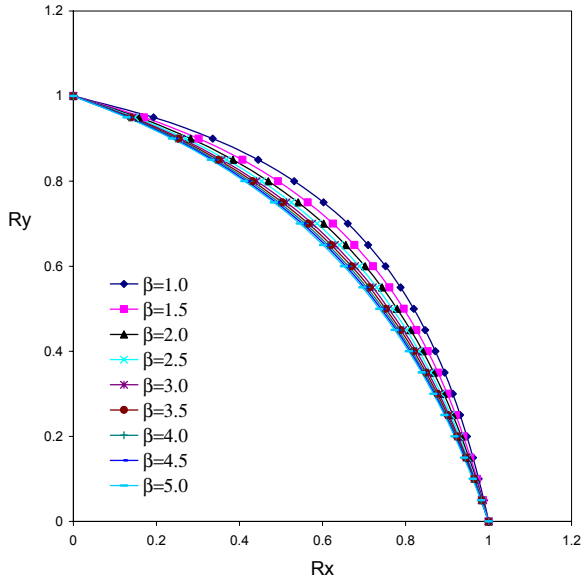

Figure 11.12 : Biaxial interaction curves provided by DNV HSLC, 1.0 < a/b < 1.5

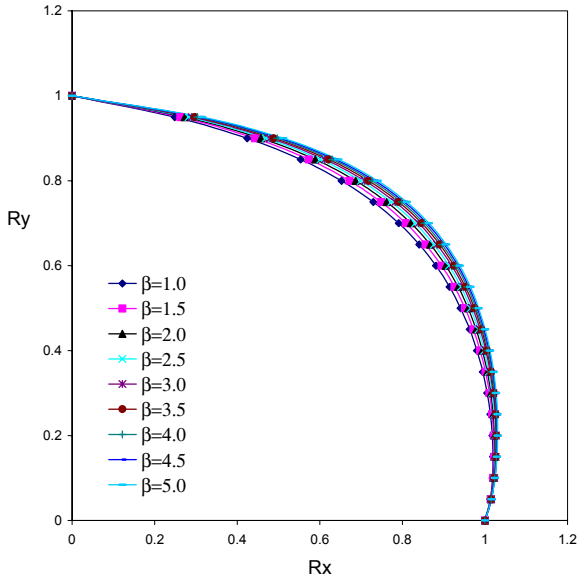

Figure 11.13 : Biaxial interaction curves provided by DNV HSLC, 1.5≤ a/b < 8

DNV 30.1 contains three different biaxial interaction formulas, one for the serviceability limit state of plates, one for the ultimate limit state of plates and one for the effective plate flange of a stiffened flange.

The details of the SLS and ULS formulations will not be given, but both formulations operates with an equivalent reduced slenderness and an equivalent stress according to Hencky-von Mises. The curves are both slenderness dependent and aspect ratio dependent. The more slender the plate is, the stronger the interaction, and the lower the value of the aspect ratio, a/b, the stronger the interaction.

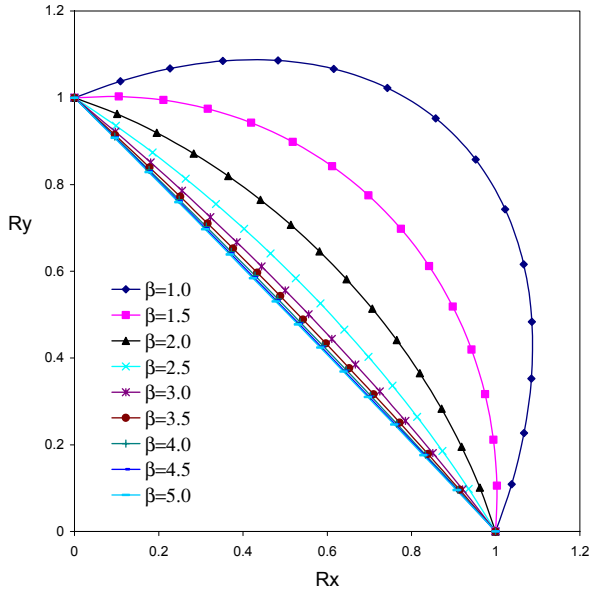

Figure 11.14 : Biaxial interaction curves given by DNV 30.1, SLS, aspect ratio, a/b=1

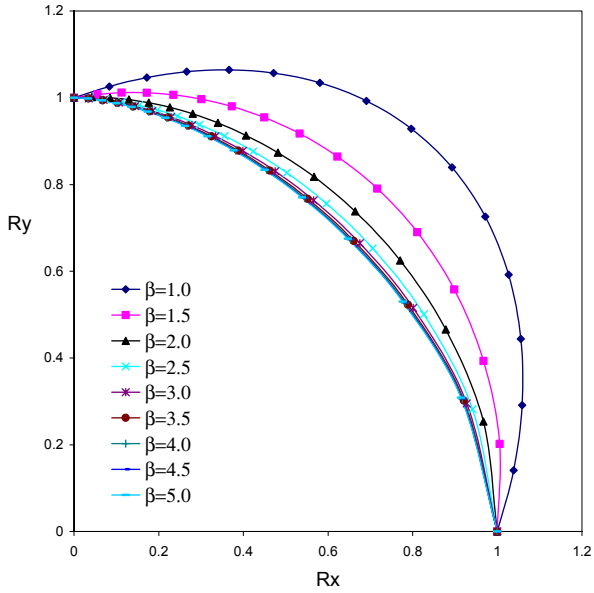

Figure 11.15 : Biaxial interaction curves given by DNV 30.1, SLS, aspect ratio, a/b=3

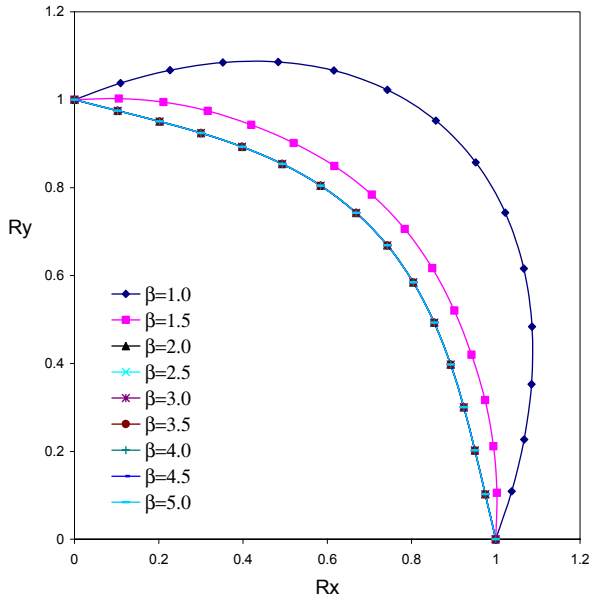

Figure 11.16 : Biaxial interaction curves given by DNV 30.1, ULS, aspect ratio, a/b=1

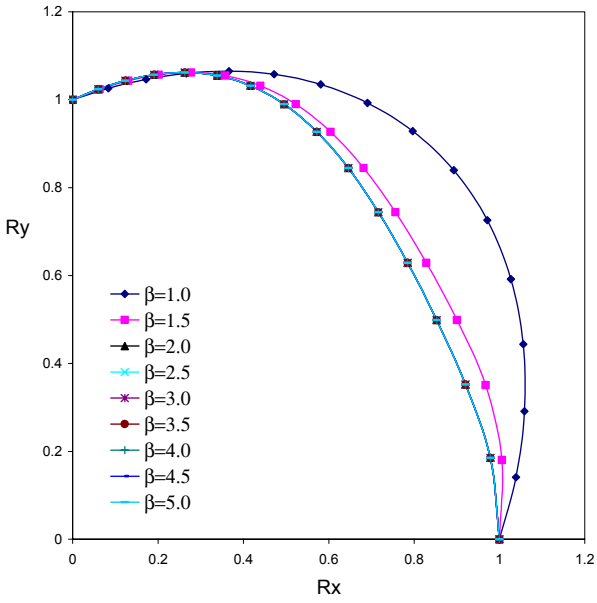

Figure 11.17 : Biaxial interaction curves given by DNV 30.1, ULS, aspect ratio, a/b=3

The effective flange formulation of DNV 30.1 has two different interaction formulas, one for aspect ratio, a/b=1, and one for aspect ratio, a/b=3. For intermediate values of the aspect ratio, a/b, linear interpolation applies. No weaker interpolation than the curve given for aspect ratio, a/b=3, is allowed even though the aspect ratio, a/b, exceeds the value of 3.

The interaction formula for aspect ratio, a/b=3, is slenderness independent, while the interaction formula for aspect ratio, a/b=1, show stronger interaction the more slender the plates become.

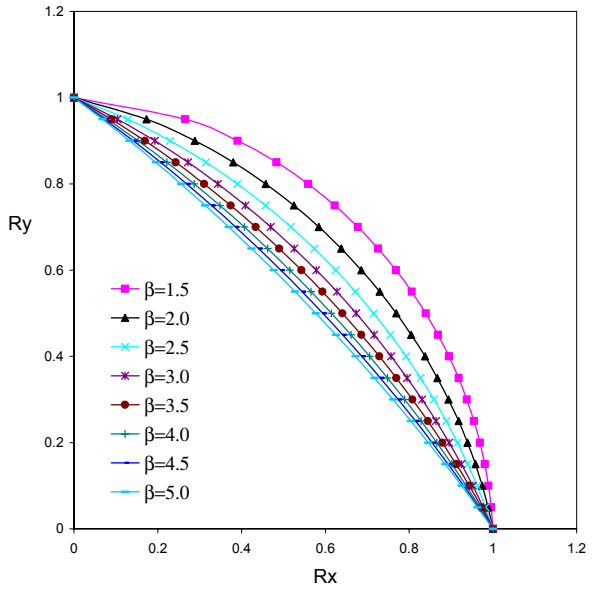

Figure 11.18 : Biaxial interaction curves given by DNV 30.1, effective flange formulation, aspect ratio, a/b=1

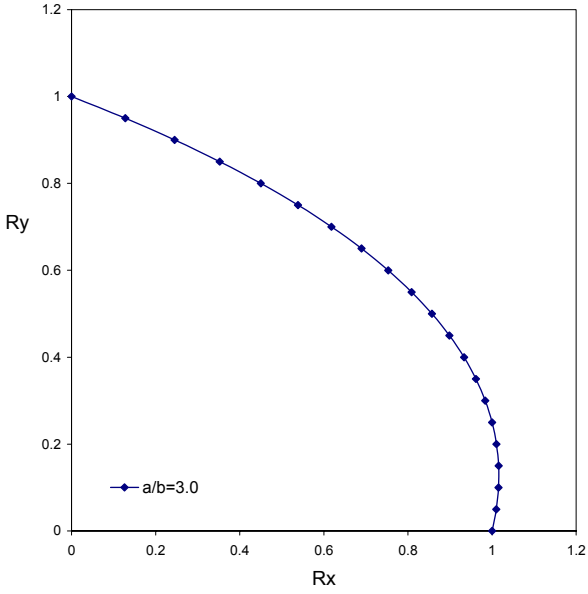

Figure 11.19 : Biaxial interaction curve given by DNV 30.1, effective flange formulation, aspect ratio, a/b=3

In Figures 11.20-11.28 the proposed biaxial interaction curves for plates with aspect ratio, a/b=3, given in Chapter 10.3.4, are compared with the presented design codes. A comparison for plates with aspect ratio, a/b=1, can be found in Appendix 7.

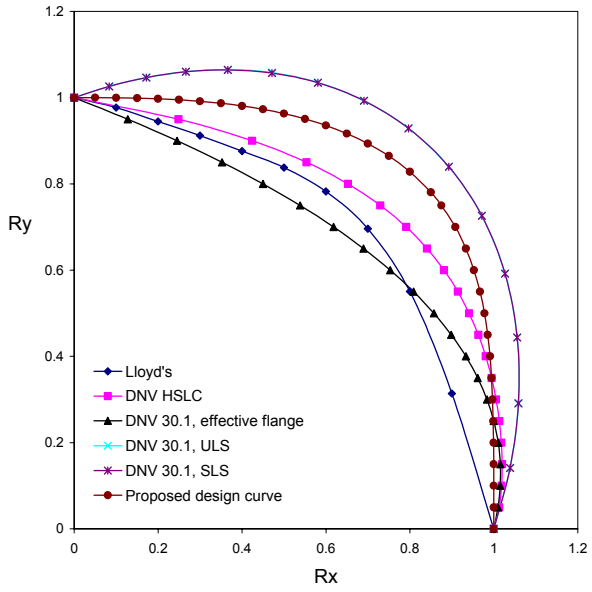

Figure 11.20 : Comparison of different code formulations for biaxial loading, aspect ratio, a/b=3, β=1.0

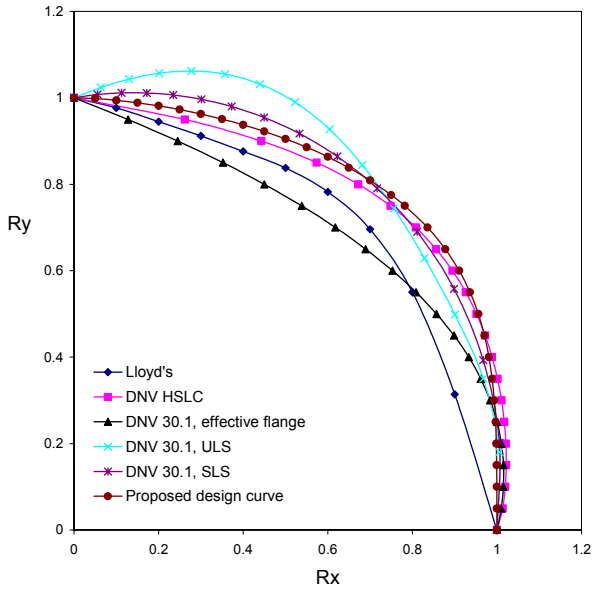

Figure 11.21 : Comparison of different code formulations for biaxial loading, aspect ratio, a/b=3, β=1.5

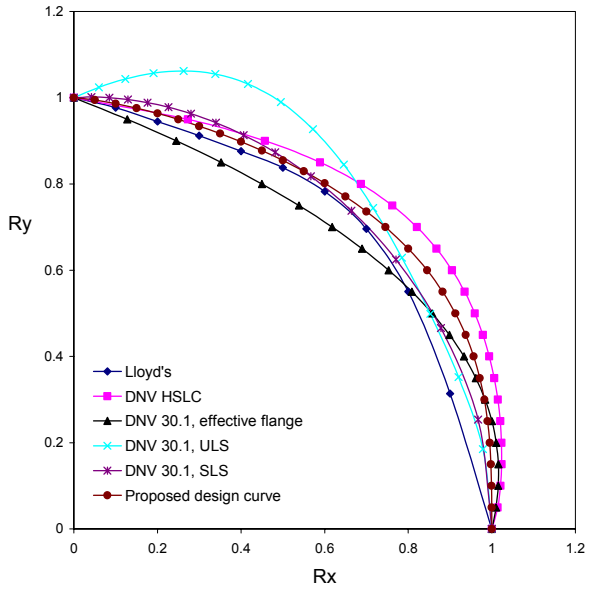

Figure 11.22 : Comparison of different code formulations for biaxial loading, aspect ratio, a/b=3, β=2.0

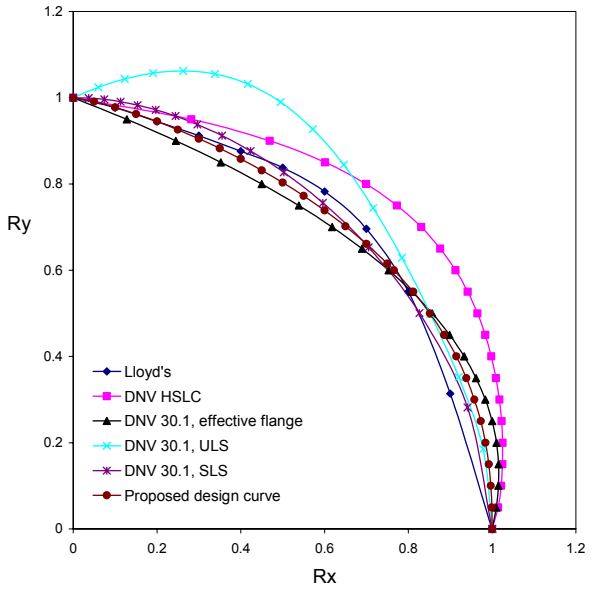

Figure 11.23 : Comparison of different code formulations for biaxial loading, aspect ratio, a/b=3, β=2.5

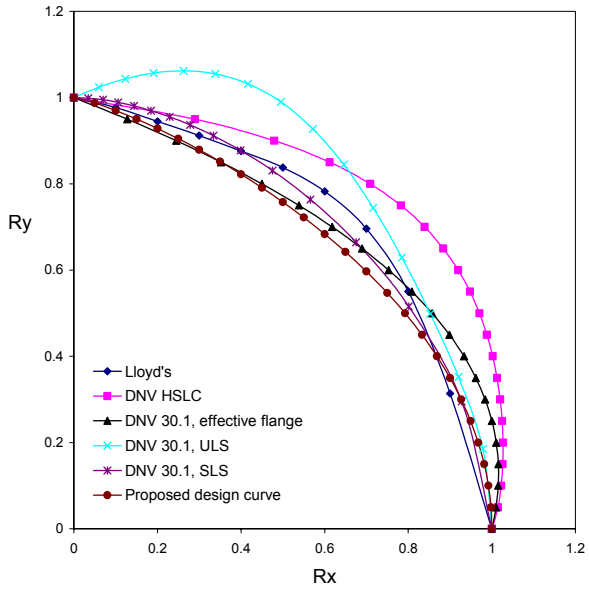

Figure 11.24 : Comparison of different code formulations for biaxial loading, aspect ratio, a/b=3, β=3.0

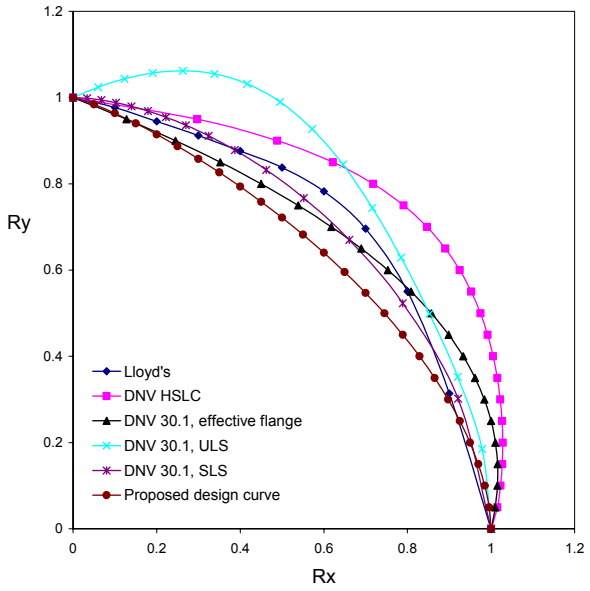

Figure 11.25 : Comparison of different code formulations for biaxial loading, aspect ratio, a/b=3, β=3.5

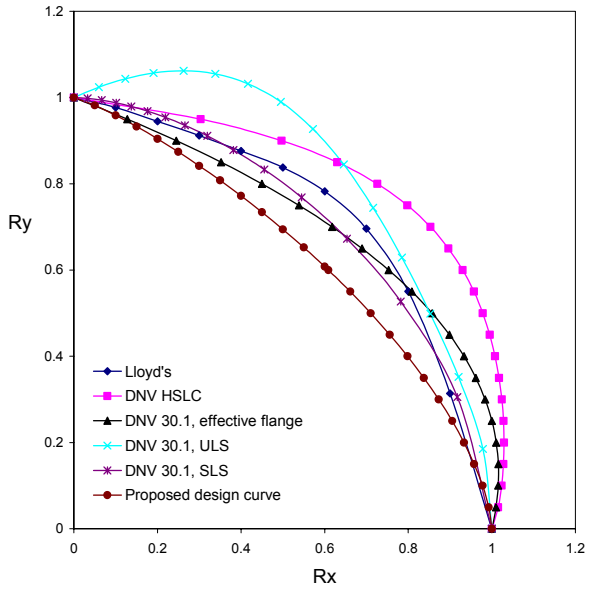

Figure 11.26 : Comparison of different code formulations for biaxial loading, aspect ratio, a/b=3, β=4.0

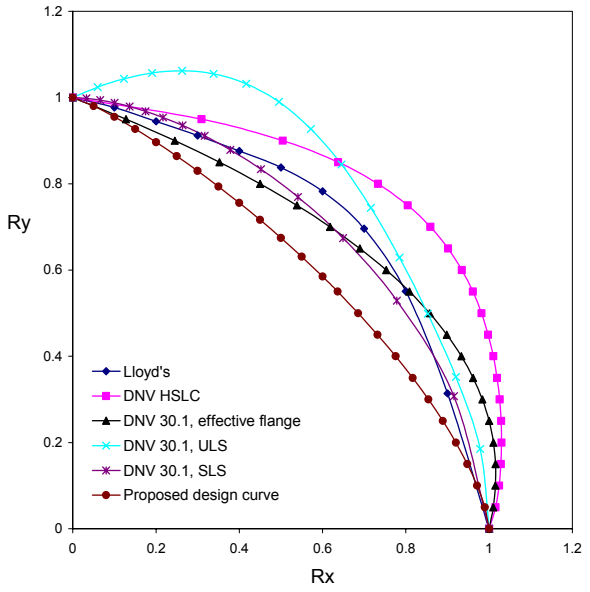

Figure 11.27 : Comparison of different code formulations for biaxial loading, aspect ratio, a/b=3, β=4.5

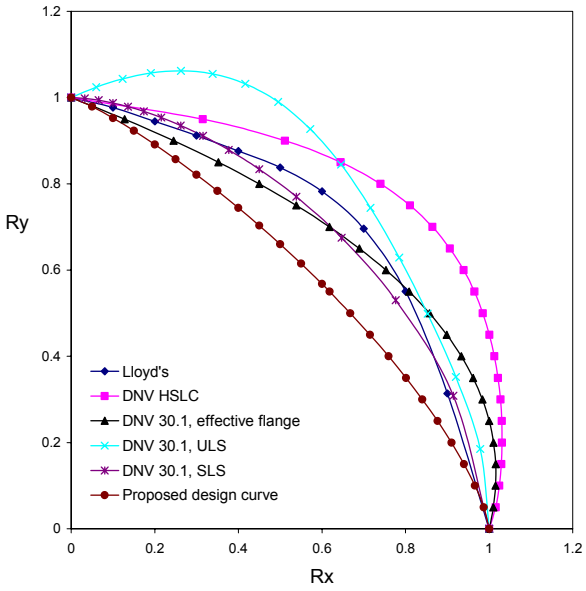

Figure 11.28 : Comparison of different code formulations for biaxial loading, aspect ratio, a/b=3, β=5.0

Because available code formulations and the proposed design curves are so different a more fundamental discussion is more informative than comparing too many details in the different plots.

The biaxial interaction curves proposed by the author show a clear and considerable slenderness dependency for all values of the aspect ratio, a/b. The higher the value of the slenderness, β, the stronger the interaction, and the differences between the interaction curves for the same absolute increase in the slenderness, β, decreases as the value of the slenderness, β, increases.

There is also a clear and considerable dependency of the aspect ratio. The higher the value of the aspect ratio, a/b, the weaker the interaction.

The biaxial interaction curves provided by Lloyd's show aspect ratio dependency with the same trend as the proposed design curves, but no slenderness dependency. Using the proposed interaction formula, which suggests linear interaction, will always be conservative, but the results are unacceptably conservative for low values of the slenderness, β.

The biaxial interaction curves given in DNV HSLC show both aspect ratio dependency and slenderness dependency. The aspect ratio dependency is introduced as a jump from plates with aspect ratios, a/b, less than 1.5 to plates with aspect ratios, a/b, equal to or larger than 1.5. The numerical analyses show that there should be a continuous transition. The biaxial interaction curves given in DNV HSLC also show a slenderness dependency, but the interaction curves for the lowest and the highest slenderness values are much more alike than the proposed design curves. It is also a mystery why the plates with aspect ratios equal to or larger than 1.5 have stronger interaction the more compact the plates become, but the explanation may be as simple as a printing error.

The DNV 30.1 effective flange formula for aspect ratio, a/b=1, is in good agreement with the proposed design formula. It has a little weaker interaction for plates with slenderness, β, equal to or lower than 3.0 and an almost identical fit for plates with higher values of the slenderness, β. The DNV 30.1 effective flange formula for plates with aspect ratio, a/b=3, on the other hand, is slenderness independent and is fundamentally different from the proposed design formula.

The DNV 30.1 SLS and ULS interaction formulas are both slenderness dependent and aspect ratio dependent, but they will only occasionally coincide with the proposed design curves.

For plates with aspect ratio, a/b=1, the DNV 30.1 ULS formula gives highly non-conservative interaction curves for all values of the slenderness, β, as compared to the proposed design formula. For aspect ratio, a/b=3, the DNV 30.1 ULS formula still gives non conservative-results, except for some compact plates with mainly axial loading.

If the aspect ratio, a/b=1, and the slenderness, β, is equal to or higher than 2.0, the DNV 30.1 SLS formula will give equal or conservative results as compared to the proposed design formula. For plates with aspect ratio, a/b=3, only plates with slenderness, β, equal to 1.5, 2.0 and 2.5 will have interaction curves that coincide or are conservative as compared to the proposed design interaction curves.

11.5 Pure Shear Loads

As for the axially loaded case, Lloyd's and DNV HSLC are based on linear elastic buckling with a Johnson Ostenfeld correction, and the shear stresses are not allowed to be higher than the reduced shear yield stresses in the heat affected zones. The 0.2 percent shear tensile proof stress is employed as the normalising stress.

Eurocode 9 also uses linear elastic buckling, but there is no Johnson Ostenfeld correction. There is, however, a yield check. Because the plates used for design formula development had heat affected zones extending around the entire perimeter, the yielding check simply requires that the shear stresses are not allowed to be higher than the reduced shear yield stresses in the heat affected zones.

The DNV 30.1 effective flange formulation has no equation determining the uniaxial shear stress capacity. There is only a correction formula for shear stresses acting together with axial stresses (see Chapter 11.6). The DNV 30.1 SLS and ULS equations presented in Chapter 11.2 also applies for pure shear loading. Because DNV 30.1 is a design code meant for steel, no information is provided as to handle the effect of heat affected zones.

For plates with large reduction in yield stress in the heat affected zones, and small values of β, the design curve proposed by the author utilises the material capacities in the heat affected zones so far beyond the 0.2 percent tensile proof stress that a maximum value of stress cut-off maybe should have been employed. No such cut-off is enforced in the comparisons that follow.

In Figures 11.29 and 11.30 the design curves given in DNV HSLC and Lloyd's and Eurocode 9 are compared with the proposed design curve. In Figure 11.29 the plates have no yield stress reduction in the heat affected zones, and in Figure 11.30 the plates have a 50%

reduction of yield stresses in the heat affected zones. The breadth of the heat affected zones is 25 mm. For convenience the stress corresponding to equal elastic and plastic strain is chosen to be equal to the 0.2 percent shear tensile proof stress. In Appendix 7 (Figures A7.28 - A7.33) all design codes, including the DNV 30.1 SLS and ULS formulations, are compared for different amount of reduction of yield stress in the heat affected zones.

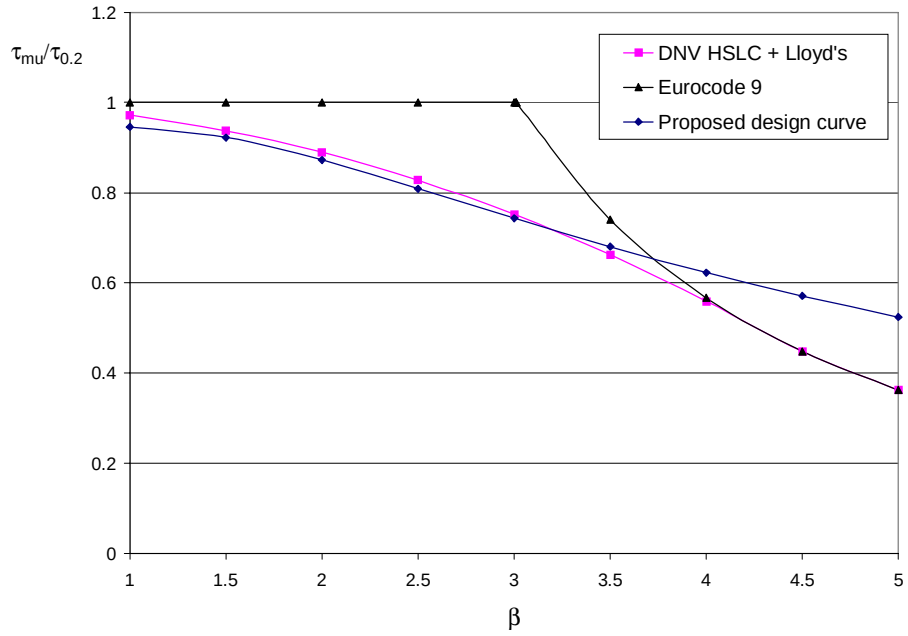

Figure 11.29 : Comparison of proposed design formula with different design codes for a non-heat treated alloy that have been welded, but without any reduction in yield strength due to welding. Aspect ratio, a/b=3.

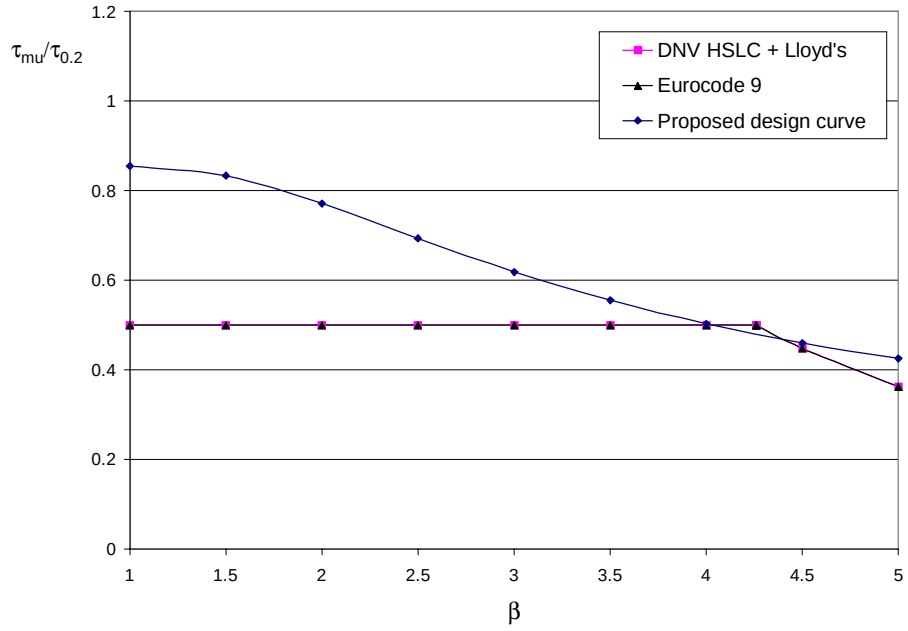

Figure 11.30 : Comparison of proposed design formula with different design codes for a heat treated alloy with heat affected zones along all edges. The breadth of the heat affected zones is 25 mm. The 0.2 percent tensile proof stress in the heat affected zones is half the value of the 0.2 percent tensile proof stress of the base material. Aspect ratio, a/b=3.

If linear elastic buckling with a Johnson Ostenfeld correction is employed, and shear stresses are not allowed to be higher than the reduced shear yield stresses in the heat affected zones (DNV HSLC and Lloyd's), the design values obtained will not show large non-conservatism as compared to design values given by the proposed design formula. The design values given by DNV HSLC ans Lloyd's can, on the other hand, be very conservative as compared to the proposed design curve. This occurs for compact plates with large reductions in yield stresses due to heat affected zones (see comments in previous paragraph).

Because Eurocode 9 does not have a Johnson Ostenfeld correction, compact plates with small or no reduction of yield stresses due to welding, may get non-conservative design values as compared to the proposed design curve.

The proposed design formula implies an increase in strength for slender plates as compared to the design codes employed for comparison. The reason for this is that the proposed design formula takes advantage of a tension field in one of the two diagonal directions. This tension field is created after first buckle has occurred (see also Chapter 3.2.4). Linear elastic buckling, used in Lloyd's, DNV HSLC and Eurocode 9, only predicts first buckle.

11.6 Axial Compression in Combination with Shear Loads

Only the shapes of the interaction curves are compared. The differences in the uniaxial capacities are discussed in their respective chapters (Chapters 11.2 and 11.5). As for plates loaded by pure shear loads, only plates with aspect ratio, a/b=3, are investigated.

If the shear stresses are less than half the uniaxial capacity, Eurocode 9 has no reduction in axial capacity due to the presence of shear stresses. For higher values of the shear stresses, the relationship between the axial capacity and shear capacity can be expressed as:

$$R_x = 1.6 - 1.2R_\tau \qquad 0.5 < R_\tau \leq 1 \qquad (11.10)$$

The biaxial formula given in Lloyd's takes account of both axial stresses, transverse stresses and shear stresses simultaneously. Assuming zero transverse stresses, and after some paraphrasing, the equation for the elastic shear capacity can be written:

$$\tau_E = \sigma_{Ex}\sqrt{\left(1-\frac{\sigma_{mx}}{\sigma_{Ex}}\right)\left(2-\frac{\sigma_{mx}}{\sigma_{Ex}}\right)} \qquad (11.11)$$

After the elastic shear capacity has been found, a Johnson Ostenfeld correction is employed if the elastic shear capacity is higher than half the shear yield stress.

The biaxial formula presented in DNV HSLC also treats axial stresses, transverse stresses and shear stresses simultaneously. Assuming zero transverse stresses the formula can be written:

$$R_x + R_\tau^2 = 1 \qquad (11.12)$$

The formula becomes identical to the Bathdorf and Stein (1947) proposal presented in Chapter 3.1.6.

DNV 30.1, effective flange formulation, uses plastic correction (see Chapter 3.2.5 for details).

$$R_x^2 + R_\tau^2 = 1 \tag{11.13}$$

The DNV 30.1 SLS and ULS interaction curves are also suitable for handling axial compression in combination with shear loads. The interaction curves taken from the different design codes are presented in Figures 11.31-11.36.

In Figure 11.37 the biaxial interaction curves from Eurocode 9, Lloyd,s, DNV HSLC and DNV 30.1 effective flange formulation are compared with the proposed design curve. The slenderness of the plates, β, is equal to 1.0. In Figure 11.38 the same design curves are compared for β=5.0. Curves also including the DNV 30.1 SLS and ULS formulations are given in Appendix 7. All the curves are for plates with aspect ratio, a/b=3.

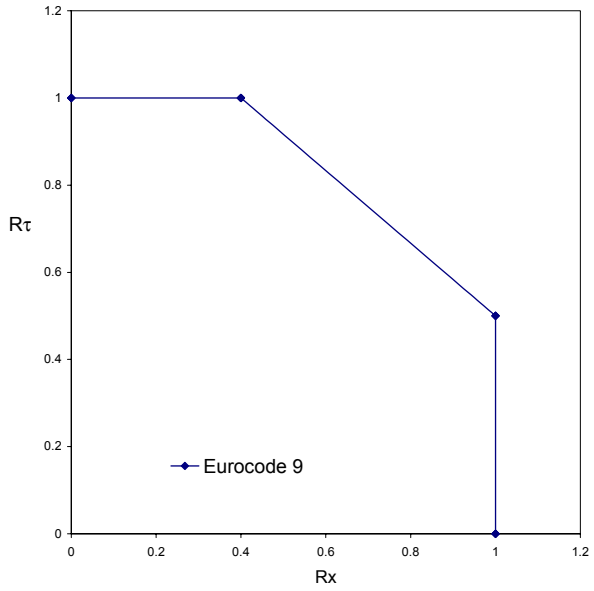

Figure 11.31 : Eurocode 9

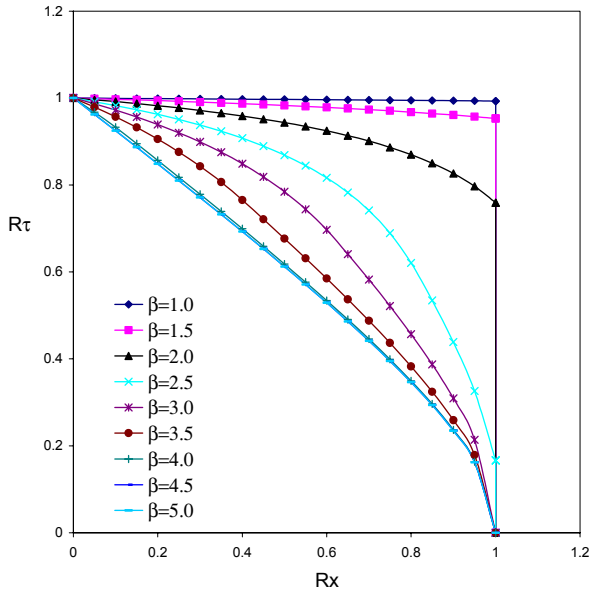

Figure 11.32 : Lloyd's

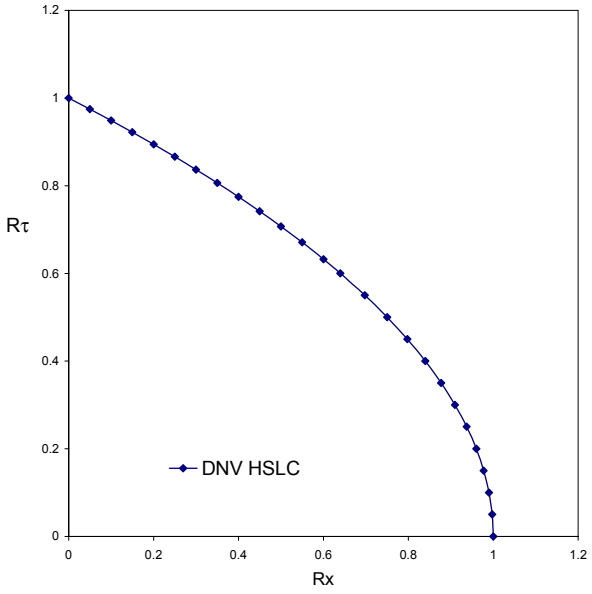

Figure 11.33 : DNV HSLC

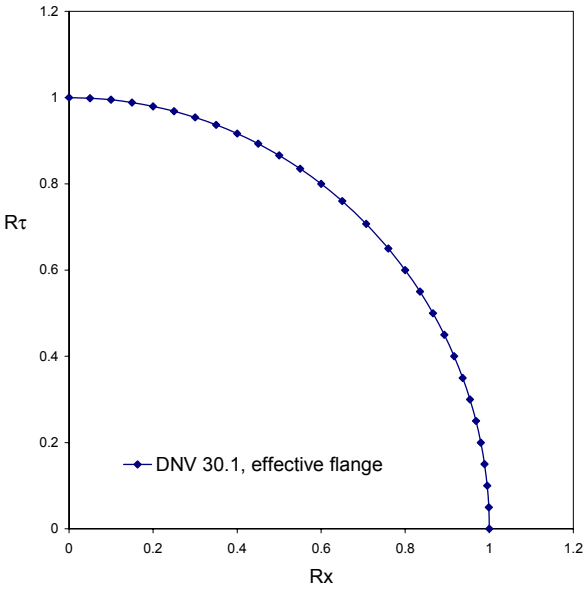

Figure 11.34 : DNV 30.1, effective flange formulation

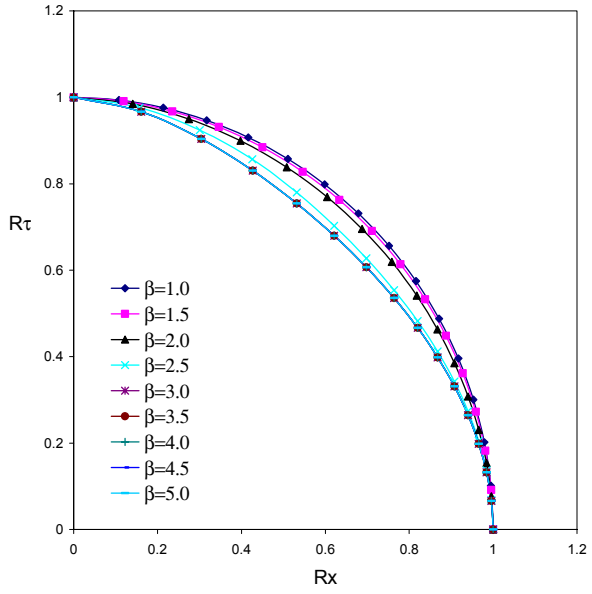

Figure 11.35 : DNV 30.1, ULS formulation

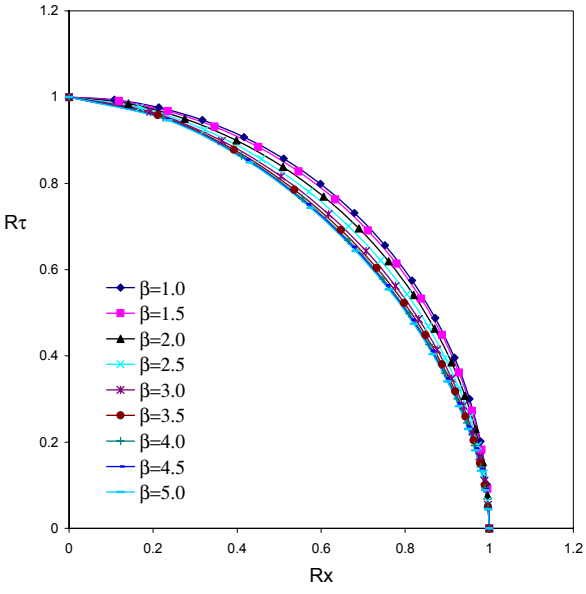

Figure 11.36 : DNV 30.1, SLS formulation

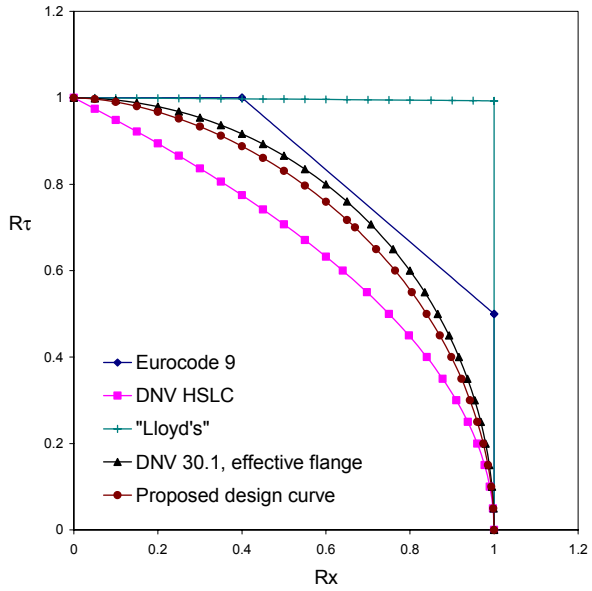

Figure 11.37 : Comparison of different design curves for β=1.0

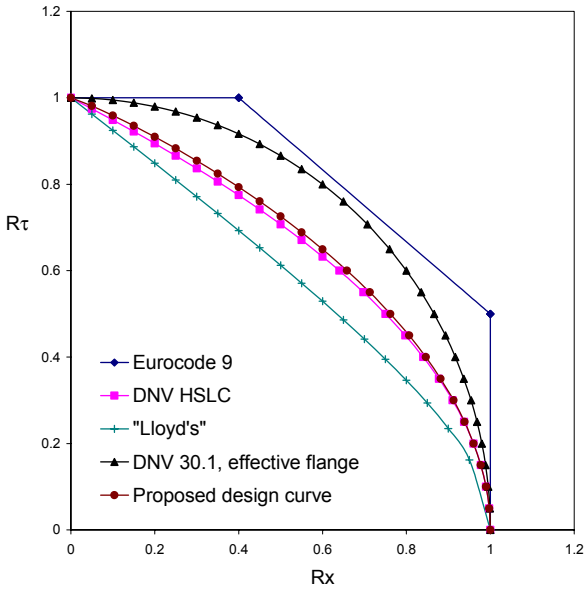

Figure 11.38 : Comparison of different design curves for β=5.0

I is observed that the proposed design curves exhibit some slenderness dependency, but it is not very significant. Eurocode 9, DNV HSLC and DNV 30.1 effective flange formulation do not have any slenderness dependency at all. The DNV 30.1 ULS and SLS formulations have a slenderness dependence that is in the same order of magnitude as the proposed design formula, and the formula employed in Lloyd's has a huge slenderness dependence, much larger than the proposed design formula.

The DNV 30.1 effective flange formulation uses plastic correction and take no buckling phenomena into consideration. This is believed to represent an upper bound for the biaxial curves and, as can be seen by studying Figure 11.37, will be in good accordance with the proposed interaction curves for extremely sturdy plates. As the slenderness grows larger, the additional reduction in strength due to buckling becomes larger and larger and the non-conservatism increases.

The interaction curve given in Eurocode 9 is above the plastic correction curve and is considered to be non-conservative.

The interaction curve presented in DNV HSLC is in close agreement with the proposed design curve for the largest value of the slenderness, β, considered. As the value of the slenderness decreases, the conservatism as compared to the proposed design formula increases. Equation 12.12 is, in other words, an excellent lower bound for the ultimate capacity of axially loaded plates in combination with shear loads.

The strong slenderness dependence expressed in Lloyd's make the interaction formula very non-conservative for sturdy plates, and fairly conservative for slender plates as compared to the proposed design formula.

Both the DNV 30.1 SLS and ULS inteaction curves have an appearance that is very similar to the shape of the proposed design curves. They allow slightly higher utilisation, and the differences are bigger for slender plates.

Chapter 12

Conclusions and Recommendations for Further Work

12.1 Conclusions

Based on a systematic study of the collapse behaviour of aluminium alloy plates carried out, design formulas for the ultimate capacity of aluminium plates have been proposed. The aluminium plates are assumed to be part of a marine structure. The support conditions, welding patterns and initial imperfections are chosen accordingly. The formulas take full advantage of non-linear material behaviour and non-linear geometric stiffness. The design formulas cover axial and transverse compression, pure shear loading, axial compression in combination with transverse compression as well as axial compression in combination with shear loading.

Using an element mesh with 24 rectangular elements of type S4R (ABAQUS, 1998, notation) over the breadth of the plates gives sufficient accuracy in the analyses.

Axially loaded plates with HAZ along loaded edges have lower ultimate capacity than plates with HAZ along unloaded (long) edges. The capacity of plates with HAZ along all edges is close to that for plates with HAZ along loaded edges.

Plates with HAZ along long edges only can be modelled to have a constant absolute reduction in axial ultimate capacity due to presence of HAZ. If the plates have HAZ along all edges or the extruded pattern of the heat affected zones, they will have the same percentage reduction in axial ultimate capacity.

The reduction in ultimate capacity can be modelled to vary linearly with the breadth of the HAZ, and the reduction in ultimate capacity can be modelled to vary linearly with the relationship between the 0.2 percent tensile proof stress in the heat affected zones and the 0.2 percent tensile proof stress of the base material.

Plates with no reduction in 0.2 percent tensile proof stress in the HAZ will have a reduction in ultimate capacities due to residual stresses only. The reduction in ultimate strength is approximately equal to the reduction in strength of plates with a 0.2 percent tensile proof stress in the HAZ which is 90 percent of that of the base material.

If the plates contain heat affected zones, the ultimate capacity of transversally loaded plates can be modelled as the sum of the strength of a square plate and a plate strip. Ultimate capacities of square plates and plate strips with relevant patterns of HAZ have to be employed.

The assumption that the ultimate capacity of transversally loaded aluminium plates can be found as the weighted sum of the capacities of a square plate and a plate strip holds for all the boundary conditions investigated, not only for plates with straight, simply supported edges.

The ultimate capacity of plate strips with HAZ along loaded edges will not be affected be the presence of the HAZ. If the plate strip has a heat affected zone in the middle of the plate strip, loss of capacity occurs due to the presence of the heat affected zone.

Biaxial interaction curves show a considerable slenderness dependence for all values of the aspect ratio, a/b, investigated. The biaxial interaction curves are only slightly affected by introduction of different patterns of heat affected zones.

Changing the aluminium alloy does not change the shape of the biaxial interaction curves.

If the biaxial interaction curves for plates with aspect ratios, a/b=1 and a/b=5, are used as basis for design, employing linear interaction for intermediate values of the aspect ratio, a/b, will be conservative.

Axially loaded plates with straight, clamped boundary conditions, and aspect ratios larger than one, are less influenced by introduction of heat affected zones than axially loaded plates with straight, simply supported boundary conditions or free, simply supported boundary conditions. For transversally loaded plates the situation is the opposite.

Plates with free, simply supported edges and straight, simply supported edges show the same percentage reductions in ultimate capacity for both axially and transversally loaded plates.

Axially loaded plates that consist of the base material only, have exact the same collapse capacity for all integer values of the aspect ratio, a/b. If heat affected zones are introduced, plates with aspect ratio, a/b=1, will have the lowest capacitiey.

Square plates with the extruded HAZ pattern show lower "transverse" capacity than plates with HAZ along all edges. This is in contrast to the "axially" loaded case in which the capacities are identical.

Because both the square plate capacity and the plate strip capacity for plates with the extruded HAZ pattern are lower than the square plate capacity and the plate strip capacity for plates with heat affected zones along all edges, transversally loaded plates with the extruded HAZ pattern will have lower ultimate capacities than transversally loaded plates with HAZ along all edges.

Compact plates are sensitive to variation of initial deflection amplitude. Very slender plates are only insignificantly affected by variations in the initial deflection amplitude.

Transversally loaded plates exhibit the lowest ultimate capacity when the fundamental linear elastic eigenmode is used as initial deflection pattern. This is the case both for plates consisting of the base material only and plates with HAZ along all edges. Axially loaded plates with HAZ along all edges also have the lowest ultimate capacity if the fundamental linear elastic eigenmode is used as the initial deflection pattern, but if the plates consist of the base material only, combining several eigenmodes will decrease the ultimate capacity for slender plates.

The stress corresponding to equal elastic and plastic strain is better suited as the normalising stress than the more commonly used 0.2 percent tensile proof stress. One design curve can be used to represent all the different aluminium alloys investigated.

By comparing the proposed design formula with the most commonly used design procedure, linear elastic buckling with Johnson Ostenfeld correction, show that axially loaded plates with no strength reduction in HAZ will have approximately coincident ultimate capacities for compact plates. For slender plates the proposed design formula suggests a huge increase in collapse capacity.

When the aluminium alloys have reductions in 0.2 percent tensile proof stresses due to welding, most marine design codes compare the mean average stresses with the 0.2 percent tensile proof stresses. They do not allow higher mean average stresses than the 0.2 percent tensile proof stresses in the HAZ. If the mean average stresses are lower than 0.2 percent tensile proof stresses, no corrections for HAZ will be performed. By doing so, most marine design codes allow lower mean axial stresses than the proposed design curve for compact plates, because the proposed design formula takes advantage of stress values beyond the proportional limit.

Even though the proposed design curve has considerable reductions in ultimate capacity due to HAZ for slender plates, the non-linear effects incorporated in the axial design formula results in much higher collapse capacities for slender plates than what is predicted by linear elastic buckling.

The proposed design formula for axial ultimate capacity give higher ultimate capacities for plates consisting of the base material than Eurocode 9, but it has larger reductions in ultimate capacity due to HAZ.

It can generally be said that linear elastic buckling with Johnson Ostenfeld correction over-predicts the collapse capacity for compact plates, and underestimate the collapse capacity for slender plates.

The biaxial interaction curves in the different design codes are very different, both regarding mode of expression and physical effects included and interpreted. Only the effective flange formulation in DNV classification note 30.1 for aspect ratio, a/b=1, has comparable structure and values as the proposed design formulas.

The proposed interaction curves for axial compression in combination with shear loading are located between the Hencky von Mises yielding correction curve and the elastic Bathdorf and Stein (1947) proposal. The interaction curve taken from Eurocode 9 shows weaker interaction than the Hencky von Mises yielding curve and is believed to be non-conservative.

12.2 Recommendations for Further Work

12.2.1 Laboratory Testing

One of the major findings in the numerical analyses is that HAZ along loaded edges of an axially loaded plate are more critical than HAZ along unloaded edges only. The loss of strength is more severe for compact plates.

The collapse mechanism is local failure at the loaded edges. If the plates are square (a/b=1) they will have HAZ along both loaded edges of the same collapse half wave and the loss in strength is at it's maximum level.

It would therefore be desirable to have a test series of compact square plates with HAZ along loaded edges and compare the results with test series of plates with HAZ along unloaded edges and test series of plates consisting of the base material only.

12.2.2 Altering the Location and the Breadth of the Longitudinal Weld in Extruded Panels

Plates with the extruded HAZ pattern loaded transversally, show poorer capacities than plates with HAZ along all edges. This is believed to be caused by the unfavourable location of the weld in the middle of the plates in longitudinal direction. It is located in the middle of the plates where the bending moments have their maximum level.

The weld in longitudinal direction does not have to be located in the middle of the plates, it can have any location along the plate breadth. It would be interesting to study the sensitivity to plate breadth location.

It is also interesting to study welding breadth variations for different locations of the longitudinal welds, although the results in Chapter 5.2.1.4 and Chapter 5.3.1.2 give good indications as what to expect.

12.2.3 Shear Ultimate Capacity for Other Aspect Ratios and Other Patterns of the Heat Affected Zones

The shear ultimate capacity design formula developed, only applies for aspect ratio, a/b=3. According to linear theory, the buckling capacity decreases as the aspect ratio, a/b, increases. This indicates that the developed formula also can be conservatively applied for aspect ratios, a/b, less than 3.0. Introducing non-linear material behaviour and non-linear geometric stiffness will in the author's opinion not alter these conclusions; if the plates consist of the base material only. Plates with smaller aspect ratios will experience stiffer support conditions, with the effect of increasing strength.

Introducing heat affected zones, on the other hand, complicates the picture. The more square the plates become, the larger the volume fracture of material with reduced material capacities. The increased susceptibility to yielding has to be weighted against the stiffer support conditions. At least limited investigations of plates with other aspect ratios have to be performed before the design formula can be used for other aspect ratios.

Plates with the extruded pattern of the heat affected zones have not been investigated for shear ultimate capacity. Doing so will complete the shear ultimate capacity design suggestions.

12.2.4 Cut-off Criteria

In the numerical analyses advantage has been taken of the whole stress-strain relationship of the materials. The materials have been modelled by the Ramberg Osgood law, but no criterion as to whether fracture occurs has been employed.

It is obvious that the local stresses can not be higher than the ultimate tensile strength of the material. This means that the local stress in the HAZ cannot be higher than the ultimate tensile strengths of the materials in the heat affected zones.

A stress check in all parts of the plates has not been performed, but if the mean average stresses become larger than the ultimate tensile stresses of the materials in the heat affected zones, such high stress levels cannot be allowed.

For most aluminium alloys, the ultimate tensile strength of the material in the annealed condition is higher than the stress corresponding to equal elastic and plastic strain in the heat treated or cold worked state, but not for all aluminium alloys. On the other hand, using the reduced 0.2 percent tensile proof stress as the cut-off criterion will be very conservative. The plates will collapse at substantially higher stress levels without any fracture occurring.

REFERENCES

ABAQUS Version 5.8 (1998). User's manual. Theory Manual. *Hibbit, Karlsson & Sorensen, Inc., USA.*

Amdahl, Jørgen, Langhelle, Nina Kristin and Lundberg, Steinar (2001). Aluminium Plated Structures at Elevated Temperatures. *Proceedings of OMAE 2001: 20th Offshore Mechanics and Arctic Engineering Conference, June 3-8, 2001, Rio De Janeiro, RJ, Brazil.*

Antoniou, A. C., Lavidas, M. and Karvounis G. (1984). On the Shape of Post-Welding Deformations of Plate Panels in Newly Built Ships. *Journal of Ship Research, Vol. 28, No. 1, March 1984, pp. 1-10.*

Antoniou A. C. (1980). On the Maximum Deflection of Plating in Newly Built Ships. *Journal of Ship Research, Vol. 24, No. 1, March 1980, pp. 31-39.*

Baehre, R. (1966). Comparison between structural behaviour of elastoplastic materials (in Swedish). *Arne Johnson Ingeniörsbyrå, Report No. 16, 1966.*

Batdorf, S. B. and Stein M. (1947). Critical Combinations of Shear and Direct Stress for Simply Supported Rectangular Flat Plates. *NACA Tech. Note 1223, 1947.*

Bayley, M. J. (1987). Materials for aluminium structures. *Proceedings of the International Conference on Steel and Aluminium Structures, Cardiff, UK, 8-10 July, 1987, Ed. R. Narayanan, Elsevier Applied Science.*

Bleich, F. (1952). Buckling Strength of Metal Structures. *McGraw-Hill, 1952.*

British Standards Institution (1991). British Standard 8118, Structural use of aluminium, Part 1, Code of practice for design. *British Standards Institution, ISBN 0 580 19209 1.*

Bruaseth, Sindre (2000). Closed section aluminium panel subjected to uniform transverse loading. *Norwegian University of Science and Technology, Faculty of Marine Technology, Department of Marine Structures.*

Caldwell, J. B. (1965). Ultimate Longitudinal Strength. *Trans. RINA, 107, 1965, p. 411.*

Carlsen, C. A. (1980). A parametric study of collapse of stiffened plates in compression. *The Structural Engineer 58B (2). 33-40.*

Carlsen, C. A. and Czujko J. (1979). The specification of post-welding distortion tolerances for stiffened plates in compression. Discussion. *The Structural Engineer/Volume 57A/No. 10/October 1979.*

Carlsen, C. A. and Czujko J. (1978). The specification of post-welding distortion tolerances for stiffened plates in compression. *The Structural Engineer 56A(5), pp. 133-141.*

Clarke, John D. (1987). Buckling of Aluminium Alloy Stiffened Plate Ship Structure. *Proc. Int. Conf. on Steel and Aluminium Structures, Cardiff, July 1987. Admiralty Research Establishment, Dunfermline, UK.*

Clarke, J. D. and Swan, J. W. (1985). Interframe Buckling of Aluminium Alloy Stiffened Plating. *Report AMTE(S) R 85104. Admiralty Research Establishment, Dunfermline, UK.*

Crisfield, M. A. (1991). Non-linear Finite Element Analysis of Solids and Structures. *John Wiley & Sons Ltd. ISBN 0 471 92956 5 (v. 1).*

Czujko, J. and Kmiecik M. (1975). Post welding distortions of ship shell plating. *Technical University of Szciencin, Ship Research Institute, Rep. No. 4-S, 1975.*

Dalåsen, Kari (1998). Capacity of Aluminium Plate Fields with Open Stiffeners (in Norwegian). *M. Sc. Thesis. Norwegian University of Science and Technology, Faculty of Civil and Environmental Engineering, Department of Structural Engineering.*

Det Norske Veritas Classification AS (1996). Rules for Classification of High Speed and Light Craft, Hull Structural Design, Aluminium Alloy. *Det Norske Veritas.*

Det Norske Veritas Classification AS (1995). Classification Notes No. 30.1, Buckling Strength Analysis. *Det Norske Veritas.*

Dwight, John (1999). Aluminium Design and Construction. E & FN SPON (ISBN 0 419 15710 7).

Dowling, P. J., Harding J. E. and Frieze P. A. (1976). Steel Plated Structures. *Crosby Lockwood Staples, London.*

European Committee for Standardization (1998). Eurocode 9 : Design of aluminium structures - Part 1-1: General rules - General rules and rules for buildings. *European Committee for Standardization, ENV 1999-1-1:1998 E.*

Faulkner, D. (1975). A Review of Effective Plating for Use in the Analysis of Stiffened Plating in Bending and Compression. *Journal of Ship Research 19 (1), March 1975, pp. 1-17.*

Felippa, Carlos A. (1996). Nonlinear Finite Element Methods. *Department of Aerospace Engineering Sciences and Center for Aerospace Structures, University of Colorado, Boulder, Colorado 80309-0429, USA. Report No. CU-CSSC-96-16.*

Fujikubo, Masahiko, Yao, Tetsuya and Varghese, Balu (1997). Buckling and Ultimate Strength of Plates Subjected to Combined Loads. *Proceedings of the Seventh International Offshore and Polar Engineering Conference, Honolulu, USA, May 25-30, 1997.*

Fukumoto, Y. and Itoh Y. (1984). Basic Compressive Strength of Steel Plates From Test Data. *Proceedings of JSCE No. 344/I-1 (Structural Eng./Earthquake Eng.), April 1984.*

Fukumoto, Y., Usami, T. and Itoh, Y. (1983). A Numerical Data-Base Approach to the Ultimate Compressive Strength of Unstiffened Plates. *Stability of metal structures, Paris, 16-17 nov. 1983, pp. 275-283.*

Hopperstad, O. S., Langseth, M. and Hanssen, L. (1997). Ultimate Compressive Strength of Plate Elements in Aluminium: Correlation of Finite Element Analyses and Tests. *Thin-Walled Structures Vol.29, Nos. 1-4, pp. 31-46.*

Hopperstad, O. S. and Langseth, M. (1994). Inelastic Buckling of Simply Supported Aluminium Plates: Comparison of Numerical and Experimental Results (in Norwegian). *Institute Report, Norwegian University of Science and Technology, Faculty of Civil and Environmental Engineering, Department of Structural Engineering.*

Hughes, Owen F. (1983). Ship Structural Design. *John Wiley & Sons, Inc., ISBN 0-471-03241-7.*

Kmiecik, M., Jastrzebski, T. and Kuzniar J. (1995). Statistics of Ship Plating Distortions. *Marine Structures 8, 1995, pp. 119-132.*

Kissel, J. R. and Ferry, L. F. (1995). Aluminium Structures. *John Wiley & Sons, Inc., New York.*

Kristensen, Odd Halvdan Holt and Moan, Torgeir (2000). Effect of HAZ Properties on the Ultimate Axial Strength of Plates Made of Different Aluminium Alloys. *Paper submitted to the seminar "Buckling and Ultimate Strength of Ship Structures" taking place at Det Norske Veritas, Høvik, Norway.*

Kristensen, Odd Halvdan Holt and Moan, Torgeir (1999). Ultimate Strength of Aluminium Plates under Biaxial Loading. Fifth International Conference on Fast Sea Transportation. *The Society of Naval Architects and Marine Engineers.*

Kristensen, Odd Halvdan Holt (1999). Ultimate Strength of Aluminium Plates Under Biaxial Loading. *NTNU Report, Norwegian University of Science and Technology, Faculty of Marine Technology, Department of Marine Structures. Report no. MK/R-139/Rev.1.*

Kristensen, Odd Halvdan Holt, Witsø, Stig Arne and Moan, Torgeir (1998). Ultimate Strength of Aluminium Plates. *NTNU Report, Norwegian University of Science and Technology, Faculty of Marine Technology, Department of Marine Structures. Report no. MK/R-134/Rev.1.*

Kristensen, Odd Halvdan Holt (1997). Strength of Plate Elements with Residual Stresses and Soft Zones. *Report no. R-41-97, Norwegian University of Science and Technology, Faculty of Civil and Environmental Engineering, Department of Structural Engineering.*

Langseth, M., Hopperstad, O. S. and Hanssen L. (1998). Buckling of Aluminium Plates. *Internal note, Norwegian University of Science and Technology, Faculty of Civil and Environmental Engineering, Department of Structural Engineering. Later published at DNV Seminar: Buckling and Ultimate Strength of Ship Structures, 20 September, 2000, Høvik, Norway.*

Little, G. H. (1981). Collapse Behaviour of Aluminium Plates. *International Journal of Mechanical Sciences, 24(1), pp. 37-45.*

Lloyd's Register of Shipping (1996). Rules and Regulations for the Classification of Special Service Craft, Volume 5, Part 7, Hull Construction in Aluminium. *Lloyd's Register of Shipping.*

Marsh, Cedric (1998). Design Method for Buckling Failure of Plate Elements. *Journal of Structural Engineering, July 1998, pp. 850-854.*

Mazzolani, Federico M. (1995). Aluminium Alloy Structures. *E & FN SPON, ISBN 0 419 17770 1.*

Mazzolani, Federico M. (1974). Proposal to classify the aluminium alloy on the basis of the mechanical behaviour. *ECCS Committee 16, Doc. 16-74-2, 1974.*

Mazzolani, Federico M. (1972). Characterisation of the σ-ε law and buckling of aluminium columns (in Italien). *Costr. Metall., 1972, No. 3.*

Moan Torgeir, Kristensen, Odd Halvdan Holt and Zha, Yufeng (1999). Ultimate Strength of Aluminium Panel Structures. *NTNU Report, Norwegian University of Science and Technology, Faculty of Marine Technology, Department of Marine Structures. Report no. MK/R-140.*

Mofflin, D. S. and Dwight, J. B. (1984). Buckling of Aluminium Plates in Compression, in Behaviour of Thin-Walled Structures (eds J. Rhodes and J. Spence). *Elsevier Applied Science, London and New York.*

Mofflin, David Shane (1983). Plate Buckling in Steel and Aluminium. Dissertation submitted to the University of Cambridge for the Degree of Doctor of Philosophy. *University Library Cambridge.*

Paik, J. K. and Pedersen, P. T. (1996). A simplified method for predicting ultimate compressive strength of ship panels. *Int. Shipbuild. Progr., Vol. 43, No. 434, 1996, pp. 139-157.*

Ramberg, W. and Osgood W. R. (1943). Description of stress-strain curves by three parameters. *NACA Techn. No. 902, 1943.*

Sharp, M. (1993). Behaviour and Design of Aluminium Structures. *MacGraw-Hill, New York, 1993.*

Soares, C. Guedes (1988). Design Equation for the Compressive Strength of Unstiffened Plate Elements with Initial Imperfections. *J. Construct. Steel Research 9 (1988) pp. 287-310.*

Soares, C. Guedes and Kmiecik, M. (1993). Simulation of the Ultimate Compressive Strength of Unstiffened Rectangular Plates. *Marine Structures 6 (1993) pp. 553-569.*

Soares, C. Guedes and Gordo J. M. (1996a). Collapse Strength of Rectangular Plates under Transverse Compression. *J. Construct. Steel Res. Vol. 36, No. 3, pp. 215-234, 1996.*

Soares, C. Guedes and Gordo J. M. (1996b). Compressive Strength of Rectangular Plates Under Biaxial Load and Lateral Pressure. *Thin-Walled Structures 24 (1996) pp. 231-259.*

Steinhardt, O. (1971). Aluminium constructions in civil engineering (in Deutsch). *Aluminium, 47, 1971.*

Syvertsen, Kåre (1992). Plate Theory (in Norwegian). *Institute teaching compendium, Norwegian University of Science and Technology, Faculty of Marine Technology, Department of Marine Structures.*

Tansøy, Renate (1998). Column Lab Tests of Aluminium Profiles with Closed Stiffeners (in Norwegian). *Project Thesis. Norwegian University of Science and Technology, Faculty of Civil and Environmental Engineering, Department of Structural Engineering.*

Teixeira, A. P. and Soares, C. Guedes (2001). Strength of compressed rectangular plates subjected to lateral pressure. *Journal of Constructional Steel Research 57 (2001) pp. 491-516.*

Timoshenko, Stephen P. and Gere, James M. (1961). Theory of Elastic Stability. *McGraw-Hill Book Company, Inc.*

Tveiten, Bård Wathne (1999). Fatigue Assessment of Welded Aluminium Ship Details. *Dr.ing. thesis, Norwegian University of Science and Technology, Faculty of Marine Technology, Department of Marine Structures. ISBN 82-471-0417-2.*

Valen, Wenche (1998). Plate Fields in Aluminium with Closed Stiffeners (in Norwegian). *M. Sc. Thesis. Norwegian University of Science and Technology, Faculty of Civil and Environmental Engineering, Department of Structural Engineering.*

Valsgård, Sverre (1980). Numerical Design Prediction of the Capacity of Plates in Biaxial In-Plane Compression. *Computers & Structures Vol. 12, pp. 729-739. Pergamon Press Ltd., 1980. Printed in Great Britain.*

Valsgård, Sverre (1979). Technical Report, Det Norske Veritas, Research Division, Ultimate Capacity of Plates in Biaxial In-Plane Compression. *Det Norske Veritas, Report no. 79-0104.*

Wang, Xiaozhi and Moan, Torgeir (1997). Ultimate Strength Analysis of Stiffened Panels in Ships Subjected to Biaxial and Lateral Loading. *International Journal of Offshore and Polar Engineering Vol. 7, No. 1, March 1997 (ISSN 1053-5381).*

Yao, T., Nikolov, P. I. and Miyagawa Y. (1991). Influences of Welding Imperfections on Stiffness of Rectangular Plates Under Thrust. *L. Karlsson, L.-E. Lindgren, M. Jonsson (Eds.), Mechanical Effects of Welding, IUTAM Symposium, Luleå/Sweden. 1991.*

Zha, Yufeng and Moan, Torgeir (2001a). Experimental and Numerical Prediction of Collapse of Flatbar Stiffeners in Aluminium Panels. *ASCE Structural Division, to appear.*

Zha, Yufeng and Moan, Torgeir (2001b). Ultimate Strength of Stiffened Aluminium Panels with Predominantly Torsional Failure Modes. *Journal of Thin Walled Structures, to appear.*

Aalberg Arne, Langseth, Magnus and Larsen, P. K. (2000). Stiffened Aluminium Panels Subjected to Axial Force. *Extract of paper submitted to Thin-Walled Structures. DNV Seminar: Buckling and Ultimate Strength of Ship Structures, 20 September, 2000, Høvik, Norway.*

Aalberg Arne, Langseth, Magnus and Larsen, P. K. (1999a). Experimental Investigation of a Stiffened Aluminium Deck System. *A sub-report to the Aluminium in Ships - research programme. Norwegian University of Science and Technology, Faculty of Civil and Environmental Engineering, Department of Structural Engineering.*

Aalberg Arne, Langseth, Magnus and Larsen, P. K. (1999b). Stiffened Aluminium Deck System - Numerical Simulation of Experiment. *A sub-report to the Aluminium in Ships - research programme. Norwegian University of Science and Technology, Faculty of Civil and Environmental Engineering, Department of Structural Engineering.*

Aalberg, A., Langseth, M., Hopperstad, O. S. and Malo K. A. (1998). Ultimate Strength of Stiffened Aluminium Plates. *International Conference on Thin-Walled Structures, Singapore, 1998.*

Appendix 1

Convergence Test Details

A1.1 Analyses Results

Table A1.1 : Buckling capacities, axial loading, base material properties only

β	1728 elements	6912 elements	27648 Elements
1.0	303.1	303.0	303.0
1.5	266.6	266.4	266.4
2.0	224.1	223.9	223.8
2.5	196.6	196.4	196.4
3.0	182.5	182.4	182.4
3.5	174.5	173.4	173.1
4.0	160.9	159.5	159.2
4.5	148.3	146.8	146.5
5.0	136.9	135.3	134.9

Table A1.2 : Buckling capacities, axial loading, soft zones and residual stresses included

β	1728 elements	6912 elements	27648 Elements
1.0	237.7	231.8	229.1
1.5	197.7	195.2	194.4
2.0	174.9	172.7	172.1
2.5	155.0	152.5	151.9
3.0	140.8	138.3	137.9
3.5	129.1	126.7	126.1
4.0	118.0	115.8	115.1
4.5	108.4	106.2	105.7
5.0	99.56	97.32	96.92

Table A1.3 : Buckling capacities, transverse loading, base material properties only

β	1728 elements	6912 elements	27648 Elements
1.0	209.8	209.6	209.6
1.5	144.2	144.0	144.0
2.0	109.0	108.9	108.9
2.5	89.18	89.08	89.05
3.0	77.52	77.43	77.41
3.5	70.45	70.38	70.37
4.0	65.08	64.44	64.30
4.5	58.32	57.80	57.68
5.0	52.88	52.32	52.20

Table A1.4 : Buckling capacities, transverse loading, soft zones and residual stresses included

β	1728 elements	6912 elements	27648 Elements
1.0	183.9	183.4	183.3
1.5	126.5	126.3	126.2
2.0	93.74	93.49	93.45
2.5	75.43	75.06	74.98
3.0	63.47	62.89	62.75
3.5	54.49	53.81	53.66
4.0	47.36	46.70	46.57
4.5	41.94	41.32	41.17
5.0	37.47	36.88	36.73

Appendix 2

Details Concerning Residual Stresses versus Soft Zones

A2.1 Residual Stresses Only

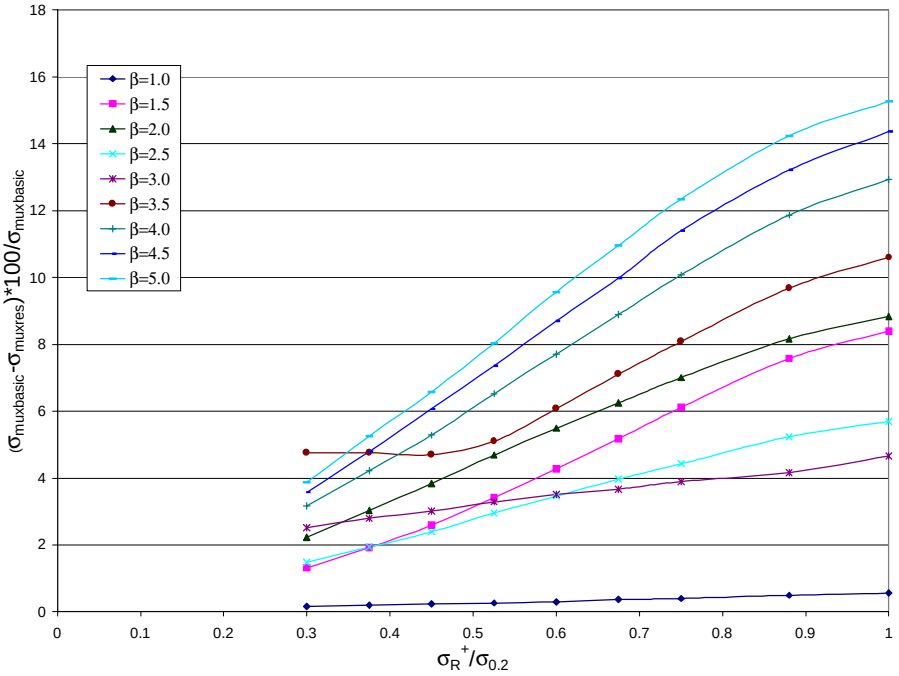

Figure A2.1 : Percentage reduction in strength caused by residual stresses only

A2.2 Soft Zones Only

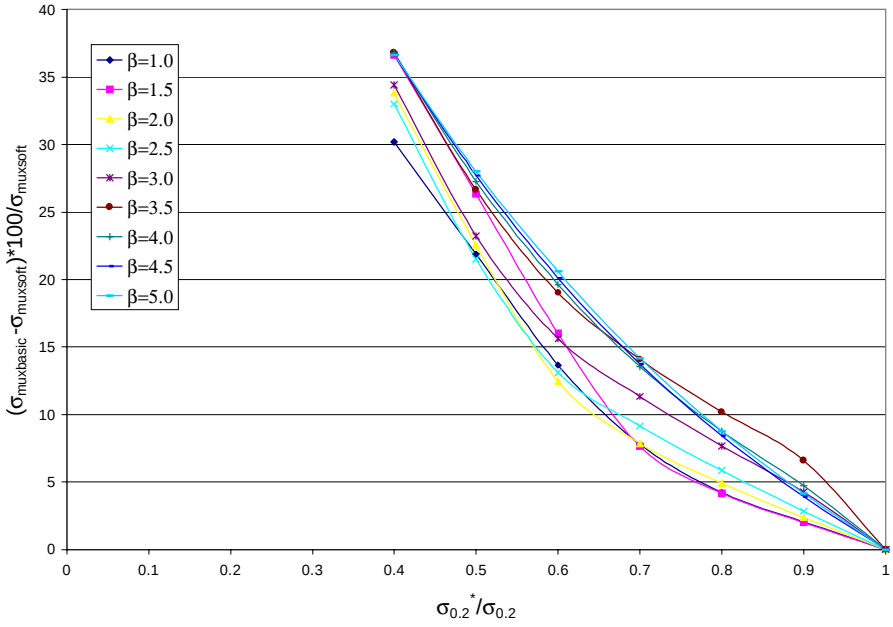

Figure A2.2 : Percentage reduction in strength caused by soft zones only

A2.3 Combined Effect of Residual Stresses and Soft Zones

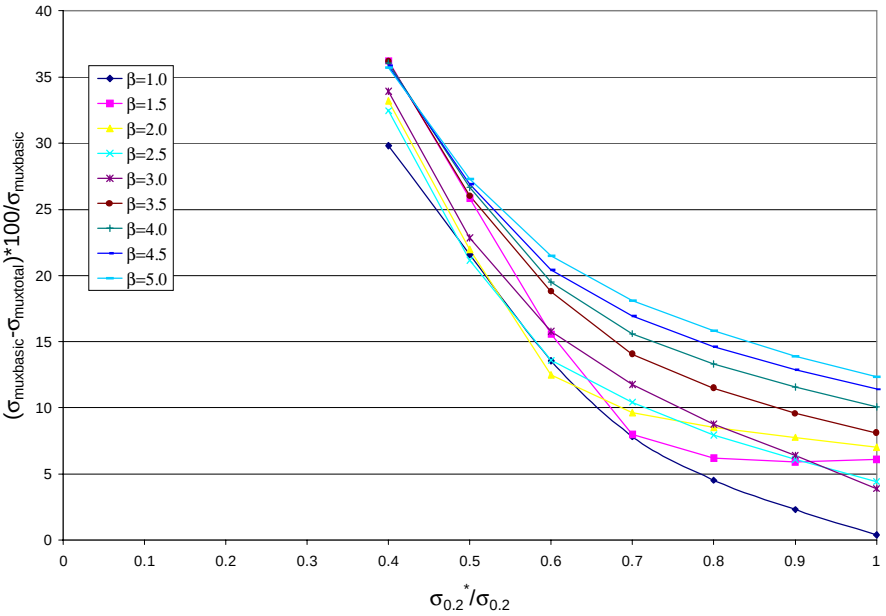

Figure A2.3 : Percentage reduction in strength caused by the combined effect of residual stresses and soft zones

Appendix 3

Details Concerning Alteration of Initial Deflection Amplitude

A3.1 Axial Compression

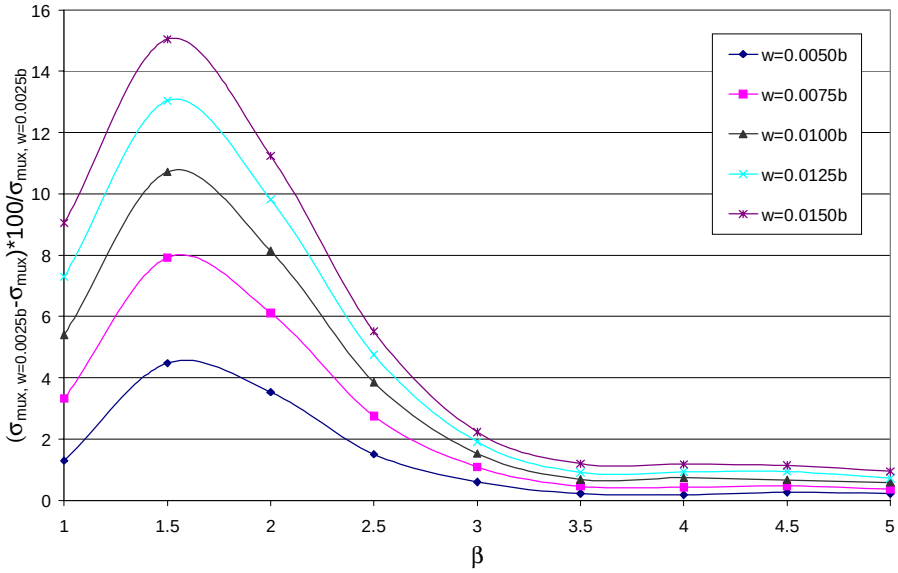

Figure A3.1 : Percentage reduction in strength as compared to analyses with the smallest maximum value of the initial out of plane deflection, w. The plates have no heat affected zones.

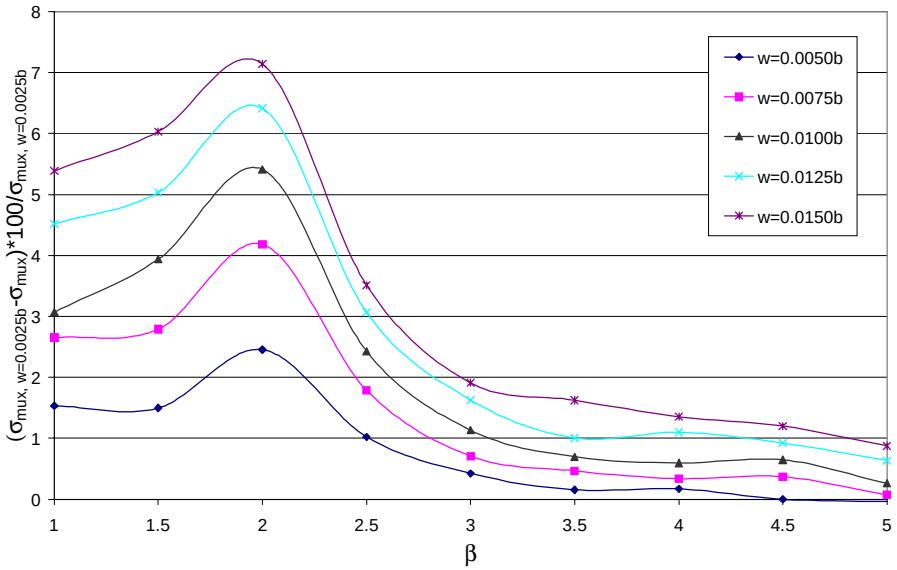

Figure A3.2 : Percentage reduction in strength as compared to analyses with the smallest maximum value of the initial out of plane deflection, w. The plates have heat affected zones along all edges.

A3.2 Transverse Compression

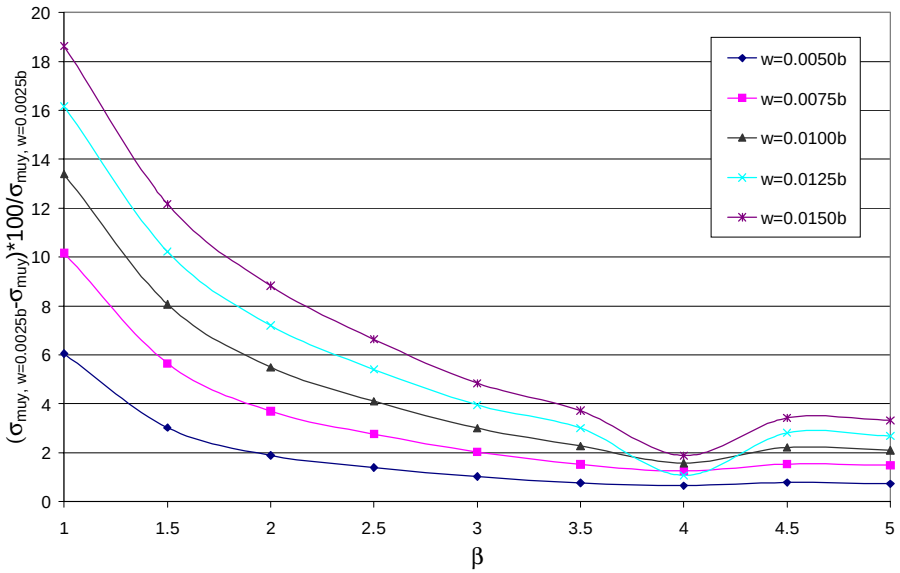

Figure A3.3 : Percentage reduction in strength as compared to analyses with the smallest maximum value of the initial out of plane deflection, w. The plates have no heat affected zones.

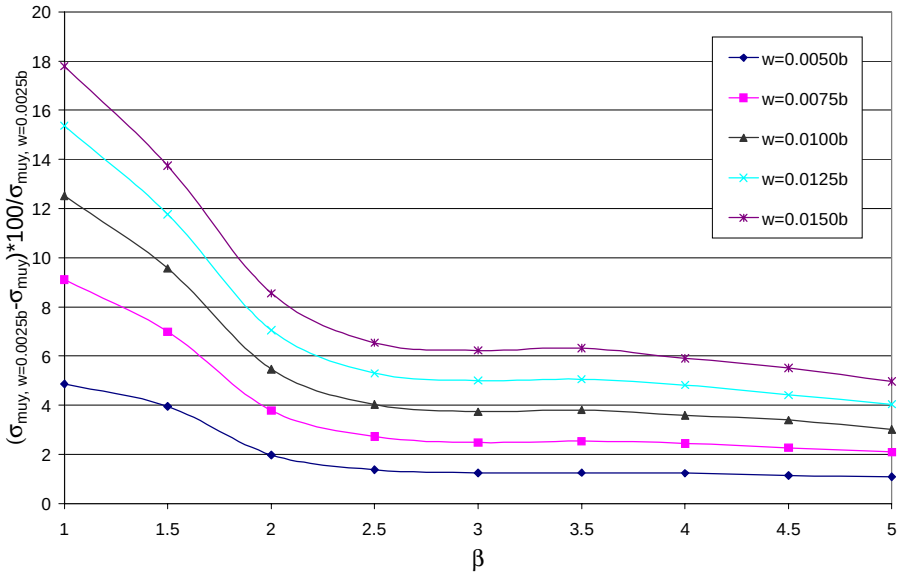

Figure A3.4 : Percentage reduction in strength as compared to analyses with the smallest maximum value of the initial out of plane deflection, w. The plates have heat affected zones along all edges.

Appendix 4

Details Concerning Change of Initial Deflection Pattern

A4.1 Axial Compression

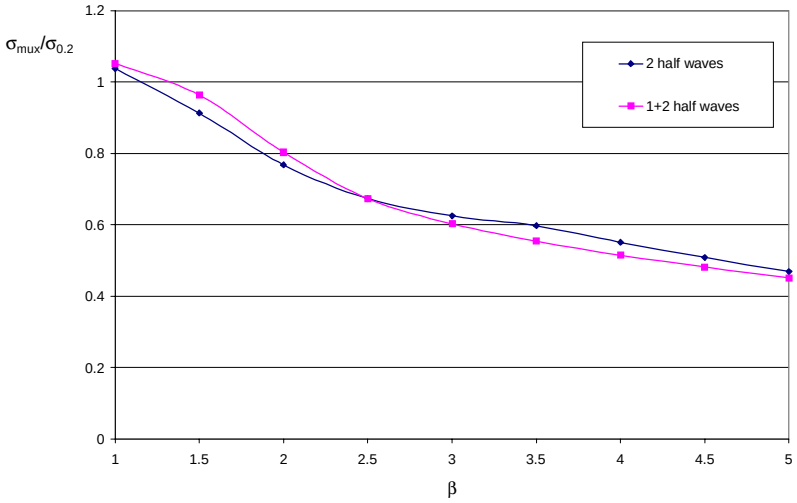

Figure A4.1 : Axial buckling capacity for different initial deflection patterns. The aspect ratio, a/b=2. The plates consist of the base material only.

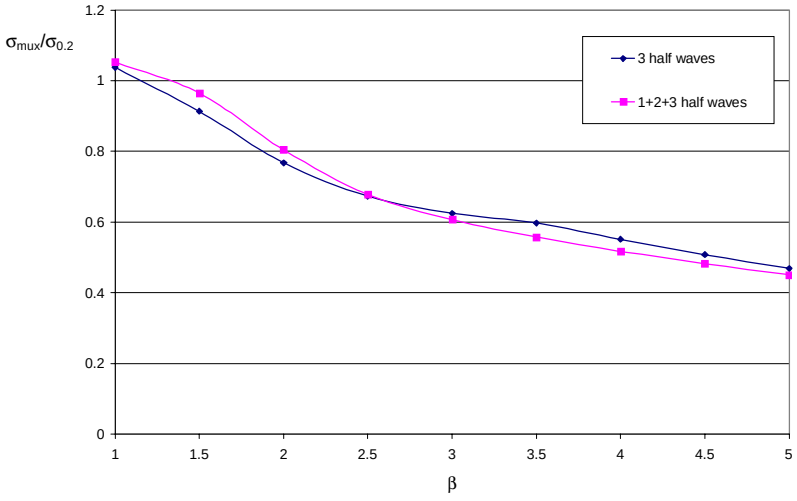

Figure A4.2 : Axial buckling capacity for different initial deflection patterns. The aspect ratio, a/b=3. The plates consist of the base material only.

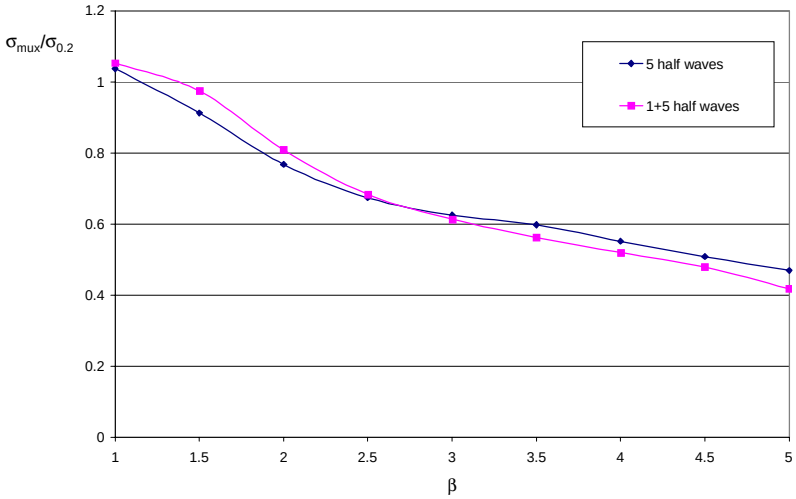

Figure A4.3 : Axial buckling capacity for different initial deflection patterns. The aspect ratio, a/b=5. The plates consist of the base material only.

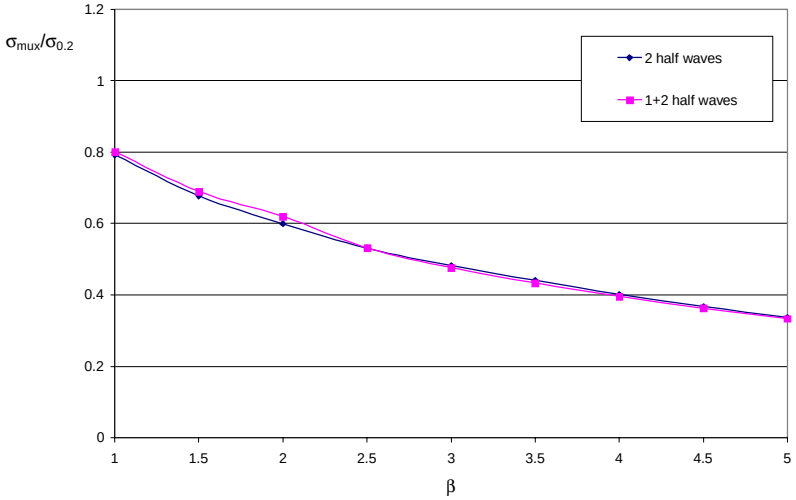

Figure A4.4 : Axial buckling capacity for different initial deflection patterns. The aspect ratio, a/b=2. The plates have heat affected zones along all edges.

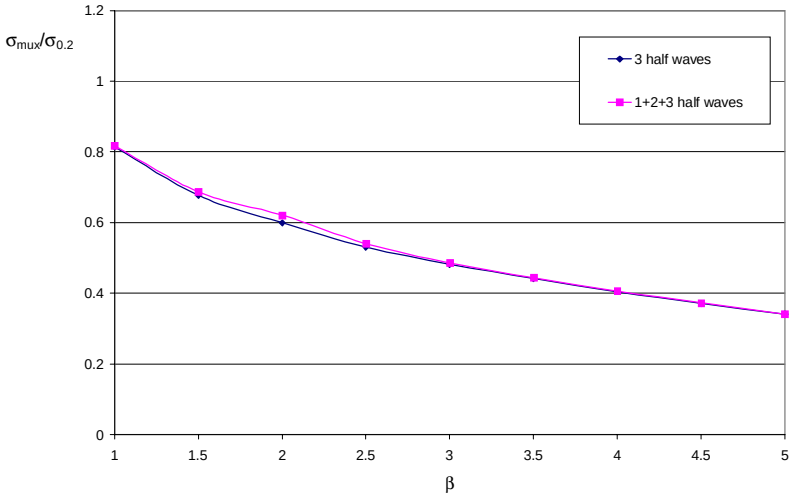

Figure A4.5 : Axial buckling capacity for different initial deflection patterns. The aspect ratio, a/b=3. The plates have heat affected zones along all edges.

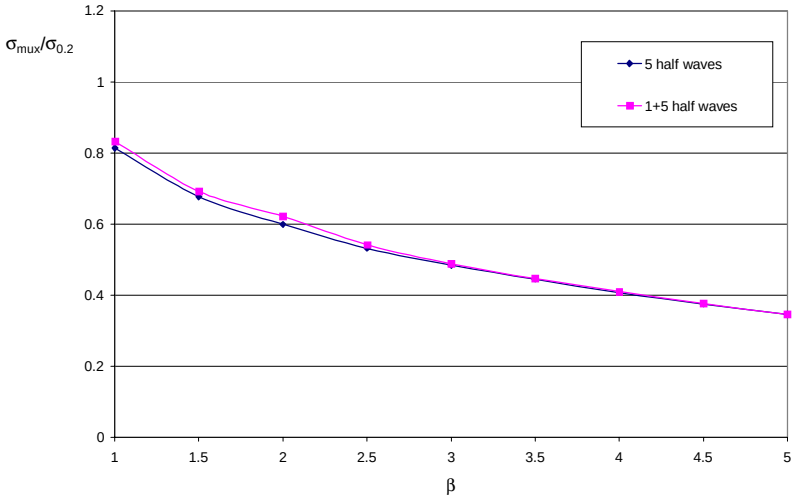

Figure A4.6 : Axial buckling capacity for different initial deflection patterns. The aspect ratio, a/b=5. The plates have heat affected zones along all edges.

A4.2 Transverse Compression

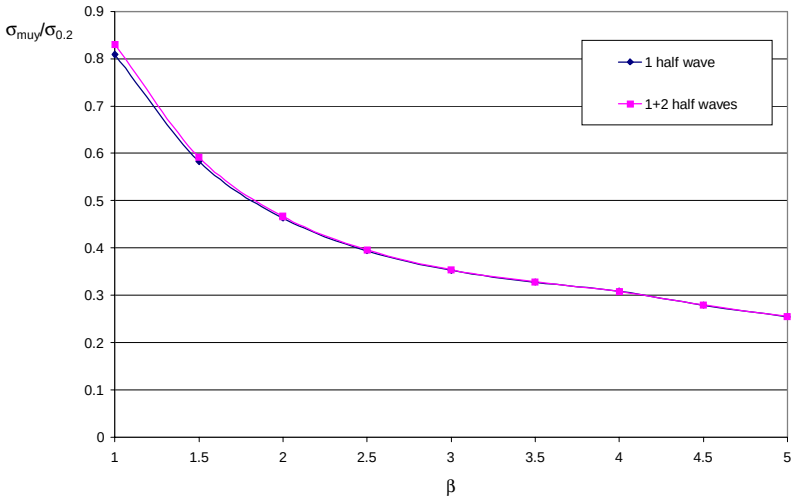

Figure A4.7 : Transverse buckling capacity for different initial deflection patterns. The aspect ratio, a/b=2. The plates consist of the base material only.

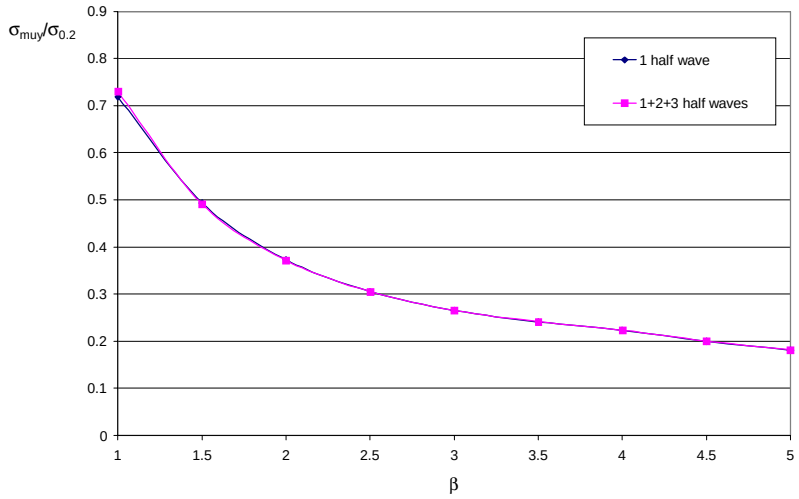

Figure A4.8 : Transverse buckling capacity for different initial deflection patterns. The aspect ratio, a/b=3. The plates consist of the base material only.

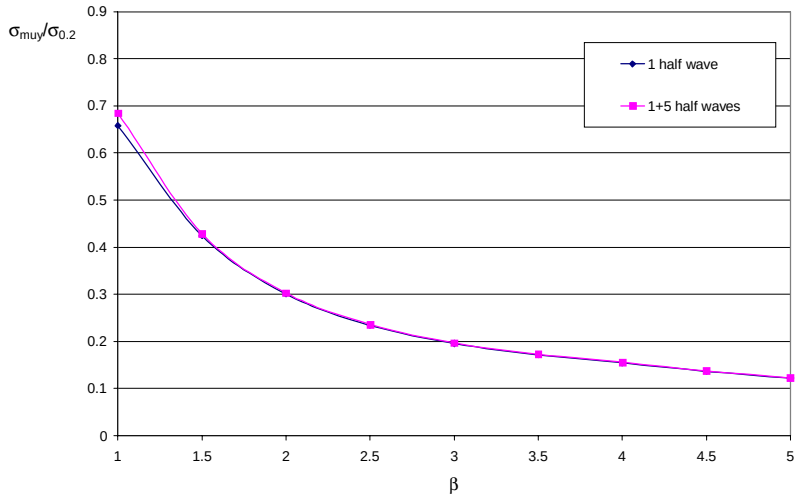

Figure A4.9 : Transverse buckling capacity for different initial deflection patterns. The aspect ratio, a/b=5. The plates consist of the base material only.

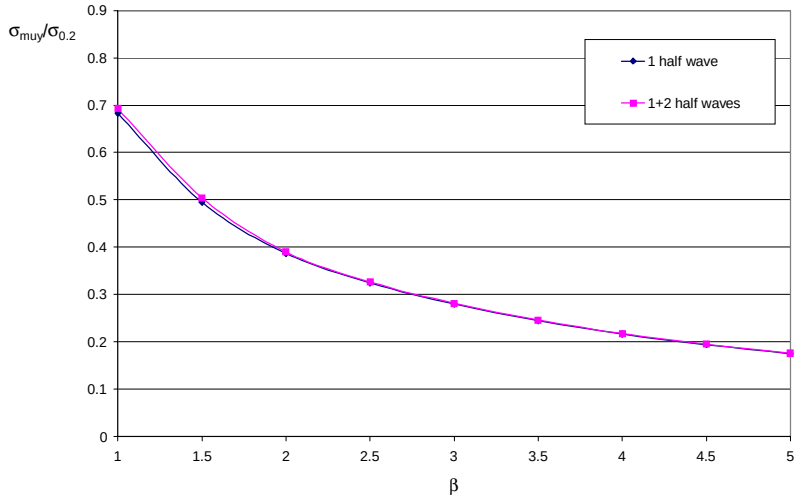

Figure A4.10 : Transverse buckling capacity for different initial deflection patterns. The aspect ratio, a/b=2. The plates have heat affected zones along all edges.

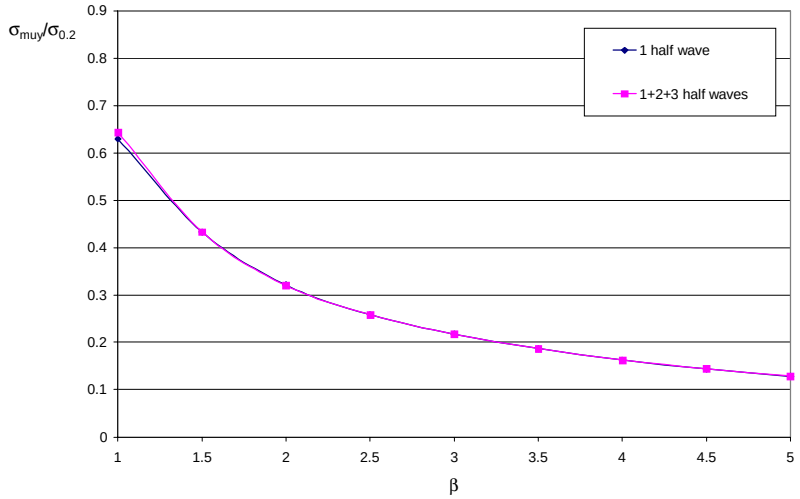

Figure A4.11 : Transverse buckling capacity for different initial deflection patterns. The aspect ratio, a/b=3. The plates have heat affected zones along all edges.

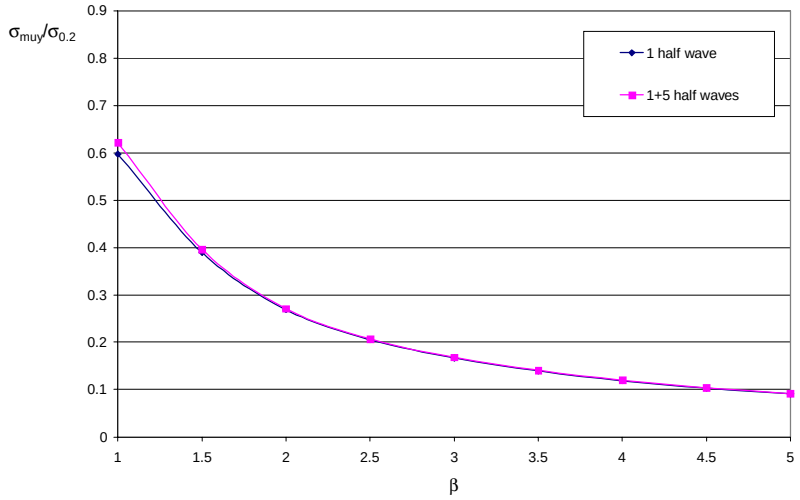

Figure A4.12 : Transverse buckling capacity for different initial deflection patterns. The aspect ratio, a/b=5. The plates have heat affected zones along all edges.

Appendix 5

Details Concerning Change of Aluminium Alloys

A5.1 Axial Loading

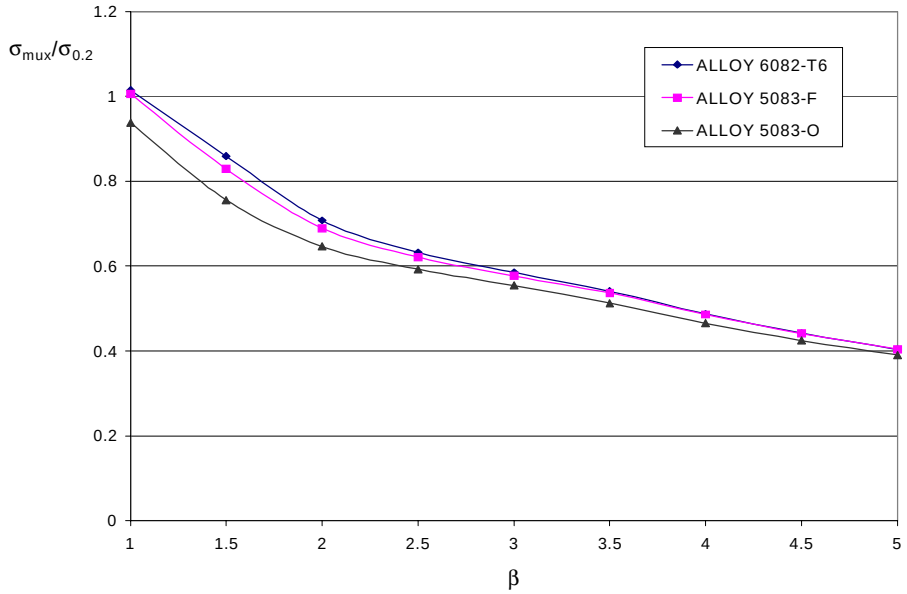

Figure A5.1 : Axial buckling capacities of different aluminium alloys. The plates have heat affected zones along all edges, and the reduction in yield strength in the heat affected zones is 10 percent. The buckling capacities have been normalised with the 0.2 percent tensile proof stress. Aspect ratio, a/b=3.

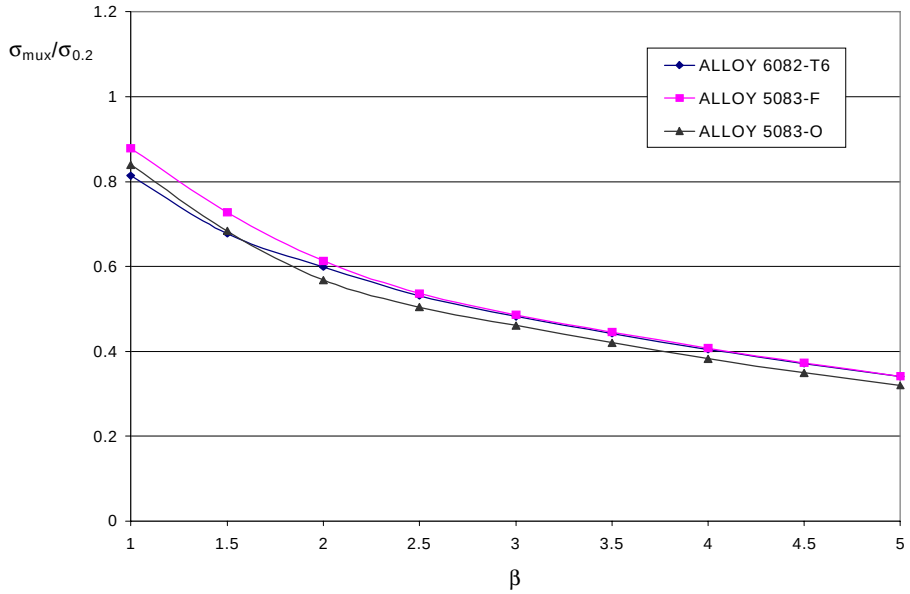

Figure A5.2 : Axial buckling capacities of different aluminium alloys. The plates have heat affected zones along all edges, and the reduction in yield strength in the heat affected zones is 50 percent. The buckling capacities have been normalised with the 0.2 percent tensile proof stress. Aspect ratio, a/b=3.

A5.2 Transverse Loading

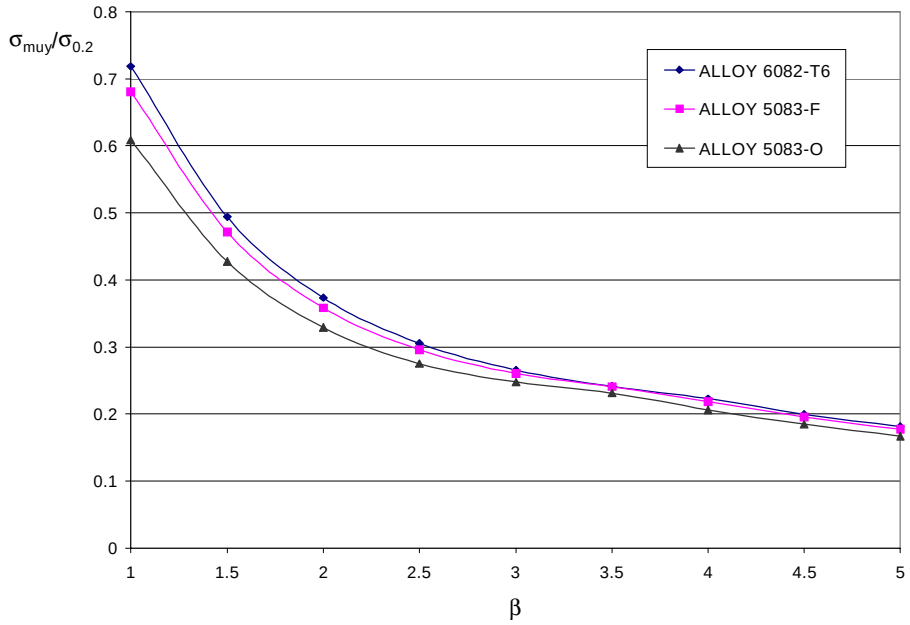

Figure A5.3 : Transverse buckling capacities of different aluminium alloys. The plates consist of the base material only, and their buckling capacities have been normalised with the 0.2 percent tensile proof stress. Aspect ratio, a/b=3.

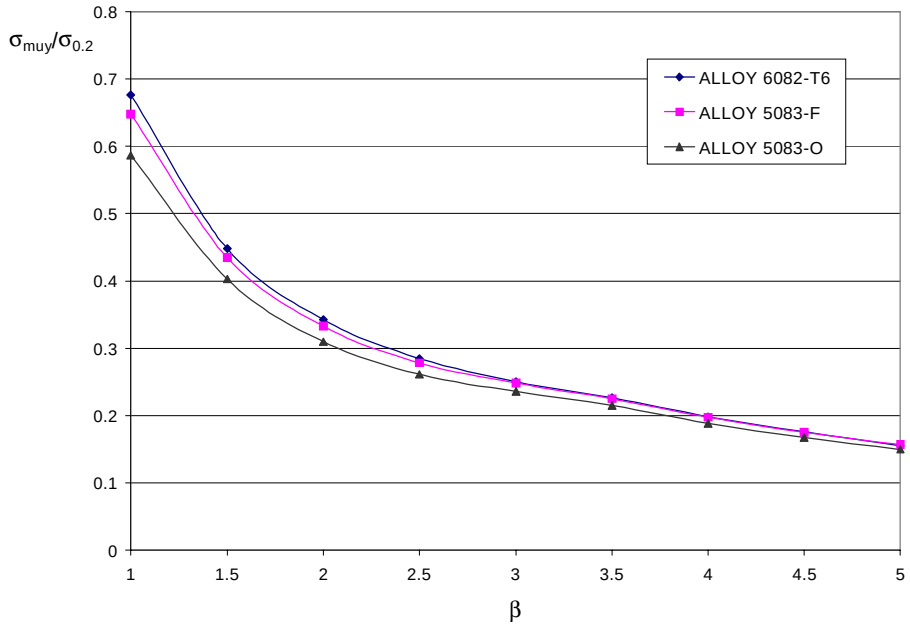

Figure A5.4 : Transverse buckling capacities of different aluminium alloys. The plates have heat affected zones along all edges, and the reduction in yield strength in the heat affected zones is 10 percent. The buckling capacities have been normalised with the 0.2 percent tensile proof stress. Aspect ratio, a/b=3.

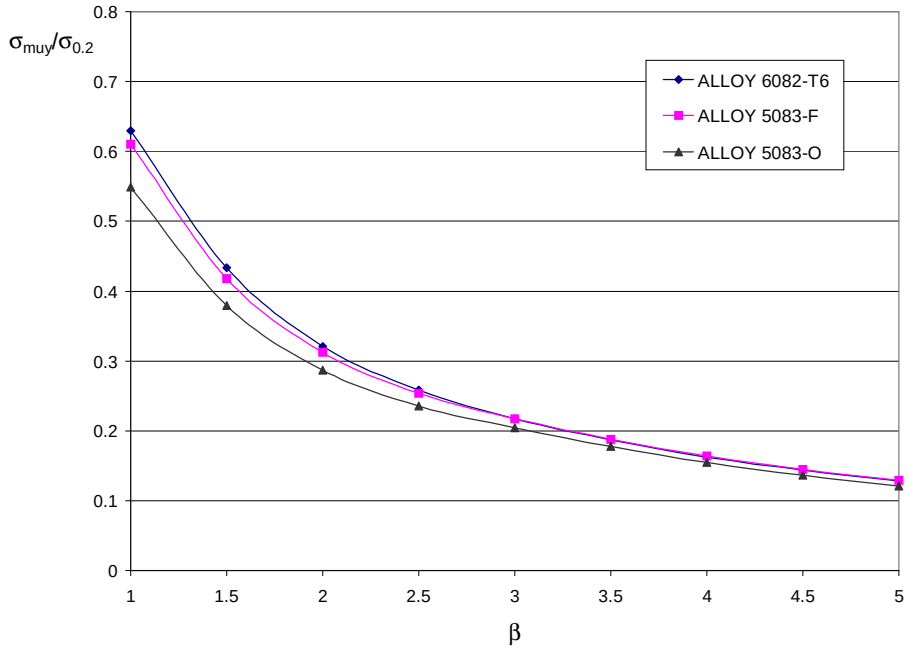

Figure A5.5 : Transverse buckling capacities of different aluminium alloys. The plates have heat affected zones along all edges, and the reduction in yield strength in the heat affected zones is 50 percent. The buckling capacities have been normalised with the 0.2 percent tensile proof stress. Aspect ratio, a/b=3.

A5.3 Plate Strip Analyses

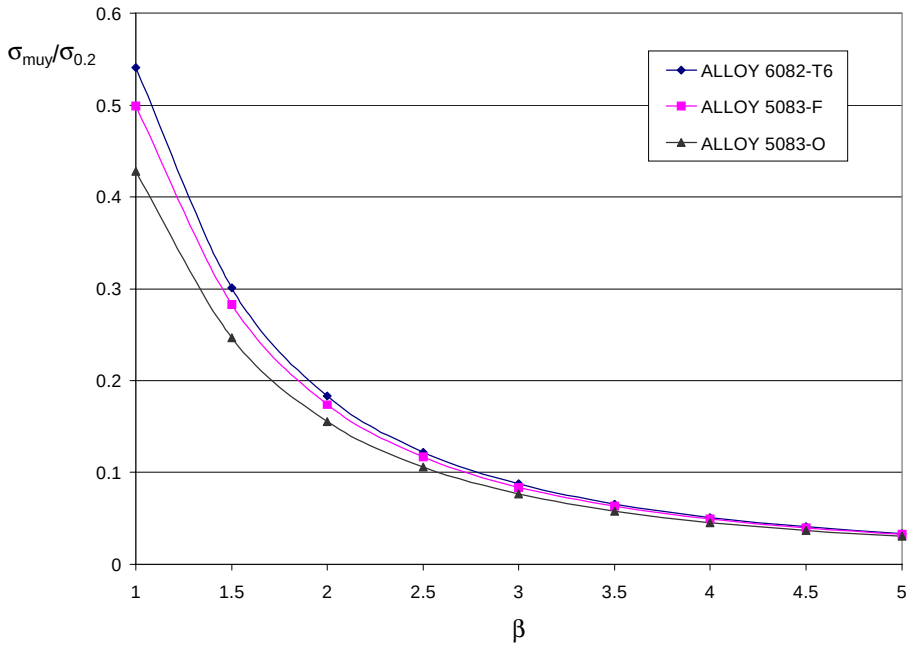

Figure A5.6 : Plate strip analyses of plates made of different aluminium alloys. The plates consist of the base material only, and their buckling capacities have been normalised with the 0.2 percent tensile proof stress.

A5.4 Biaxial Loading

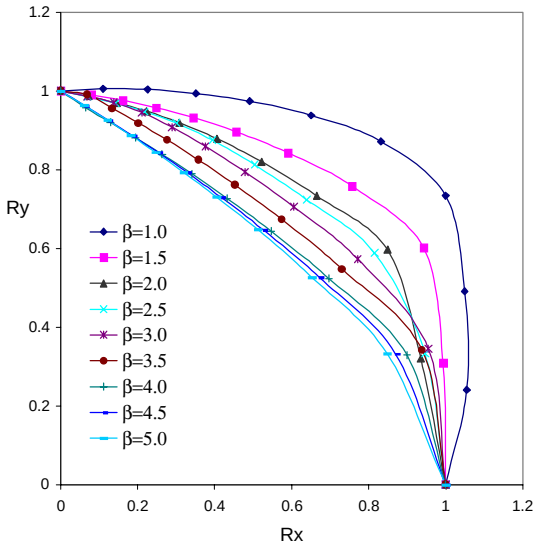

Figure A5.7 : Biaxial buckling curves for alloy 6082-T6. The plates have no heat affected zones.

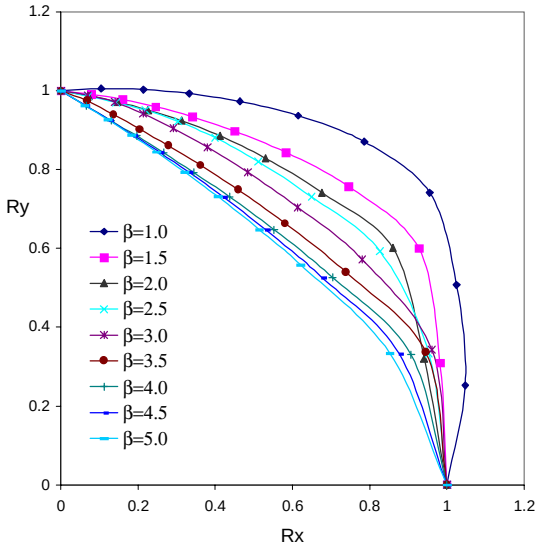

Figure A5.8 : Biaxial buckling curves for alloy 5083-F. The plates have no heat affected zones.

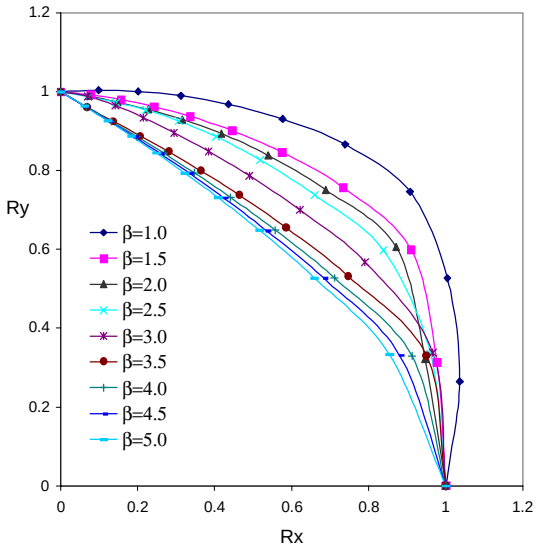

Figure A5.9 : Biaxial buckling curves for alloy 5083-O. The plates have no heat affected zones.

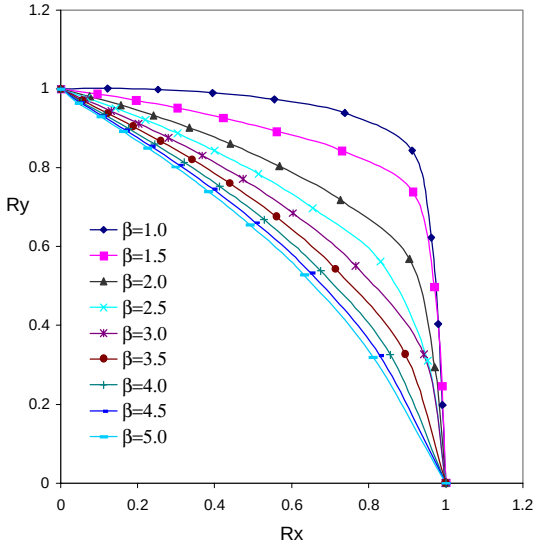

Figure A5.10 : Biaxial buckling curves for alloy 6082-T6. The plates have heat affected zones along all edges.

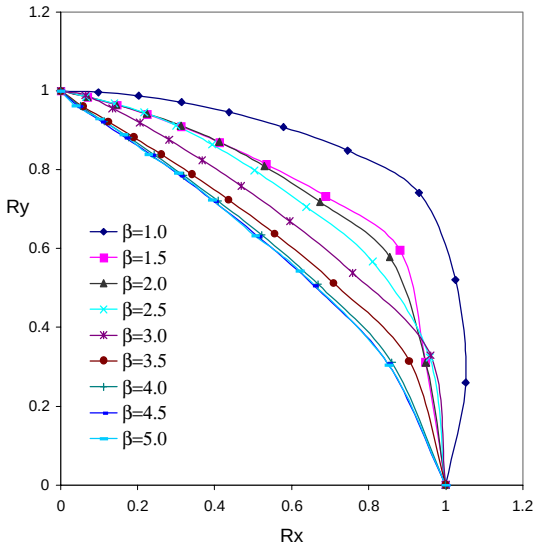

Figure A5.11 : Biaxial buckling curves for alloy 5083-F. The plates have heat affected zones along all edges.

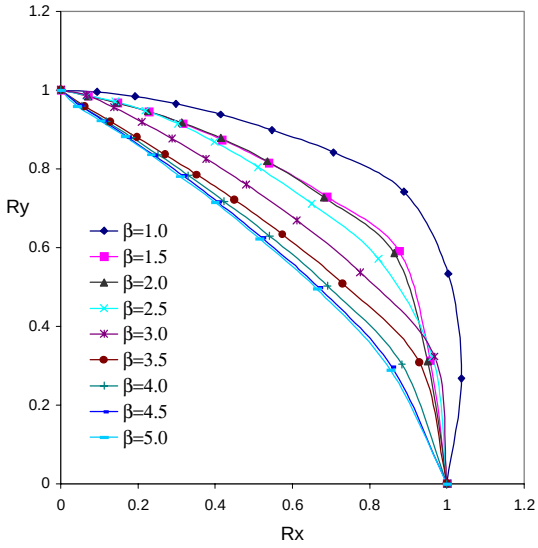

Figure A5.12 : Biaxial buckling curves for alloy 5083-O. The plates have heat affected zones along all edges.

Appendix 6

Comparison of Biaxial Interaction Curves

A6.1 a/b=1

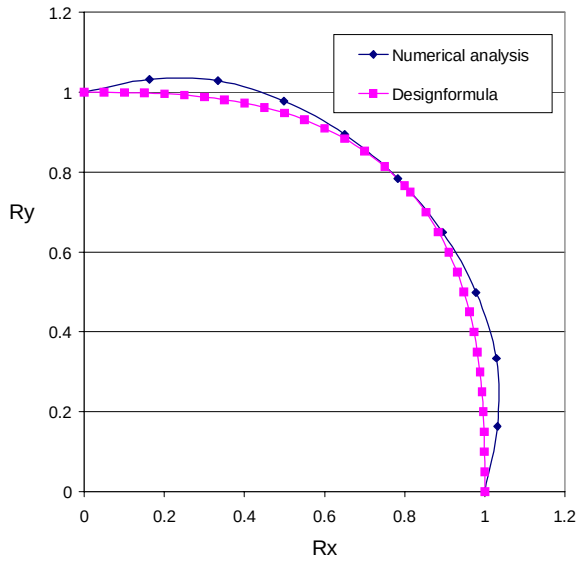

Figure A6.1 : Comparison of proposed design curve and biaxial interaction curve used as basis for design. Slenderness, β=1.0.

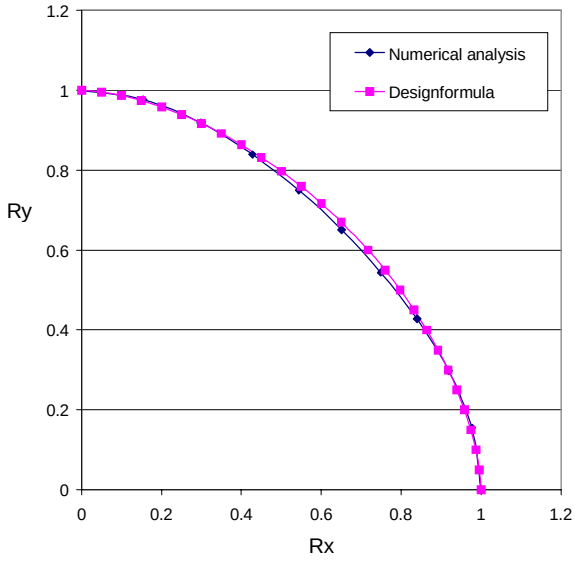

Figure A6.2 : Comparison of proposed design curve and biaxial interaction curve used as basis for design. Slenderness, β=1.5.

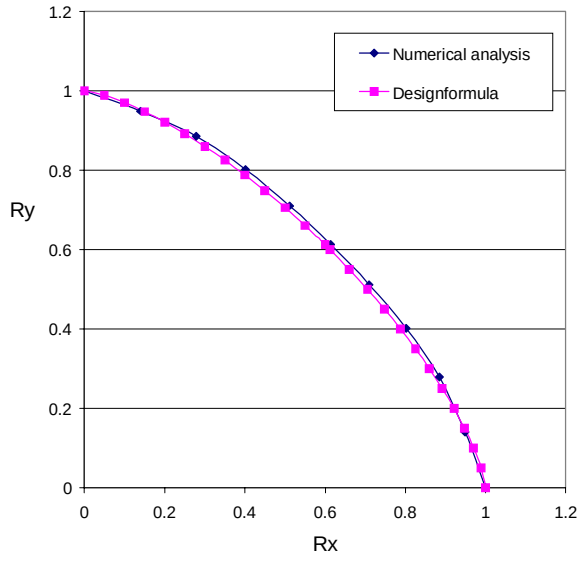

Figure A6.3 : Comparison of proposed design curve and biaxial interaction curve used as basis for design. Slenderness, β=2.0.

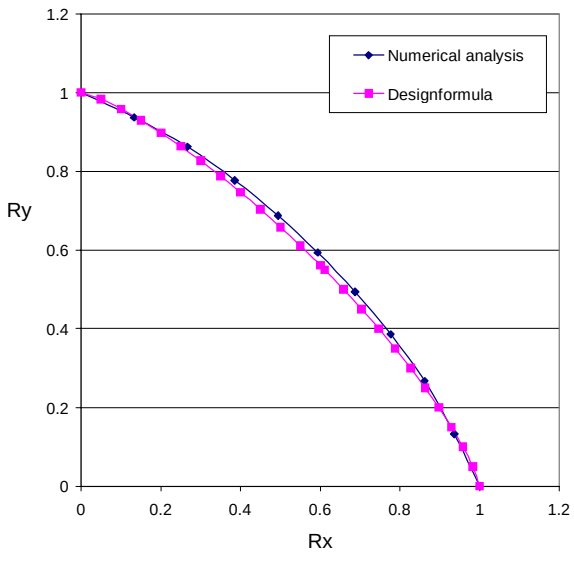

Figure A6.4 : Comparison of proposed design curve and biaxial interaction curve used as basis for design. Slenderness, β=2.5.

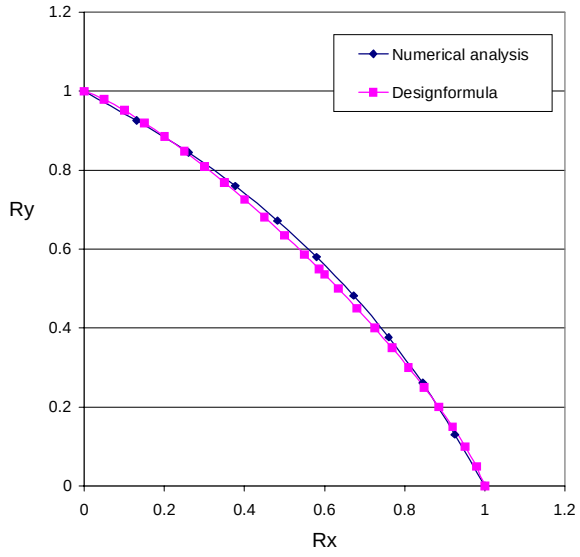

Figure A6.5 : Comparison of proposed design curve and biaxial interaction curve used as basis for design. Slenderness, β=3.0.

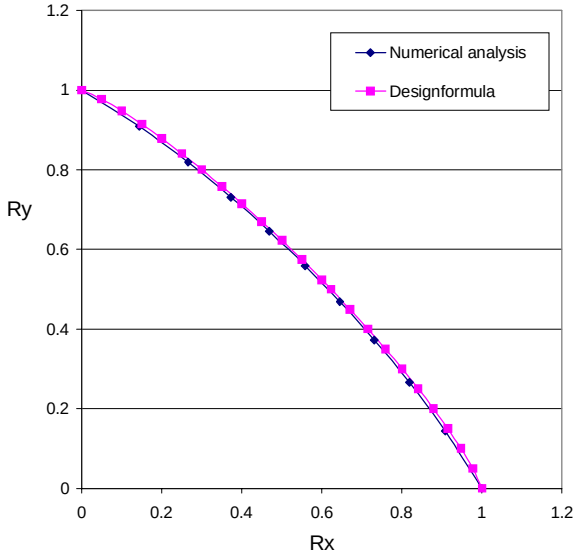

Figure A6.6 : Comparison of proposed design curve and biaxial interaction curve used as basis for design. Slenderness, β=3.5.

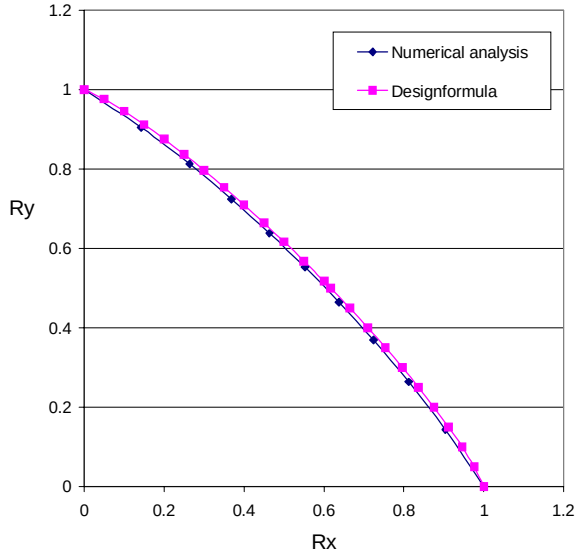

Figure A6.7 : Comparison of proposed design curve and biaxial interaction curve used as basis for design. Slenderness, β=4.0.

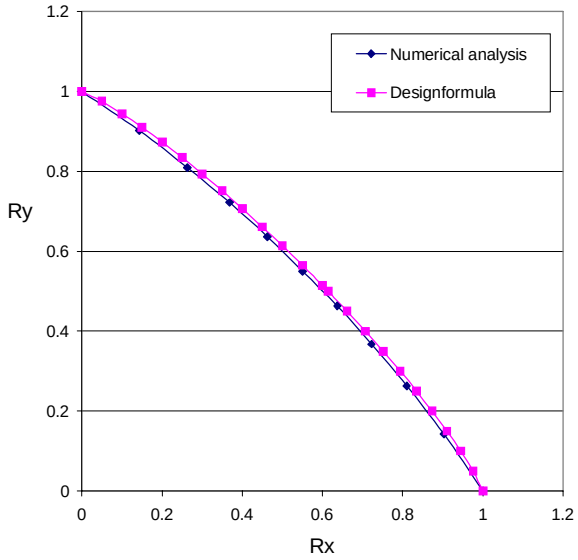

Figure A6.8 : Comparison of proposed design curve and biaxial interaction curve used as basis for design. Slenderness, β=4.5.

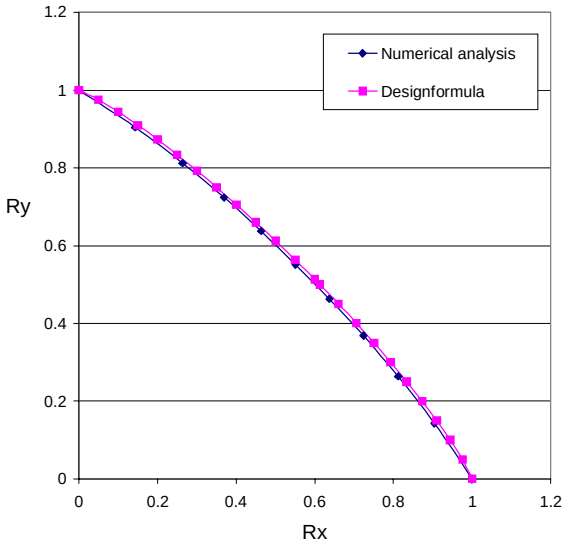

Figure A6.9 : Comparison of proposed design curve and biaxial interaction curve used as basis for design. Slenderness, β=5.0.

A6.2 a/b=2

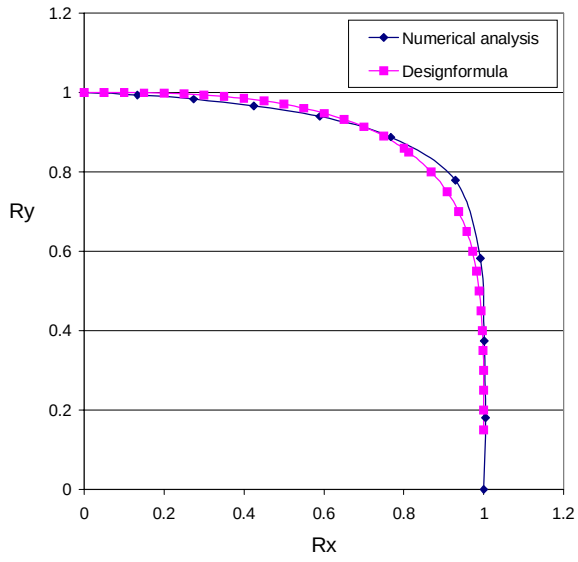

Figure A6.10 : Comparison of proposed design curve and biaxial interaction curve used as basis for design. Slenderness, β=1.0.

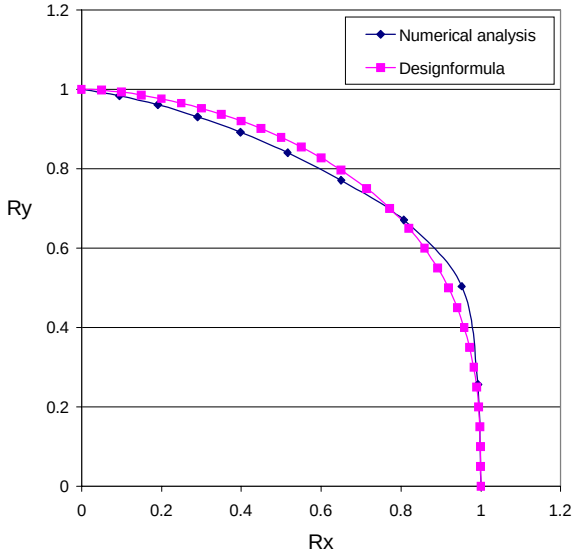

Figure A6.11 : Comparison of proposed design curve and biaxial interaction curve used as basis for design. Slenderness, β=1.5.

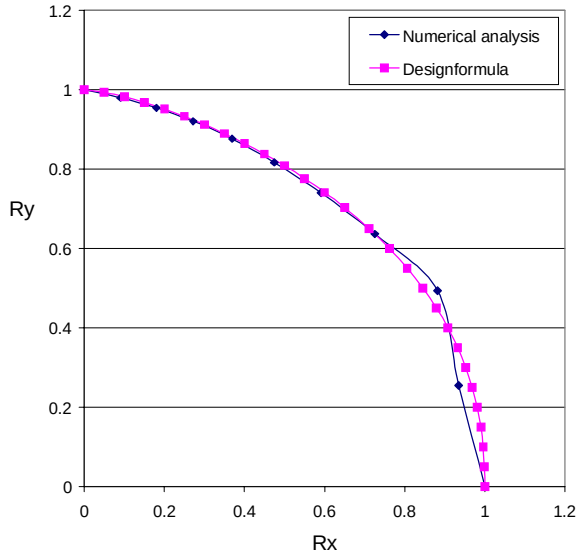

Figure A6.12 : Comparison of proposed design curve and biaxial interaction curve used as basis for design. Slenderness, β=2.0.

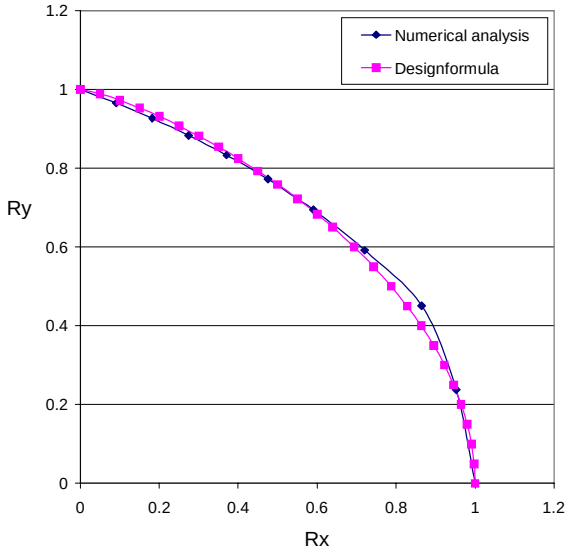

Figure A6.13 : Comparison of proposed design curve and biaxial interaction curve used as basis for design. Slenderness, β=2.5.

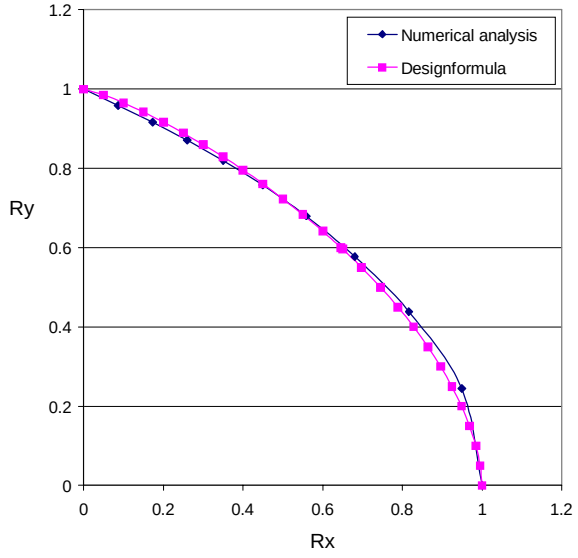

Figure A6.14 : Comparison of proposed design curve and biaxial interaction curve used as basis for design. Slenderness, β=3.0.

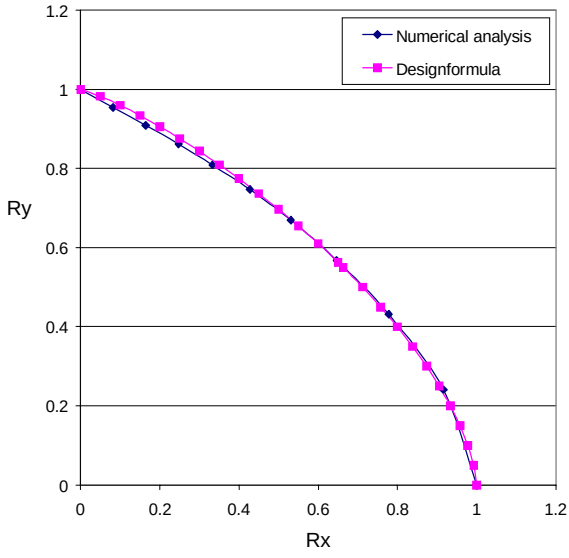

Figure A6.15 : Comparison of proposed design curve and biaxial interaction curve used as basis for design. Slenderness, β=3.5.

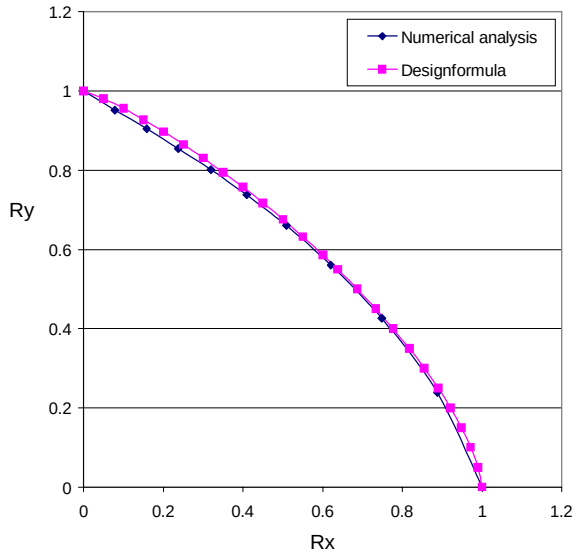

Figure A6.16 : Comparison of proposed design curve and biaxial interaction curve used as basis for design. Slenderness, β=4.0.

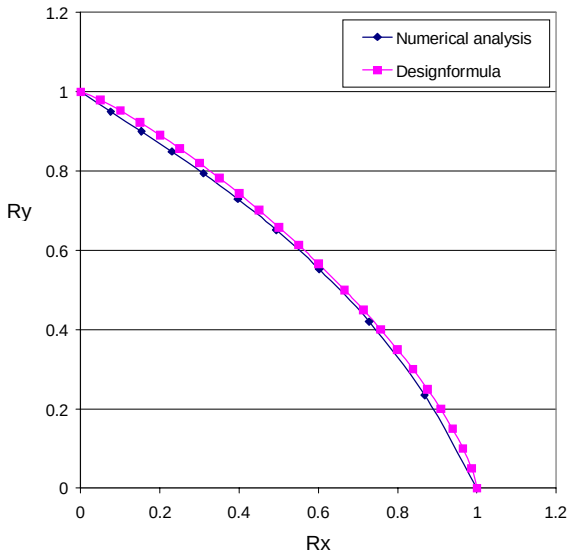

Figure A6.17 : Comparison of proposed design curve and biaxial interaction curve used as basis for design. Slenderness, β=4.5.

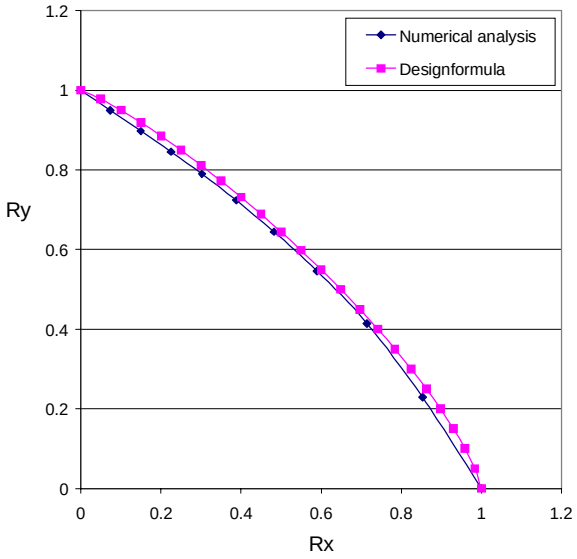

Figure A6.18 : Comparison of proposed design curve and biaxial interaction curve used as basis for design. Slenderness, β=5.0.

A6.3 a/b=3

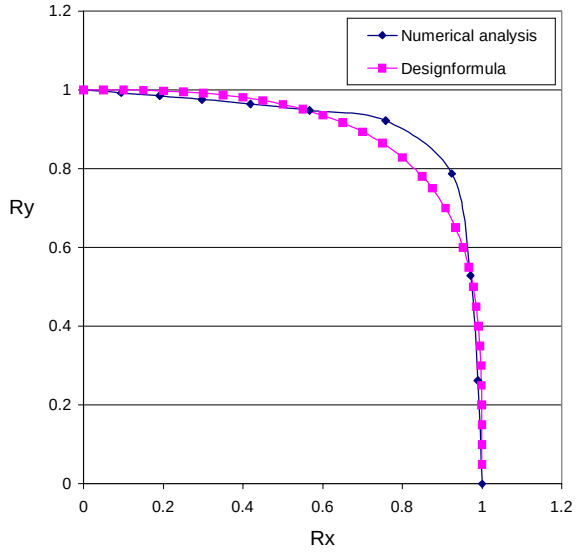

Figure A6.19 : Comparison of proposed design curve and biaxial interaction curve used as basis for design. Slenderness, β=1.0.

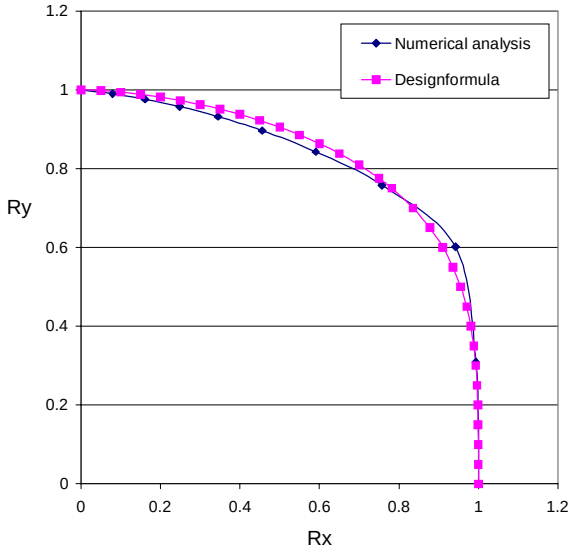

Figure A6.20 : Comparison of proposed design curve and biaxial interaction curve used as basis for design. Slenderness, β=1.5.

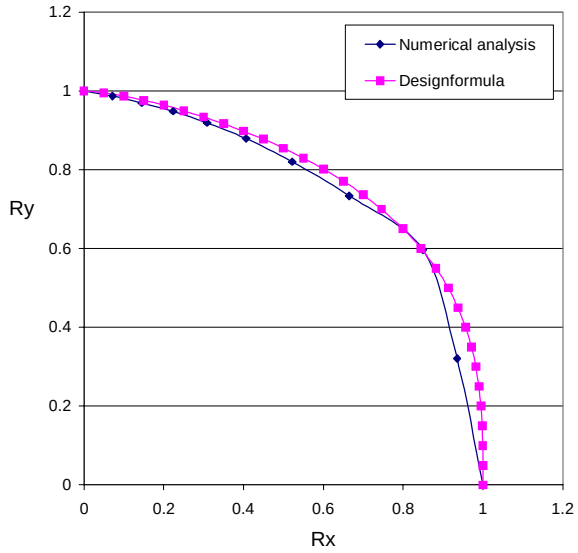

Figure A6.21 : Comparison of proposed design curve and biaxial interaction curve used as basis for design. Slenderness, β=2.0.

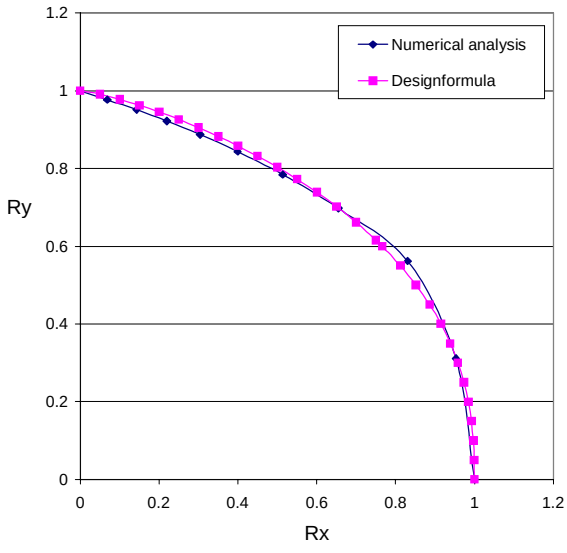

Figure A6.22 : Comparison of proposed design curve and biaxial interaction curve used as basis for design. Slenderness, β=2.5.

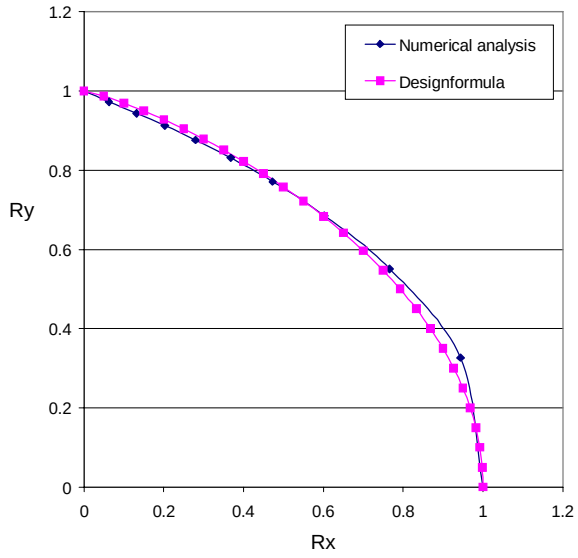

Figure A6.23 : Comparison of proposed design curve and biaxial interaction curve used as basis for design. Slenderness, β=3.0.

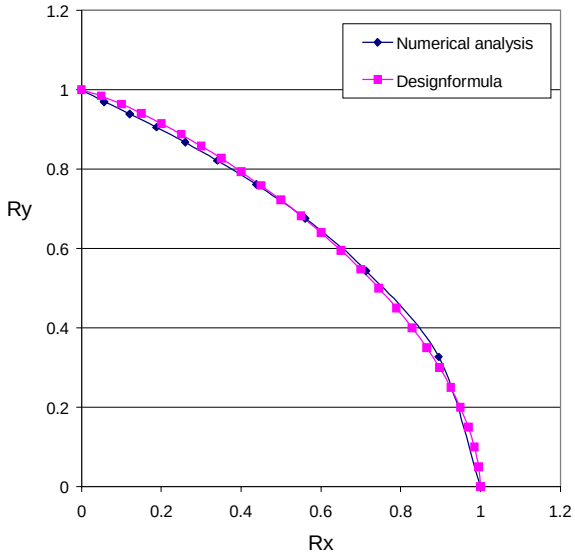

Figure A6.24 : Comparison of proposed design curve and biaxial interaction curve used as basis for design. Slenderness, β=3.5.

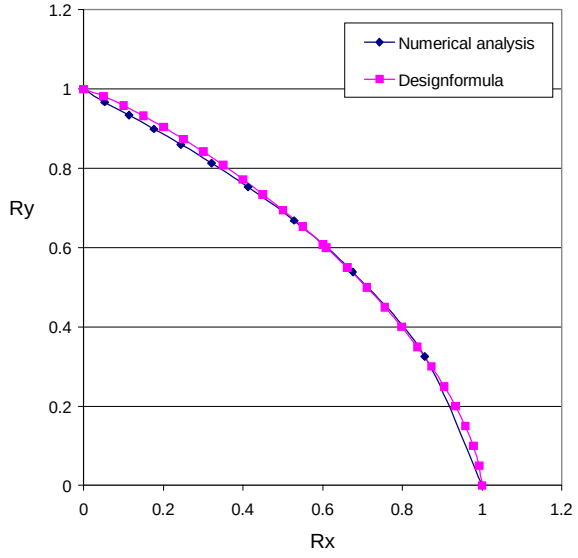

Figure A6.25 : Comparison of proposed design curve and biaxial interaction curve used as basis for design. Slenderness, β=4.0.

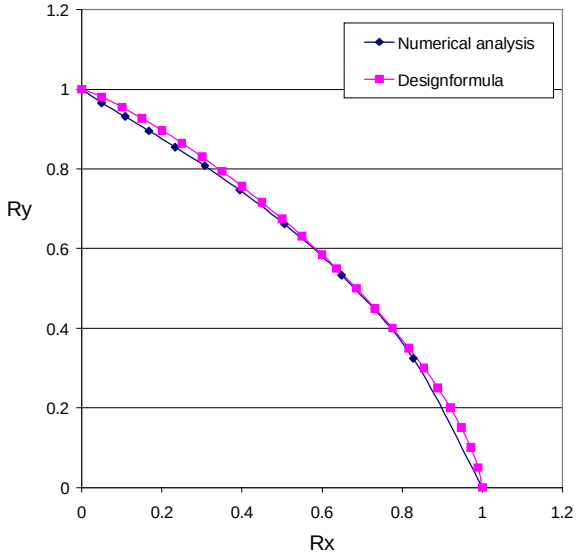

Figure A6.26 : Comparison of proposed design curve and biaxial interaction curve used as basis for design. Slenderness, β=4.5.

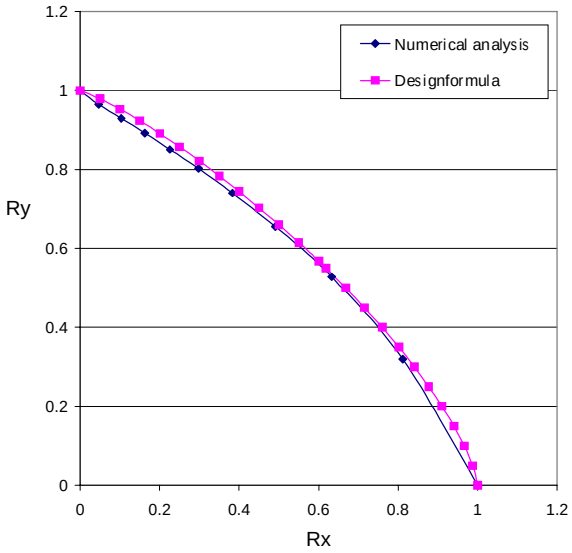

Figure A6.27 : Comparison of proposed design curve and biaxial interaction curve used as basis for design. Slenderness, β=5.0.

A6.4 a/b=5

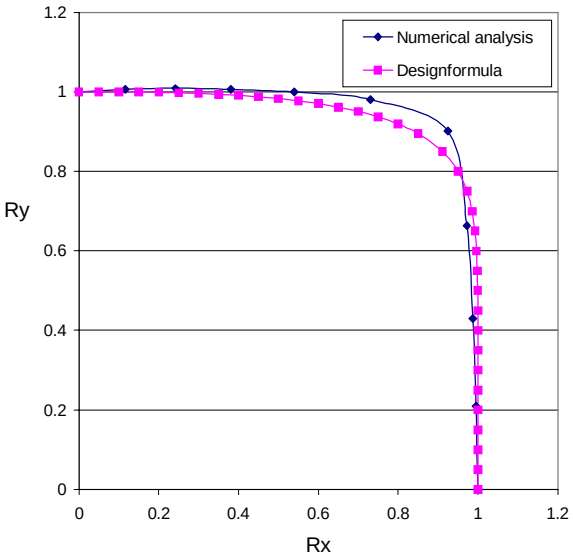

Figure A6.28 : Comparison of proposed design curve and biaxial interaction curve used as basis for design. Slenderness, β=1.0.

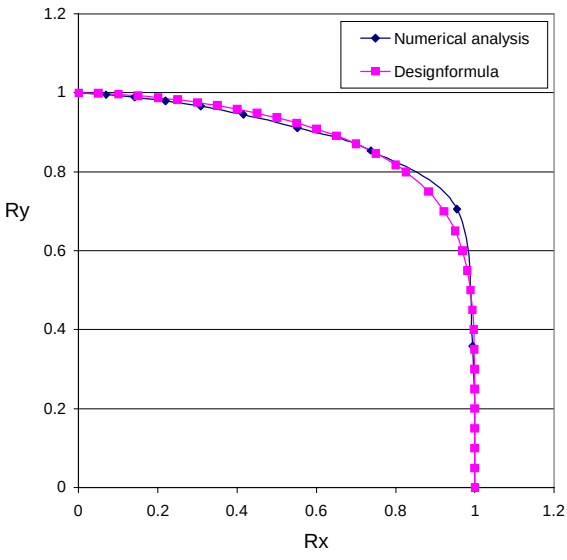

Figure A6.29 : Comparison of proposed design curve and biaxial interaction curve used as basis for design. Slenderness, β=1.5.

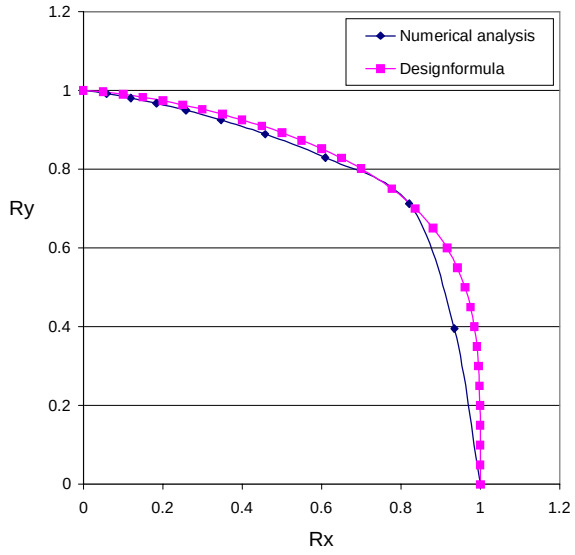

Figure A6.30 : Comparison of proposed design curve and biaxial interaction curve used as basis for design. Slenderness, β=2.0.

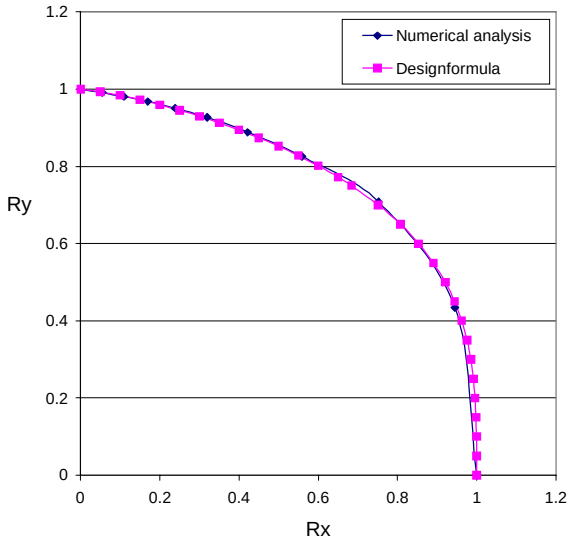

Figure A6.31 : Comparison of proposed design curve and biaxial interaction curve used as basis for design. Slenderness, β=2.5.

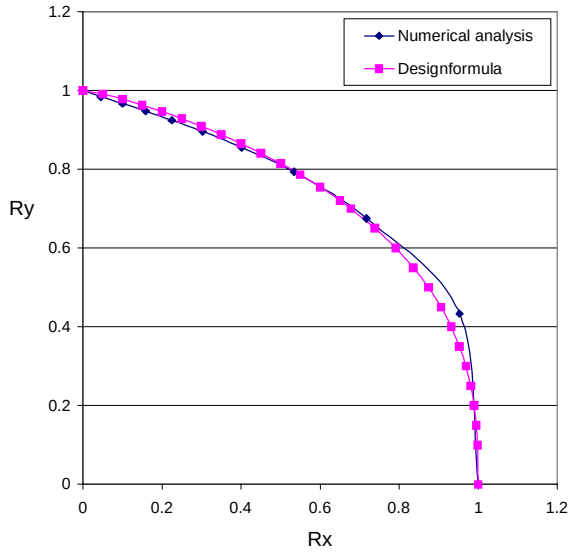

Figure A6.32 : Comparison of proposed design curve and biaxial interaction curve used as basis for design. Slenderness, β=3.0.

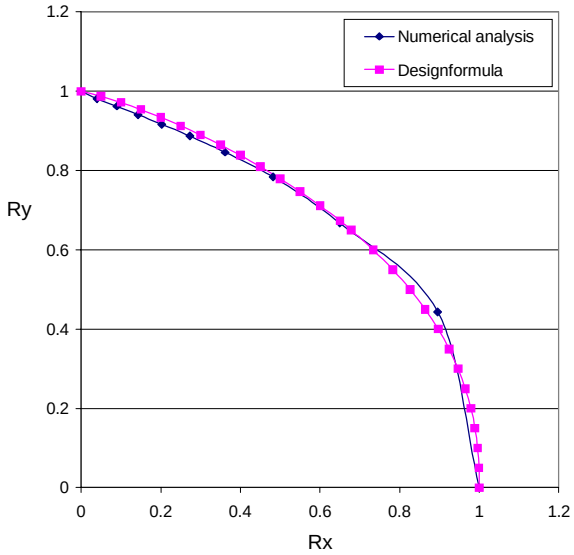

Figure A6.33 : Comparison of proposed design curve and biaxial interaction curve used as basis for design. Slenderness, β=3.5.

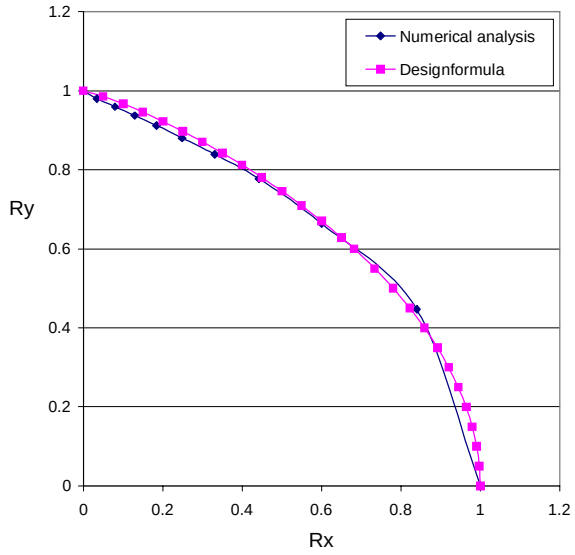

Figure A6.34 : Comparison of proposed design curve and biaxial interaction curve used as basis for design. Slenderness, β=4.0.

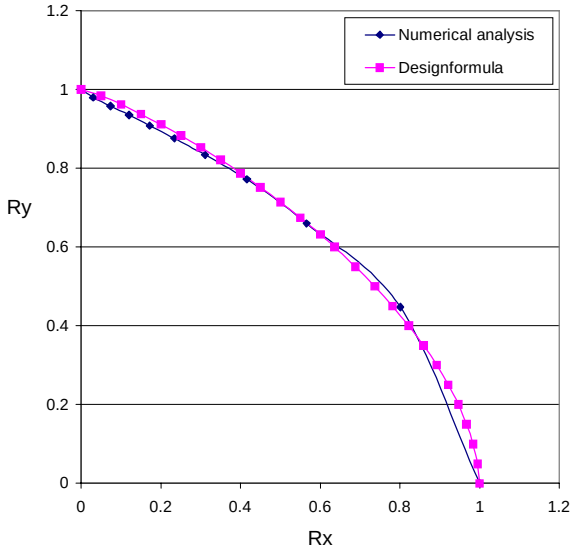

Figure A6.35 : Comparison of proposed design curve and biaxial interaction curve used as basis for design. Slenderness, β=4.5.

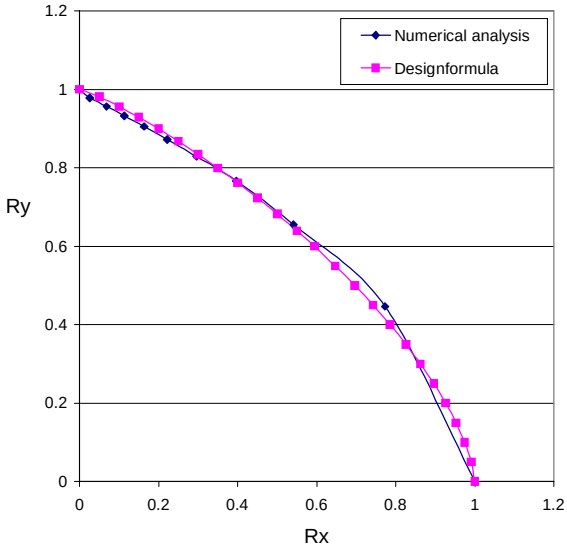

Figure A6.36 : Comparison of proposed design curve and biaxial interaction curve used as basis for design. Slenderness, β=5.0.

Appendix 7

Details in Design Codes

A7.1 Axial Buckling Curves in Present Design Codes

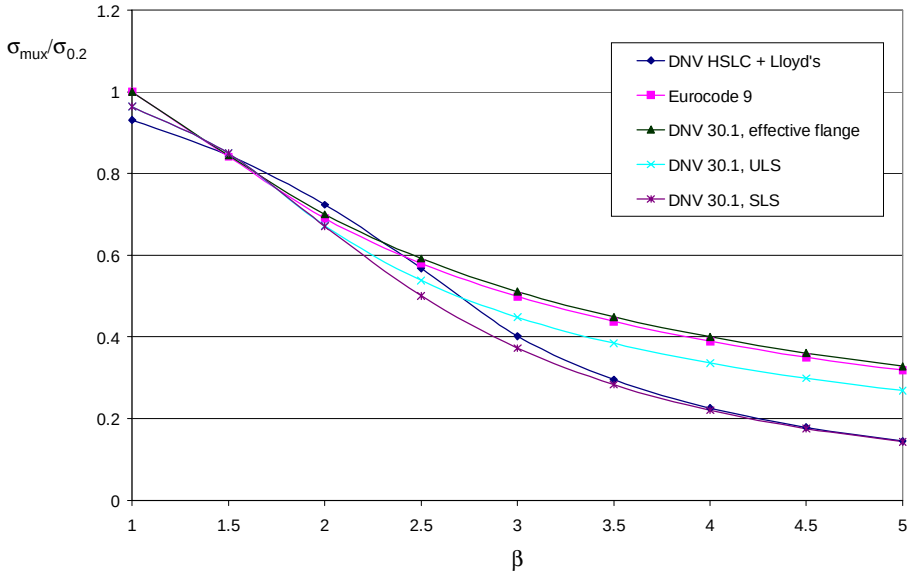

Figure A7.1 : Axial buckling capacities in present design codes (heat treated, welded plates, but no reduction in 0.2 percent tensile proof stress due to welding)

A7.2 Comparison between Proposed Design Formula and DNV HSLC+Lloyd's

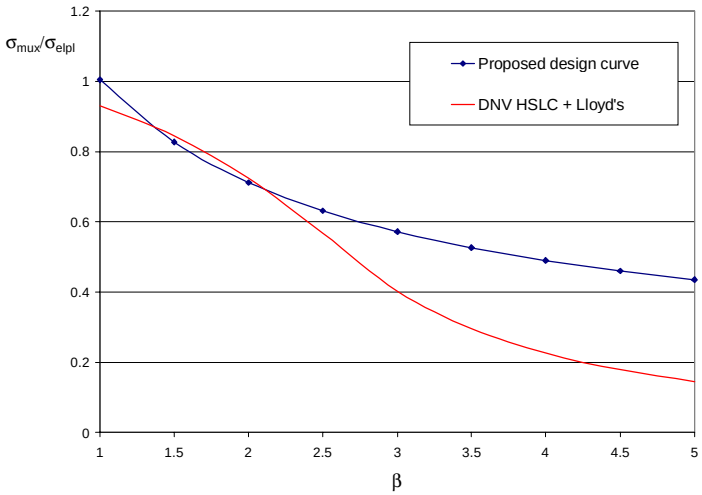

Figure A7.2 : Buckling curves from proposed design formula compared with linear elastic buckling with Johnson-Ostenfeld correction. $\sigma_{0.2}{}^{*}/\sigma_{0.2}=1.0$.

URN:NBN:no-1307

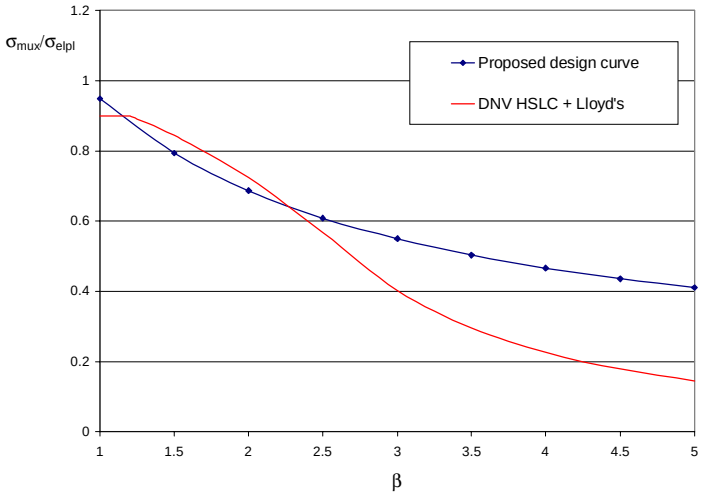

Figure A7.3 : Buckling curves from proposed design formula compared with linear elastic buckling with Johnson-Ostenfeld correction. $\sigma_{0.2}^{*}/\sigma_{0.2}=0.9$.

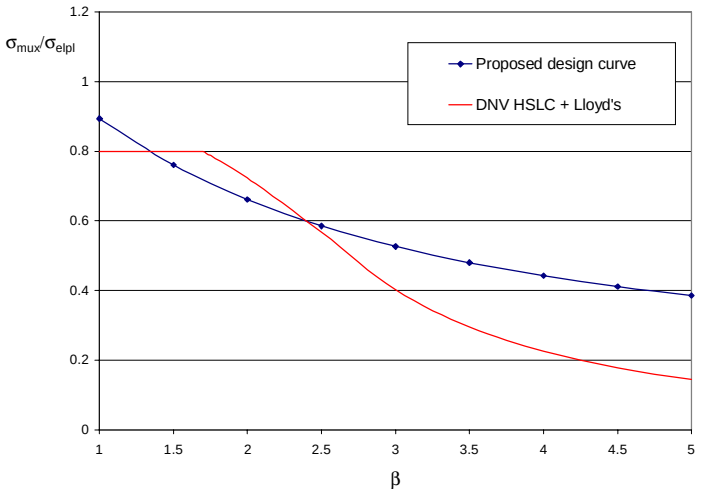

Figure A7.4 : Buckling curves from proposed design formula compared with linear elastic buckling with Johnson-Ostenfeld correction. $\sigma_{0.2}^{*}/\sigma_{0.2}=0.8$.

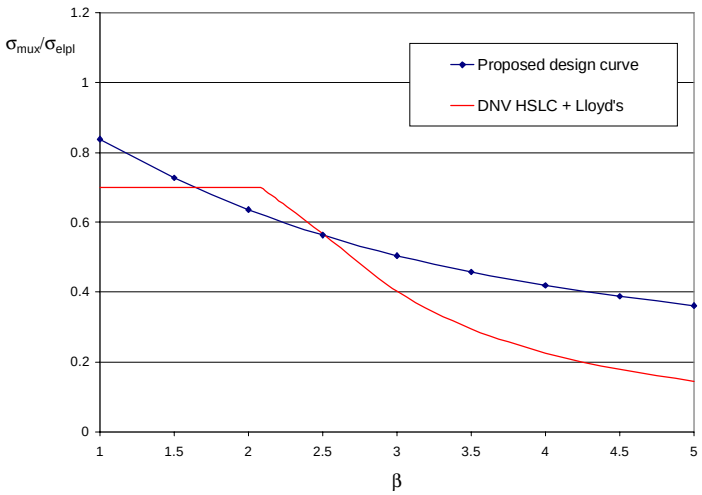

Figure A7.5 : Buckling curves from proposed design formula compared with linear elastic buckling with Johnson-Ostenfeld correction. $\sigma_{0.2}^{*}/\sigma_{0.2}=0.7$.

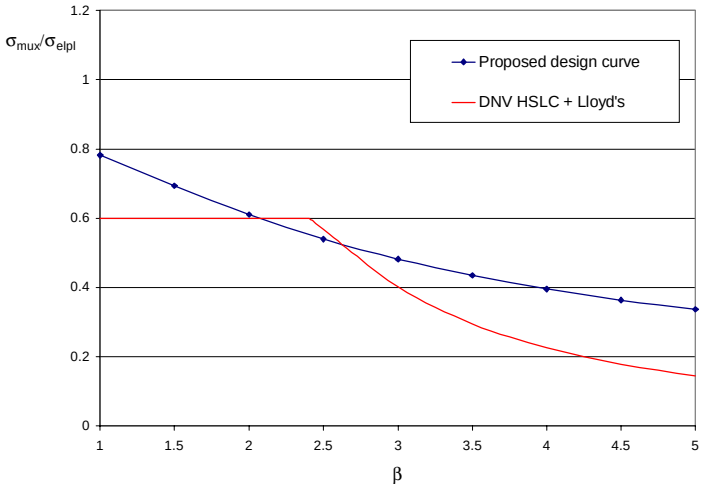

Figure A7.6 : Buckling curves from proposed design formula compared with linear elastic buckling with Johnson-Ostenfeld correction. $\sigma_{0.2}^{*}/\sigma_{0.2}=0.6$.

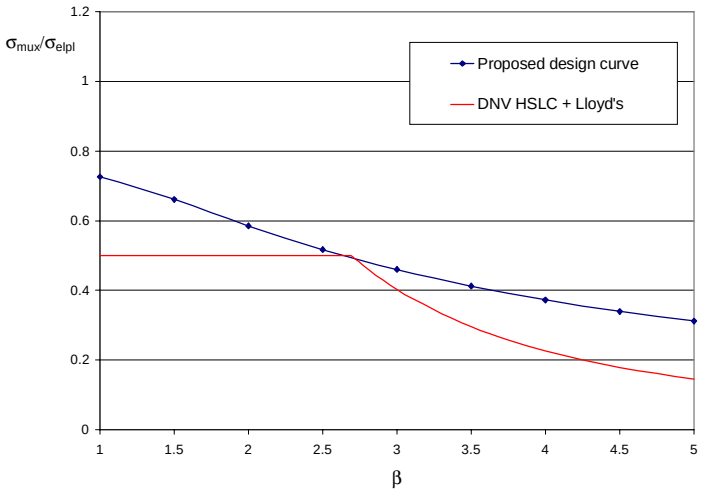

Figure A7.7 : Buckling curves from proposed design formula compared with linear elastic buckling with Johnson-Ostenfeld correction. $\sigma_{0.2}^{*}/\sigma_{0.2}=0.5$.

A7.3 Comparison between Proposed Design Formula and Eurocode 9

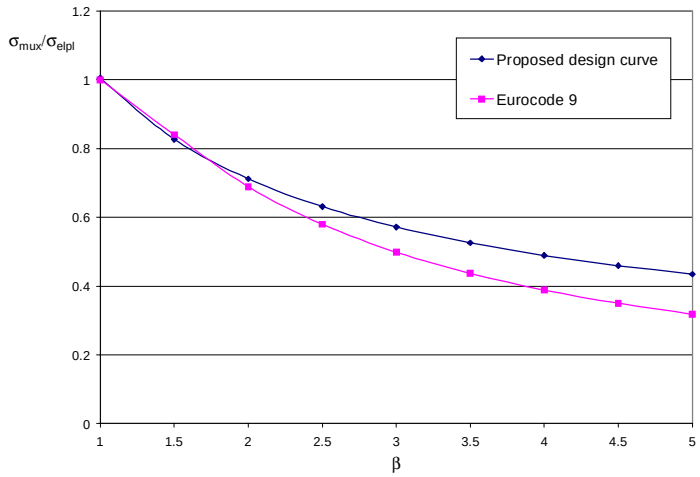

Figure A7.8 : Buckling curves from proposed design formula compared with Eurocode 9. The plates are made of a heat treated and welded alloy. $b_{HAZ}/b=1/12$. $\sigma_{0.2}^{*}/\sigma_{0.2}=1.0$.

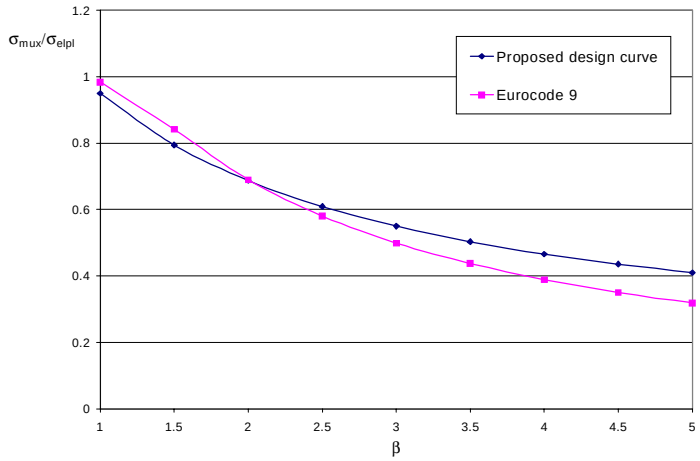

Figure A7.9 : Buckling curves from proposed design formula compared with Eurocode 9. The plates are made of a heat treated and welded alloy. $b_{HAZ}/b=1/12$. $\sigma_{0.2}^{*}/\sigma_{0.2}=0.9$.

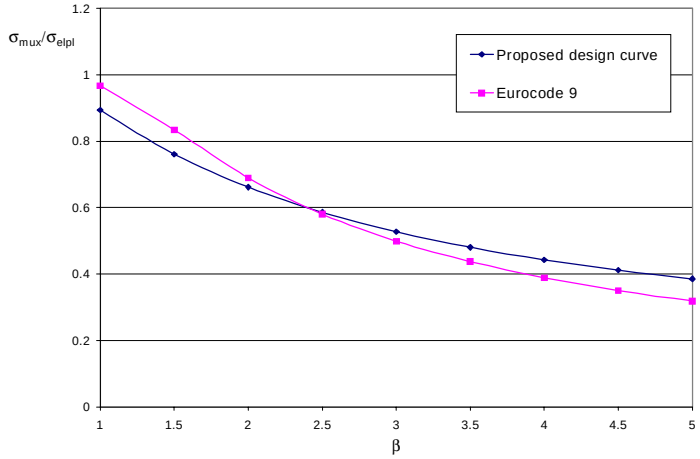

Figure A7.10 : Buckling curves from proposed design formula compared with Eurocode 9. The plates are made of a heat treated and welded alloy. $b_{HAZ}/b=1/12$. $\sigma_{0.2}^{*}/\sigma_{0.2}=0.8$.

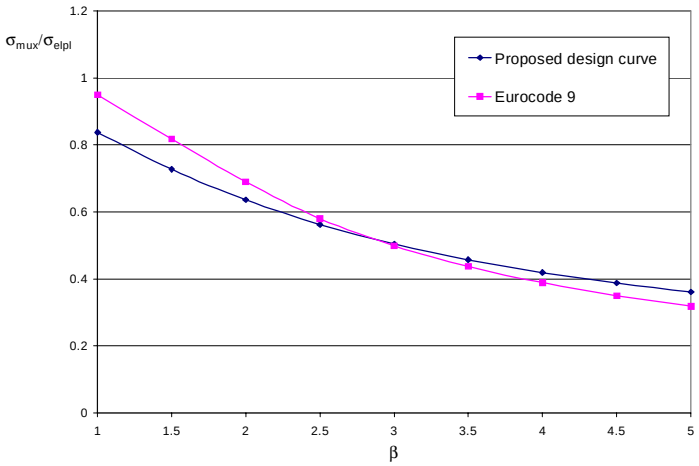

Figure A7.11 : Buckling curves from proposed design formula compared with Eurocode 9. The plates are made of a heat treated and welded alloy. $b_{HAZ}/b=1/12$. $\sigma_{0.2}^{*}/\sigma_{0.2}=0.7$.

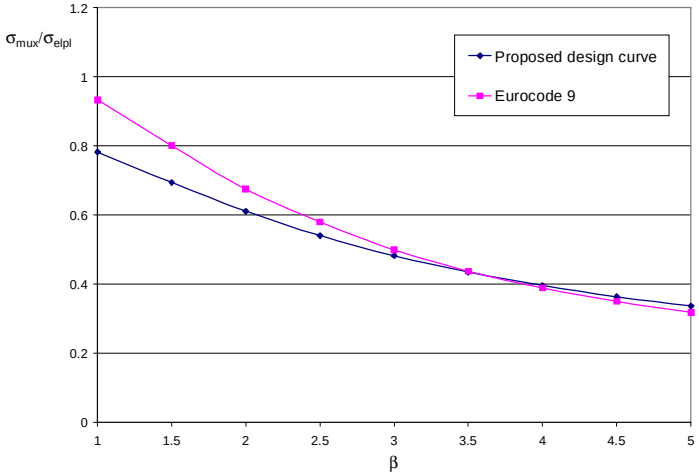

Figure A7.12 : Buckling curves from proposed design formula compared with Eurocode 9. The plates are made of a heat treated and welded alloy. $b_{HAZ}/b=1/12$. $\sigma_{0.2}^{*}/\sigma_{0.2}=0.6$.

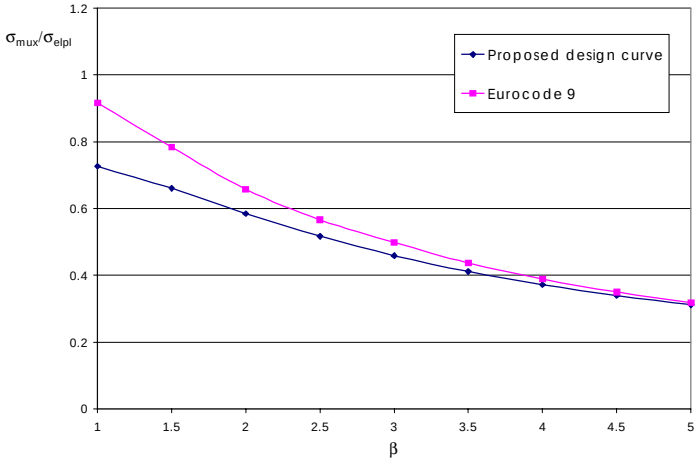

Figure A7.13 : Buckling curves from proposed design formula compared with Eurocode 9. The plates are made of a heat treated and welded alloy. $b_{HAZ}/b=1/12$. $\sigma_{0.2}^{*}/\sigma_{0.2}=0.5$.

A7.4 Transverse Plate Strip Curves

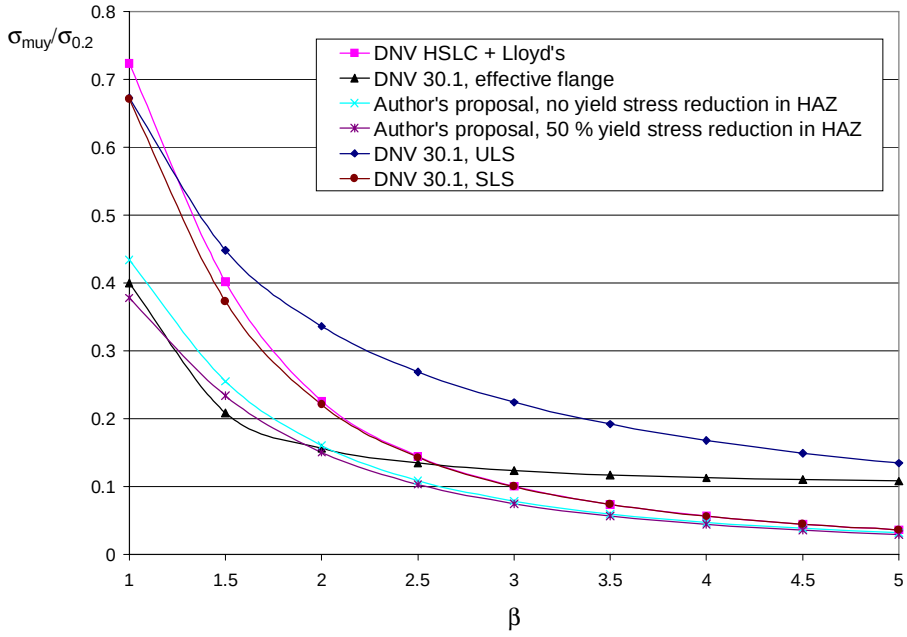

Figure A7.14 : Plate strip capacities obtained from different design rules and proposed design formula.

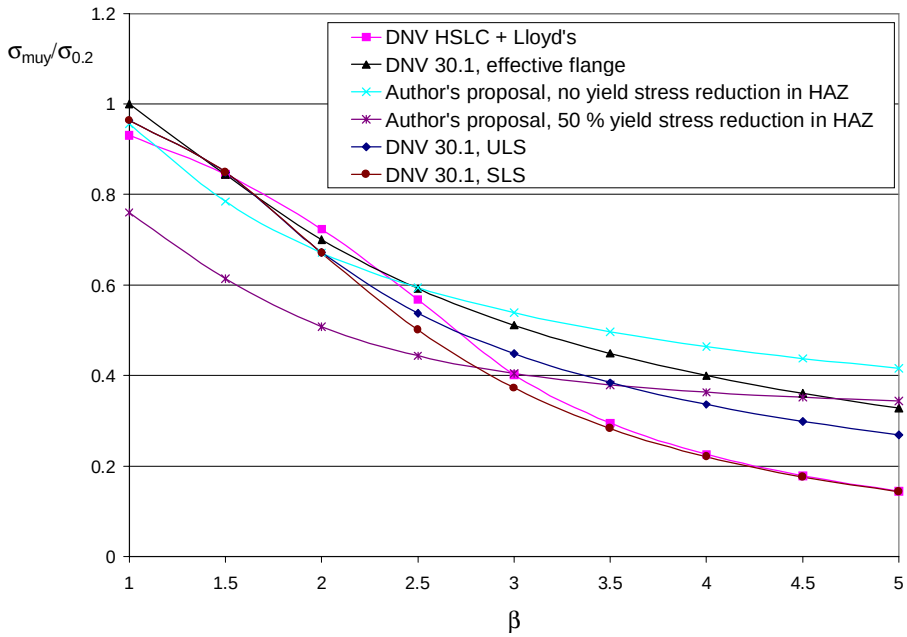

Figure A7.15 : Transverse buckling capacities obtained from different design rules and proposed design formula. Aspect ratio, a/b=1.

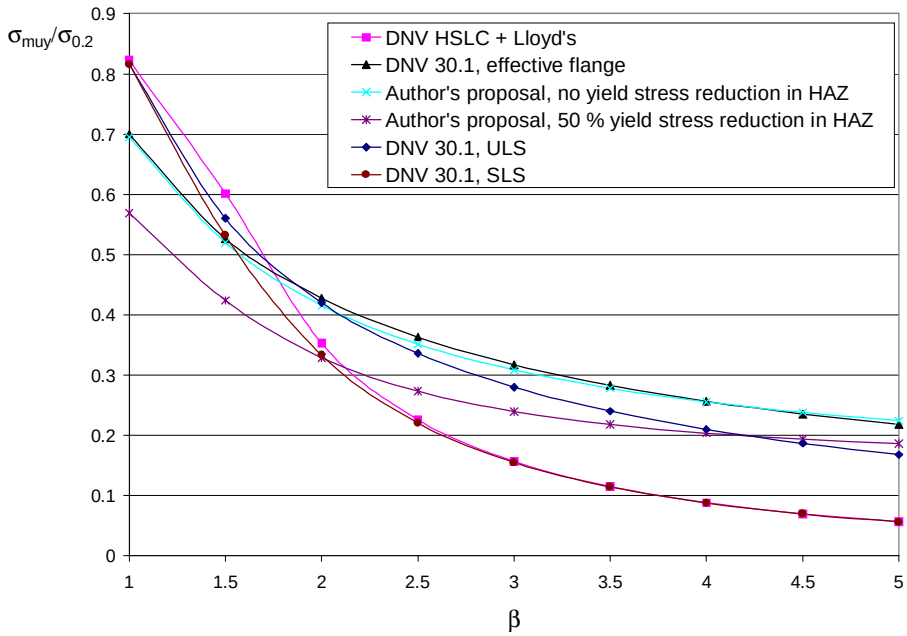

Figure A7.16 : Transverse buckling capacities obtained from different design rules and proposed design formula. Aspect ratio, a/b=2.

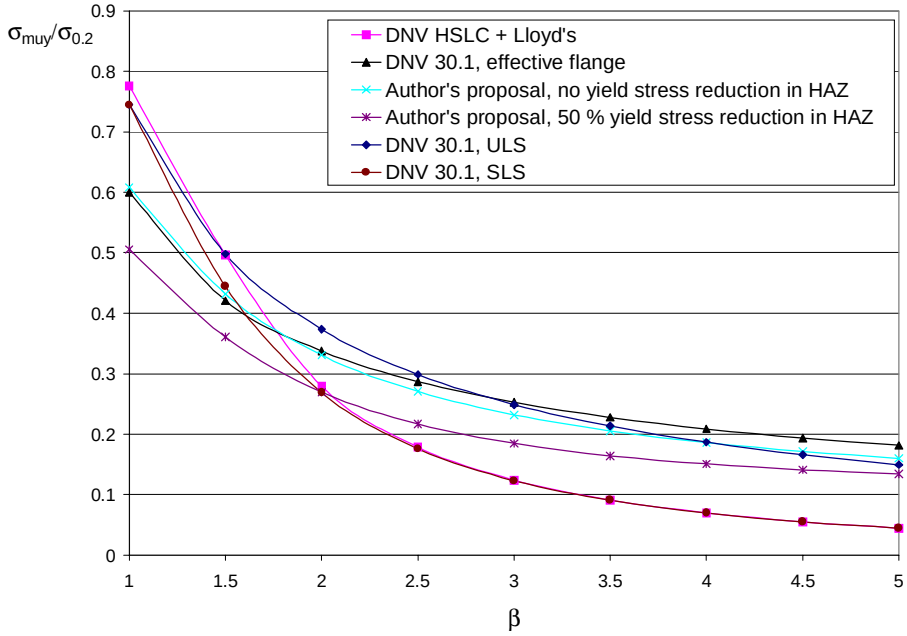

Figure A7.17 : Transverse buckling capacities obtained from different design rules and proposed design formula. Aspect ratio, a/b=3.

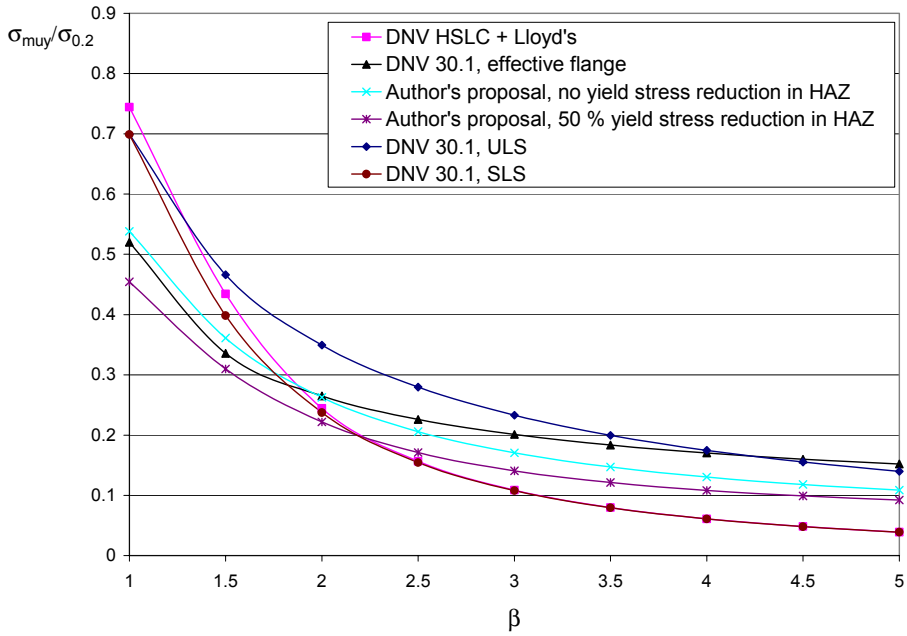

Figure A7.18 : Transverse buckling capacities obtained from different design rules and proposed design formula. Aspect ratio, a/b=5.

A7.5 Comparison of Biaxial Interaction Curves for Aspect Ratio, a/b=1.

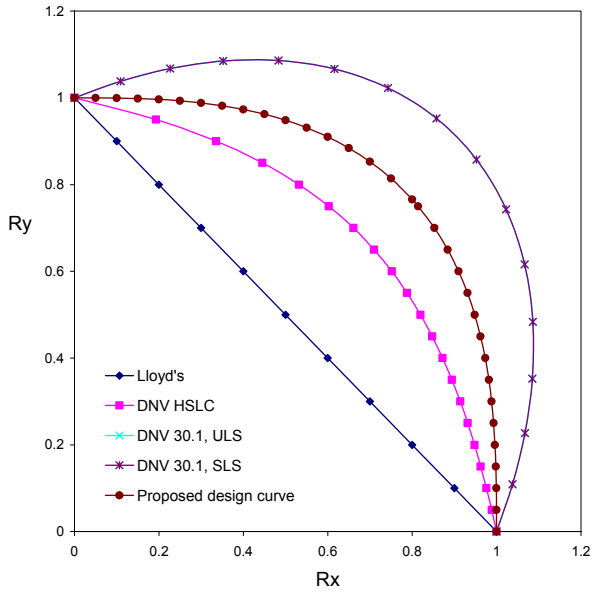

Figure A7.19 : Comparison of different biaxial design codes and proposed design formula, aspect ratio, a/b=1, β=1.0

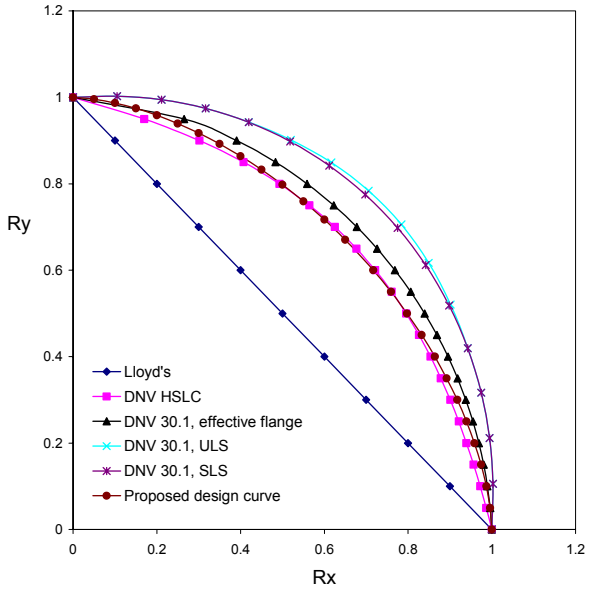

Figure A7.20 : Comparison of different biaxial design codes and proposed design formula, aspect ratio, a/b=1, β=1.5

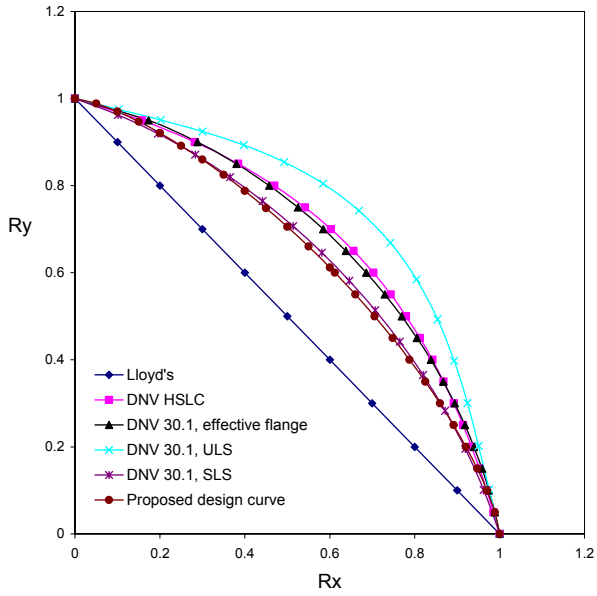

Figure A7.21 : Comparison of different biaxial design codes and proposed design formula, aspect ratio, a/b=1, β=2.0

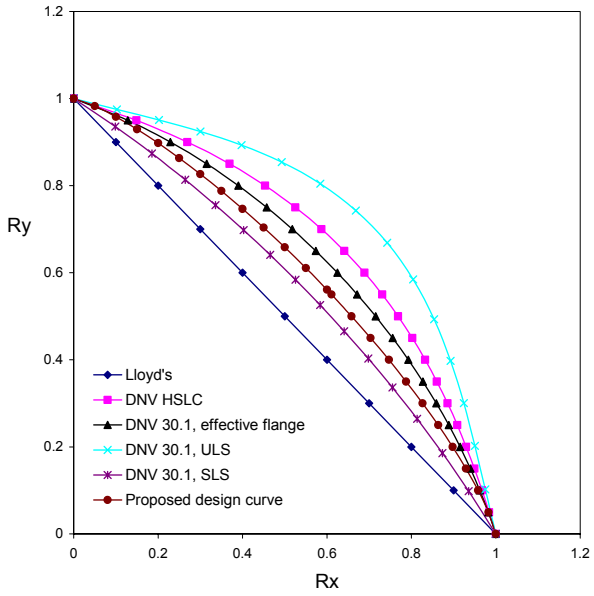

Figure A7.22 : Comparison of different biaxial design codes and proposed design formula, aspect ratio, a/b=1, β=2.5

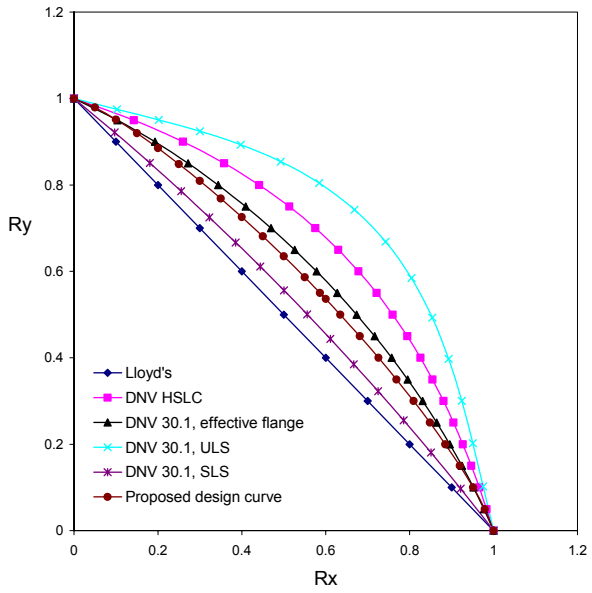

Figure A7.23 : Comparison of different biaxial design codes and proposed design formula, aspect ratio, a/b=1, β=3.0

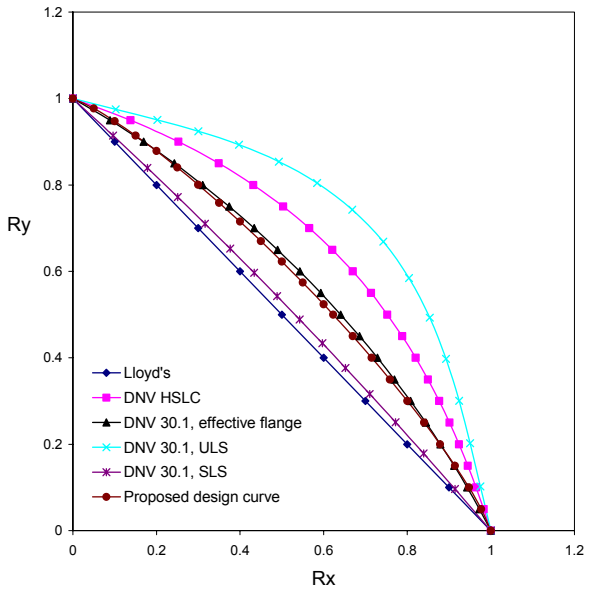

Figure A7.24 : Comparison of different biaxial design codes and proposed design formula, aspect ratio, a/b=1, β=3.5

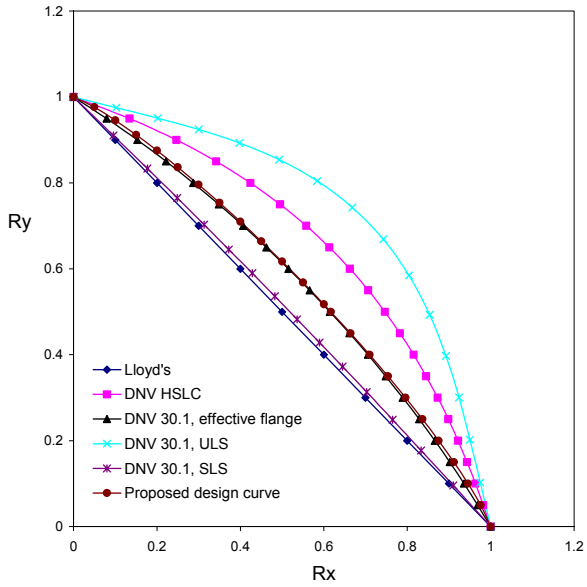

Figure A7.25 : Comparison of different biaxial design codes and proposed design formula, aspect ratio, a/b=1, β=4.0

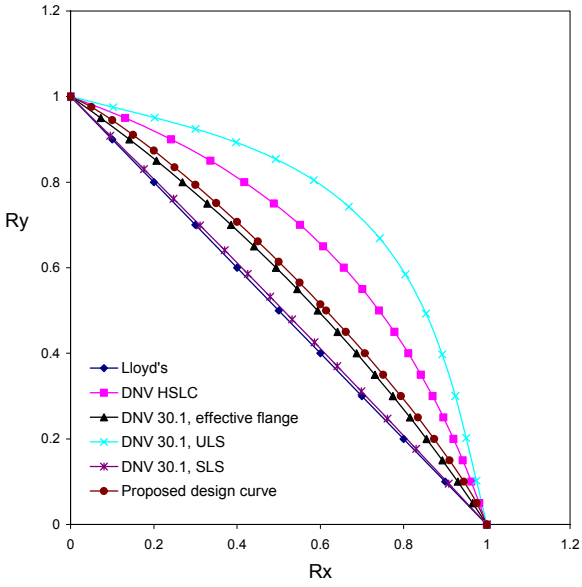

Figure A7.26 : Comparison of different biaxial design codes and proposed design formula, aspect ratio, a/b=1, β=4.5

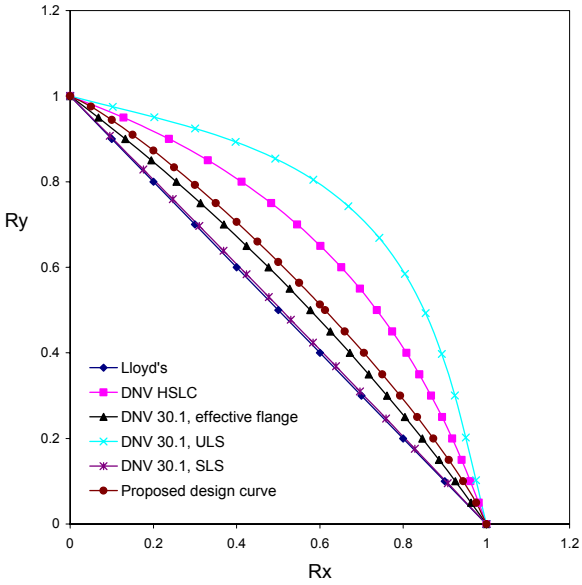

Figure A7.27 : Comparison of different biaxial design codes and proposed design formula, aspect ratio, a/b=1, β=5.0

A7.6 Comparison of Shear Design Curves

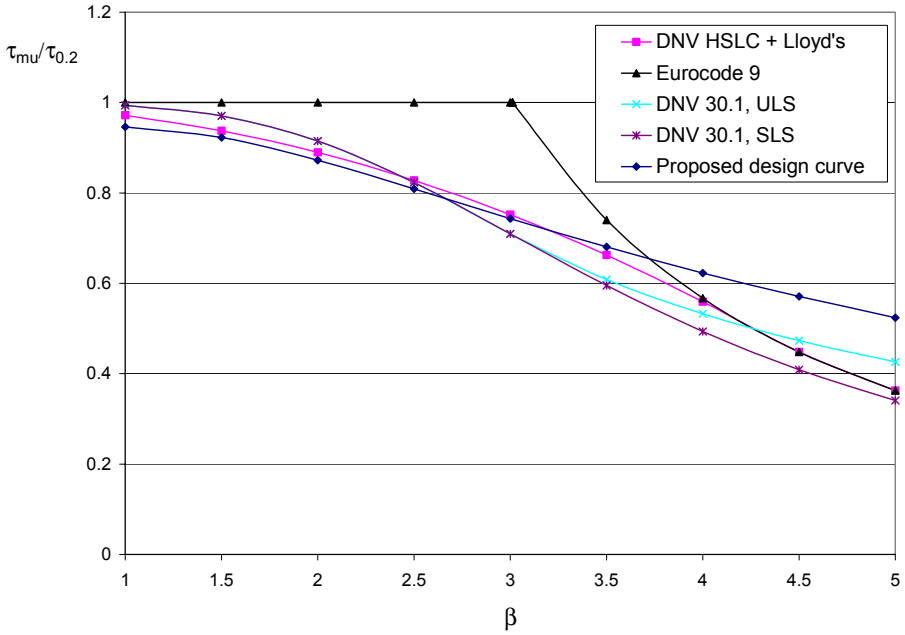

Figure A7.28 : Buckling curves from proposed design formula compared with different design formulations. $\sigma_{0.2}^{*}/\sigma_{0.2}$=1.0. Aspect ratio, a/b=3.

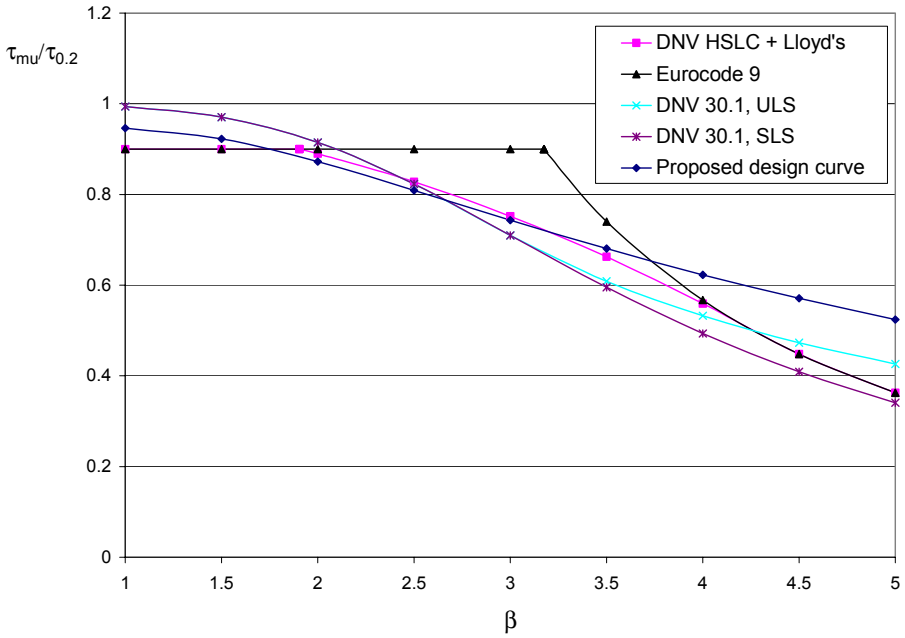

Figure A7.29 : Buckling curves from proposed design formula compared with different design formulations. $\sigma_{0.2}^{*}/\sigma_{0.2}$=0.9. Aspect ratio, a/b=3.

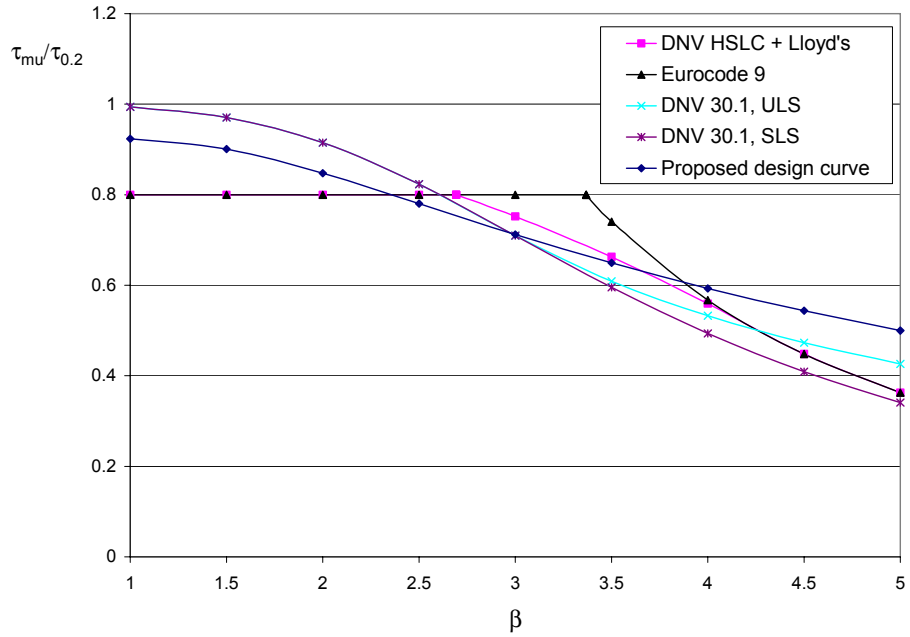

Figure A7.30 : Buckling curves from proposed design formula compared with different design formulations. $\sigma_{0.2}^{*}/\sigma_{0.2}$=0.8. Aspect ratio, a/b=3.

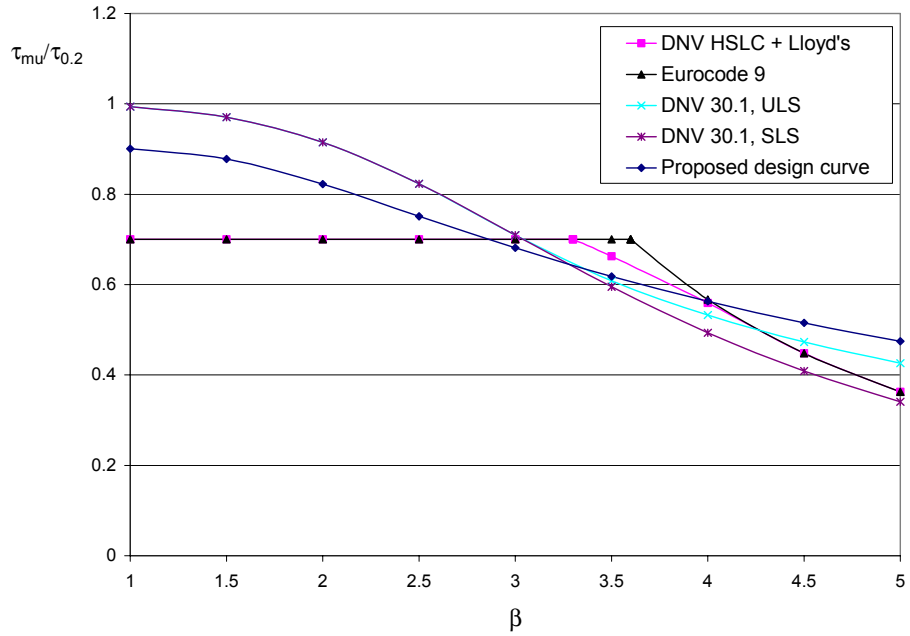

Figure A7.31 : Buckling curves from proposed design formula compared with different design formulations. $\sigma_{0.2}^{*}/\sigma_{0.2}$=0.7. Aspect ratio, a/b=3.

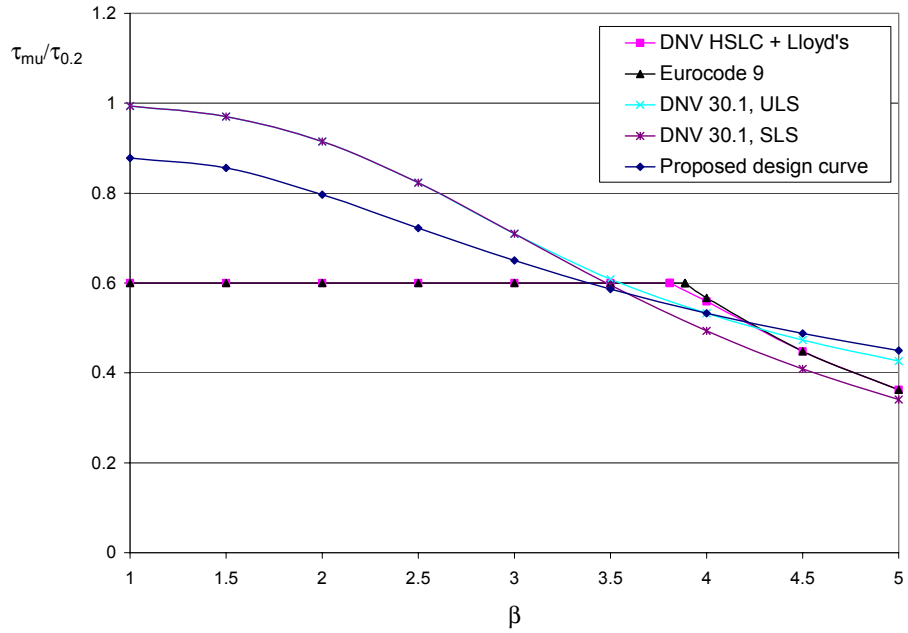

Figure A7.32 : Buckling curves from proposed design formula compared with different design formulations. $\sigma_{0.2}^{*}/\sigma_{0.2}$=0.6. Aspect ratio, a/b=3.

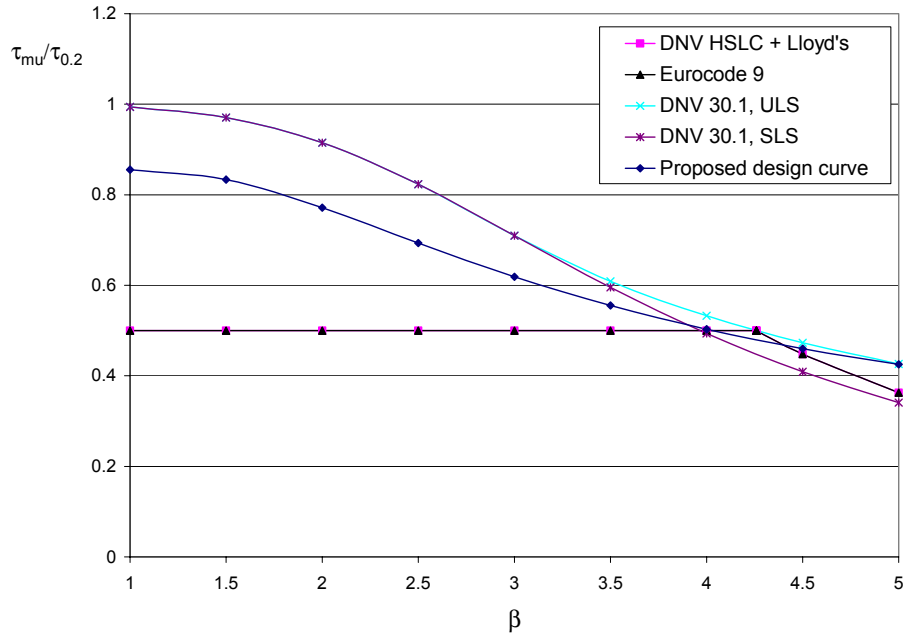

Figure A7.33 : Buckling curves from proposed design formula compared with different design formulations. $\sigma_{0.2}^{*}/\sigma_{0.2}$=0.5. Aspect ratio, a/b=3.

A7.7 Axial Compression in Combination with Shear Loads

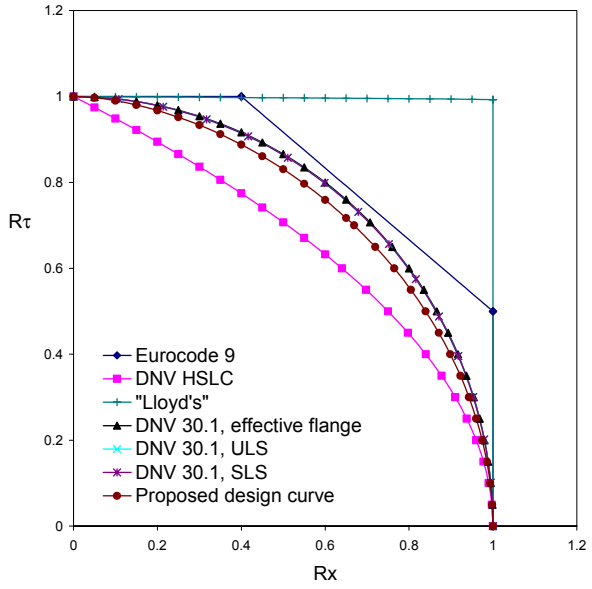

Figure A7.34 : Comparison of different design curves for β=1.0

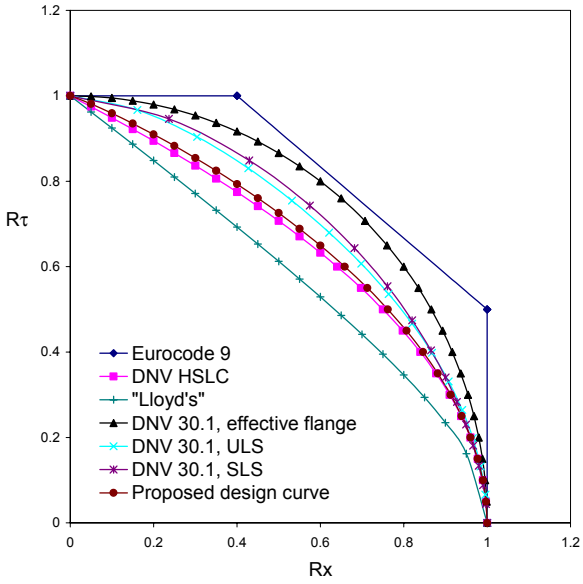

Figure A7.35 : Comparison of different design curves for β=5.0

PREVIOUS DR.ING. THESES

Department of Marine Structures

Kavlie, Dag	:	Optimization of Plane Elastic Grillages. 1967.
Hansen, Hans R.	:	Man-Machine Communication and Data-Storage Methods in Ship Structural Design. 1971.
Gisvold, Kaare M.	:	A Method for non-linear mixed -integer programming and its Application to Design Problems.
Lund, Sverre	:	Tanker Frame Optimalization by means of SUMT-Transformation and Behaviour Models. 1971.
Vinje, Tor	:	On Vibration of Spherical Shells Interacting with Fluid. 1972.
Lorentz, Jan D.	:	Tank Arrangement for Crude Oil Carriers in Accordance with the new Anti-Pollution Regulations. 1975.
Carlsen, Carl A.	:	Computer-Aided Design of Tanker Structures. 1975.
Larsen, Carl M.	:	Static and Dynamic Analysis of Offshore Pipelines during Installation. 1976.
Hatlestad, Brigt	:	The Finite Element Method used in a Fatigue Evaluation of Fixed Offshore Platforms. 1979.
Valsgård, Sverre	:	Finite Difference and Finite Element Method Applied to Non-Linear Analysis of Plated Structures. 1979.
Pettersen, Erik	:	Analysis and Design of Cellular Structures. 1979.
Nordsve, Nils T.	:	Finite Element Collapse Analysis of structural Members considering Imperfections and Stresses due to Fabrication. 1980.
Fylling, Ivar J.	:	Analysis of towline Forces in Ocean towing Systems. 1980.
Haver, Sverre	:	Analysis of Uncertainties related to the stochastic Modelling of Ocean Waves. 1980.
Odland, Jonas	:	On the Strength of welded Ring stiffened cylindrical Shells primarily subjected to axial Compression. 1981.
Engesvik, Knut	:	Analysis of Uncertainties in the fatigue Capacity of Welded Joints. 1982.
Eide, Oddvar Inge	:	On Cumulative Fatigue Damage in Steel Welded Joints. 1983.
Mo, Olav	:	Stochastic Time Domain Analysis of Slender Offshore Structures. 1983.
Amdahl, Jørgen	:	Energy absorption in Ship-platform impacts 1983.
Czujko, Jerzy	:	Collapse Analysis of Plates subjected to Biaxial Compression and Lateral Load. 1983.

Soares, C. Guedes	:	Probabilistic models for load effects in ship structures. 1984.
Mørch, Morten	:	Motions and mooring forces of semi submersibles as determined by full-scale measurements and theoretical analysis. 1984.
Engseth, Alf G.	:	Finite Element Collapse Analysis of Tubular Steel Offshore Structures. 1985.
Baadshaug, Ola	:	Systems Reliability Analysis of Jacket Platforms. 1985. (Confidential)
Hessen, Gunnar	:	Fracture Mechanics Analysis of Stiffened Tubular Members. 1986.
Taby, Jon	:	Ultimate and post-ultimate strength of dented tubular members. 1986.
Wessel, Heinz-J.	:	Fracture mechanics analysis of crack growth in plate girders. 1986.
Leira, Bernt Johan	:	Gaussian Vector-processes for Reliability Analysis involving Wave-induced Load Effects. 1987.
Xu JUN	:	Non-linear Dynamic Analysis of Space-framed Offshore Structures. 1988.
Guoyang Jiao	:	Reliability Analysis of Crack Growth under Random Loading considering Model Updating. 1989.
Olufsen, Arnt	:	Uncertainty and Reliability Analysis of Fixed Offshore Structures. 1989.
Wu Yu-Lin	:	System Reliability Analyses of Offshore Structures using improved Truss and Beam Models. 1989.
Farnes, Knut-Aril	:	Long-term Statistics of Response in Non-linear Marine Structures. 1990.
Sotberg, Torbjørn	:	Application of Reliability Methods for Safety Assessment of Submarine Pipelines. 1990.
Hoen, Christopher	:	System Identification of Structures Excited by Stochastic Load Processes. 1991.
Sødahl, Nils	:	Methods for Design and Analysis of Flexible Risers. 1991.
Haugen, Stein	:	Probabilistic Evaluation of Frequency of Collision between Ships and Offshore Platforms. 1991.
Ormberg, Harald	:	Non-linear Response Analysis of Floating Fish Farm Systems. 1991.
Marley, Mark J.	:	Time Variant Reliability Under Fatigue Degradation. 1991.
Bessason, Bjarni	:	Assessment of Earthquake Loading and Response of Seismically Isolated Bridges. 1992.
Sævik, Svein	:	On Stresses and Fatigue in Flexible Pipes. 1992.
Dalane, Jan Inge	:	System Reliability in Design and Maintenance of Fixed Offshore Structures. 1993.

Karunakaran, Daniel	:	Nonlinear Dynamic Response and Reliability Analysis of Drag-dominated Offshore Platforms. 1993.
Passano, Elizabeth	:	Efficient Analysis of Nonlinear Slender Marine Structures. 1994.
Bech, Sidsel M.	:	Experimental and Numerical Determination of Stiffness and Strength of GRP/PVC Sandwich Structures. 1994.
Hovde, Geir Olav	:	Fatigue and Overload Reliability of Offshore Structural Systems, Considering the Effect of Inspection and Repair. 1995.
Wang, Xiaozhi	:	Reliability Analysis of Production Ships with Emphasis on Load Combination and Ultimate Strength. 1995.
Hellan, Øyvind	:	Nonlinear Pushover and Cyclic Analyses in Ultimate Limit State Design and Reassessment of Tubular Steel Offshore Structures. 1995.
Hermundstad, Ole A.	:	Theoretical and Experimental Hydroelastic Analysis of High Speed Vessels. 1995.
Eknes, Monika Løland	:	Escalation Scenarios Initiated by Gas Explosions on Offshore Installations. 1996.
Halse, Karl Henning	:	On Vortex Shedding and Prediction of Vortex-Induced Vibrations of Circular Cylinders. 1997.
Igland, Ragnar Torvanger	:	Reliability Analysis of Pipelines during Laying, Considering Ultimate Strength under Combined Loads. 1997.
Vikestad, Kyrre	:	Multi-Frequency Response of a Cylinder Subjected to Vortex Shedding and Support Motions. 1998
Azadi, Mohammad R. E.	:	Analysis of Static and Dynamic Pile-Soil-Jacket Behaviour. 1998.
Videiro, Paulo Mauricio	:	Reliability Based Design of Marine Structures. 1998.
Mainçon, Philippe	:	Fatigue Reliability of Long Welds Application to Titanium Risers. 1999.
Langhelle, Nina Kristin	:	Experimental Validation and Calibration of Nonlinear Finite Element Models for Use in Design of Aluminium Structures Exposed to Fire. 1999.
Berstad, Are Johan	:	Calculation of fatigue damage in ship structures. 1999.
Tveiten, Bård Wathne	:	Fatigue Assessment of Welded Aluminum Ship Details. 1999.
Sagli, Gro	:	Model Uncertainty and Simplified Estimates of Long Term Extremes of Hull Girder Loads in Ships. 2000.
Tronstad, Harald	:	Nonlinear Analysis and Design of Cable Net Structures Like Fishing Gear Based on the Finite Element Method. 2000.
Wang, Lihua	:	Probabilistic Analysis of Nonlinear Wave-induced Loads on Ships. 2001.